Institut für Hydrologie
Albert-Ludwigs-Universität Freiburg im Breisgau

Andreas Hartmann

Process-based modelling of karst springs in Mt. Hermon, Israel

Diplomarbeit unter Leitung von Prof. Dr. M. Weiler

Freiburg im Breisgau

September 2008

Institut für Hydrologie

Albert-Ludwigs-Universität Freiburg im Breisgau

Andreas Hartmann

Process-based modelling of karst springs in Mt. Hermon, Israel

Referent: Prof. Dr. M. Weiler

Koreferent: Dr. Jens Lange

Diplomarbeit unter Leitung von Prof. Dr. M. Weiler

Freiburg im Breisgau

September 2008

Acknowledgments

I would like to thank the following people for their support during the thesis and the studies

- First of all my two supervisors, Alon Rimmer and Jens Lange, for supervision of my thesis and a lot of inspiring discussions and support.
- Prof. Dr. Markus Weiler for being my consultant.
- Prof. Dr. Leibundgut for the allocation of the thesis' theme and for support on my search for karst literature.
- Ora Hadas, Diti Viner-Mutzini, Yuri Lechinsky and Werner Eckart of the Yigal Allon Kinneret Limnological Laboratory for their valuable advice and support in all matters.
- Christina Hauger, Emil Blattmann and Jürgen Strueb of the Institute of Hydrology Freiburg for their help in organisatorical and technical questions.
- The German Academic Exchange Service, the Fördervein Hydrologie and the Freunde der Albert-Ludwigs Universität for their generous financial support.
- My parents who financed my whole studies for more than 5 years.
- My office mates in the Rheinstrasse for allways having time for discussion about more or less relevant issues.

Table of contents

Table of contents ..... **I**

List of figures ..... **V**

List of tables ..... **XIII**

List of symbols ..... **XVII**

Summary ..... **XXI**

Zusammenfassung ..... **XXIII**

Ehrenwörtliche Erklärung ..... **XXVII**

1 Introduction **1**

1.1 General Introduction 1

1.2 Objective 2

2 Study area **5**

2.1 Available data 6

2.2 Climate 7

2.3 Geology and Geomorphology 8

2.3.1 Banias Spring 11

2.3.2 Dan Spring 11

2.4 Soils 12

2.5 Vegetation and Land Use 13

2.6 Hydrology 13

2.6.1 Banias Spring 14

2.6.2 Dan Spring 15

2.7 Hydrochemistry 16

2.8 Conclusions 17

3 Karst hydrology **19**

3.1 Principles of karst hydrology 19

3.2 Modelling of karst systems 24

3.2.1 Global models 25

3.2.2 Distributive models 27

3.2.3 Modelling of the epikarst 32
3.3 Conclusions 36

4 Limitations for Mt. Hermon karst modelling 39

5 HYMKE - a HYdrological Model for Karst Environments 41

5.1 Model structure 41
5.2 Limitations of HYMKE 43
5.3 Conclusions 48

6 Consideration of hydrochemical knowledge 49

6.1 Solutes used for spring water characterization 50
6.2 Hydrochemical characterization 51
6.2.1 Banias Spring 52
6.2.2 Dan Spring 54
6.3 Comparison of both springs 56
6.3.1 Results of comparison 56
6.3.2 Summary of comparison 59
6.4 Hydrograph separation 59
6.4.1 Banias Spring 59
6.4.2 Dan Spring 65
6.4.3 Summary of hydrograph separations 66
6.5 Measurement campaign 67
6.5.1 Preparation 67
6.5.2 Results 68
6.5.3 Summary of measurement campaign 70
6.6 Conclusions 70

7 Development of a new model of groundwater flow: HYMKE_modified 73

7.1 Incorporation of the duality of groundwater flow 73
7.2 Mathematical application of the new conceptual model 74
7.2.1 Analytical solution for flows 74
7.2.2 Analytical solution for mixing 79
7.2.3 Acknowledgments 85

8 Application of HYMKE_modified 87

8.1 Sensitivity analysis of the modified groundwater routine 87

8.2 Application of HYMKE_modified on the real data 96
8.3 Intermediate conclusions 101

9 Incorporation of all major karst processes: HYMKE_DUAL 103

9.1 Snowmelt routine 103
9.2 Soil-Epikarst routine 107
9.3 Groundwater routine 111
9.4 Mixing routine for the soil-epikarst routine 119
9.5 Mixing for groundwater 121
9.6 Conclusions 128

10 Application of HYMKE_DUAL 131

10.1 Input data 131
10.1.1 Precipitation 131
10.1.2 Temperature 132
10.1.3 Evaporation 133
10.1.4 Plant uptake and release of NO_3 in the soil 135
10.2 Sensitivity analysis of the HYMKE_DUAL routines 139
10.2.1 The snowmelt routine 139
10.2.2 The soil/epikarst routine 142
10.2.3 The groundwater routine 158
10.3 Application of HYMKE_DUAL on the real data 171
10.4 Intermediate conclusions 179

11 Final discussion and conclusions 181

11.1 Discussion of flow simulations 182
11.2 Discussion of solute concentration simulations 184
11.3 Conclusions 186

12 Outlook 189

13 References 191

A Appendix 201

A.1 Long term data of hydrochemical variables for Banias and Dan Spring 201
A.2 Data used for the Piper and Schoeller diagrams 207
A.3 Data used for the three-component hydrograph separation 208

A.4 Photos of Dan Spring measurement campaign 209
A.5 Source codes of the modified groundwater routine 210
A.6 Source codes of the model routines of HYMKE_DUAL 213
A.6.1 Source code of the snow melt routine 213
A.6.2 Source code of the soil/epikarst routine 214
A.6.3 Source code of the groundwater routine 216
A.6.4 Source code of the soil-epikarst mixing routine 219
A.6.5 Source code of the groundwater mixing routine 222
A.7 Input data 224
A.7.1 Source code for down-scaling of nitrogen mineralization and immobilization observations 224
A.7.2 Source code for interpolation and regionalization of temperature data 225
A.7.3 Source code for regionalisation of potential evaporation data 226

List of figures

FIGURE 1: The study area: Mt. Hermon range and its position in the Middle East 5

Figure 2: Map of the main faults in the northern Jordan Rift Valley (Brielmann, 2008, after Heimann, 1990 and Zilberman, 2000)..... 9

FIGURE 3: The topography of the Mount Hermon region and its hydrological network (GUR ET AL., 2003, adapted from GILAD AND SCHWARTZ, 1978) 10

FIGURE 4: Geological cross section of Banias Spring (GUR ET AL., 2003, adapted fromb GILAD AND SCHWARTZ, 1978) 11

Figure 5: Geological cross section of Dan Spring (Gur et al., 2003, adapted from Gilad and Schwartz, 1978) 12

Figure 6: Precipitation at Ma'ayan Barukh station and discharge of Banias and Dan Spring from 1973/1974 to 1982/ 1983..... 15

FIGURE 7: Precipitation at Ma'ayan Barukh station and discharge of Banias and Dan Spring from 1990/1991 to 1999/2000..... 15

Figure 8: Conceptual model of a karst aquifer (Doerflinger, 1999)..... 21

FIGURE 9: Schematic relationship between soil CO_2, rate of limestone solution, and fissuring beneath the soil (WILLIAMS, 1983) 22

FIGURE 10: Schematic picture of the epikarst (WILLIAMS, 1983)..... 23

Figure 11: Interacting between water strored in fissures and water in the conduits of a karstich system (Seiler, 1989; modified)..... 24

FIGURE 12: A two-reservoir model as proposed by GEYER ET AL. (2008) 27

FIGURE 13: Classification of distributive karst modelling methods; EPM= equivalent porous medium approach, DC= double continuum approach, CDC= combined discrete-continuum (hybrid) approach, DFN= discrete fracture network approach, DCN= discrete channel network approach (GOLDSCHEIDER AND DREW, 2007) 28

Figure 14: Double Continuum approach by Mohrlock (1996; modified) 30

Figure 15: Conceptual model of karstic groundwater reservoir (Maloszewski, 2002, modified) 31

FIGURE 16: Recharge functions for the conduit system (dark grey) and to the fissured aquifer (bright grey), and resulting spring hydrographs under different numerical configurations (GEYER ET AL., 2008) 33

FIGURE 17: Soil reservoir applied in FLEURY ET AL. (2007) 34

FIGURE 18: Conceptualization of the soil and epikarst by PERRIN ET AL. (2003) 35

FIGURE 19: Geometry of the epikarst reservoir modelled with FEFLOW yielding the best results created by PERRIN ET AL. (2003) 36

Figure 20: Conceptual model of HYMKE (Rimmer and Salingar, 2006, modified) 42

Figure 21: Modelled baseflow (by HYMKE) and measured (base flow separated) discharge of Dan Spring from 1990/1991 to 1999/2000 43

Figure 22: Modelled baseflow (by HYMKE) and measured (base flow separated) discharge of Banias Spring from 1990/1991 to 1999/2000 43

Figure 23: Variations of NO_3 in Dan Spring between 1990/1991 and 1999/2000 45

Figure 24: Variations of SO_4 in Dan Spring between 1990/1991 and 1999/2000 45

Figure 25: Variations of Cl in Dan Spring between 1990/1991 and 1999/2000 46

Figure 26: variation of NO_3 in Banias Spring between 1990/1991 and 1999/2000 47

Figure 27: variation of SO_4 in Banias Spring between 1990/1991 and 1999/2000 47

Figure 28: variation of Cl in Banias Spring between 1990/1991 and 1999/2000 48

FIGURE 29: Schematic illustration of temporal variations of discharge and basic hydrochemical parameters (GOLDSCHEIDER AND DREW, 2007) 50

Figure 30: Piper diagram of Banias Spring major ion concentrations under different discharge conditions 52

Figure 31: Schoeller diagram of Banias Spring concentrations for different seasons (rainy or dry) under different pre-conditions 53

Figure 32: Piper diagram of Dan Spring major ion concentrations under different discharge conditions 54

Figure 33: Schoeller diagram of Dan Spring concentrations for rainy or dry season under different pre-conditions 55

FIGURE 34: Hydrographs and chemographs of Cl of Banias Spring and Dan Spring from 1973/1974 to 1982/1983 56

FIGURE 35: Hydrographs and chemographs of NO_3 of Banias Spring and Dan Spring from 1973/1974 to 1982/1983 58

FIGURE 36: Hydrographs and chemographs of SO_4 of Banias Spring and Dan Spring from 1973/1974 to 1982/1983 58

FIGURE 37: Mean and median variations of Cl, NO_3 and SO_4 of Banias Spring 62

FIGURE 38: Mixing diagram of Cl and SO_4; red dots represent the end-members and the green dots the median mixing composition of the respective month 64

FIGURE 39: Contributions of the three components to total discharge 64

FIGURE 40: Air pressure and air temperature collected by the BARO DIVER 68

FIGURE 41: Water level, conductivity and , water temperature collected by the CTD DIVER, pH and O_2 saturation collected by the YSI Multiparameter Water Quality Sonde 69

Figure 42: New conceptual model for the groundwater module in HYMKE 74

Figure 43: Schematic concept of the modified groundwater reservoir 75

FIGURE 44: Response of the modified reservoir on a synthetic event using different K_Es and K_1=5 days; left: response of conduit outlet, right: response of exchange flow; the black bar represents the recharge event 88

FIGURE 45: Response of the modified reservoir on a synthetic event using different K_Es and K_1=15; left: response of conduit outlet, right: response of exchange flow; the black bar represents the recharge event 89

FIGURE 46: Response of the modified reservoir on a synthetic event using different K_Es and K_1=25; left: response of conduit outlet, right: response of exchange flow; the black bar represents the recharge event 89

FIGURE 47: Hydrochemical response of the modified reservoir on a synthetic event with gradually decreasing concentration of input (bars) using different K_Es and K_1=5; left: response of conduit outlet, right: response of exchange flow 91

FIGURE 48: Hydrochemical response of the modified reservoir on a synthetic event with gradually decreasing concentration of input (bars) using different K_Es and K_1=15; left: response of conduit outlet, right: response of exchange flow 91

FIGURE 49: Hydrochemical response of the modified reservoir on a synthetic event with gradually decreasing concentration of input (bars) using different K_Es and K_1=25; left: response of conduit outlet, right: response of exchange flow 92

FIGURE 50: Hydrochemical response of the modified reservoir on a synthetic event with constant flux of mass to the fissured aquifer and a constant input concentration (bars) using different K_Es and K_1=5; left: response of conduit outlet, right: response of exchange flow 93

FIGURE 51: Hydrochemical response of the modified reservoir on a synthetic event with constant flux of mass to the fissured aquifer and a constant input concentration (bars) using different K_Es and K_1=15; left: response of conduit outlet, right: response of exchange flow 94

FIGURE 52: Hydrochemical response of the modified reservoir on a synthetic event with constant flux of mass to the fissured aquifer and a constant input concentration (bars) using different K_Es and K_1=25; left: response of conduit outlet, right: response of exchange flow 94

Figure 53: Output of the surface layer routine which serves as input for the simulations..... 96

FIGURE 54: Discharge and concentrations of Cl, NO_3 and SO_4 at Dan Spring from 1990/1991 to 1999/2000 predicted by the old HYMKE and the modified HYMKE compared to the measured (base flow separated) and hydrochemical data 98

Figure 55: Discharge and concentrations of Cl, NO_3 and SO_4 at Banias Spring from 1990/1991 to 1999/2000 predicted by the old HYMKE and the modified HYMKE compared to the measured (base flow separated) and hydrochemical data 100

FIGURE 56: Altitude distribution of Mt. Hermon Range calculated by RIMMER AND SALINGAR (2006); grey lines indicate border between two altitude strips 105

FIGURE 57: Geometry of the new soil-epikarst module 108

FIGURE 58: Geometry of the new groundwater module 112

FIGURE 59: Schematic picture of the groundwater mixing model 125

FIGURE 60: WHOLE MODEL STRUCTURE OF HYMKE_DUAL 128

FIGURE 61: Daily precipitation of Ma'ayan Barukh, Yiiftah and Malkya meteorological stations from 1973 to 1983 131

FIGURE 62: Temperature time series of Zefat station from 1973 to 1983 132

FIGURE 63: Seasonal pan coefficient corrected seasonal tren of pan A evaporation by RIMMER AND SALINGAR (2006) and fitted Thornthwaite evaporation for altitude strip 4 135

FIGURE 64: Variations of soil N-NO3, N-NH4, N-NO2 and total N [ppm] from May 2004 to January 2006 below the Yatir Forest shrub land as observed by GELFAND AND YAKIR (2008) 136

FIGURE 65: Accumulated nitrogen mineralization [ppm] for seven incubation periods from October 1985 to June 1986 observed by (JOFFRE, 1990) 137

FIGURE 66: Accumulated plant nitrogen immoblization [ppm] for three periods from October 1985 to June 1986 observed by (JOFFRE, 1990) 138

FIGURE 67: Effective mineralization of nitrogen, negative values stand for effective plant immobilization; data obtained from JOFFRE (1990). 139

FIGURE 68: Results of sensitivity analysis of snow melt rotine 141

FIGURE 69: Sensitivity analysis for the thickness of the soil layer *RD* 146

FIGURE 70: Sensitivity analysis for the thickness of the upper epikarst h_{Up} 147

FIGURE 71: Sensitivity analysis for the thickness of the lower epikarst h_{Low} 148

FIGURE 72: Sensitivity analysis for the saturation water content of the soil and upper epikarst $\theta_{Sat,Up}$ 149

FIGURE 73: Sensitivity analysis for the residual water content of the soil and upper epikarst $\theta_{Rest,Up}$ 150

FIGURE 74: Sensitivity analysis for the saturated hydraulic conductivity of the soil and upper epikarst $K_{Sat,Up}$ 151

FIGURE 75: Sensitivity analysis for parameter which is related to the Brooks-Corey grain size index for the soil and upper epikarst m_{Up} 152

FIGURE 76: Sensitivity analysis for the saturation water content of the lower epikarst $\theta_{Sat,Low}$ 153

FIGURE 77: Sensitivity analysis for the residual water content of lower epikarst $\theta_{Rest,Low}$ 154

FIGURE 78: Sensitivity analysis for the saturated hydraulic conductivity of lower epikarst $K_{Sat,Low}$ 155

FIGURE 79: Sensitivity analysis for parameter which is related to the Brooks-Corey grain size index for the lower epikarst m_{Low} 156

FIGURE 80: Sensitivity analysis for the storage coefficient of the Dan conduit system K_1 163

FIGURE 81: Sensitivity analysis for the storage coefficient of the Banias conduit system K_2 164

FIGURE 82: Sensitivity analysis for the exchange coefficient K_E 165

FIGURE 83: Sensitivity analysis for the conduit porosity n_1 166

FIGURE 84: Sensitivity analysis for the fissure porosity n_2 167

FIGURE 85: Sensitivity analysis for the altitude difference between Dan and Banias Spring outlet H_2 168

FIGURE 86: Sensitivity analysis for the fraction of Dan Spring subsurface catchment on the whole catchment area *a* (inverse to this the fraction of Banias Spring subsurface catchment area *b*) 169

FIGURE 87: Output of soil epikarst routine; on the top: discharge to the fissures, matrix flow to the conduits and preferential flow to the conduits; below: concentrations of the sum of matrix and preferential flow to the conduits and flow to the fissures 173

FIGURE 88: Output of groundwater routine for Banias Spring; on the top: observed and measured discharge; below: observed and measured concentrations of Cl, NO_3 and SO_4 177

FIGURE 89: Output of groundwater routine for Dan Spring; on the top: observed and measured discharge; below: observed and measured concentrations of Cl, NO_3 and SO_4 178

FIGURE 90: Discharge, electric conductivity, temperature. pH value and turbidity courses of Banias Spring from 1990 to 2000 201

FIGURE 91: Major cation courses of Banias Spring from 1990 to 2000 202

FIGURE 92: Major anion courses of Banias Spring from 1990 to 2000 203

FIGURE 93: Discharge, electric conductivity, temperature. pH value and turbidity courses of Dan Spring from 1990 to 2000 204

FIGURE 94: Major cation courses of Dan Spring from 1990 to 2000 205

FIGURE 95: Major anion courses of Banias Spring from 1990 to 2000 206

FIGURE 96: DIVER fixed on cable and lock 209

Figure 97: Hydrologist Yuri Lechinsky, Kinneret Limnological Laboratory staff, installing the DIVER in the Dan stream 210

List of tables

Table 1: Data provided by the Allon Yigal Kinneret Limnological Laboratory 6

Table 2: General classification of the main Jordan tributaries in the Mt. Hermon range; AMaF: absolute maximum flow, MHF: mean annual high flow, MF: mean annual flow, MLF: mean annual low flow and AMiF: absolute minimum flow (Brielmann, 2008) 14

Table 3: Composition of Mt. Hermon rain/snow samples; nd: not detected (Brielmann, 2008) 17

TABLE 4: Contribution of event water (P_E) and pre-event water (P_{PE}) for the hydrological years 2002/2003 and 2003/2004 established by BRIELMANN (2008) 60

TABLE 5: Concentrations representing event and pre-event components for $\delta^{18}O$ (C_E and C_{PE}), rain and snow (C_{RS}), vadose zone (C_{VAD}) (i.e. the soil and epikarst) and diffuse matrix flow components (C_{DF}) for SO_4 for the hydrological years 2002/2003 and 2003/2004 (BRIELMANN, 2008) 60

TABLE 6: Contribution of rain and snow (P_{RS}), vadose zone (P_{VAD}) and diffuse matrix flow (P_{DF}) for the hydrological years 2002/03 and 2003/04 established by BRIELMANN (2008) 61

TABLE 7: End member composition of rain/snow, soil/epikarst, and the diffuse matrix flow component 63

TABLE 8: End-member concentrations for the hydrological years 2002/03 and 2003/04 at Dan Spring (BRIELMANN, 2008) 65

TABLE 9: Contribution of event (E) and pre-event (PE) water to total discharge in 2002/03 and 2003/04 calculated with $\delta^{18}O$, SO_4 and Cl (BRIELMANN, 2008) 65

TABLE 10: Summary of impact of K_I and K_E on discharge and concentrations in the conduits and the fissured aquifer 95

TABLE 11: Parameters for seasonal pan A evaporation trend determined by RIMMER AND SALINGAR (2006) 133

TABLE 12: Different sets of parameters applied in the HBV snow melt routine..... 139

TABLE 13: Summary of the soil/epikarst routine parameters and description 142

TABLE 14: Parameter ranges chosen for sensitivity analysis of the soil/epikarst routine and their default values 143

TABLE 15: Influence of soil/epikarst routine parameters on output variables (+++: strong influence, ++: moderate influence, +: low influence, -: no influence)..... 157

TABLE 16: Parameters included in the groundwater routine, their descriptions and units..... 158

TABLE 17: Storage coeffcients for conduit and fissure systems found in other studies..... 159

TABLE 18: Parameter ranges chosen for sensitivity analysis of the groundwater routine and their default values 160

TABLE 19: Parameters chosen for the snow melt routine..... 171

TABLE 20: Parameters chosen for the soil/epikarst routine..... 172

TABLE 21: Parameters chosen for the groundwater routine 174

TABLE 22: Input concentration for HYMKE_DUAL mixing routines 175

Table 23: Banias Spring major ion concentrations for different seasons (rainy or wet) under different pre-conditions in the year before..... 207

TABLE 24: Dan Spring major ion concentrations for different seasons (rainy or wet) under different pre-conditions in the year before..... 207

TABLE 25: median, mean, minimum and maximum monthly concentrations of Cl; n is the total number of samples taken for the respective calculations..... 208

TABLE 26: median, mean, minimum and maximum monthly concentrations of NO_3; n is the total number of samples taken for the respective calculations 208

TABLE 27: median, mean, minimum and maximum monthly concentrations of SO_4; n is the total number of samples taken for the respective calculations 209

List of symbols

A	area of the whole catchment	[km²]
a	parameter for Thornthwaite method	[mm/day/°C/h]
a_E	constant for seasonal evaporation trend of potential evaporation	[mm/day]
AG	temperature gradient	[°C/100m]
A_i	area of a certain altitude strip	[km²]
Alt_i	mean level of a certain altitude strip	[m]
Alt_{Zefat}	level of Zefat meteorological station	[m]
A_R	amplitude in empirical precipitation-elevation-seasonal equation	[mm/m]
a_R	coefficient in empirical precipitation-elevation-seasonal equation	[m]
B	matrix containing the concentrations of components in hydrograph separation	[mg/l]
b_E	constant for seasonal evaporation trend of potential evaporation	[mm/day]
b_R	coefficient in empirical precipitation-elevation-seasonal equation	[mm]
$c_1(t)$	solute concentration in the conduits in HYMKE_modified	[g/m³]
c_{10}	initial solute concentration in the conduits in HYMKE_modified	[g/m³]
$c_2(t)$	solute concentration in the fissures in HYMKE_modified	[g/m³]
c_{20}	initial solute concentration in the fissures in HYMKE_modified	[g/m³]
$c_{Cond}(t)$	solute concentration of whole flow to conduits	[g/m³]
$c_{Cond,i}(t)$	solute concentration of flow to conduits of a certain altitude strip	[g/m³]
C_E	pan A coefficient	[-]
$c_{E1}(t)$	concentration of exchange flow between Dan Spring conduits and the fissure system HYMKE_DUAL	[g/m³]
$c_{E2}(t)$	concentration of exchange flow between Banias Spring conduits and the fissure system HYMKE_DUAL	[g/m³]
$c_{Fis}(t)$	solute concentration of whole flow to fissures	[g/m³]
$c_{Fis,i}(t)$	solute concentration of flow to fissures of a certain altitude strip	[g/m³]
c_{in1}	concentration of inflow to the Dan Spring conduit system in HYMKE_DUAL	[g/m³]
c_{in2}	concentration of inflow to the Banias Spring conduit system in HYMKE_DUAL	[g/m³]
c_{in3}	concentration of inflow to fissure system in HYMKE_DUAL	[g/m³]
$c_{out1}(t)$	concentration in Dan Spring conduits HYMKE_DUAL	[g/m³]
$c_{out2}(t)$	concentration in Banias Spring conduits HYMKE_DUAL	[g/m³]
$c_{out3}(t)$	concentration in fissures in HYMKE_DUAL	[g/m³]
ddf	degree day factor	[mm/°C/day]
$E_p(JD)$	seasonal evaporation trend of potential evaporation	[mm/day]

$E_{pt}(JD)$	evaporation by Thornthwaite method	[mm/day]
Ept_{Thres}	parameter defining the minimum water content from which on actual evaporation equals potential evaporation	[-]
$Evap(t)$	actual evaporation	[mm]
$Evap_{pot}(t)$	potential evaporation	[mm]
F_j	daily average factor for regionalisation of precipitation	[-]
$h_1(t)$	water level in Dan Spring conduit system in HYMKE_DUAL	[m]
$h_1(t)$	level of the water in the conduits in HYMKE_modified	[m]
h_{10}	initial water level in the conduits in HYMKE_modified	[m]
h_{10}	initial water level in Dan Spring conduits in HYMKE_DUAL	[m]
H_2	level difference of Dan and Banias Spring outlet	[m]
$h_2(t)$	water level in Banias Spring conduit system in HYMKE_DUAL	[m]
$h_2(t)$	level of the water in the fissure aquifer in HYMKE_modified	[m]
h_{20}	initial water level in the fissures in HYMKE_modified	[m]
h_{20}	initial water level in Banias Spring conduits in HYMKE_DUAL	[m]
$h_3(t)$	water level in fissure system in HYMKE_DUAL	[m]
h_{30}	initial water level in the fissures in HYMKE_DUAL	[m]
HC	holding capacity of snow pack	[-]
$h_E(t)$	difference of water level of the conduit reservoir and the fissured aquifer in HYMKE_modified	[m]
$h_{E1}(t)$	water level in Dan Spring conduits in HYMKE_DUAL	[m]
$h_{E2}(t)$	water level in Banias Spring conduits in HYMKE_DUAL	[m]
h_{low}	thickness of lower epikarst layer	[m]
h_{up}	thickness of upper epikarst layer	[m]
$h_{up,Evap}$	thickness of soil layer	[m]
I	parameter for Thornthwaite method	[-]
JD	Julian Day number	[-]
JD_R	Julian day number of 15th day of the month	[-]
K_1	storage coefficient of Dan Spring conduits in HYMKE_DUAL	[day]
K_1	storage coefficient of the conduit reservoir in HYMKE_modified	[day]
K_2	storage coefficient of Banias Spring conduits in HYMKE_DUAL	[day]
K_E	exchange coefficient	[day]
K_{E1}	exchange coefficient including the conduit porosity	[day]
K_{E2}	exchange coefficient including the fissure porosity	[day]
$K_{sat,low}$	unsaturated conductivity of the lower epikarst	[-]
$K_{sat,up}$	unsaturated conductivity of the soil and upper epikarst layer	[-]
λ	Brooks-Corey grain size distribution index	[-]
$l(t)$	vector containing the contribution of components in hydrograph separation	[-]

l_E	angular frequency for seasonal evaporation trend of potential evaporation	[rad]
l_R	angular frequency in empirical precipitation-elevation-seasonal equation	[rad]
$LWRC$	liquid water retaining capacity of snow pack]	[mm]
$m_1(t)$	solute mass stored in the conduits in HYMKE_modified	[g/m²]
$m_1(t)$	solute mass stored in Dan Spring conduit system in HYMKE_DUAL	[g/m²]
$m_2(t)$	solute mass stored on the fissures in HYMKE_modified	[g/m²]
$m_2(t)$	solute mass stored in Banias Spring conduit system in HYMKE_DUAL	[g/m²]
$m_3(t)$	solute mass stored in fissure system in HYMKE_DUAL	[g/m²]
m_{add1}	constant flux of mass to Dan Spring geogene mass reservoir	[g/m²/day]
m_{add2}	constant flux of mass to Banias Spring geogene mass reservoir	[g/m²/day]
m_{dif}	intrinsic input of solute mass to the fissures in HYMKE_modified	[g/m²/day]
$m_E(t)$	exchange of solute mass between the conduit and fissure reservoir in HYMKE_modified	[g/m²/day]
$m_{geo1}(t)$	mass stored in Dan Spring geogene mass reservoir	[g/m²]
$m_{geo2}(t)$	mass stored in Banias Spring geogene mass reservoir	[g/m²]
m_{in1}	constant input of mass into the conduits in HYMKE_modified	[g/m²/day]
m_{in2}	constant input of mass into the fissures in HYMKE_modified	[g/m²/day]
m_{low}	parameter related to the Brooks-Corey grain size distribution index for lower epikarst layer	[-]
$m_{out1}(t)$	outflow of solute mass from the conduits in HYMKE_modified	[g/m²/day]
m_{up}	parameter related to the Brooks-Corey grain size distribution index for the soil and upper epikarst layer	[-]
$m_{UpRel}(t)$	solute mass uptake and release by micro-organisms and vegetation in the soil layer	[g/m²/day]
n_1	effective porosity of the conduits	[-]
n_2	effective porosity of the fissures	[-]
N_M	number of days of a certain month	[-]
$q_1(t)$	specific discharge of the conduits in HYMKE_modified	[m/day]
$q_1(t)$	outflow of Dan Spring conduit system in HYMKE_DUAL	[m/day]
$q_2(t)$	outflow of Banias Spring conduit system in HYMKE_DUAL	[m/day]
$q_{Cond,i}(t)$	specific flow to the conduits from a certain altitude strip	[m/day]
$q_E(t)$	specific flow between the conduit reservoir and the fissured aquifer in HYMKE_modified	[m/day]
$q_{E1}(t)$	flow from the fissure reservoir to Dan Spring conduits in HYMKE_DUAL	[m/day]
$q_{E2}(t)$	flow from the fissure reservoir to Banias Spring conduits in HYMKE_DUAL	[m/day]

$q_{Fis,i}(t)$	specific flow to the fissures from a certain altitude strip	[m/day]
q_{in1}	inflow to the conduits in HYMKE_modified	[m/day]
q_{in1}	inflow to the Dan Spring conduit system in HYMKE_DUAL	[m/day]
q_{in2}	inflow to the fissures in HYMKE_modified	[m/day]
q_{in2}	inflow to the Banias Spring conduit system in HYMKE_DUAL	[m/day]
q_{in3}	inflow to the fissure system in HYMKE_DUAL	[m/day]
$\theta_{low}(t)$	volumetric water content in the lower epikarst	[-]
q_{melt}	calculated snowmelt	[mm/day]
$q_{out1}(t)$	outflow of Dan Spring conduits HYMKE_DUAL	[m/day]
$q_{out2}(t)$	outflow of Banias Spring conduits HYMKE_DUAL	[m/day]
q_{refr}	calculated refreezing rate of liquid water in snow pack	[mm/day]
$\theta_{rest,low}$	residual relative water content for the lower epikarst layer	[-]
$\theta_{rest,up}$	residual relative water content for the soil and upper epikarst layer	[-]
$\theta_{sat,low}$	saturated relative water content of the lower epikarst layer	[-]
$\theta_{sat,up}$	saturated relative water content of the soil and upper epikarst layer	[-]
$\theta_{up}(t)$	volumetric water content in the upper epikarst layer	[-]
$\theta_{up,Evap}(t)$	volumetric water content in the soil layer	[-]
RF	refreezing factor	[-]
R_{ij}	precipitation at a certain altitude at a certain day	[mm]
R_j	catchment wide precipitation at a certain day	[mm]
RLW	retained liquid water in snow pack	[mm]
R_M	monthly precipitation for empirical precipitation-elevation-seasonal equation	[mm]
R_{nj}^*	precipitation measured at a certain station at a certain day	[mm]
S_0	mean daily astronomic sunshine length	[h]
SWE	snow water equivalent of snow pack	[mm]
T_{AIR}	mean daily air temperature for snow melt calculations	[°C]
$T_i(t)$	mean daily temperature for a certain altitude strip	[°C]
T_M	melting temperature	[°C]
$T_{Zefat}(t)$	mean daily temperature at Zefat meteorological station	[°C]
w_E	phase shift for seasonal evaporation trend of potential evaporation	[-]
w_R	phase shift in empirical precipitation-elevation-seasonal equation	[-]
$x(t)$	vector containing solute concentration of observations in hydrograph separation	[mg/l]
z	elevation of gauging stations used for regionalisation	[m]

Summary

The hydrological behavior of karst systems is characterised by a duality of recharge, flow and storage. In order to model the karstic behavior different approaches can be applied which generally form two groups: global models and distributive models. Distributive models require a large amount of spatial system information which is not always available, in particular for large-scale basins. Despite of that global models only require the input and output data of the system. To provide output predictions they use system functions. If these functions include processes and storages which are really abundant in the hydrological system under consideration the global models are also called “grey box” models. Since in the case of Mt. Hermon hydrological system there is nearly no system-inside information available RIMMER AND SALINGAR (2006) developed a “grey box” of this system: HYMKE (hydrological model for karst environments). This model yielded good results for the discharge predictions but coupling of its flow predictions with solute concentration predictions showed that the observed solute concentrations of the system outflow could not be reproduced. This was considered as an indicator that at least one storage or process was missing in the HYMKE model structure. As the structure of HYMKE is based only on observations of the flow behavior of the system hydrochemical data of the major springs, Dan and Banias Spring, was also considered aiming on identifying the missing storage or process. The analysis showed that both spring receive water from three different sources: rain and snow, soil and epikarst, and diffuse matrix flow water. The contribution of theses sources varies between the springs and during the seasons. In order to incorporate this knowledge in HYMKE two different approaches were applied: (1) Identification of the most important missing storage or process and incorporating it in HYMKE: development of HYMKE_modified. (2) Modification of all HYMKE routines in a manner that they represent the three sources identified in the hydrochemical analysis: development of HYMKE_DUAL. As most important missing storage a fissure storage, representing diffuse matrix flow, was identified. Thus the difference of the first version of HYMKE and HYMKE_modified is a modified groundwater routine which includes a fissure storage and a conduit storage which exchange water dependent on their water level difference. Despite of that the incorporation of the three recognized sources in HYMKE_DUAL consisted of the development of a snow melt routine, a modification of the HYMKE surface routine to better represent the soil and epikarst, and a further development of the HYMKE_modified groundwater routine. Hereby the snow melt routine and the new soil/epikarst routine were distributed over 56 elevation

zones. With these new features both approaches provided good discharge predictions even though the structures of HYMKE_modified and HYMKE_DUAL were different, particularly in the routines superimposed on their groundwater routines: in HYMKE_modified a combination of a one-layer soil/epikarst routine and a linear storage representing the vadose zone provided the recharge to the groundwater routine. Despite of that in HYMKE_DUAL a more complex three-layer soil/epikarst routine provided the recharge. Similar to the first version of HYMKE mixing equations were coupled with the flow predictions of the new models to proof that their structure is representing the real system behavior. As a consequence of the combination of a fast reacting conduit storage and a slow reacting fissure storage in their groundwater routines both approaches were able to rapidly transform hydrochemical signals to the output leading to good predictions of solute concentrations for both approaches. Hence the identification of the fissure storage was proven to be the most important missing process in the first version of HYMKE. However regarding the concentrations of recharge to the groundwater routines showed that only the three-layer soil/epikarst routine of HYMKE_DUAL was able to transfer event water concentrations, which is rain and snow melt, to the groundwater routine and to the system outlet as it was identified in the hydrochemical analysis during the rainy season. Nevertheless HYMKE_modified could reproduce the seasonal variations of solute concentrations but without contribution of event water.

Altogether the good discharge and hydrochemical predictions showed that HYMKE_modified and HYMKE_DUAL both include the major processes and storages of the Mt. Hermon hydrological system even though they are represented by differing routines. HYMKE_modified has a lumped structure and therefore it needs only a few parameters whereas HYMKE_DUAL requires more parameters due to its complex representation of the soil and epikarst; additionally its parameters can be distributed over the different elevation zones. This allows the application of spatial information and to obtain spatial distributed results. Unfortunately in Mt. Hermon no spatial information was available – the same estimated parameters had to be applied on every elevation zone. Hence the potential advantages of HYMKE_DUAL did not yield significant improvements compared to HYMKE_modified.

Zusammenfassung

Das hydrologische Verhalten von Karstsystemen zeichnet sich durch eine Dualität von Grundwasserneubildung, Fließen und Speicherung aus. Zur Modellierung dieses Verhaltens gibt es verschiedene Ansätze, welche generell in zwei Gruppen unterteilt werden können: Globale Modelle und distribuierte Modelle. Distribuierte Modelle benötigen eine große Menge an räumlich aufgelösten Daten über das System, welche gerade in großen Einzugsgebieten nicht immer verfügbar ist. Im Gegensatz dazu benötigen globale Modelle nur Eingangs- und Ausgangsdaten des betrachteten Systems. Um Ausgangsdaten vorherzusagen benutzen sie so genannte Systemfunktionen. Berücksichtigen diese Funktionen Prozesse und Speicher, die im betrachteten System wirklich vorkommen, so bezeichnet man sie auch als "grey box" Modelle. Da im Falle des hydrologischen System des Mt. Hermon kaum räumlich aufgelöste Daten vorhanden sind, entwickelten RIMMER UND SALINGAR (2006) ein "grey box" Modell, genannt HYMKE (*hydrological model for karst environments*). Die Abflussvorhersagen dieses Modells waren zwar gut, jedoch zeigte eine Erweiterung des Modells um Mischungsrechnungen, dass es nicht fähig war, die am Systemauslass beobachteten Konzentrationen wiederzugeben. Dies wurde als ein Anzeichen dafür interpretiert, dass mindestens ein wichtiger Prozess oder Speicher nicht durch die Modellstruktur berücksichtigt wurde. Da die Struktur von HYMKE nur aufgrund von Beobachtungen der Abflüsse gewählt wurde, wurden nun zusätzlich hydrochemische Beobachtungen der beiden wichtigsten Quellen des Mt. Hermon Systems, der Dan- und der Baniasquelle, herangezogen, um den fehlenden Prozess, beziehungsweise Speicher, zu identifizieren. Die Analyse der hydrochemischen Daten zeigte, dass beide Quellewässer eine Mischung aus Regen- und Schneeschmelzwasser, Boden- und Epikarstwasser und Wasser einer diffus fließenden Matrixkomponente darstellten. Der Beitrag der jeweiligen Komponenten variierte zwischen den Quellen und während den Jahreszeiten. Um diese Erkenntnisse in HYMKE zu integrieren, wurden zwei Ansätze gewählt: (1) Die Identifizierung des wichtigsten fehlenden Prozesses oder Speichers und dessen Einarbeitung in HYMKE: Entwicklung von HYMKE_modified. (2) Die Modifizierung aller Modellroutinen von HYMKE, so dass sie die drei in der hydrochemischen Analyse identifizierten Komponenten repräsentieren: Entwicklung von HYMKE_DUAL. Als wichtigster fehlender Speicher würde der Kluftspeicher identifiziert, welcher verantwortlich für das diffuse Matrixfließen ist. Damit besteht der Unterschied zwischen HYMKE und HYMKE_modified in einer modifizierten Grundwasserroutine, welche aus einem

Kluftspeicher und einem Karstkanalspeicher besteht, die abhängig von ihrem Wasserstandunterschied Grundwasser austauschen. Im Gegensatz dazu bestand die Einarbeitung der drei identifizierten Komponenten in HYMKE_DUAL in der Entwicklung einer Schneesschmelzroutine, einer Modifizierung der ursprünglichen HYMKE Oberflächenroutine, um das Verhalten des Bodens und des Epikarsts besser darzustellen, und einer Weiterentwicklung der Grundwasserroutine von HYMKE_modified. Dabei wurde eine Distribuierung der Schneeschmelz- und der Boden- und Epikarstroutine in 56 Höhenstreifen vorgenommen. Mit diesen Veränderungen lieferten beide Modelle gute Abflussvorhersagen obwohl sie sich in ihrer Struktur unterschieden, speziell in den Routinen welche der Grundwasserroutine vorgeschaltet waren. HYMKE_modified benutzt einen einschichtigen Boden/Epikarstspeicher, welcher einem Linearspeicher, der die vadose Zone repräsentieren soll, vorgeschaltet ist. In HYMKE_DUAL hingegen wird die Grundwasserneubildung durch einen dreischichtigen Boden- und Epikarstspeicher erzeugt. Ähnlich wie bei der ersten Version von HYMKE, wurden die Abflussberechnungen mit Mischungsrechungen gekoppelt, um die Wahl der richtigen Modellstruktur zu bestätigen. Durch die Kombination eines schnell reagierenden Karstkanalspeichers mit einem langsam reagierenden Kluftspeicher konnten die Eingangskonzentrationen zur Grundwasserroutine schnell zum Auslass übertragen werden, was bei beiden Modellen zu guten hydrochemischen Vorhersagen führte. Somit kann die Identifizierung des Kluftspeichers als wichtigstes fehlendes Glied in der ersten Version von HYMKE bestätigt werden. Betrachtet man die Grundwasserneubildungskonzentrationen beider Modelle, zeigt sich jedoch, dass nur die Boden- und Epikarstroutine von HYMKE_DUAL fähig war, Ereigniswasserkonzentrationen, d.h. Regen- und Schneeschmelzwasserkonzentrationen, bis zur Grundwasserroutine, und damit zum Teil auch bis zum Auslass, zu übertragen. Dass dieser Prozess wirklich stattfindet wurde durch die hydrochemische Analyse bewiesen. In HYMKE_modified konnten hingegen nur die saisonalen Variationen der beobachteten Konzentrationen dargestellt werden. Es war nicht fähig Ereigniswasserkonzentrationen bis zur Grundwasserroutine zu übertragen.

Insgesamt zeigten die guten Abfluss- und Konzentrationsvorhersagen von HYMKE_modified und HYMKE_DUAL dass beide Modelle die wichtigsten Prozesse und Speicher vom hydrologischen System des Mt. Hermon beinhalten, auch wenn sie durch verschiedenartige Routinen wiedergegeben werden. Die flächenkonzentrierte Struktur von HYMKE_modified benötigt nur eine geringe Zahl an Parametern, wo hingegen HYMKE_DUAL aufgrund des komplexen Aufbaus seiner Boden- und Epikarstroutine deutlich mehr Parameter benötigt. Zusätzlich erlaubt dieses Modell die räumliche Verteilung der verschiedenen Parameter, was

den Einsatz von räumlich verteilter Information erlaubt, womit auch räumlich verteilte Ergebnisse produziert werden können. Leider ist für den Mt. Hermon keine räumliche Information verfügbar, daher konnten nur einheitlich abgeschätzte Parameter für alle Höhenzonen angewandt werden. Somit führten diese potentiellen Vorteile von HYMKE_DUAL zu keiner signifikanten Verbesserung der Abfluss- und Konzentrationsvorhersagen.

Ehrenwörtliche Erklärung

Hiermit erkläre ich, dass die Arbeit selbstständig und nur unter der Verwendung der angegebenen Hilsfsmittel angefertigt wurde.

Freiburg im Breisgau, den 5. September 2008

_____

(Andreas Hartmann)

1 Introduction

1.1 General Introduction

"And when Caesar had further bestowed upon him another additional country, he built there also a temple of white marble, hard by the fountains of Jordan: the place is called Panium, where is a top of a mountain that is raised to an immense height, and at its side, beneath, or at its bottom, a dark cave opens itself; within which there is a horrible precipice, that descends abruptly to a vast depth; it contains a mighty quantity of water, which is immovable; and when any body lets down any thing to measure the depth of the earth beneath the water, no length of cord is sufficient to reach it. Now the fountains of Jordan rise at the roots of this cavity outwardly; and, as some think, this is the utmost origin of Jordan: but we shall speak of that matter more accurately in our following history."

This citation is taken from "History of the Jewish War" written by Flavius Josephus 70 AD and translated by WHISTON (1987). Such early mentioning of the Jordan River and its sources outlines its importance in the past. The Jordan River is small but well known because (1) it is a holy river where Jesus was baptized by John the Baptist, and (2) it is located in an area suffering from scarcity of water (JU'UB AND SCHETELING, 2004). The part of the Jordan River between its main sources and Lake Tiberias is called Upper Jordan River. In Israel nearly all available surface water is used for water supply and irrigation. This is also true for the inflows of the Upper Jordan River into Lake Tiberias: nearly all water flowing in the lake is pumped out again; it is conducted to the coastal plain from where it is distributed by the National Water Carrier from the north to the Negev south (HÖTZL, 2004). Using this distribution system Lake Tiberias water contributes about 30% of the Israeli water demand and about 55% of its drinking water (GOPHEN, 2004). In the first half of this century all of the countries in the Middle East were able to satisfy their water demands through access to indigenous water resources. Although the region has always experienced seasonal and often annual water shortages the inhabitants had been able to cope except in the most severe droughts (BEAUMONT ET AL., 1988). The main reason for this was that prior to the twentieth century local communities had only been using a fraction of the renewable water resources which are available. Nowadays most of the renewable water resources of the region have been

committed to human use. In dry years water sources are even over-exploited which causes in the case of Lake Tiberias that water table sometimes reaches critical levels also with regard to the rising of water salinity and salt water intrusions. This might be problematic since a sufficient availability of water was found to be the key for prosper economical development (HÖTZL, 2004). The date when a country fully utilizes its renewable water resources marks an critical landmark but does not represent the end of its economic development (BEAUMONT, 2000). In the case of the Jordan River however this landmark also reaches a political dimension since the Jordan River waters are used by five countries: Lebanon, Syria, Israel, Jordan and Palestine (JU'UB AND SCHETELING, 2004). The effect of rising water demands will be aggravated by the climate change. Climate scenarios predict a raise of 1.1 to 3.1 °C until the end of this century (IPCC, 2007). In Israel climate change will lead to a temperature decrease in winter and a temperature increase in summer thus seasonal temperature variability will increase (BEN-GAI, 1999). Additional the rainy season will shorten while rain intensities increase (PE'ER AND SAFRIEL, 2000). Annual amount of precipitation is predicted to decrease for Israel's neighboring countries but for Israel an increase is predicted (STEINBERGER AND GAZIT-YAARI, 1996 in ALPERT, 2004). The impact of these changes on groundwater resources is difficult to assess (SEILER AND GAT, 2007). Also the Upper Jordan River is fed by springs supplied from groundwater. Therefore impact of climate change on their hydrological system, in particular on their groundwater recharge mechanisms, has to be estimated in order to develop water protection and management strategies for the future conditions.

1.2 Objective

In order to transform future climate scenarios into hydrological scenarios hydrological models have to be applied on the output data of the climate simulation models. Such models require an adequate representation of hydrological processes to maintain their predictive ability under changing climatic conditions. So-called "black-box" models are not applicable for this task because they just transfer a certain input of rain into a certain output regardless of the real processes. Thus they are just valid at the most for the actual climatic conditions. In this diploma thesis the hydrological system of the source area of the Upper Jordan River, Mt. Hermon range, will be characterized using information on meteorology, hydrology and hydrochemistry with special focus on karst specific processes. The objective is the development of a process based hydrological model representing the groundwater system of Mt. Hermon in order to provide a hydrological tool to assess impact of climate change on the

Upper Jordan River and therfore on the major inflow into Lake Tiberias. This will be done by two different approaches which will be compared in a final discussion.

2 Study area

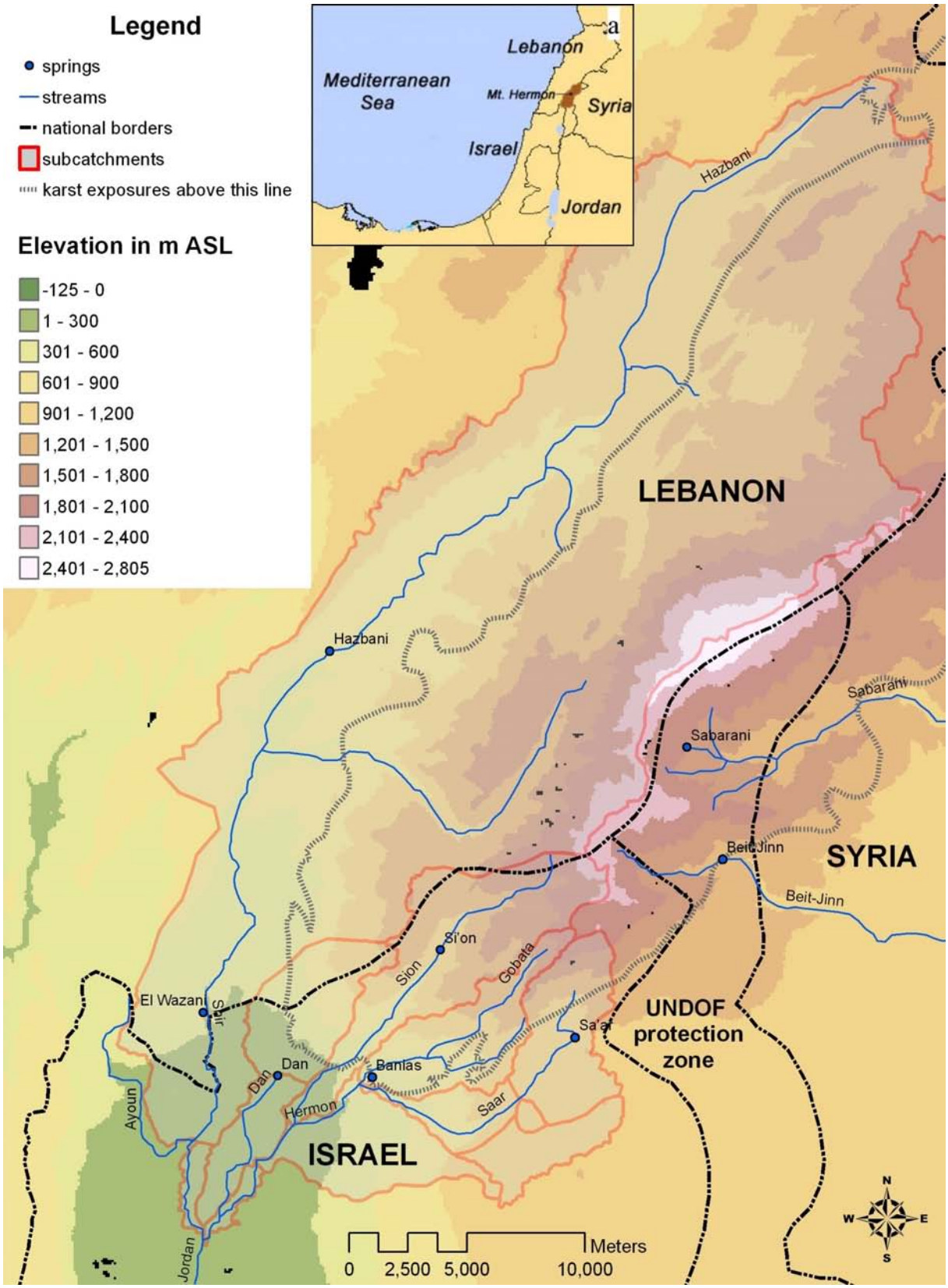

FIGURE 1: The study area: Mt. Hermon range and its position in the Middle East (RIMMER AND SALINGAR, 2006; modified)

The Mt. Hermon range is located in the Middle East at the borders of Israel, Syria and Lebanon. It contains the major sources of the Upper Jordan River, which are Hazbani Spring, Banias Spring and Dan Spring (FIGURE 1). Their discharge contributes to the main tributaries of the Upper Jordan River: The Dan, the Snir (also known as Hazbani) and the Hermon (also known as Banias), with a total catchment area of 783 km². The Upper Jordan River is the major inflow to Lake Tiberias (also known as Lake Kinneret). From there the Jordan River flows out south towards the Dead Sea. However the major part of the lake waters is consumed for drinking and agricultural water supplies (see chapter 1). In this paper, the focus will be on the hydrological and geochemical characteristics of the Dan and the Banias Springs.

2.1 Available data

The Yigal Allon Kinneret Limnological Laboratory provided data from several Israeli authorities listed in TABLE 1. Additional data of precipitation, snowmelt and various Mt. Hermon springs was provided from Heike Brielmann, sampled during her PhD thesis in 2008 (BRIELMANN, 2008). Her data helped significantly to understand the runoff generation of Dan and Banias Spring.

TABLE 1: Data provided by the Allon Yigal Kinneret Limnological Laboratory (IHS, Israeli Hydrological Service; IMS, Israeli Meteorological Service; IS, Israeli Survey; WA, Water Authority; Mekorot, National Water Supply Company)

Type of data	Years	Source	Time scale	Remarks
Streamflow from four gauging stations in the UCJR	1969-2004	IHS	Daily	
Rainfall from 74 rain stations in the north of Israel	19##-2002	IMS	Daily	## Various starting dates
Pan evaporation from three stations within the UCJR region	1969-2001	IMS	Daily	
Water consumption from all pumping stations (~170) in the UCJR	1974-2002	WA	Monthly	Dan consumption since 1969
Discharge of springs in the UCJR region	19##-2002	IHS	Monthly	## Various starting dates
Hydrochemical data of springs in the UCJR region	1972-2005	Mekorot	Weekly/Monthly	Dan hydrochemistry since 1969
Digital Terrain Model (DTM) data. Detailed topographic and land use maps	-	IS	-	

Furthermore, an own measurement campaign was performed at Dan Spring (see chapter 6). Therefore, devices to log pH value, oxygen content, temperature, water level and conductivity in a high time resolution were installed close to the Dan Spring outlet.

2.2 Climate

The higher regions of Mt. Hermon Range (> 1000 m ASL) receive the most precipitation in Israel (> 1300 mm/a) between October and April. Between December and March precipitation usually falls as snow and can persist in the higher regions (> 1400 m ASL) until March to June. Typical daily precipitation measurements in the Upper Jordan River region, at 240 m ASL, are shown in FIGURE 6 and FIGURE 7 (Ma'ayan Barukh meteorological station, hydrological years 1973/74 - 1982/83 and 1990/91 - 1999/2000).

Mean annual temperatures of the Upper Jordan River catchments lie between 13 and 18 °C (KLAER, 1962). Temperature changes with season and altitude. Previous studies indicate a temperature gradient of about -0.5 to -0.6 °C per 100 m (BRIELMANN, 2008 according to KESSLER, 1980). The coldest month of the year is January with average temperatures of 5 to 10 °C in the valleys and 0 to 5 °C in the mountainous regions. The warmest month is August with average temperatures of 20 to 25 °C in the valley and 10 to 15 °C in the mountainous regions (TAHA ET AL., 1981).

In general, seasons in Mt. Hermon can be defined referring to synoptic systems that dominate the Eastern Mediterranean (ALPERT ET AL., 2004a, 2004b):

- Autumn (mid of September to beginning of December): Red Sea trough, which is characterized by south/south-easterly winds, low humidity, and medium to high temperatures.

- Winter (beginning of December to end of March): Cyprus low, which is associated with low temperature, strong winds, and high-intensity precipitation.

- Spring (end of March to end of May): Sharav low, which brings hot and dusty winds, low humidity and medium to high temperatures.

- Summer (end of May to mid of September): Persian trough, which is accompanied by high temperatures and high humidity, and by north/north-easterly winds.

Data about evaporation is only available as mean potential evaporation based on long term daily pan A measurements (1970 to 2000) which give a mean annual value of 1900 mm (RIMMER AND SALINGAR, 2006). There are too few stations in Mt. Hermon to obtain information about the spatial variation of actual evaporation which is assumed to vary with altitude, soil and vegetation cover. Recently, new meteorological stations have been installed by the Kinneret Limnological Laboratory but their data series are too short to be used for characterization.

2.3 Geology and Geomorphology

The Mt. Hermon is an elongated anticline which is mostly composed of Jurassic limestone with a thickness of more than 2000 m trending from north-north-east to south-south-west. Its area is about 55 km * 25 km and its summit is at an altitude of 2814 m ASL. Mt. Hermon and its northern extension, the Anti-Lebanon Mountains, are part of the Syrian Arc fold system, which is a semi-continuous belt extending from western Egypt through the North Sinai, the Negev Desert and the adjacent offshore waters of the south-eastern Mediterranean to Syria in the east (BRIELMANN, 2008). Additional to the anticline, Mt. Hermon is exalted as a Horst towards its western valleys (WOLFART, 1967).

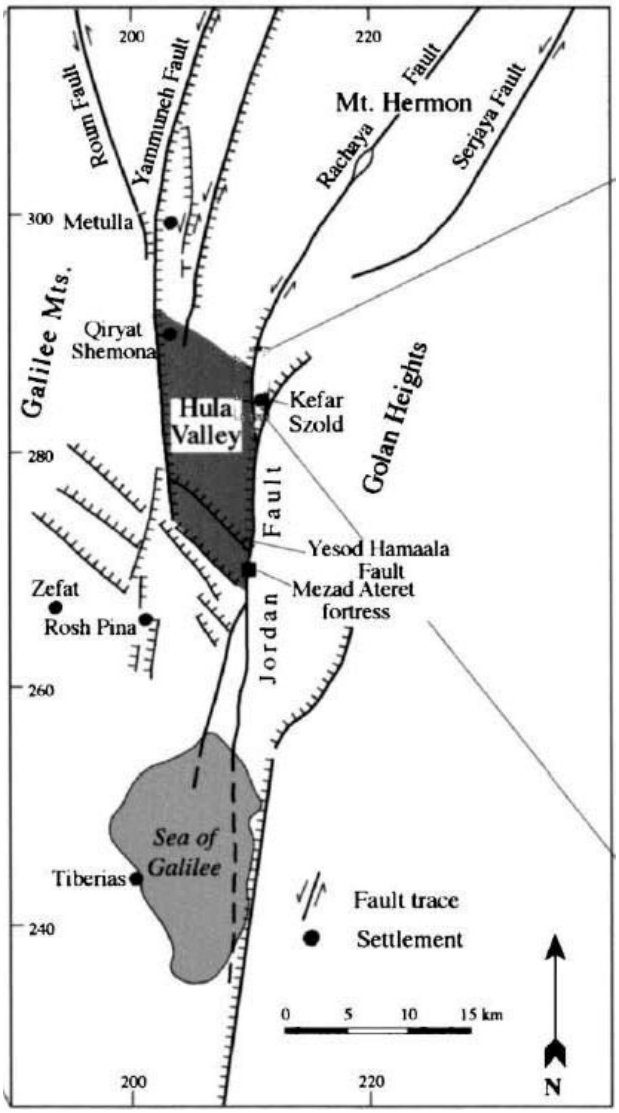

FIGURE 2: Map of the main faults in the northern Jordan Rift Valley (BRIELMANN, 2008, AFTER HEIMANN, 1990 and ZILBERMAN, 2000).

The Sion-Rachaya fault (FIGURE 2) parallels the Hermon anticline. It separates the Mt. Hermon range into two main blocks: On the western side, the Sion shoulder (Har Dov/Arkub Ridge in FIGURE 3), and on the central and eastern side Mt. Hermon range, which includes the Sion and Hermon Ridges (FIGURE 3). According to SHIMRON (1989), the eastern block, which consists of limestone partially overlain by marls and shales, is known for its abundance of basaltic rocks, dolomitization, and mineralization. In contrast to the eastern block, none of this is found in the western side of Mt. Hermon range, where limestones and sandstones are dominating (BRIELMANN, 2008). The thickness of exposed limestones was estimated by GOLDBERG ET AL. (1981) to be about 2700 m.

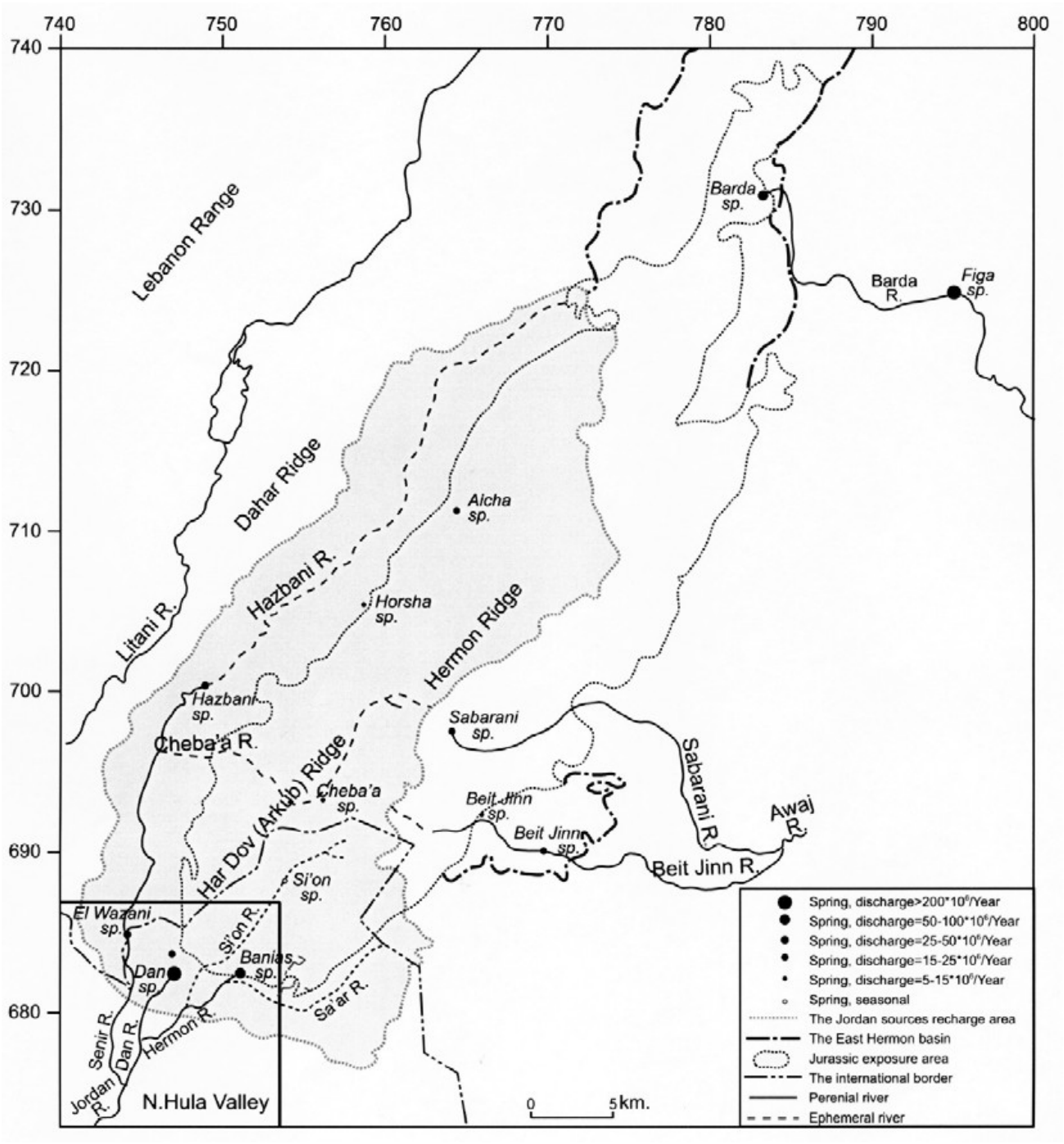

FIGURE 3: The topography of the Mount Hermon region and its hydrological network (GUR ET AL., 2003, adapted from GILAD AND SCHWARTZ, 1978)

2.3.1 Banias Spring

Banias Spring is the spring contributing most of the discharge to the Hermon stream. It is located at an altitude of 360 m ASL in the northern-east of Dan Spring (FIGURE 1) along a vertical interface between the Mt. Hermon carbonates and low-permeable quaternary sediments (FIGURE 4). In their study GUR ET AL. (2003) stated that Banias Spring is governed by two different discharge components, which are conduit and diffusive flow. This hypothesis will be picked up in the following chapters.

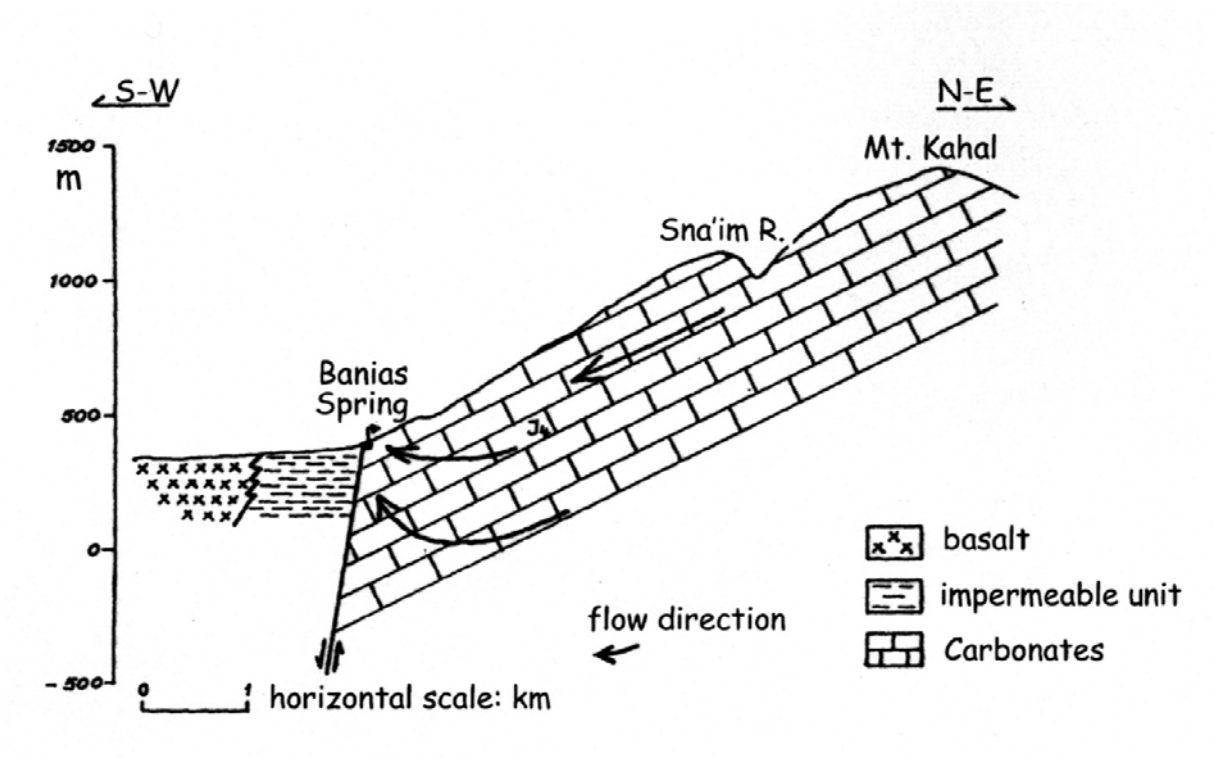

FIGURE 4: Geological cross section of Banias Spring (GUR ET AL., 2003, adapted fromb GILAD AND SCHWARTZ, 1978)

2.3.2 Dan Spring

Dan Spring is located at the top of a Horst structure at an altitude of 200 m ASL (FIGURE 5). It is developed along an underground fault line which allows waters to pass overlying sandstones and marls. They perform as an aquiclude which overly the limestone at altitudes below the karstic exposures (FIGURE 1). GUR ET AL. (2003) conclude that Dan Spring is fed by a relatively shallow and well-washed karstic system, which is recharged over the flanks of Mt. Hermon (BRIELMANN, 2008).

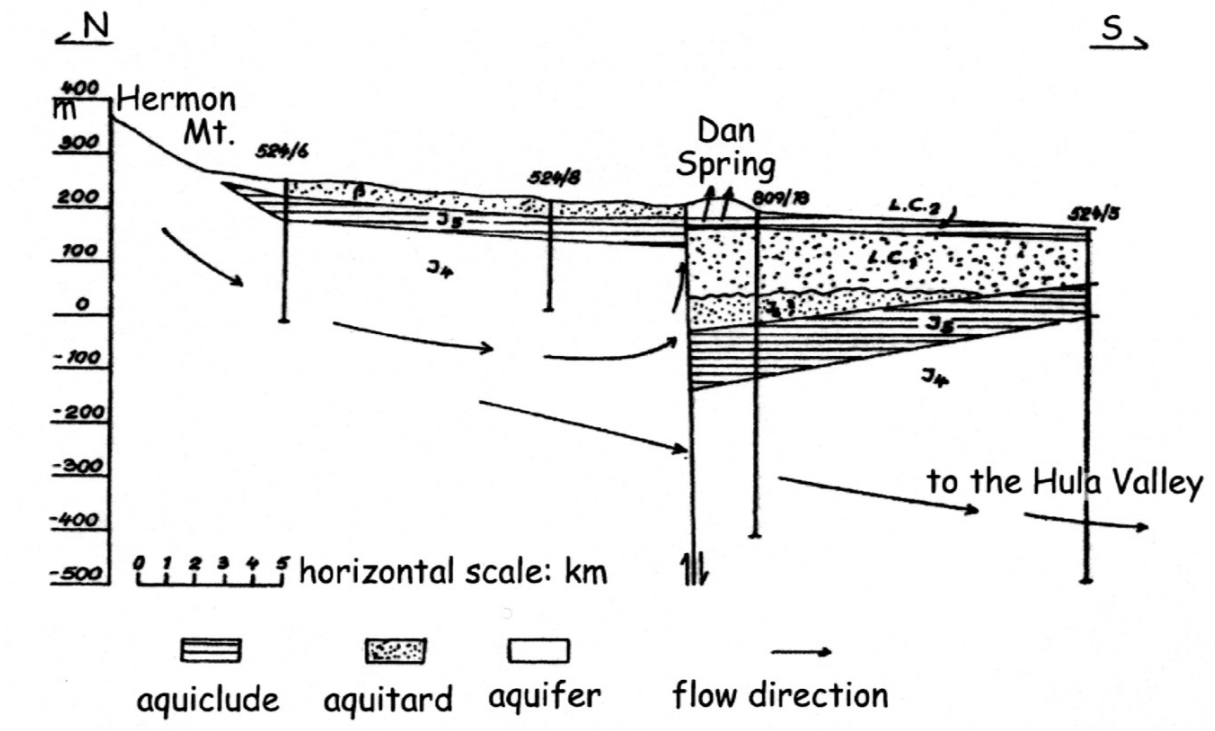

FIGURE 5: Geological cross section of Dan Spring (GUR ET AL., 2003, adapted from GILAD AND SCHWARTZ, 1978)

2.4 Soils

In general, soils in Mt. Hermon range are thin and even decrease in thickness with increasing altitude and slope (BRIELMANN, 2008). Excess of rain over evapo-transpiration during the winter leads to dissolution of the carbonate rocks and it enhances hydrolytic weathering of silicate minerals. Additionally, aeolian dust can play a significant role on soil formation as recognized by YAALON AND GANOR (1973), MACLEOD (1980) and NIHLEN AND OLSSON (1995). An aeolian dust contribution to soil development of up to 50% was claimed by YAALON (1997). And GANOR AND MAMANE (1982) assessed that the annual dust deposition in Israel is 20 to 40 t/km². Dust deposition can have various different influences on soil horizon differentiation, physical and hydraulic soil properties, and levels of fertility (SIMONSON, 1995).

The weathering of the calcareous limestone of Mt. Hermon range led to the development of soil types like Terra Rossa, which is the most prevailing soil type, Brown Rendzina and Pale Rendzina (BRIELMANN (2008) according to DAN ET AL. (1983)). Since carbonates and sulfides are easily washed out, only silicates and oxides remain in the soil and can contribute to soil

formation. Factors which influence the soil development are the pedoclimate, biotic activity, organic matter content, pH value, redox and soil water conditions. If dry and warm pedoclimates prevail, formation of hematite can occur. This causes the characteristic red colour of Terra Rossa soils. However, in higher regions and if wet soil conditions prevail, Brown Rendzina soils can be found. They gain their yellow brown colour by the Goethite that develops under such conditions on gentil slopes, in top soils or on soft limestones with low iron contents (BRIELMANN (2008) according to CORNELL AND SCHWERTMANN (1996) and SINGER ET AL. (1998)).

2.5 Vegetation and Land Use

In the lower regions (< 1300 m) of Mt. Hermon, mediterranean wood- and shrub lands dominate. Above 1300 m ASL, oro-mediterranean mountainous vegetation is dominating. Altogether, there are more than 900 different plant species which are adapted to their particular topography and its resulting microclimate. So called “cushion- plants” can be found on west facing, wind exposed, often desiccated slopes. These plants are spiny, rounded, dense and small shrubs like *Astragalus cruentiflorus, Onobrychis cornuta, Acantholimon libanoticum, Acantholimon echinus and Astragalus echinus*, which once again create environments for geophytes, annuals and other plants with soft stems. After snowmelt, temporally wet areas can accommodate *Romulea nivalis* and *Ranunculus demissu.* And the waterlogged soils of dolinas can be covered with *Polygonum cedrorum* (BRIELMANN, 2008, according to DANIN, 2004).

Land use in Mt. Hermon range did not undergo significant changes the last three decades because of the sensitivity of its water resources and the desire to keep the status quo (RIMMER AND SALINGAR, 2006). Just some orchards and olive groves can be found in the lower Hermon managed by the resident Druze population (BRIELMANN, 2008).

2.6 Hydrology

The three tributaries of the Upper Jordan River, which originate in Mt. Hermon range (Snir, Dan and Hermon) show the behaviour of a pluvio-nival discharge regime. This means that discharge of these streams is mainly due to precipitation, but also influenced by snowmelt. The major part of precipitation reaches the streams as discharge of springs that are situated at the interfaces of the main faults and the impermeable alluvia of the valleys (GUR ET AL., 2003). A general classification of the tributaries and the Upper Jordan River is given in TABLE

2 by BRIELMANN (2008). Dan discharge values had to be corrected, because some amount of spring water was already pumped out upstream of the gauging station. This was done by RIMMER AND SALINGAR (2006) using the water consumption data provided by the Water Authority (TABLE 1). Specific discharges refer to the respective surface drainage area, which is nearly zero in the case of Dan spring. This shows that specific discharges calculated with the superficial catchment area could lead to a wrong impression of specific discharge patterns. For karstic systems reliable values of specific discharge can only be calculated knowing the subsurface catchment area which unfortunately is unknown for Mt. Hermon range.

TABLE 2: General classification of the main Jordan tributaries in the Mt. Hermon range; AMaF: absolute maximum flow, MHF: mean annual high flow, MF: mean annual flow, MLF: mean annual low flow and AMiF: absolute minimum flow (BRIELMANN, 2008)

	Dan	Hermon	Snir	Jordan
period	1969-2000	1969-2000	1969-2000	1991-2000
station (HSI)	30131	30128	30122	30175
AMaF [1000 m³/d]	1071.36	3335.04	9244.8	10895.04
	08.02.1993	02.06.1992	12.02.1994	02.06.1992
MHF [1000 m³/d]	734.4	475.2	691.2	1900.8
MF [1000 m³/d]	691.2	285.12	293.76	1175.04
MLF [1000 m³/d]	665.28	216	181.44	889.92
AMiF[1000 m³/d]	276.48	60.48	43.2	241.92
	12/19/1990	09.06.1999	12/13/1999	6/16/1999
volume [Mio. m³]	254	105	108	430
surface drainage area [km²]	0	158	563	1380
yield [l/s/km²]		21.1	6.1	9.9
runoff [mm/d]		1.8	0.5	0.9

2.6.1 Banias Spring

As mentioned above Banias Spring is the major source of the Hermon stream, which has a. catchment area of 158 km² with 74 km² of karst exposures (RIMMER AND SALINGAR, 2006). It contributes about 67 * 10^6 m³ of annual discharge. Unfortunately, the hydrograph of the Banias spring is limited to monthly measured data. However, a long continuous hydrograph time series is available for the Hermon stream. By comparing Banias Spring and Hermon stream discharge it was concluded, that the daily Banias Spring discharge may be estimated fairly well by the Hermon stream flow. This estimation was performed by multiplying the Hermon stream flow by the ratio of Banias Spring to Hermon stream accumulated flow from 1973 to 1983 (and yielded a rescaling factor of 0.64; calculations performed by the author of this thesis). Therefore in the following analysis, the rescaled Hermon stream flow (FIGURE 6

and FIGURE 7) was regarded as Banias Spring hydrograph, while hydrochemical data derived directly from Banias Spring outlet. The hydrological years from 1973/1974 to 1982/1983 and 1990/1991 to 1999/2000 were selected because further investigations were performed in these two time periods.

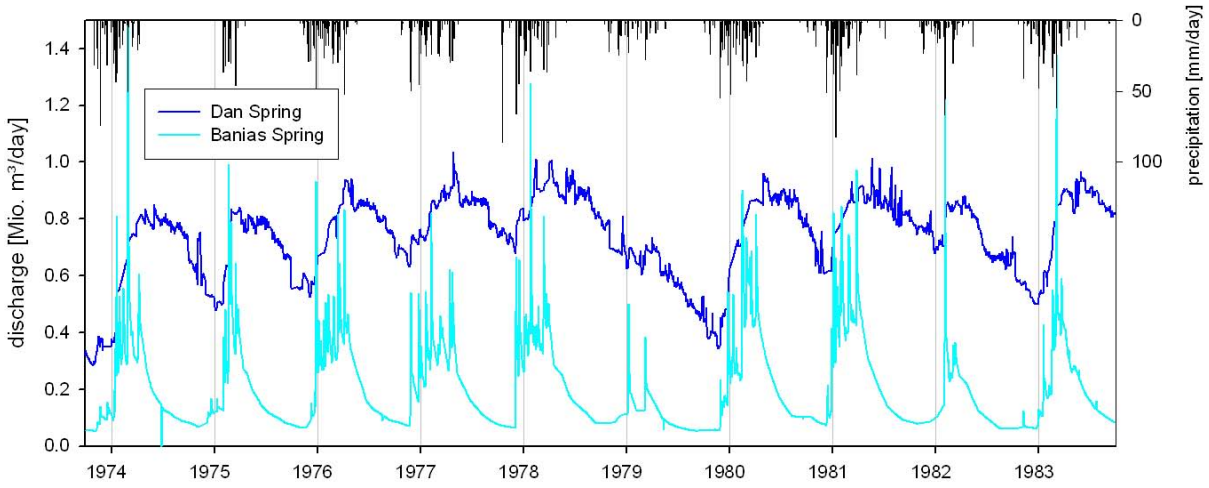

FIGURE 6: Precipitation at Ma'ayan Barukh station and discharge of Banias and Dan Spring from 1973/1974 to 1982/ 1983

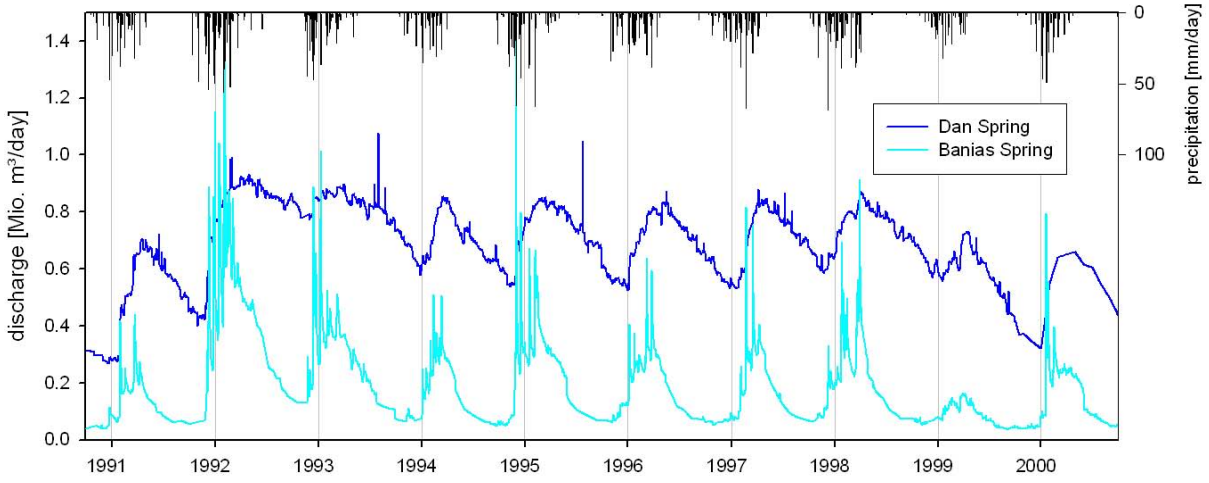

FIGURE 7: Precipitation at Ma'ayan Barukh station and discharge of Banias and Dan Spring from 1990/1991 to 1999/2000

2.6.2 Dan Spring

With its annual discharge of 254 * 10^6 m³ it represents the biggest spring in the region. Its superficial catchment area is just 24 km² with 15 km² of karst exposures, but its huge annual

discharge suggests that its subsurface is much larger. In the period from 1969 to 2004 a daily mean discharge of 691 * 10^3 m^3 was measured, respectively. The mean annual minimum and maximum are 277 * 10^3 and 734 * 10^3 m^3/d respectively (TABLE 2). Daily discharges from 1973 to 1983 and from 1990 to 2000 are given in FIGURE 6 and FIGURE 7.

2.7 Hydrochemistry

According to BRIELMANN (2008) Mt. Hermon springs are fresh water springs of the Ca-Mg-HCO_3 type with low salinities. Nearly no change in land use occurred the last decades (RIMMER AND SALINGAR, 2006) so low NO_3 concentrations (< 10 mg/l) can be regarded as non anthropogenic (KAFRI ET AL., 2002). Differences in the hydrochemistry between the Mt. Hermon springs can be explained by changes in lithology, residence time of water and distance from sea. This can be observed by comparing Dan and Banias Spring waters: Banias Spring water is characterized by higher contents of SO_4, Cl, Li, Rb, Sr and V as well as higher equivalent SO_4/Cl and Na/Cl ratios (BRIELMANN, 2008). Reason for this difference is the abundance off basaltic volcanism, dolomitization and mineralization within the Banias Spring intake area (BRIELMANN, 2008, according to SHIMRON, 1989, and KAFRI ET AL., 2002). Using ^{18}O measurements, SIMPSON AND CARMI (1983) distinguished different catchments for the main Jordan springs and came to the conclusions that interflow occurs in the near-surface part of the regional groundwater reservoir (BRIELMANN, 2008). They also conducted a tritium analysis which let them suggest that the majority of groundwater is less than 3 years old. Long term data of electric conductivity, temperature, pH value, turbidity and major ions from 1990 to 2000 can be found in the Appendix A.1: Long term data of hydrochemical variables for Banias and Dan Spring.

An estimation of the chemical composition of rain is given by BRIELMANN (2008), who analysed 92 samples of rain and snow in this area. TABLE 3 shows the results for two rain stations (Tel Dan and Banias, located close to the equally named spring) and snow at various locations on Mt. Hermon. This analysis showed the following ion sequences at the south-eastern foot slopes and higher altitudes of Mt. Hermon (BRIELMANN, 2008):

$$[Ca_2^+]>[Na^+]>[Mg_2^+]>[K^+] \text{ and } [HCO_3^-]>[Cl^-]>[SO_4^{2-}].$$

This sequence is similar to the results performed by NATIV AND MAZOR (1987) for the Maktesh Ramon basin (Negev). BRIELMANN (2008) infers that for precipitation in Israel two

distinct sources of ions can be distinguished: First, Ca and HCO_3, which can be attributed to dust derived from chalk and limestone (according to GANOR AND MAMANE, 1982; NATIV AND MAZOR, 1987). Second, Na, Mg, Cl and SO_4, which can be assumed to derive from cloud-borne sea spray.

TABLE 3: Composition of Mt. Hermon rain/snow samples; nd: not detected (BRIELMANN, 2008)

Location		n	Na+	K+	Ca2+	Mg2+	SO42-	Cl-	NO3	HCO3-	EC
			mg/l	mg/l	mg/l	mg/l	mg/l	mg/l	mg/l	mg/l	µS/cm
Banias	Median	27	1.8	0.3	6.3	0.5	2.6	3.6	1.2	-	-
	Mean		3.3	0.6	8.6	0.7	3.4	4.5	2.2	-	-
Tel Dan	Median	23	1.9	0.2	3.1	0.5	2.3	2.8	1.2	-	-
	Mean		3.7	0.4	4.5	0.6	3	4.3	1.6	-	-
Snow Mt. Hermon	Median	42	0.7	0.1	0.7	0.4	0.9	1.3	1.4	21.4	15
	Mean		1.3	0.2	1.4	0.7	0.9	2.6	1.3	25.6	20

2.8 Conclusions

The big amount of available data particularly for Banias and Dan Spring yields the base for this diploma thesis. Although its resolution is partly very rough it is good enough to reflect the seasonal behaviour of the springs. Unfortunately there is just general information about the inside properties of the Mt. Hermon system. There is no spatial data about precipitation, evaporation, geology, soil types, soil thickness, vegetation, land use, etc. Hence the general knowledge about the system and the big amount of system input and output data knowledge have to suffice for the system characterization and the further develeopments. In order to adequately understand Mt. Hermon hydrological system the special features of karst hydrology have to be reviewed.

3 Karst hydrology

3.1 Principles of karst hydrology

In a classical hydrological system, flow can be divided into surface flow and subsurface flow. Surface flow reaches the outlet of the system faster than the subsurface flow (FETTER, 1994). This is explained by the different paths and the different conductivities of the media passed by the subsurface flow. There are many different concepts which describe first the subdivision of effective precipitation into surface and subsurface flow and second the different kinds of subsurface flow (BEVEN, 2001). The dominance of different kinds of flow depends on various factors such as the local climate, soil structure, vegetation, geology, slope, shape of the catchment and morphology. Thus in a karstic system, which represents a special type of morphology, an adapted concept has to be developed.

A typical karstic system can be found in the Karst Mountains in former Yugoslavia where actually the name “karstic” originates from. In such a system calcareous rock, which is limestone and dolomite, is dissolved:

$$CO_2 + H_2O \leftrightarrow H_2CO_3 \tag{1}$$

$$H_2CO_3 \leftrightarrow HCO_3^- + H^+ \tag{2}$$

$$CaCO_3 \leftrightarrow Ca^{2+} + CO_3^{2-} \tag{3}$$

$$CO_3^{2-} + H^+ \leftrightarrow HCO_3^- \tag{4}$$

$CaCO_3$ represents the limestone ($CaMg(CO_3)_2$ would represent dolomite) and H_2O the water. CO_2 can be of atmospheric origin and of biogenic origin produced by respiration of plant roots and bacterial decomposition of buried plant remains. Products of these reactions are calcium and bicarbonate. The solubility product of corresponding to equation (3) is quite small. However because the carbonate ion CO_3^{2-} is “removed” by protonation (equation (4)) dissolution of carbonate minerals can proceed to a significant extent. This is depending on the quantity of carbonic acid that is available and delivers protons (equation (2)). The whole reaction can be summarized by:

$$CaCO_3 + H_2O + CO_2 \leftrightarrow Ca^{2+} + 2HCO_3^{2-} \tag{5}$$

This dissolution can be observed on the surface in many different ways: dissolution fissures, cavities, caves and sinkholes can be found. As a consequence of dissolution part of subsurface flow in karstic systems occurs in open conduits (MAZOR, 2004). Thus in a karstic system there can be two types of porosity: first the primary porosity which develops directly with genesis of the carbonate rock and a secondary porosity which develops later on. Primary porosity includes all kinds of small voids between crystals, grains and fossil fragments (intercrystalline, intergranular or interstitial porosity); whereas secondary porosity comprises all types of fractures and conduits. In karst hydrology intergranular pores and small fissures are often generally termed as matrix porosity, in contrast to the conduit porosity (GOLDSCHEIDER AND DREW, 2007).

PERRIN (2003) divides a karstic system in four sub-systems: the first is the infiltration sub-system where recharge can be either via high permeability channels and voids (concentrated) or via low permeability areas (diffuse). The flow of this subsystem enters the second sub-system, which is the soil and epikarst, which will be introduced later in this section. There parts of the water can be stored for some time and lateral flow can take place. The outflow from this sub-system enters the third sub-system, the unsaturated zone, which is usually named the vadose zone. The flow in this sub-system is mainly vertical and can happen through conduits or fissures (concentrated and diffuse). The vadose zone connects the soil and epikarst with the fourth sub-system, the phreatic zone. When water reaches the phreatic zone it is either stored in the high permeability conduits or the low permeability fissures. From there it flows fast (through the conduits) or slowly (leaving the fissures) to the karstic spring (FIGURE 8, following DOERFLINGER, 1999). If there is no soil, the surface flow can be neglected and the outflow behaviour is controlled by the fast draining of the conduits and the slow draining of the fissures (JEANNIN AND GRASSO, 1997).

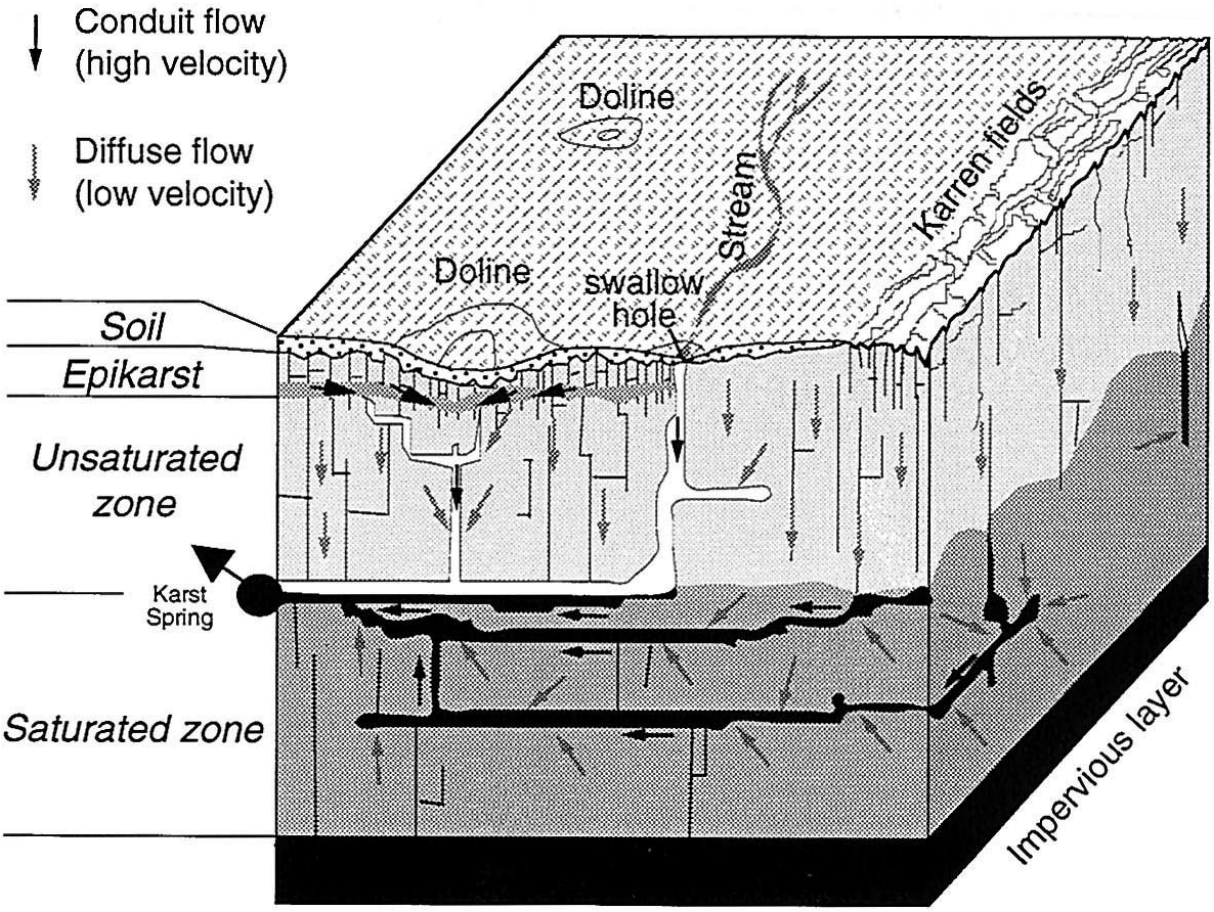

FIGURE 8: Conceptual model of a karst aquifer (DOERFLINGER, 1999)

KIRALY (1998) schematises karst aquifers by a high permeability, generally unknown channel network, which is immersed in a low permeability fractured limestone volume and which is well connected to a local discharge area. A so developing duality is a direct consequence of this structure (KIRALY, 1998):

- Duality of the infiltration processes: diffuse or slow infiltration into the low permeability volumes, concentrated or rapid infiltration into the channel network.

- Duality of subsurface flow field: Low flow in the fractures, fast flow in the conduits

- Duality of discharge conditions: Diffuse seepage from the low permeability parts, concentrated discharge from the conduits at the karst springs.

Besides this duality of karst processes, KIRALY (1998, according to MANGIN, 1975) acknowledges that additional to rivers disappearing in swallowholes the concentrated infiltrations could be enhanced by the rapid drainage in a high conductivity “skin” at shallow

depth: the epikarst. It develops as a consequence of a higher dissolution activity nearby the surface. According to FORD AND WILLIAMS (2007) in WILLIAMS (2008) about 70% of solutional denudation in a karst catchment is usually accomplished within the top 10 m of the limestone outcrop and the effectiveness of corrosional attack gradually diminishes with distance from the surface CO_2 supply (FIGURE 9). The epikarst is regarded to act as important temporary storage and distribution system for infiltrating water into the karst system (GOLDSCHNEIDER AND DREW, 2007).

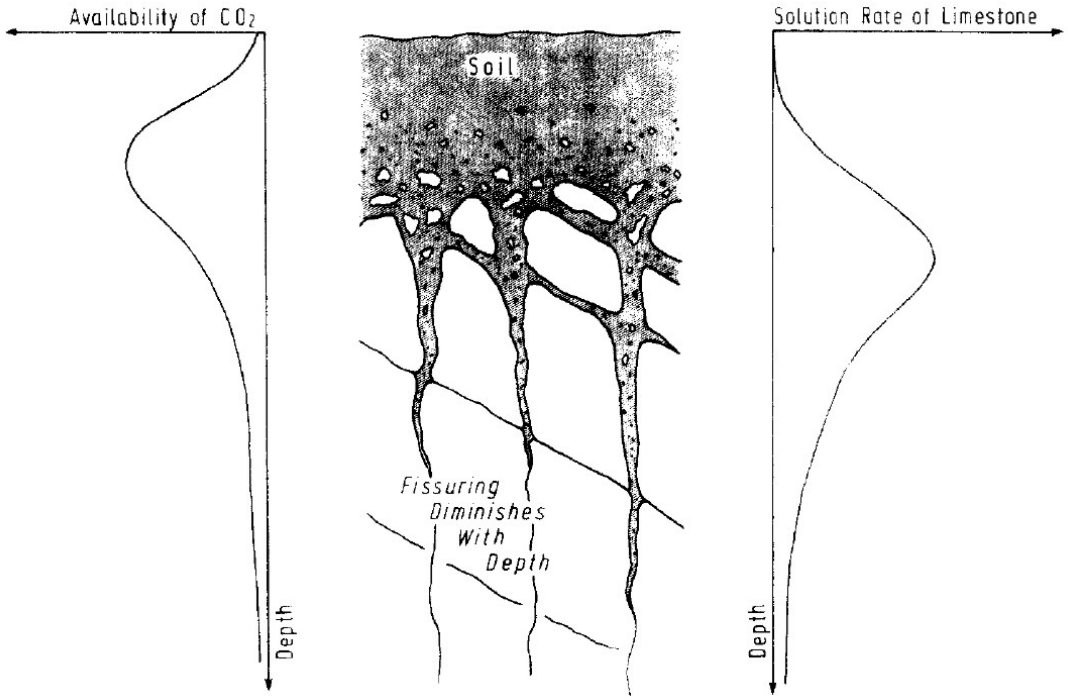

FIGURE 9: Schematic relationship between soil CO_2, rate of limestone solution, and fissuring beneath the soil (WILLIAMS, 1983)

.

According to WILLIAMS (1983, FIGURE 10) both slow percolation into tight fissures and rapid percolation via enlarged joints can occur. Since the maximum percolation rate to the fissures is smaller than the infiltration capacity into the upper epikarst water can be ponded back above the lower epikarst and then flows laterally to enlarged joints with higher conductivity. This leads to a more dynamic behaviour of flow through the enlarged joints and a more continuous flow to the fissures. Thus the duality of karst processes as mentioned above can also be attributed to the epikarst.

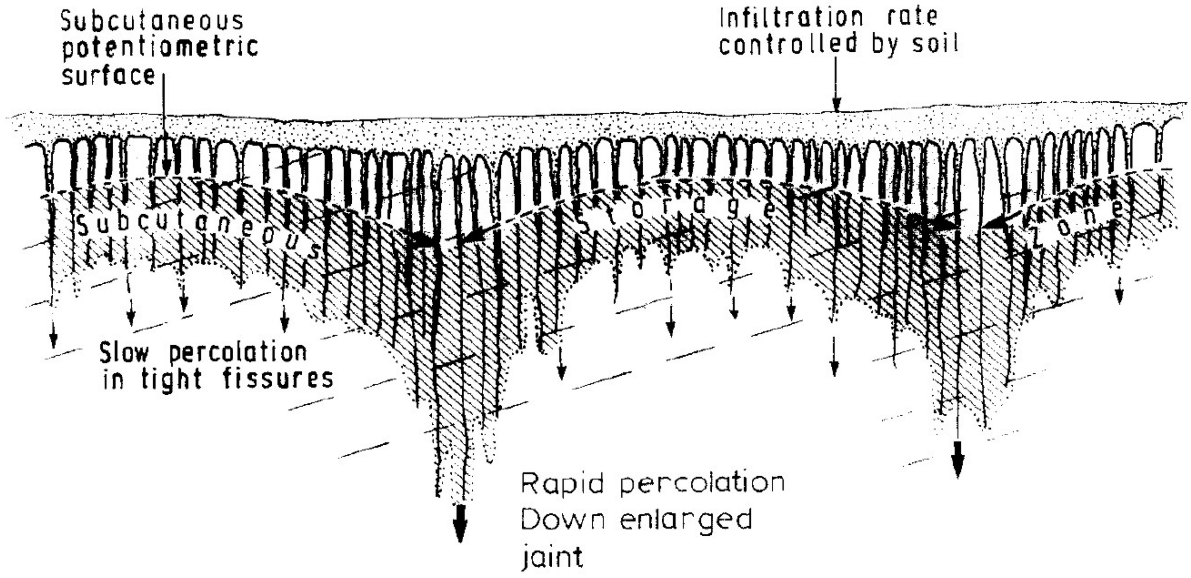

FIGURE 10: Schematic picture of the epikarst (WILLIAMS, 1983)

In the phreatic zone subsystem the duality of the subsurface flow field of a karstic system is the reason for a duality of storages that leads to exchange of water under different conditions. As shown by MALOSZEWSKI ET AL. (2002) the matrix storage contains thereby the largest amount of water but strongest dynamics can be found in the conduit system. If we attribute low flow in the fractures to the matrix storage and fast flow in the conduits to the conduit storage the exchange between them can be described as follows: when there is no recharge, the matrix storage drains to the conduits which discharge at the spring outlet. But if recharge is taking place the hydraulic head in the conduits rises above the hydraulic head in the matrix storage and water flows from the conduits to the fissures (SEILER, 1989, FIGURE 11). This process is a direct consequence of the different porosities of fissures and conduits, the double porosity.

A summarizing description of all these dualities and the epikarst has already been shown by DOERFLINGER (1999) in FIGURE 8. In the following chapters various concepts to incorporate that dual behaviour of karst systems into mathematical and numerical models will be introduced.

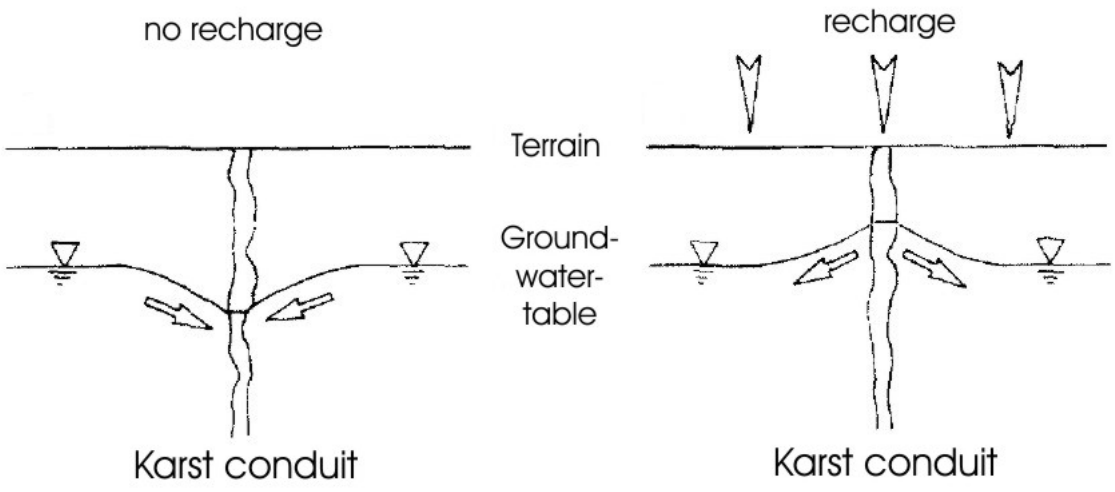

FIGURE 11: Interacting between water strored in fissures and water in the conduits of a karstich system (SEILER, 1989; MODIFIED)

3.2 Modelling of karst systems

To reproduce the hydraulic behaviour of a karstic system numerical models have to be applied in order to reconstruct a groundwater flow field (KIRÁLY, 2002). Therefore the karstic system hydraulic conductivity field and its boundary conditions have to be known. Due to the large heterogeneities abundant in karstic systems this is not always possible or certain methodologies have to be applied to consider the special features influencing a karstic groundwater flow field (PALMER ET AL., 1999).

More than in other hydrological systems simplifying assumptions have to be made to construct a conceptual model and to apply numerical methods. The uncertainties related to them are thus transformed to the model output data.

After GOLDSCHNEIDER AND DREW (2007) a sound conceptual model of a karst system incorporates heterogeneity and accordingly the duality of hydraulic flow processes which has already been mentioned in the chapters above. According to this most conceptual models include a soil zone and epikarst, an unsaturated or vadose zone, and a phreatic zone.

GOLDSCHNEIDER AND DREW (2007) mark the conceptual model proposed by KIRÁLY (1975, 2002) and KIRÁLY ET AL. (1995) which involves the epikarst and a hierarchical organisation of the conduit networks (see FIGURE 8 for a schematic representation). It also considers the carbonate aquifer as consisting of interactive units of a high permeability karst channel network with a low permeability fissured rock matrix. Since it was tested quantitatively and it was verified by numerical models (KIRÁLY AND MOREL 1976a, 1976b; KIRÁLY ET AL., 1995) it can be regarded as an acceptable conceptualisation. (GOLDSCHNEIDER AND DREW, 2007)

There are two fundamentally different approaches for studying and characterising karst hydrogeological systems (GOLDSCHEIDER AND DREW, 2007): global models, which are lumped parameter models, and distributive models.

3.2.1 Global models

Global models can be considered as transducers of an input to an output. They imply the analysis of input and output series to obtain a transformation or system function which sometimes may be used for the estimation of hydraulic parameters and conduit spacing which then again can be used in the distributive models. Since they just consider recharge and discharge global models cope with integrated information on the hydraulic behaviour of the entire system. GOLDSCHEIDER AND DREW (2007) divide them in two sub-types: single event models and time series analysis.

Time series analyses investigate the hydrological response of karst systems to rainfall events. They are based solely on mathematical analysis and thus do not provide information on the physical functioning of the karstic system. They were principally developed by JENKINS AND WATTS (1968) and first applied in karst hydrology by MANGIN (1971, 1975, 1981 and 1984). They find their application in prediction and data compilation purposes. GOLDSCHEIDER AND DREW (2007) distinguish between univariate and bivariate time series analysis. The former just uses discharge time series whereas the latter uses both rainfall and discharge time series. A univariate method is for instance the auto-correlation method which was successfully applied in karstic systems by MANGIN (1982), GRASSO AND JEANNIN (1994) and EISENLOHR (1997). Another univariate method is the spectral analysis which in turn has been successfully applied in karstic systems by BOX AND JENKINS (1976) and MANGIN (1984). Bivariate methods are the cross-spectral analysis and the cross-correlation method (applied successfully in karstic systems by JENKINS AND WATTS, 1968, BOX AND JENKINS, 1976, MANGIN, 1981, 1982, 1984, PADILLA AND PULIDO-BOSCH, 1995, LAROCQUE ET AL., 1998, GRASSO, 1998, and GRASSO AND JEANNIN, 1998).

Single event models try to synthesise the integrated recharge, storage and transmission mechanism which is mostly done by determining integral parameters

of karst properties in a qualitative but not quantitative sense. Mostly they are more or less sophisticated cascades of reservoirs. Sometimes they involve physical phenomena and semi-quantitative relationships between the pattern of the global hydraulic response and hydraulic parameters as well as some geometric properties of an aquifer. In this case they can be regarded as "grey box models" rather than "black-box models". The most common single event model is provided by MAILLET (1905). It is used for the analysis of the base flow recession after a storm event over a karst terrain. It describes the volume dependent outflow of a reservoir:

$$Q(t) = Q_0 e^{-\alpha t} \tag{6}$$

Where *Q(t)* is the discharge at time *t*, Q_0 is the initial discharge, and α is the recession coefficient, usually expressed in [1/day].

According to KOVÁCS (2003) and KOVÁCS ET AL. (2005) the baseflow recession coefficient can be used to derive important information about aquifer hydraulic parameters and conduit network characteristics. Flow types are divided in matrix-restrained flow regime and conduit influenced flow regime. For each flow type a relationship between hydraulic system parameters and recession coefficient is provided. Thus using the single event model approaches of MAILLET (1905), KOVÀCS (2003) and KOVÁCS ET AL. (2005) input parameters for distributed models can be derived.

By using more than one reservoir and thus more then one recession coefficient it is possible to associate different components of discharge to different origins. This was done by MANGIN (1975) who used two recession coefficients; one representing the unsaturated zone and another one representing the saturated zone (GOLDSCHEIDER AND DREW, 2007). Similarly GEYER ET AL. (2008) attributed the fissured matrix storage and the conduit storage to a low permeability reservoir and a highly permeable reservoir (FIGURE 12). Recharge enters both storages whereby water from the highly permeable reservoir directly leaves the system and water from the low permeability reservoir drains into the highly permeable reservoir before it leaves the system. This is just partly consistent with the

conceptualisation proposed above since there is no option for exchange between the reservoirs in both directions.

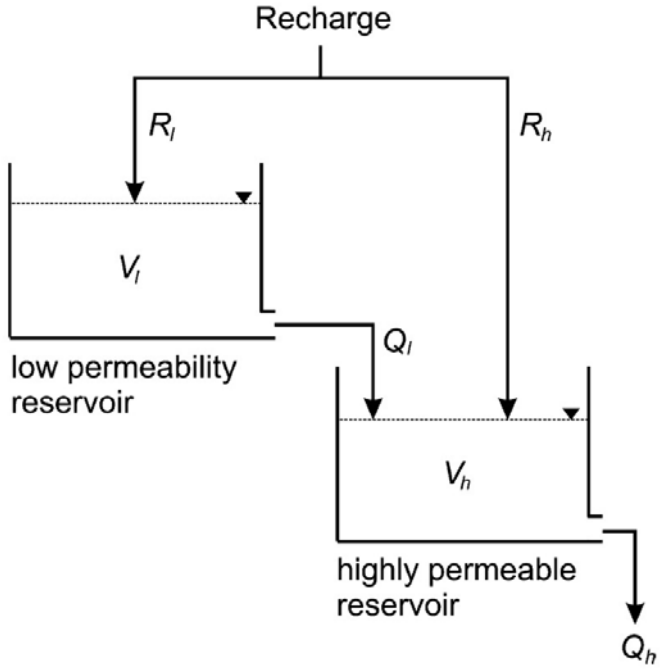

FIGURE 12: A two-reservoir model as proposed by GEYER ET AL. (2008)

3.2.2 Distributive models

Distributive models discretise a hydrogeological system into homogeneous sub-units and allow the assignment of characteristic hydraulic parameters to each of them. This involves the discretisation of differential equations describing the groundwater flow. The principal formula for groundwater flow is Dracy's law which bases on conservation of momentum and mass:

$$S_S \frac{\partial H}{\partial t} = \nabla(K \nabla H) + i \tag{7}$$

Where S_S is the specific storage coefficient, K the hydraulic conductivity, H is the hydraulic head, t is time, and i is a source term. For discretisation, the finite differences method or the finite elements method can be used which are farther described in KINZELBACH (1986), WANG AND ANDERSON (1982), and HUYAKORN AND PINDER (1983).

Distributed parameter flow models can be divided in two different concepts: the discrete concept and the continuum concept. The former considers flow within individual fractures or conduits. The latter incorporates heterogeneities as model parameters with a spatial distribution. After TEUTSCH AND SAUTER (1991, 1998) these concepts can be sub-divided into five different approaches referring to the geometric nature of the conductive features represented in the model: The Equivalent Porous Medium Approach, the Double Continuum Approach, the Combined Discrete-Continuum (Hybrid) Approach, the Discrete Fracture Network Approach and the Discrete Channel Network Approach (FIGURE 13). (GOLDSCHEIDER AND DREW, 2007)

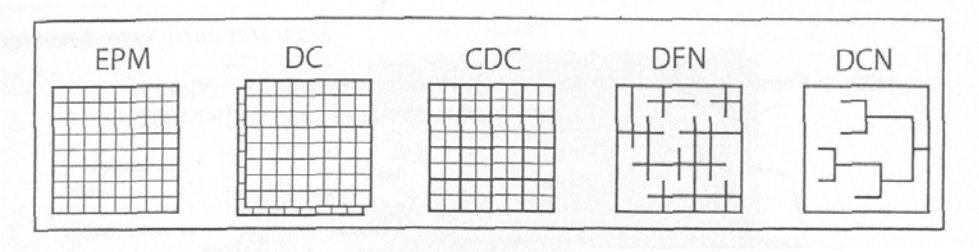

FIGURE 13: Classification of distributive karst modelling methods; EPM= equivalent porous medium approach, DC= double continuum approach, CDC= combined discrete-continuum (hybrid) approach, DFN= discrete fracture network approach, DCN= discrete channel network approach (GOLDSCHEIDER AND DREW, 2007)

The **Equivalent Porous Medium Approach** uses discretisation units of similar size. It implies that the representative volume remains nearly constant over the whole model domain and an insignificant change of hydraulic parameters in neighbouring units of discretisation, which is rarely found in karstic systems. This means the replacement of strongly heterogeneous rocks by an equivalent porous medium. Since this transformation, which in fact is an up-scaling, has always been of high interest it was performed in various studies (for example in ODA, 1995). By discretising a fracture network in grid cells EPM properties for each grid cell can be derived. If the discretisation is fine enough the hydraulic behaviour of the underlying fractured medium can be reproduced. However it fails to reflect the hydraulic behaviour of karstic systems if the discretisation is too coarse (GOLDSCHEIDER AND DREW, 2007).

The **Double Continuum Approach** was developed because of (1) the difficulties of gaining enough information about discrete fracture or conduit networks and (2) because of the inability of the Equivalent Porous Medium Approach to consider the strong heterogeneity of karstic systems. TEUTSCH (1988), who adapted the original concept of BARENBLATT ET AL. (1960), first solved numerically the Double Continuum Approach. In this approach the conduit network and the fissured medium are both represented by continuum formulations. Another successful mathematical implementation of the Double Continuum Approach was introduced by MOHRLOCK (1996; FIGURE 14). Each continuum possessed its own hydraulic properties and exchange between the continua was controlled by a so called "exchanger" (Equation (8)).

$$q_\alpha = \alpha_0 (h_a - h_b) \tag{8}$$

Whereby $(h_a - h_b)$ is the difference of water level of continuum *a* and continuum *b*, α_0 a specific exchange coefficient and q_α the specific flux between the two continua. The flow inside both continua was described by Darcy's law (Equations (9)).

$$\begin{aligned} div\left(K_{fa}\, grad\left(h_a(t)\right)\right) &= S_{0a}\frac{\partial h_a(t)}{\partial t} - W_{0a} + q_\alpha \\ div\left(K_{fb}\, grad\left(h_b(t)\right)\right) &= S_{0b}\frac{\partial h_b(t)}{\partial t} - W_{0b} - q_\alpha \end{aligned} \tag{9}$$

Here, K_{fa} and K_{fb} are the hydraulic conductivity tensors, h_a and h_b the water levels, S_{0a} and S_{0b} the specific storage coefficients, and W_{0a} and W_{0b} the specific inflows into continuum *a* and *b*. Note that the specific flux between the two continua q_α is positive for continuum *a* and negative for continuum *b*, which means that inflow in continuum *a* means an outflow of continuum *b* and vice versa.

The Double Continuum Concept is able to describe adequately the dual behaviour of karst aquifers. It just has to be kept in mind that hydraulic parameters

distributions are the averaged parameters of the real parameters and they are normally found by calibration (GOLDSCHEIDER AND DREW, 2007).

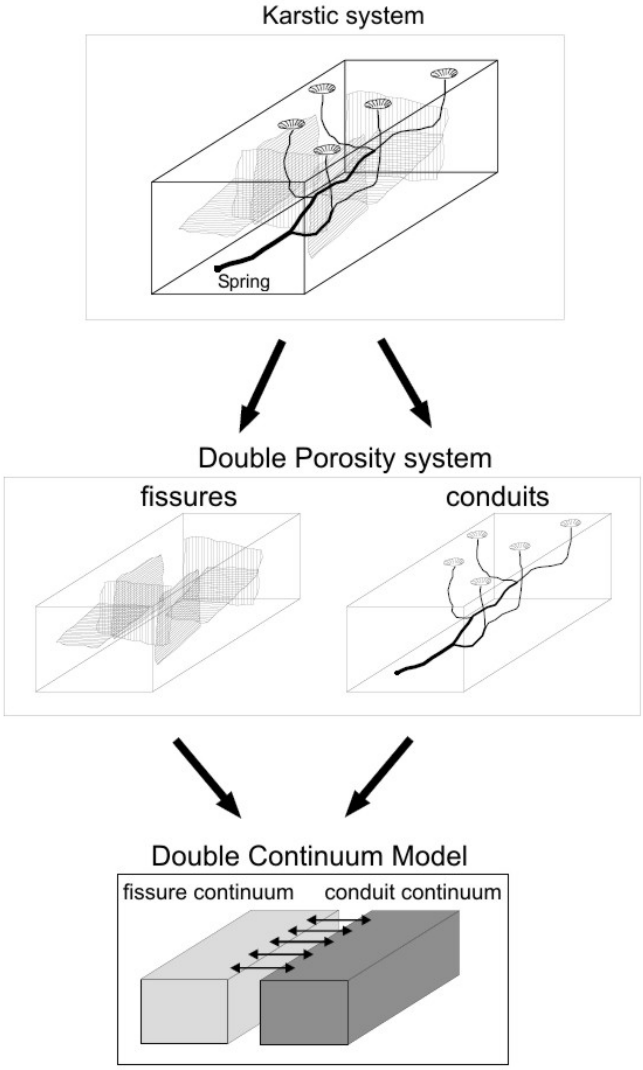

FIGURE 14: Double Continuum approach by MOHRLOCK (1996; modified)

The idea of two continua interacting with each other was also adapted by MALOSZEWSKI ET AL. (2002). They conceptualised a karstic groundwater reservoir by two interconnected parallel flow systems of a fissured-porous aquifer and karstic (drainage) channels (FIGURE 15). The fissured-porous aquifer contains mobile water in the fissures and quasi-stagnant or stagnant water in the micro-porous matrix. Infiltrating water enters either to the conduits or the fissured porous aquifer. From the conduits it can either enter the fissured-porous matrix or leave the system at the karstic spring. From the fissured-porous aquifer it enters the channels and leaves the system as well. The transit times of both systems differ in orders of magnitude so that if there is an input event a fast response due

to channel flow and a slow response due to flow through the fissured-porous aquifer will occur.

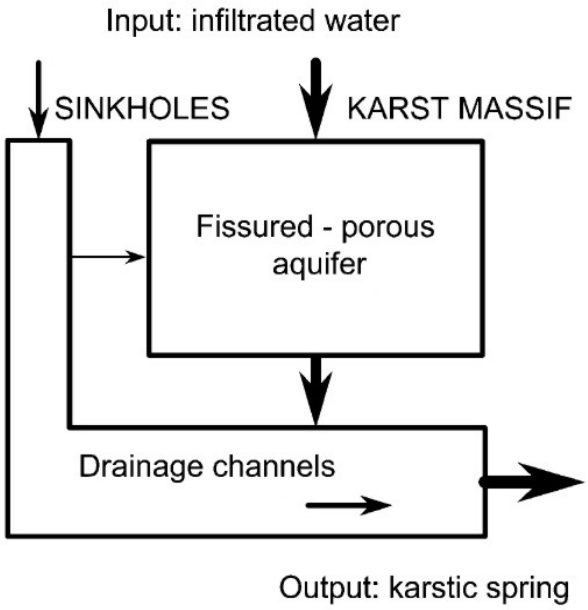

FIGURE 15: Conceptual model of karstic groundwater reservoir (MALOSZEWSKI, 2002, MODIFIED)

Another implementation of the idea of two continua exchanging with each other depending on reservoir content was performed by SUGARAWA (1995). He conceptualised a double porous soil by the exchange flow T between to parallel reservoirs:

$$T = K\left(\frac{X_1}{S_1} - \frac{X_2}{S_2}\right) \tag{10}$$

Whereby K is an exchange constant, X_1 and X_2 the volume of water in reservoir 1 and 2, and S_1 and S_2 are the maximum volumes of reservoirs 1 and 2, respectively. Both, MOHRLOCK (1996) and SUGARAWA (1995), used some measure to describe the difference of storage volume, which was then multiplied by a fixed exchange constant to obtain the exchange flow between the two media with different porosities.

The **Combined Discrete-Continuum (hybrid) Approach** is capable of handling the discontinuities that exist in all scales of a karstic system. This is done by

embedding them as a network of different order of magnitude. This approach can explain as well the duality of karst as the scale effect on hydraulic conductivity (KIRALY, 1975). Since it uses the finite elements method it can combine one-, two-, or three-dimensional elements (KIRÁLY 1979, 1985, 1988; KIRÁLY ET AL. 1995; KIRÁLY AND MOREL. 1976a). Thus karst conduits can be modelled as one-dimensional elements which are set in a low permeability matrix of three dimensions. In the same way two dimensional elements like fissures and fractures can be incorporated.

The Combined Discrete-Continuum (hybrid) Approach is unique in its capability to incorporate directly observed aquifer parameters and measured hydraulic parameters. Consequently, it can be used to test conceptual models of karst systems as shown by KOVÁCS (2003) and KOVÁCS ET AL. (2005).

The **Discrete Fracture Network Approach** considers only certain sets of fractures to be permeable. Matrix flow is neglected and the system is simplified to a network of two-dimensional fracture planes. Even though it is mainly applicable to fractured systems it can also be used for the representation of karst channels by introducing one-dimensional elements or increased transmissivity zones along individual fractures representing dissolution voids (DERSHOWITZ ET AL., 2004).

The **Discrete Conduit Network Approach** simulates flow in one dimensional pipes which represent the karst conduits or connections between fracture centres. The network geometry can be determined directly by observations, or it can be derived from stochastic discrete conduit networks by geometric transformations. Some applications can be found in CACAS ET AL. (1990), DVERSTOP ET AL. (1992), and DERSHOWITZ ET AL. (1998).

3.2.3 Modelling of the epikarst

Since the approaches introduced above consider mainly water behaviour after passing the soil and the epikarst some particular concepts to model epikarst behaviour will be discussed in this section. As mentioned by GOLDSCHEIDER AND DREW (2007) and shown by WILLIAMS (1983) in FIGURE 10 the epikarst is an important storage and distribution system for infiltrating water. The conceptualisation of its behaviour and its mathematical application in simulation routines has been performed in very simple to very complex ways.

A very simple approach of the epikarst was applied by GEYER ET AL. (2008). They assessed recharge to a slow reacting storage representing the fissure aquifer and a fast reacting storage, which is considered as the conduit system, by simple trapezoidal functions (FIGURE 16). For each trapezoid four times where given to indicate the beginning of the raising tail of the recharge, the beginning of constant time of recharge, the end of the constant time of recharge, and the end of the falling tail of recharge.

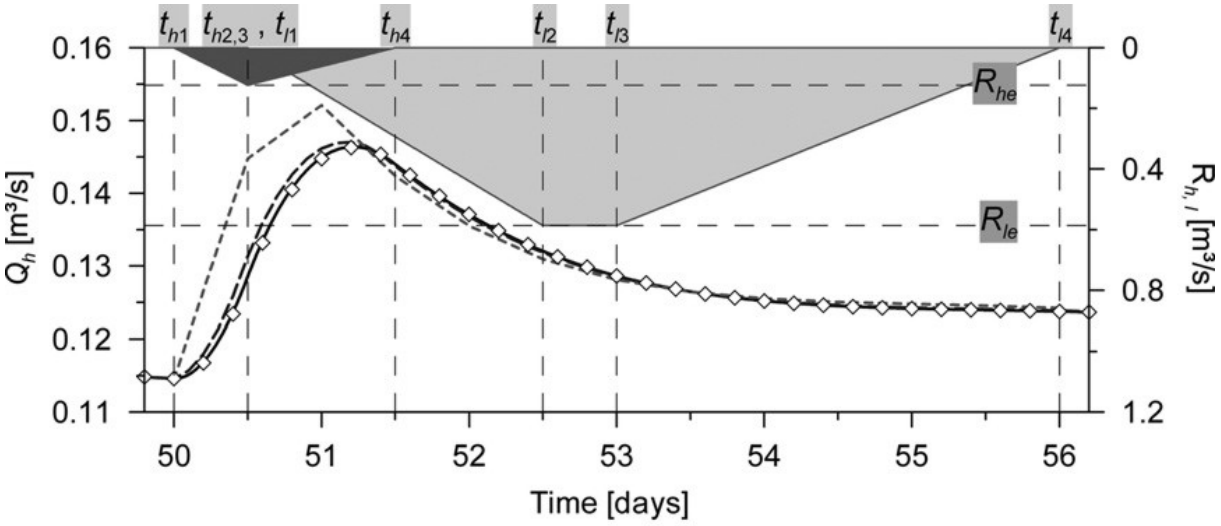

FIGURE 16: Recharge functions for the conduit system (dark grey) and to the fissured aquifer (bright grey), and resulting spring hydrographs under different numerical configurations (GEYER ET AL., 2008)

Compared to GEYER ET AL. (2008) FLEURY ET AL. (2007) already used a soil reservoir which had to fill until a certain water level H_0 (Figure 17). Overflow is then transmitted to two storages representing a fissure aquifer and a conduit system similar to GEYER ET AL. (2008). H_{min} represents an under-saturation threshold which is a level, under which no more evaporation takes place. Division of flows to the fissure aquifer and to the conduit system is performed by a constant factor determined by recession analysis.

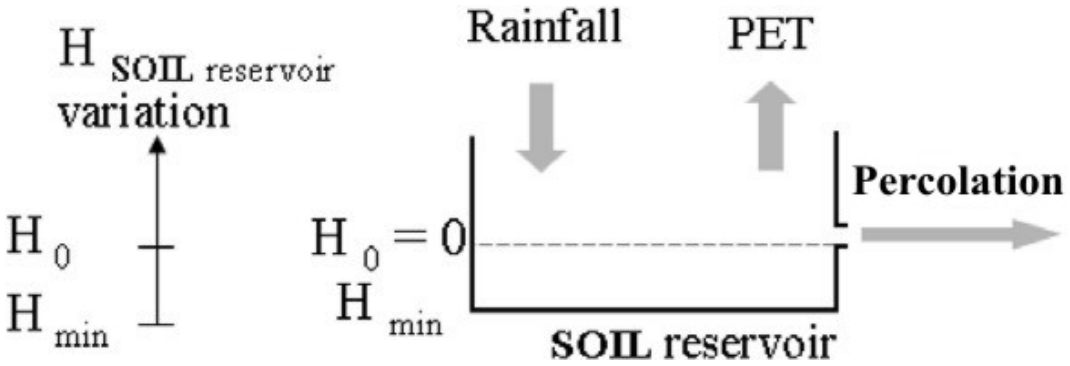

FIGURE 17: Soil reservoir applied in FLEURY ET AL. (2007)

However in the approach of FLEURY ET AL. (2008) there is still no description of water movement in the soil, and no consideration of epikarst specific processes at all. If water level passes H_0 all water is directly transferred to the ground water system.

Both approaches of the soil and epikarst behaviour introduced above are very simplistic and can by far not be regarded as process-based. In contrast, PERRIN ET AL. (2003) used a more complex approach which led to good results and which was additionally corroborated by hydrochemical simulations. According to their conceptual model of the epikarst (FIGURE 18) it should reproduce sharp hydraulic responses but damped solute concentrations. Its total desired functioning is listed as follows (PERRIN ET AL., 2003):

> **Hydraulics of the conceptual model:** The soil splits rainfall R_r into evapo-transpiration *ETR* and actual infiltration I_a. The epikarst distributes flow into base flow Q_b and quick flow Q_q. In case of high I_a, infiltrating water in excess bypasses the soil-epikarst reservoir as fresh water Q_f.
>
> **Non-reactive transport in the conceptual model:** Water leaving the epikarst reservoir (Q_b and Q_q) has the solute concentration C_b which is a weighted average of rain solute concentration C_r. Soil may partly transform C_r into C_b. Freshwater Q_f has the concentration of rain C_r. From field data the authors found a maximum infiltration capacity over which bypass flow, i.e. Q_f is produced. Below the infiltration capacity water leaving the soil-epikarst system has the concentration C_b.
>
> **Towards numerical modelling:** The soil-epikarst reservoir should account for (1) the progressive concentration of flow in the vertical direction (bottleneck

effect described by Williams, 1983; FIGURE 10), (2) storage and mixing, and (3) piston flow allowing rapid hydraulic pulses and delayed concentration response. Moreover non-linearity in flow and transport has to be introduced with a temporary outlet functioning when a given hydraulic head is reached.

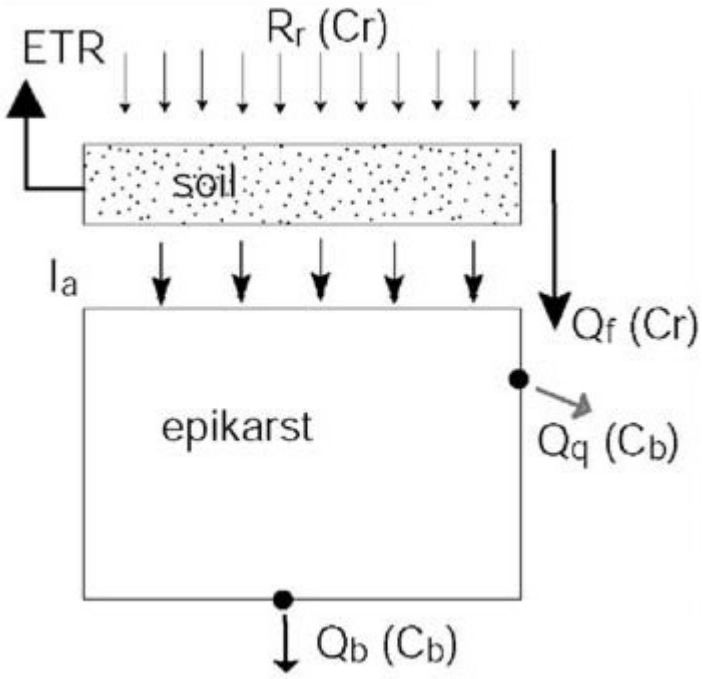

FIGURE 18: Conceptualization of the soil and epikarst by PERRIN ET AL. (2003)

This concept was implemented by modelling the epikarst as a confined aquifer in a vertical plane. Software used was the FEFLOW groundwater model provided by the Wasy GmbH. In order to incorporate the decreasing hydraulic conductivity with decreasing depth of the epikarst three layers with decreasing conductivities (10^{-4}, 10^{-5} and 10^{-6} m/s from top to the bottom) where created. These values are in agreement with estimations by JEANNIN (1996) and WILLIAMS (1985). Tries with different configurations showed that soil-epikarst behaviour could be best reproduced by an epikarst reservoir with a depth of 3.5 m and a length of 10 m each (FIGURE 19). Additionally an anisotropy factor of 0.1 has been introduced to account for decrease of horizontal conductivity of a factor 10. Two outlets were created: one at the bottom of the right side of the epikarst reservoir and one at the top of the right side. The outlet at the right side of the reservoir was chosen to create lateral flow because water entering near the left side end of the reservoir has to travel trough the whole reservoir to reach at least one of the outlets. Above a 1 m soil layer was superimposed likewise with a length of 10 m and a hydraulic conductivity of 10^{-4} m/s.

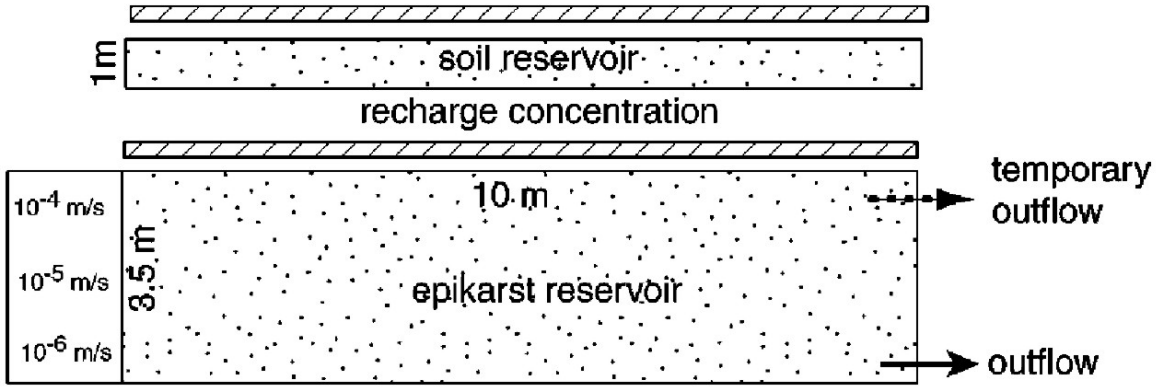

FIGURE 19: Geometry of the epikarst reservoir modelled with FEFLOW yielding the best results created by PERRIN ET AL. (2003)

Since with the actual configuration only piston flow-like behaviour could be produced but no mixing which was observable in their measurements though, PERRIN ET AL. (2003) replaced the soil layer by a linear reservoir and applied mixing equations. The assumption of complete mixing in the soil was explained by part of the water bypassing the soil reservoir through macro pores during an event and mixing with the matrix water which is completely mobile due to the saturation of the soil.

With this modification it was possible to reproduce hydrographs and chemographs at the measurement points. Thus the conceptual model introduced above seems to be adequately representing the soil and epikarst flow as well as solute transport behaviour. According to the authors the adaptation of non-saturated flow methods as introduced by SIMUNEK ET AL. (2003) could even lead to better results.

3.3 Conclusions

The different concepts described above provide various approaches to model a karst system as described in the first section of this chapter. They are dependent on available data and desired degree of precision. For a high degree of precision the distributive models a more favourable because they are physically based and yield spatial and temporal distributions of groundwater heads and flow. However they require a large amount of input data including a lot of system inside information. Hence these models were mostly applied in well measured small scale catchments. In the opposite there are the global models. They are applicable in every scale but their predictive capability as well for time series analysis as for single event models is quite small. “Grey box” approaches consisting of series of reservoirs, representing real processes and storages of a karstic system, are an alternative way to incorporate karst specific processes

instead of using a distributive model with its large demand for data. However the “grey box” approaches introduced above just represent insufficiently the duality of karst hydrological behaviour.

As described in chapter 2 there is a scarceness of spatial information inside the Mt. Hermon system. This is the major problem for building up a modelling system for this area. The whole lack of data is summarized in the following chapter.

4 Limitations for Mt. Hermon karst modelling

The most recent model of the Mt. Hermon hydrological system was developed by RIMMER AND SALINGAR (2006). In order to manage this they had to cope with a big lack of knowledge which is summarized as follows (RIMMER AND SALINGAR, 2006):

- Precipitation (either snow or rain) was never measured systematically for long periods of time due to the inaccessibility of most parts of the mountain and the difficulties in maintenance of meteorological stations at altitudes above 2000 m ASL (GILAD AND BONNE, 1990). Previous studies had to deal with data from lower altitude stations (GILAD AND SCHWARTZ, 1978; SIMPSON AND CARMI, 1983). New meteorological data for Mt. Hermon high altitudes are available since 2006 (Alon Rimmer, Pers. Com.) but these data could not contribute to the current research, which was based on historical data.

- The streams and springs in the east and northeast region of Mt. Hermon are located in Syria and Lebanon and there is no hydrological data sharing between Israel, Syria and Lebanon because of political reasons.

- Many hydrological parameters and variables inside the region are unknown (like thickness and borders of the aquifers, water level fluctuations, hydraulic characteristics, rainfall distribution, annual recharge, etc.).

- The location of the different aquifers and their recharge area to the three tributaries of the Jordan River are unknown. However, it is obvious that these recharge areas are not correlated to their superficial catchment areas.

This lack of information inhibits the application of distributive models. However, the huge database of the hydrology of the Jordan River and the long term precipiation and evaporation data (TABLE 1) gives good conditions for the development of a global model. Hereby a system approach of the type $y(t) = \Phi[x(t)]$ (RIMMER AND SALINGAR, 2006) was applied. In this case $x(t)$ represents the input to the Mt. Hermon system, which is the amount of precipitation and evaporation, $y(t)$ represents the output of the system, which is the discharge, and $\Phi(x)$

represents the system function - a set of equations and parameters which transfers the input $x(t)$ to the output $y(t)$. Since input and output are known and the system function is unknown, the problem of identifying the characteristics of Mt. Hermon is an inverse problem. The process of solving this type of inverse problem is recognized as "system identification" and includes the choice of a physically acceptable solution, out of numerous mathematically acceptable solutions (see for example CAMBI AND DRAGONI, 2000). Criteria for this choice depend on the nature of the inverse problem (SINGH, 1988). A model developed with these guidelines can be regarded as a "grey box" model since it already includes processes and storages that really exist inside the model. Given the limitations listed above and the objective of a proper system identification RIMMER AND SALINGAR (2006) developed a conceptual model of the Mt. Hermon hydrological system using only the water input and output. Hereby hydrochemical data was not included yet. This system is described in the following chapter.

5 HYMKE - a HYdrological Model for Karst Environments

5.1 Model structure

The hydrological model for karst environment (HYMKE) developed by RIMMER AND SALINGAR (2006) consists of four routines: the surface layer routine, the vadose zone routine, the groundwater routine and the surface flow routine. The surface layer routine represents the soil and the epikarst (similarly to JEANNIN AND GRASSO, 1997). During an event precipitation is filling surface layer storage until a certain saturation value is reached. Then it generates preferential flow and surface flow. Surface flow is excluded from the subsurface system and reaches the stream via the surface flow routine. The preferential flow bypasses the soil and enters directly the vadose zone routine while evaporation is only affecting the water stored in the surface layer storage. The outflow of the surface layer water is controlled by its water content according to the models applied by THORNTHWAITE AND MATHER (1955, 1957), STEENHUIS AND VAN DER MOLEN (1986) and PERANGINANGIN ET AL. (2004). Therefore water reaching the vadose zone consists of preferential flow bypassing the surface layer and surface layer outflow depending on the water content. The vadose zone routine is a reservoir which drains linearly to its storage content. From there the output feeds the groundwater routine's reservoir which is a linear reservoir again. This finally gives the outflow of the system. Because of the different groundwater discharge patterns this routine was separated into three groundwater reservoirs, which represent the three main tributaries of the Jordan River, and a fourth reservoir, which takes into account the unknown groundwater component that drains to the eastern part of Mt. Hermon in the area of Syria. The sum of the outflow of the three groundwater reservoirs draining to the tributaries and of the surface flow model creates the main stream: the Jordan River.

In order to calibrate surface flow and groundwater flow separately RIMMER AND SALINGAR (2006) used the "recursive digital filter" method of ECKHARD (2005) originating from signal processing (see also NATHAN AND MCMAHON, 1990; SMAKHTIN, 2001; HUGHES ET AL., 2003). This method separates high from low-frequency signals. Surface flow was attributed to high frequency signals and groundwater flow was attributed to low frequency signals, respectively. However the "recursive digital filter" cannot distinguish between fast conduit response of karst system and superficial flow. This has to be remembered in the following parts of the paper.

This diploma thesis focuses on the hydrochemistry and discharge modelling of the Dan Spring and Banias Spring. Therefore FIGURE 20 only illustrates the conceptual structure of the model just for these parts of the system. The fractions of water from the vadose zone, which enter the different groundwater reservoirs, were determined by RIMMER AND SALINGAR (2006) via calibration. They represented the proportion of the whole catchment area which contributes to the respective groundwater reservoir. Calibration of discharge predictions was performed by fitting the simulated spring discharges to the separated low frequency part of the particular spring; also referred to as separated base flow.

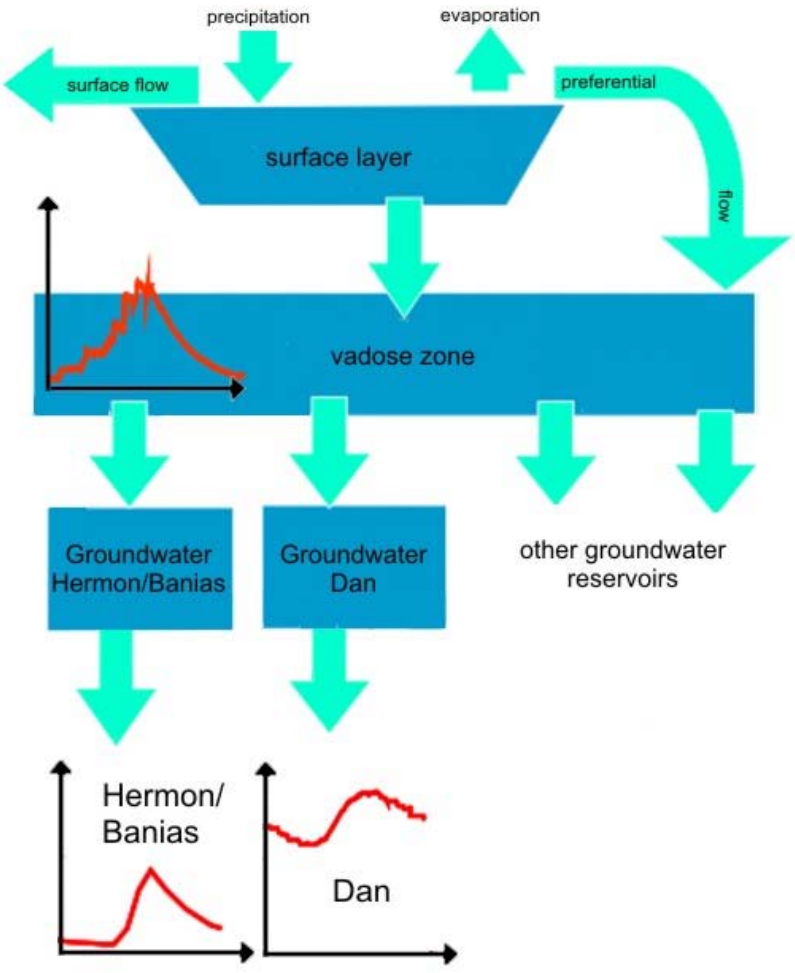

FIGURE 20: Conceptual model of HYMKE (RIMMER AND SALINGAR, 2006, modified)

5.2 Limitations of HYMKE

HYMKE simulated discharge and separated base flow from the hydrological years 1990/1991 to 1999/2000 can be seen in FIGURE 21 and FIGURE 22. Under average conditions, from 1994/1995 to 1997/1998, the measured discharge of both springs is well approximated by the model. However during extremely wet or dry years, 1991/1992 or 1998/1999, the model predictions show relatively strong deviations in particular for Dan Spring. Predictions strongly overestimate the peak discharge in the wet year of 1991/1992 while following the dry year of 1998/1999 it underestimates the peak and overestimates the minimum discharge. Deviations for Banias Spring are less obvious during the wet years but following dry seasons the falling tail of the hydrograph differs sometimes from the base flow separated discharge.

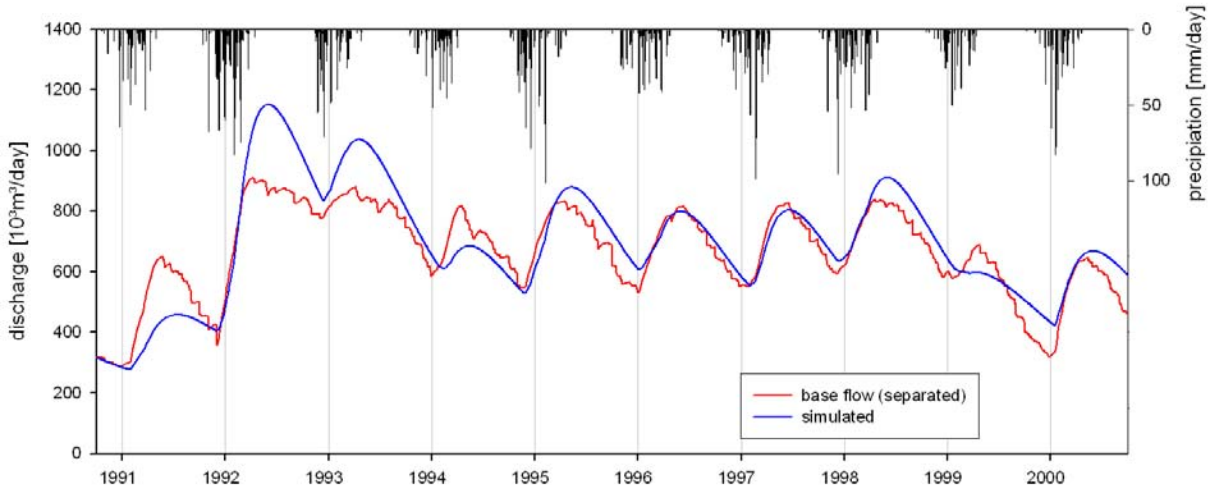

FIGURE 21: MODELLED BASEFLOW (BY HYMKE) AND MEASURED (BASE FLOW SEPARATED) DISCHARGE OF DAN SPRING FROM 1990/1991 TO 1999/2000

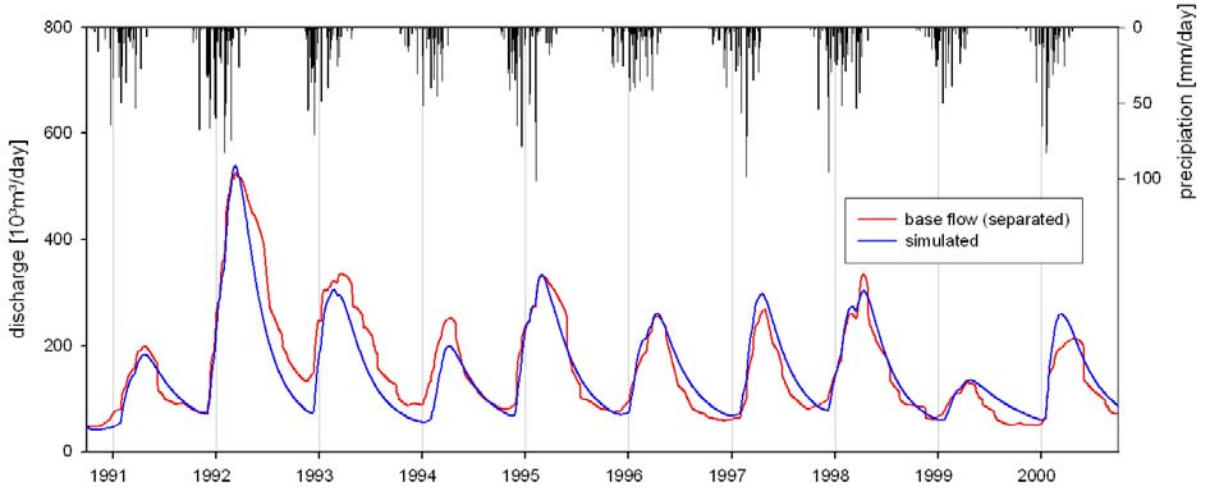

FIGURE 22: Modelled baseflow (by HYMKE) and measured (base flow separated) discharge of Banias Spring from 1990/1991 to 1999/2000

To examine how far the first version of HYMKE (RIMMER AND SALINGAR, 2006) was able to predict solute concentrations at the spring outlets simple mass balance equations were applied to each routine similar to the approach already used by HORNBERGER ET AL. (1994) to incorporate mixing of dissolved organic carbon into TOPMODEL (BEVEN AND KIRBY, 1979). The principal assumption of these equations is that the sum of input, output and change of storage equals zero. This was applied for the water flows as well as for the NO_3, Cl and SO_4 using the following equations:

$$Q_{in}(t) + Q_{out}(t) + \frac{\partial S(t)}{\partial t} = 0 \tag{11}$$

$$m_{in}(t) + m_{out}(t) + \frac{\partial m_S(t)}{\partial t} = 0 \tag{12}$$

Whereby $Q_{in}(t)$ and $Q_{out}(t)$ are the inflows and outflows, and $m_{in}(t)$ and $m_{out}(t)$ are the mass of solutes which enter and leave the reservoir at time *t*. $\partial S(t)/\partial t$ and $\partial m_S(t)/\partial t$ are the change of stored water and the change of stored mass inside the reservoir. This approach implies the assumption of complete and instantaneous mixing which may not always be expected. To account for partial mixing in the vadose zone its mixing volume was set the half of the actual volume of this storage. Time delay effects of transition of the partial mixing concentration to the vadose zone outlet were considered to be negligible. Of course solute transport processes are not exactly represented by this approach but it will be sufficient to show if the actual model structure is at least able to reproduce trends of discharge concentrations or not.

For the surface layer reservoir this means that infiltrating water, with a certain solute concentration, can mix with the water stored already inside this reservoir. The stored water is enriched in time because water which leaves this reservoir via evaporation has evidently a concentration equals zero leading to a higher concentration is the residual water. Accordingly high concentrations of soil water solutes can be expected as a result of high evaporation and high residence times while low concentration can be expected for low evaporation conditions. Finally, for this part of the system, the outflow of the soil mixes with the bypassing preferential flow, which has the same concentration as the water entering the soil before it was mixed in the surface layer reservoir and exposed to evaporation.

For the following reservoirs, which are the vadose zone and the groundwater storage, an attenuation of the signal will occur. That is because these two storages are set as series and each time water enters one of the storages it is mixed with the water which already residues in the respective storage. The hydrochemical signal is smoothed dependent on the volume of water already stored in the reservoir: strong attenuation can be expected for mixing with large volumes while weak attenuation can be expected for mixing with small volumes. This can be observed in the results of the application of the mass balance equation to HYMKE (FIGURE 23, FIGURE 24 and FIGURE 25 for Dan Spring, FIGURE 26, FIGURE 27 and FIGURE 28 for Banias Spring).

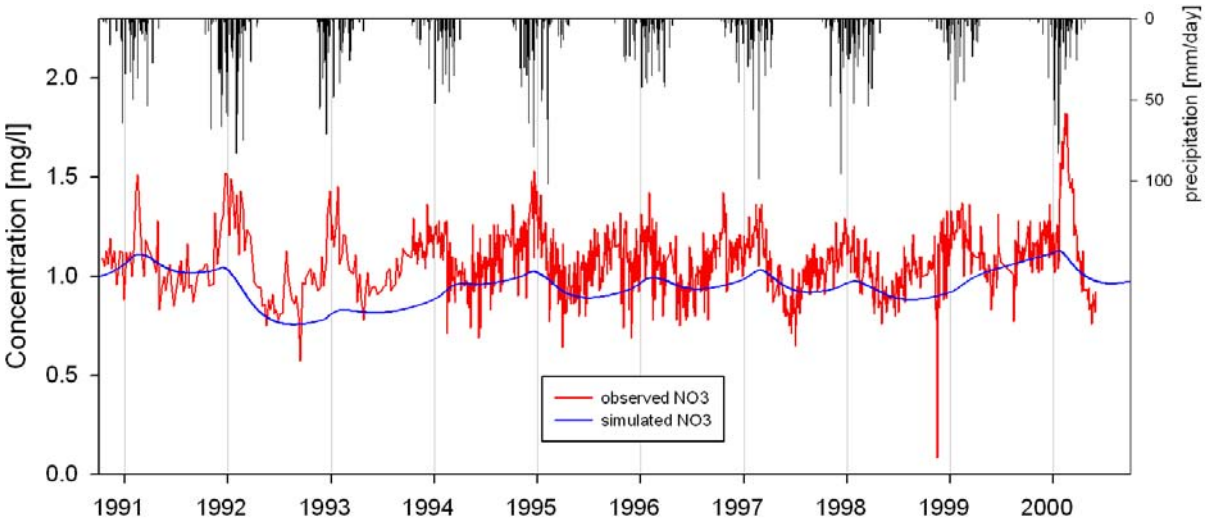

FIGURE 23: Variations of NO_3 in Dan Spring between 1990/1991 and 1999/2000

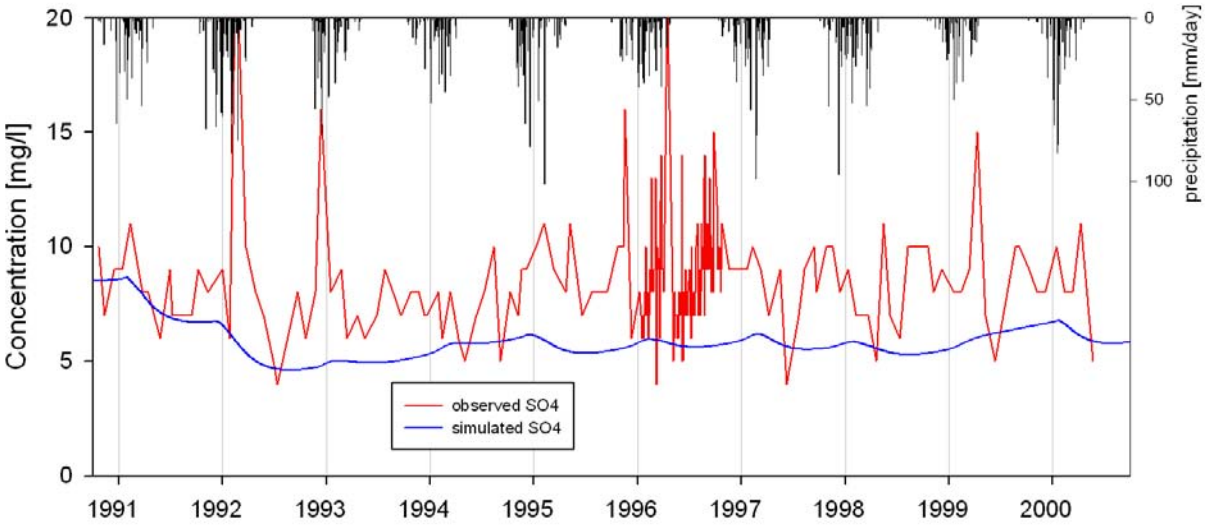

FIGURE 24: Variations of SO_4 in Dan Spring between 1990/1991 and 1999/2000

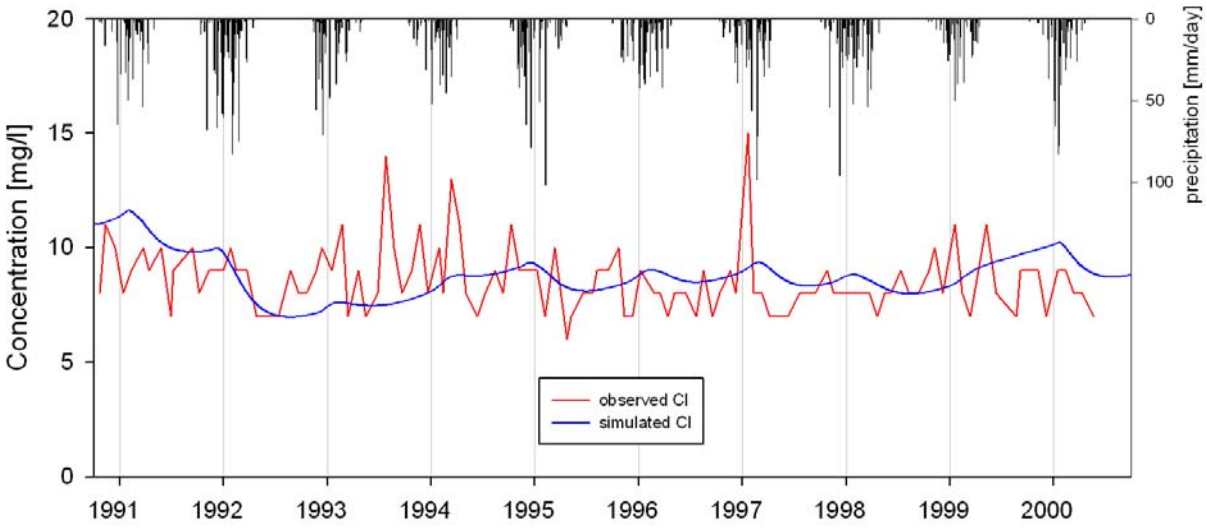

FIGURE 25: Variations of Cl in Dan Spring between 1990/1991 and 1999/2000

The model predicts strong dilution for the Dan which takes place as a result of its large groundwater reservoir. Although the peaks are close to the measured peaks, the modelled amplitude is far too small. This can be observed best for NO_3 (FIGURE 23).

The results for the Banias Spring show a weaker dilution as a consequence to the relatively small groundwater reservoir which does not attenuate much the vadose zone output concentration. Attention should be given to the amplitude of SO_4 in Banias Spring which acts totally different to the other solutes. Its amplitude is about seven times larger than the SO_4 amplitude of the Dan Spring. These variations cannot be reproduced at all by the model.

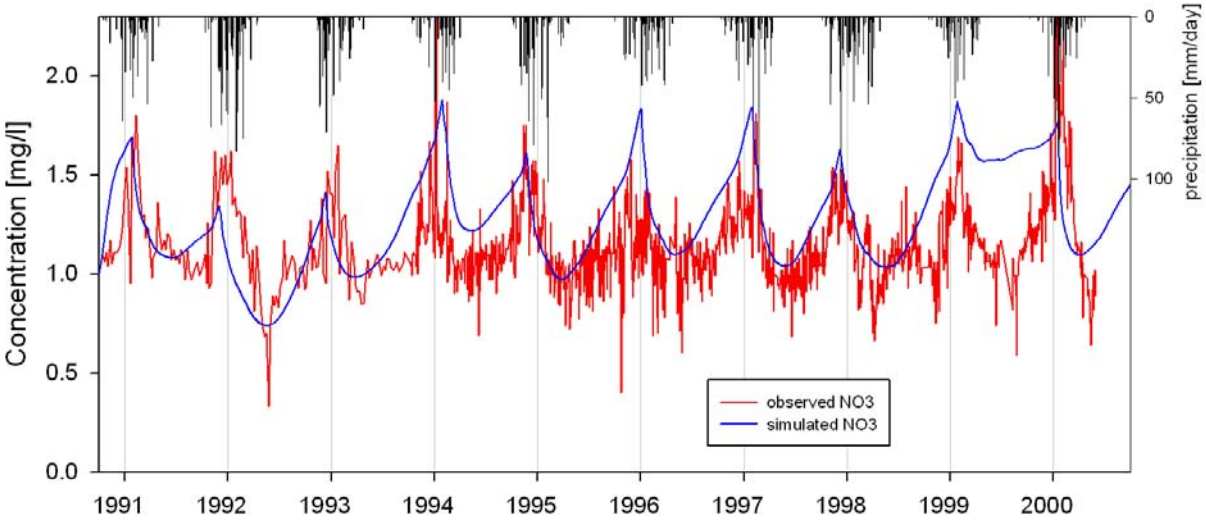

FIGURE 26: variation of NO_3 in Banias Spring between 1990/1991 and 1999/2000

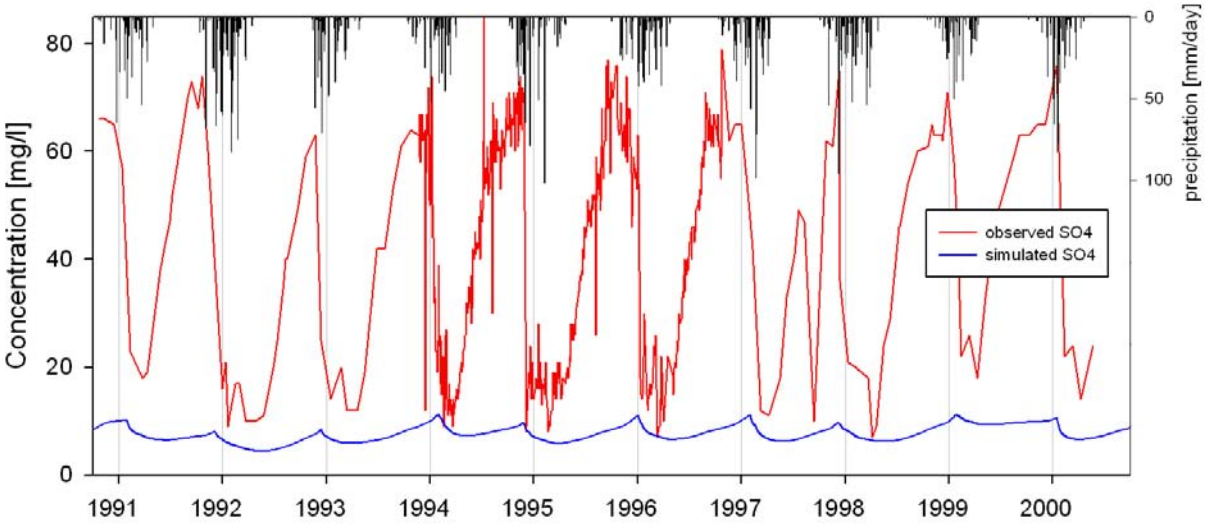

FIGURE 27: variation of SO_4 in Banias Spring between 1990/1991 and 1999/2000

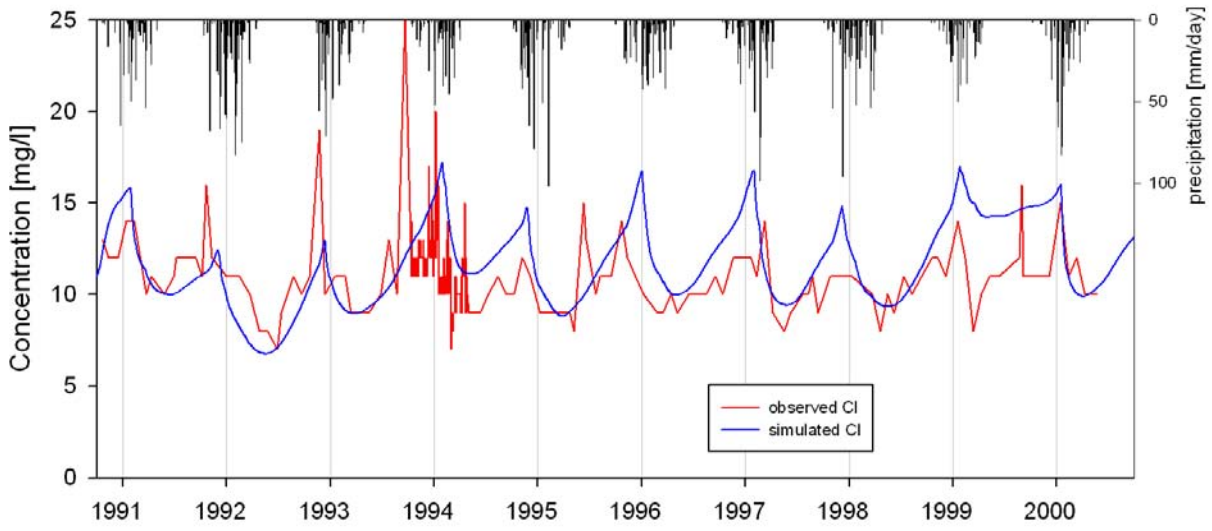

FIGURE 28: variation of Cl in Banias Spring between 1990/1991 and 1999/2000

5.3 Conclusions

The conclusion of this analysis was that although the system of HYMKE resulted in fair results for the discharge predictions it was clearly not suitable for the predictions of solute concentrations at the spring outlets: at Dan Spring the amplitude of variations were too small and at Banias Spring the dry season peaks of SO_4 could not be reproduced. This indicates that HYMKE structure was missing one or more important processes which are responsible for the solute concentrations observed at the springs' outlet. In order to identify these processes hydrochemical data was integrated in the development of a new conceptual model of the Mt. Hermon hydrological system. This is the major objective of the following chapter.

6 Consideration of hydrochemical knowledge

Most features of the Mt. Hermon karst system identified and conceptualized in HYMKE derived from hydrograph analysis. However, these data do not yield information about actual transit or residence time and on location of storages (epikarst, unsaturated or saturated zone). Hydrochemical techniques, if a sufficient contrast of the considered variables exists, provide answers to these questions and also help to locate and quantify the acquisition of mineralization by the water (GOLDSCHEIDER AND DREW, 2007). The most fundamental data set for characterising a karst system are rainfall, discharge, electrical conductivity and temperature. Electrical conductivity is mostly the choice because it is highly correlated with Ca, HCO_3, total dissolved solids and hardness (GOLDSCHEIDER AND DREW, 2007). FIGURE 29 shows the variation of these data including additionally turbidity and DOC. At the initial phase of the rising hydrograph no hydrochemical reaction can be observed at all. This is due to a pressing out of old water already stored in the conduit system. After that, during the peak time of discharge, also conductivity reaches its peak value. This is attributed to the pressing out of higher mineralised water from the epikarst. This pressing out of old and epikarst water is considered as piston flow mechanism (GOLDSCHEIDER AND DREW, 2007). At the falling tail of the hydrograph temperature and conductivity are decreasing before they slowly begin to recover to medium values. This is attributed to dilution by event water which looses its influence after the rain event. Despite of that turbidity and DOC have their peaks at the falling tail of the hydrograph coinciding with the largest contribution of event water. This can be explained by the source of spoiling elements and of DOC which is the shallow soil and the surface.

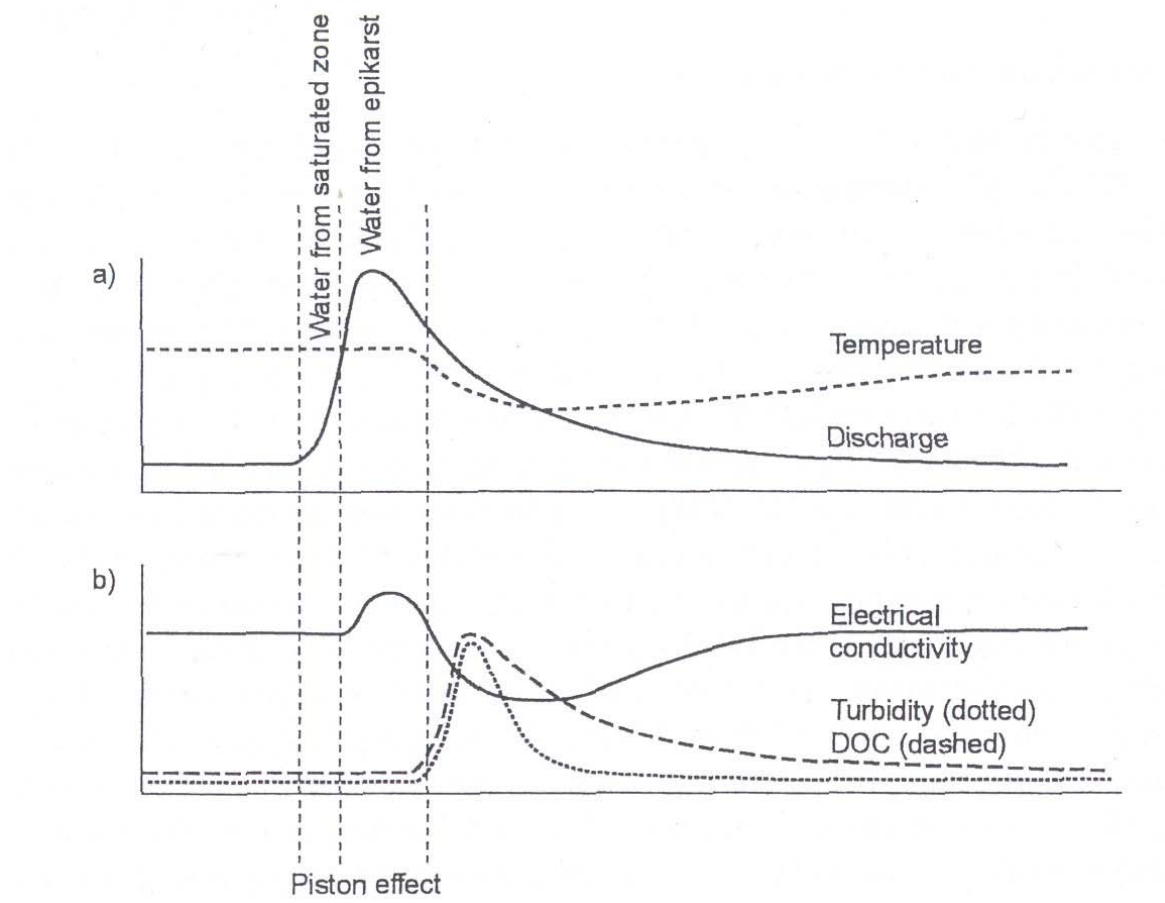

FIGURE 29: Schematic illustration of temporal variations of discharge and basic hydrochemical parameters (GOLDSCHEIDER AND DREW, 2007)

This example demonstrates how hydrochemical analysis can provide information about the functioning of karst aquifers (successfully performed for example by AQUILINA ET AL., 2006, or DESMARAIS, 2002). To gain more understanding of the Mt. Hermon hydrological system these ideas, considering the concepts introduced in chapter 3, will be applied to the hydrochemical data available for the Banias and Dan Spring. This will include a hydrochemical characterization of springs, a direct comparison using the long term data (TABLE 1), hydrograph separations, and an own measurement campaign at Dan Spring. The aim is to identify karst specific processes which are not yet included in the HYMKE approach on order to improve its predictions regarding the solutes. With this it could be shown that the choice of newly incorporated processes would be based on real processes.

6.1 Solutes used for spring water characterization

To gain a picture about the general hydrochemistry of both springs Piper and Schoeller diagrams were established using major ion concentrations (sampled by the Mekorot according

to Standard Methods (EATON ET AL., 2005)). For a deeper insight, and later for the simulations of solute concentrations, the anions Cl, SO_4 and NO_3were considered more thoroughly. Their origins and conservative or non-conservative behaviour will be discussed later in this chapter.

The accuracy of sampling of these anions depends on the method used for its evaluation. For NO_3 two different methods were applied: For low solute concentrations (< 0.6 mg/l), Mekorot used the cadmium-copper method, which has a precision of $\pm 0.50/\sqrt{n}$ µmol/l (STRICKLAND AND PARSONS, 1968). Where n is the number of evaluations of one sample. Since Mekorot only evaluates once per sample, n = 1. Thus, using the atomic weight of NO_3, the precision for NO_3 samples with concentrations below 0.6 mg/l is ± 0.0031 mg/l. For NO_3 concentrations above 0.6 mg/l, the NAS method is used (SZEKELY, 1979), which has a precision of about 0.1 mg/l. For the SO_4 measurements the so called turbidimetric method was applied (EATON ET AL., 2005). Its precision is given by a standard deviation of 0.13 mg/l and a coefficient of variation of 1.7% (using a sample with a mean concentration of 7.45 mg/l SO_4). At last, Cl content was determined by the potentiometric method (EATON ET AL., 2005). Its precision is about 0.12 mg/l or 2.5% of the amount in the sample if there are no interfering substances (for a sample with a mean concentration of 5 mg/l).

6.2 Hydrochemical characterization

For the general hydrochemical characterization major ions were regarded under different states of discharge. Two major groups were distinguished: (1) major ion concentrations during the rainy and (2) concentrations during the dry season of the respective year. Additionally it was distinguished between dry and wet preceding years to see if there is a memory effect for the major ions inside the system. With these data (Appendix, TABLE 23, TABLE 24) Piper diagrams and Schoeller diagrams were created.

6.2.1 Banias Spring

The Piper diagram of Banias Spring (FIGURE 30) under different pre-conditions shows an obvious dominance of the Ca-HCO_3 type of water. But in the dry season as well under wet as under dry pre-conditions there is a shift towards the Ca-SO_4 type. HCO_3 still remains the major anion but the SO_4 contribution is not negligible. The Schoeller diagrams in FIGURE 31 (sorted by decade) indicate that the salinity during dry season always is higher than during rainy season, primarily for SO_4. The same effect, though not so pronounced, can be observed for the Mg.

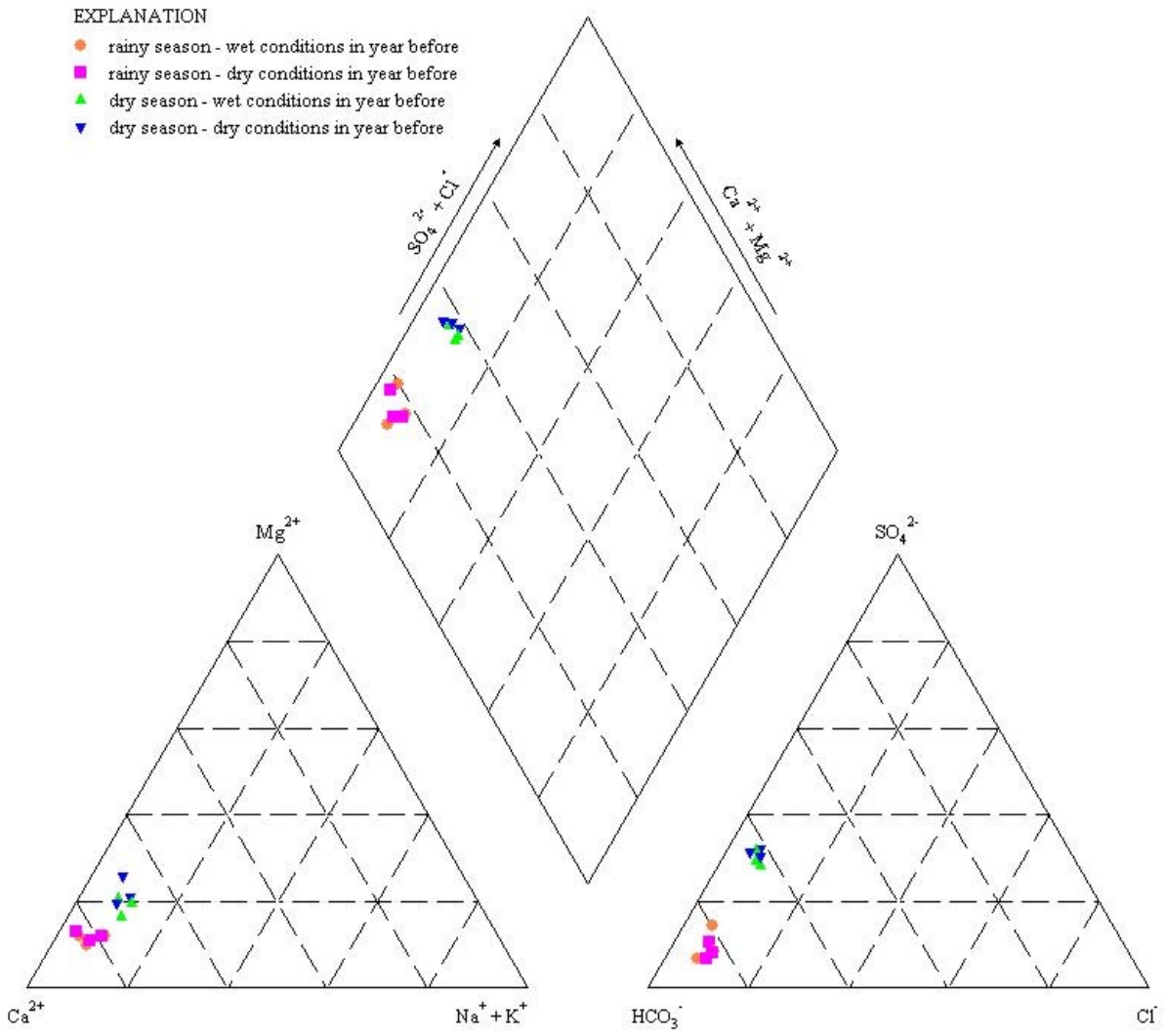

FIGURE 30: Piper diagram of Banias Spring major ion concentrations under different discharge conditions

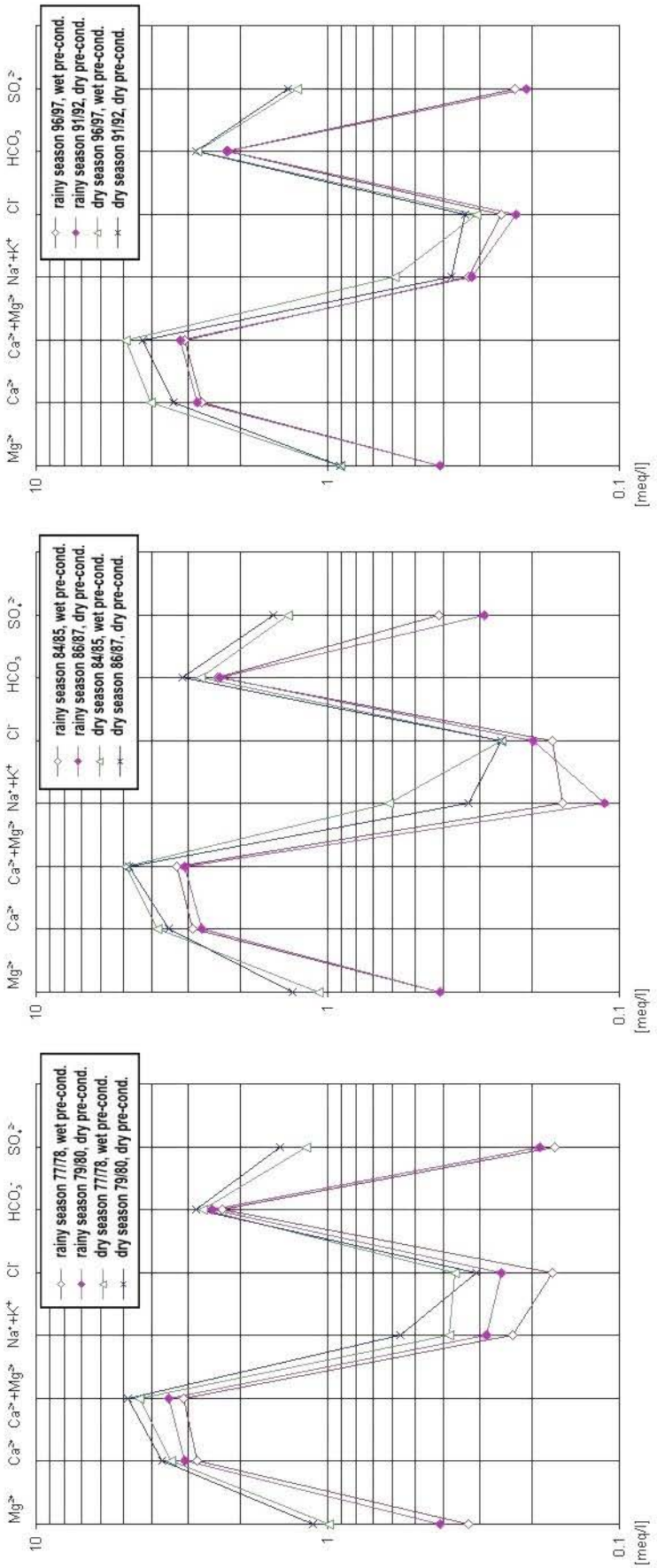

FIGURE 31: Schoeller diagram of Banias Spring concentrations for different seasons (rainy or dry) under different pre-conditions

6.2.2 Dan Spring

Piper and Schoeller diagrams of Dan Spring for different seasons under different pre-conditions can be seen in FIGURE 32 and FIGURE 33. In FIGURE 32 values for all different states of discharge and different preceding conditions plot very near to each other: They all represent the Ca-HCO_3 type. Similarly the same data plotted in Schoeller diagrams in FIGURE 33 show no significant differences for the rainy and dry season under different pre-conditions. To maintain a clear arrangement an individual fingerprint diagram was plotted for each decade.

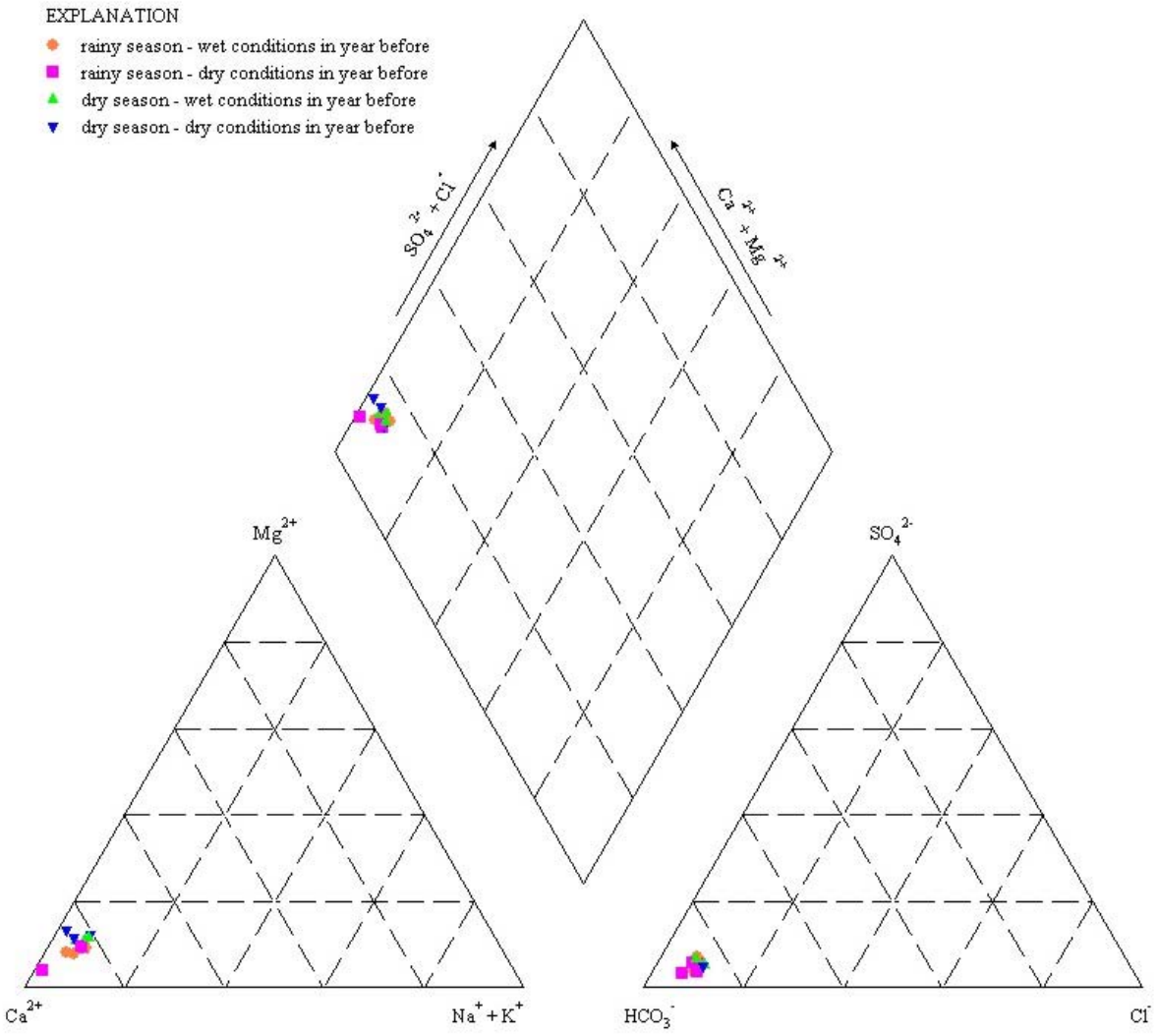

FIGURE 32: Piper diagram of Dan Spring major ion concentrations under different discharge conditions

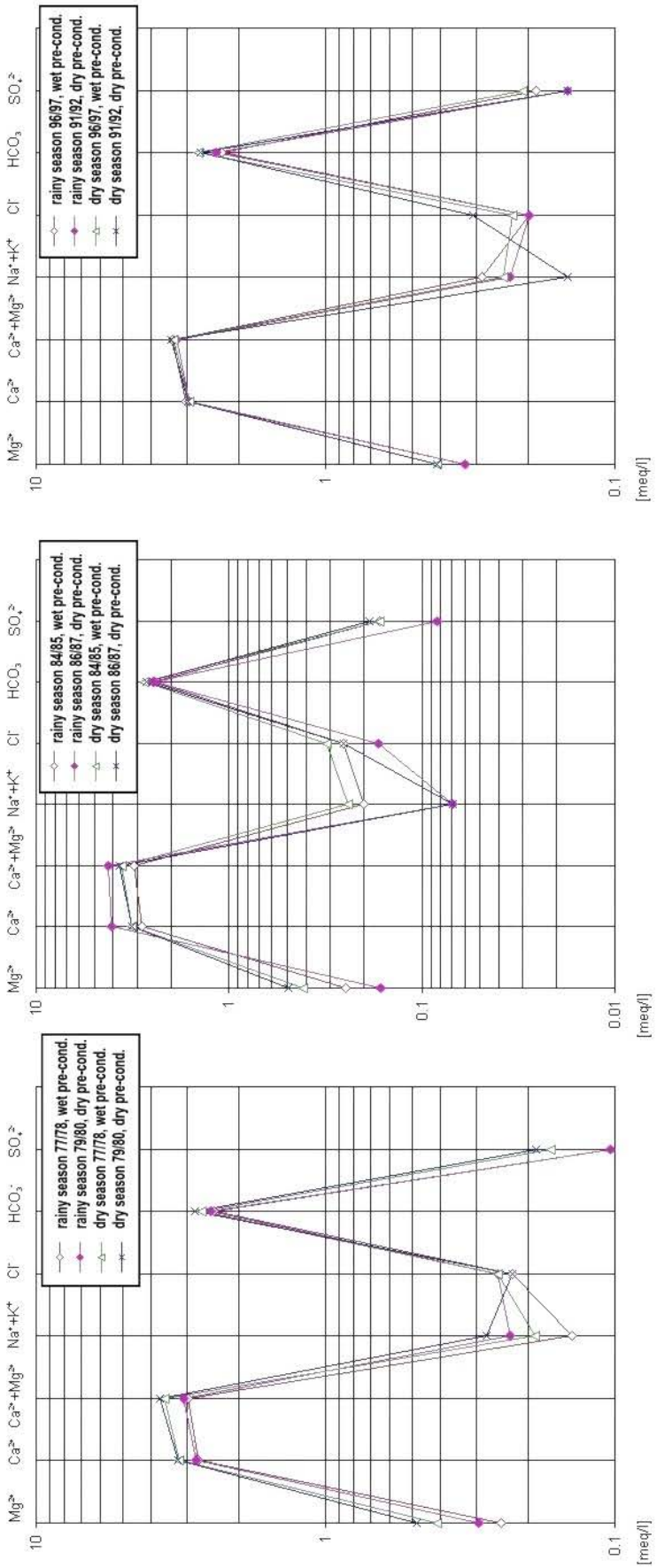

FIGURE 33: Schoeller diagram of Dan Spring concentrations for rainy or dry season under different pre-conditions

6.3 Comparison of both springs

6.3.1 Results of comparison

In order to compare between the two springs common solute concentration courses were plotted in one diagram including the hydrographs for both springs (FIGURE 34 for Cl, FIGURE 35 for NO_3 and FIGURE 36 for SO_4). The figures show that Banias Spring discharge has a far bigger amplitude than Dan Spring. This means that inter-annual variations of Banias Spring are much stronger than inter-annual variations of Dan Spring. Dan Spring reacts slower at the beginning of wet season and its peak is later than the Banias Spring peak. The recession of Dan Spring also is slower than the recession of Banias Spring and shows the concave shape which is typical for this spring. Dan Spring discharge stays relatively high even in dry years. RIMMER AND SALINGER (2006) explained this behaviour by the much larger size of the reservoir which is feeding this spring and by the fact that its outlet lies 159 m below the outlet of Banias Spring. This can also be the reason for the faster reaction of Banias Spring: Its fluctuations indicate that its outlet is closer to the recharge area than Dan Spring outlet. GILAD AND SCHWARTZ (1978) suggested that the Dan Spring's hydraulic head is much higher than its topographic level. These proposed differences between the two springs are also supported by other studies which show that the more intermittent springs have a higher altitude than the perennial springs (JENNINGS, 1985; CAMBI AND DRAGONI, 2000).

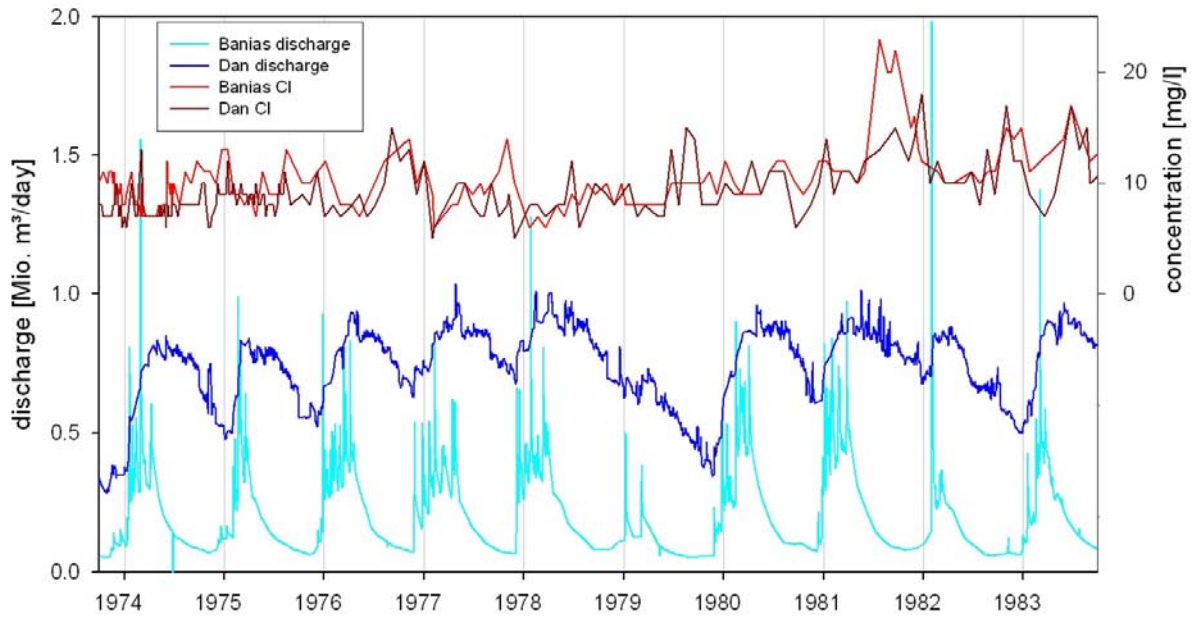

FIGURE 34: Hydrographs and chemographs of Cl of Banias Spring and Dan Spring from 1973/1974 to 1982/1983

Comparing the solute variations (FIGURE 34, FIGURE 35 and FIGURE 36) demonstrates that the hydrochemistry time series of NO_3 and SO_4 show significant seasonal trends whereas Cl seasonal fluctuations are not obviously showing seasonality. However Cl and NO_3 show very similar behaviour at both springs despite of their very distinct discharge variations. NO_3 maximum peaks are at the beginning of the raising tail and their minima at the falling tail of the Banias Spring seasonal discharge variations and close to the peak discharges of Dan Spring.

In contrast to the Cl and NO_3 fluctuations there is a big difference of SO_4 seasonal trend of both springs. Maximum values of SO_4 in the Banias Spring are up to seven times larger than the Dan Spring concentrations. Its maximum is at the minimum peak of discharge and its minimum at the maximum peak of discharge. According to SHIMRON, (1989) and KAFRI ET AL. (2002) BRIELMANN (2008) suggested that the difference of Dan and Banias Springs hydrochemistry is caused by a difference of bedrocks of the respective intake areas. In a slow diffusive process groundwater travels down to deeper layers where it gets in contact with the bedrock, where evaporites can be abundant, and it returns later to the shallow groundwater regions. This conclusion is also supported by NISSENBAUM (1978) who investigated the sulphur isotope distribution in SO_4. The results of his study showed that SO_4 contributions of surface water in the Upper Jordan River Catchments derive only from precipitation, with the exception of the Hermon stream, which also has a large contribution of marine SO_4, especially in summer.

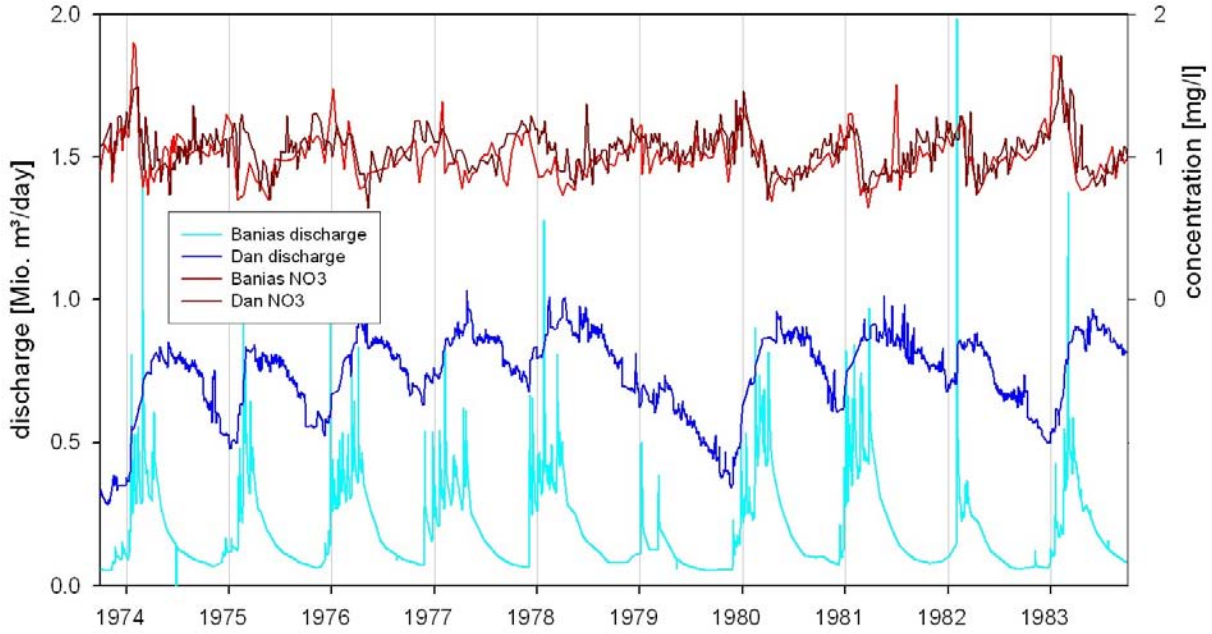

FIGURE 35: Hydrographs and chemographs of NO_3 of Banias Spring and Dan Spring from 1973/1974 to 1982/1983

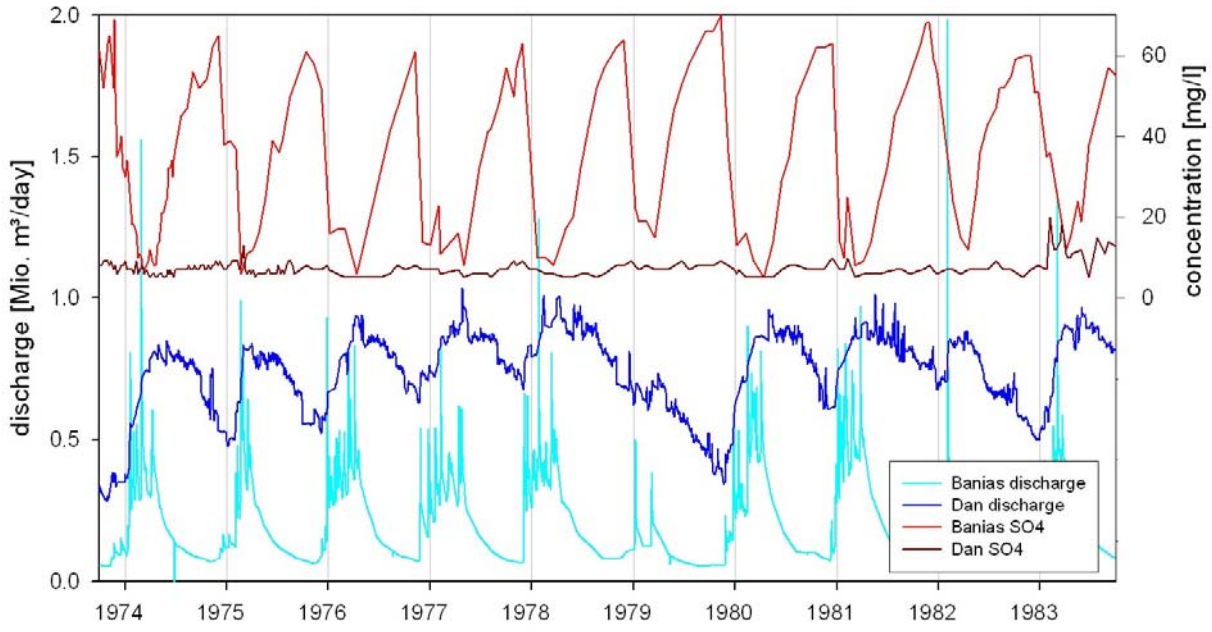

FIGURE 36: Hydrographs and chemographs of SO_4 of Banias Spring and Dan Spring from 1973/1974 to 1982/1983

6.3.2 Summary of comparison

The comparison between Cl, NO_3 and SO_4 variations of the both springs can be summarized as follows: since Cl and NO_3 variations of both springs are very similar it could be assumed that the origin of these waters is the same for both springs. Since it is assumed that there are no anthropogenic sources of NO_3 in Mt. Hermon input must be due to atmospheric deposition and decomposition of bio mass. Thus its variations might be caused by evaporation and biological processes. However, the variations of Cl seem to be produced by another mechanism which should be the same for both springs as well. The similar trend, in particular for NO_3, also indicates that Dan Spring is receiving also a big amount of surface near water. The significant differences in SO_4 variations could be an indicator for flow of a different kind which is water that came into contact with SO_4 containing bedrock, e.g. evaporites. As mentioned above this water is attributed to a slow travelling diffuse matrix component which might move through the fissure matrix of the bedrock. But just because the high SO_4 concentrations appear only in Banias Spring waters this is no proof that Dan Spring is not receiving waters from the same type of flow as well. It might just not have been got in contact with other rock because the geological conditions of the western side of the Sion-Rachaya fault are different as described in chapter 2. This theory could be proved by the differences of hydrographs: Dan Spring is acting far more continuously than Banias Spring. That might indicate that a diffuse matrix component is feeding the spring at least in the dry season.

6.4 Hydrograph separation

In order to identify the contribution of different origins hydrograph separations performed by BRIELMANN (2008) were reviewed and an own hydrograph separation was conducted.

6.4.1 Banias Spring

To separate event and pre-event water in Banias Spring BRIELMANN (2008) performed a two-component hydrograph separation according to SKLASH AND FARVOLDEN (1979). As tracer BRIELMANN (2008) used $\delta^{18}O$ values. Isotopic ratios for event and pre-event water are given in TABLE 5. The $\delta^{18}O$ ratio for pre-event water was taken from the spring discharge at baseflow conditions. The $\delta^{18}O$ ratio for event water was taken from the transsect of local enrichment lines from different springs and the local meteoric water line. The results are shown in TABLE 4. In both years pre-event water is yielding the major part of flow. Event

water contribution increases with the rainy season in December and January, and reaches its maximum in February 2002/2003 and March 2003/2004. The differences of the two years can be explained by the difference of annual precipitation: the year 2002/2003 was a relatively dry year whereas 2003/04 was a year with average annual precipitation (BRIELMANN, 2008).

TABLE 4: Contribution of event water (P_E) and pre-event water (P_{PE}) for the hydrological years 2002/2003 and 2003/2004 established by BRIELMANN (2008)

	Oct	Nov	Dec	Jan	Feb	Mar	Apr	May	Jun	Jul	Aug	Sep
2002/03												
P_E [%]		0	5	16	23	20	-	-	15	-	-	-
P_{PE} [%]		100	95	84	77	80	-	-	85	-	-	-
2003/04												
P_E [%]			0	20	21	42	35	17	6	4	-	-
P_{PE} [%]			100	80	80	58	65	83	94	96	-	-

It can be assumed that event water is representing at least a part of the karst conduit water. But it is not reasonable to attribute the pre-event water to the diffuse matrix flow alone (BRIELMANN, 2008). In chapter 3 the epikarst was already introduced as an important part of a karst system (also shown by PERRIN ET AL., 2003, EINSIEDL, 2005, or LEE AND KROTHE, 2003). Water which is originating from the epikarst has an own hydrochemical composition deriving from evaporation as well as from chemical and biological processes. Hence it should be identifiable as well.

For a three-component hydrograph separation BRIELMANN (2008) used again the $\delta^{18}O$ value and additionally SO_4 (the same combination of tracers used in LEE AND KROTHE, 2001) to distinguish a soil and epikarst component, a diffuse component, and a rain and snow component. The concentrations representing each component are listed in TABLE 5. SO_4 concentration of the rain and snow component is estimated by direct sampling (TABLE 3). Soil and epikarst concentrations were assumed to be represented by Si'on Spring (FIGURE 1) under baseflow conditions. Finally, the concentration of the diffusive matrix flow component was considered to be the concentration of Banias Spring discharge under baseflow conditions as well.

TABLE 5: Concentrations representing event and pre-event components for $\delta^{18}O$ (C_E and C_{PE}), rain and snow (C_{RS}), vadose zone (C_{VAD}) (i.e. the soil and epikarst) and diffuse matrix flow components (C_{DF}) for SO_4 for the hydrological years 2002/2003 and 2003/2004 (BRIELMANN, 2008)

Hydrological	$\delta^{18}O$		SO_4		
year	C_E [‰]	C_{PE} [‰]	C_{RS} [‰]	C_{VAD} [‰]	C_{DF} [‰]
2002/03	-8.19	-7.35	0.9	4.6	62.2
2003/04	-8.19	-7.4	0.9	4.6	57.2

Results of the separation can be seen in TABLE 6. They show that after separating pre-event water into two components the contribution of the diffuse matrix flow component is not as big as possibly supposed. Its contribution decreases to percentages of sometimes 10%, whereas the soil and epikarst component exceeds the 50% threshold in both of the years. In the dry year 2002/03 it even passes the 60% mark. In June 2003/04 epikarst contribution still yields a third of total spring discharge. This indicates that epikarst is also an important distribution and storage system in the Mt. Hermon hydrological system. It is responsible that there still is a contribution of shallow waters long after the end of the rainy season (BRIELMANN, 2008).

TABLE 6: Contribution of rain and snow (P_{RS}), vadose zone (P_{VAD}) and diffuse matrix flow (P_{DF}) for the hydrological years 2002/03 and 2003/04 established by BRIELMANN (2008)

	Oct	Nov	Dec	Jan	Feb	Mar	Apr	May	Jun	Jul	Aug	Sep
2002/03												
P_{RS} [%]		0	5	16	23	20	-	-	15	-	-	-
P_{VAD} [%]		0	25	60	65	66	-	-	55	-	-	-
P_{DF} [%]		100	70	24	12	14	-	-	30	-	-	-
2003/04												
P_{RS} [%]		0	20	21	42	35	17	6	4	-	-	
P_{VAD} [%]		0	42	70	48	47	54	43	32	-	-	
P_{DF} [%]		100	38	10	10	18	29	51	64	-	-	

To gain more understanding of the long term behaviour of Banias Spring mean and median monthly concentrations of the Cl, NO_3 and SO_4 were calculated using the whole range of available hydrochemical data. Results are shown in FIGURE 37 and the respective data in the Appendix in chapter A.3. Then the monthly median variations of Cl and SO_4 were used for another three-component hydrograph separation, also known as end-member mixing analysis, according to CHRISTOPHERSEN AND HOOPER (1992) and CHRISTOPHERSEN ET AL. (1990):

$$x(t) = l(t) \cdot B \tag{13}$$

Hereby, *x(t)* is 1 x *p* vector with the *p*-1 observed solute concentration at time t in the first columns and a one in the last column (representing the discharge), *l(t)* a 1 x *k* vector containing the contributions of the *k* components which are ought to be separated and *B* is a *k* x *p* matrix containing the chemical composition of the end-members in the first *p*-1 columns and ones in the last column (representing once again the discharge). Inverting matrix *B* gives the contribution of each component at time *t*:

$$l(t) = x(t) \cdot B^{-1} \tag{14}$$

In this case there are two solute observations, one discharge observation in each time step and three components. Thus $p = 3$ and $k = 3$ what means B is a square matrix and inverting it is fairly straightforward.

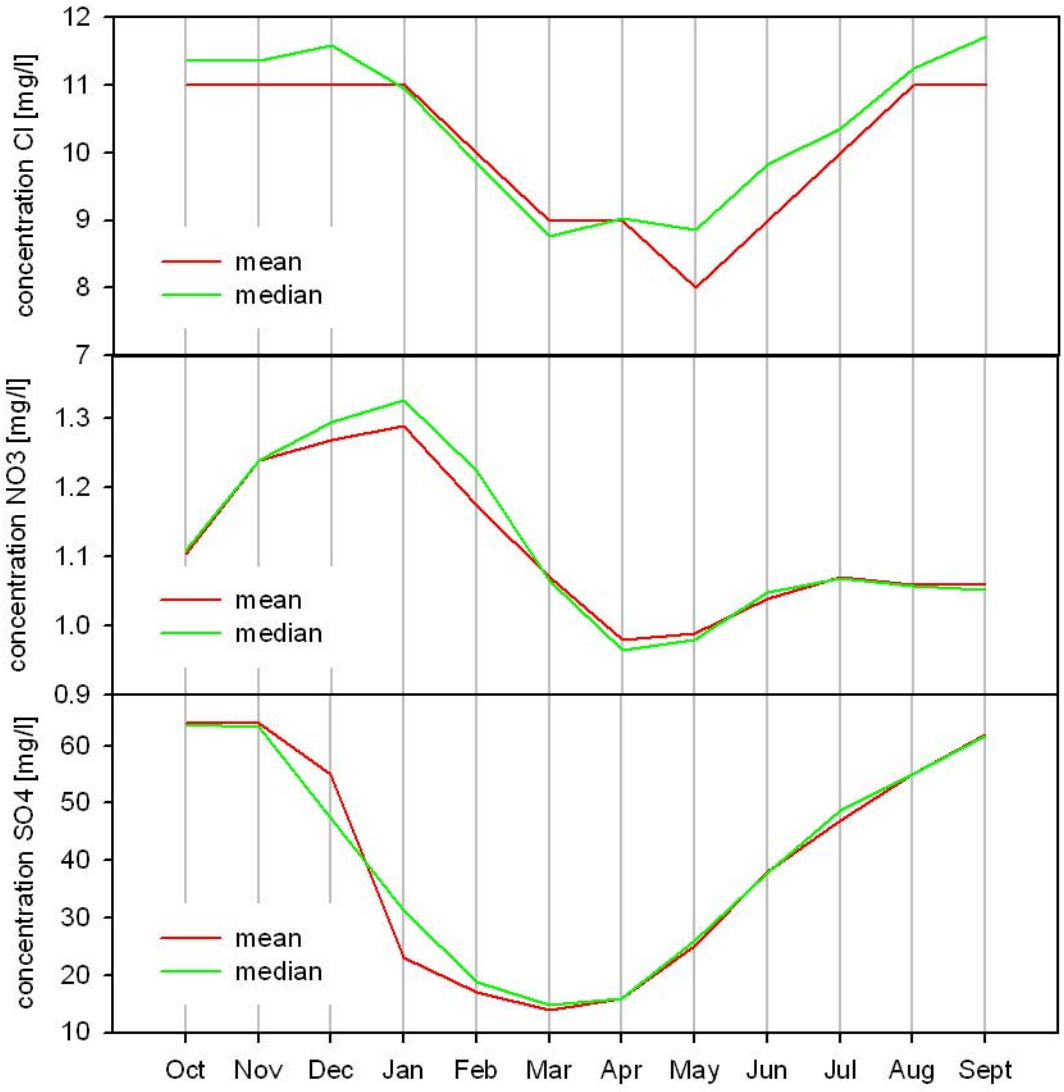

FIGURE 37: Mean and median variations of Cl, NO_3 and SO_4 of Banias Spring

As components for separation the same end-members as used in BRIELMANN (2008) were distinguished: snow and rain water, soil and epikarst water and diffuse matrix flow water. Concentrations for each component are listed in TABLE 7. Cl and SO_4 concentrations of the rain and snow component were taken from the rain and snow samples drawn by BRIELMANN (2008) (TABLE 3). Diffuse matrix flow concentrations were estimated equally to BRIELMANN

(2008) as the discharge concentrations of Cl and SO_4 under baseflow conditions. The SO_4 concentration of the soil and epikarst component was also adapted from BRIELMANN (2008). The estimation of the Cl concentration of the soil and epikarst component was done firstly by setting it equal to the diffuse matrix flow concentration (assuming that there is no additional source of Chloride). Secondly the end-members and median solute variations were then plotted into a mixing diagram (FIGURE 38). It can be seen that for all 12 months, values plot inside or very near to the triangle set by the end-members in TABLE 7 which indicates a proper choice of end-member concentrations.

TABLE 7: End member composition of rain/snow, soil/epikarst, and the diffuse matrix flow component

component	conc. Cl [mg/l]	conc. SO_4 [mg/l]
rain/snow	1.3	0.9
soil/epikarst	11	4.6
diffuse matrix flow	11	63

Applying equations (13) and (14) on these end-members and the median concentrations gives the median contribution of the three components each month which is shown in FIGURE 39. Contributions below zero and above one can be attributed to values slightly outside the end-member triangle in FIGURE 38. From January to April the soil and epikarst component yields the major part of discharge. From June to December it is the diffuse matrix flow component which dominates runoff. The rain and snow component contributes to discharge from February to July with contributions < 0.3 which can also be seen qualitatively in FIGURE 38: all values plot all in the right part of the mixing diagram. In May all three components contribute about the same parts.

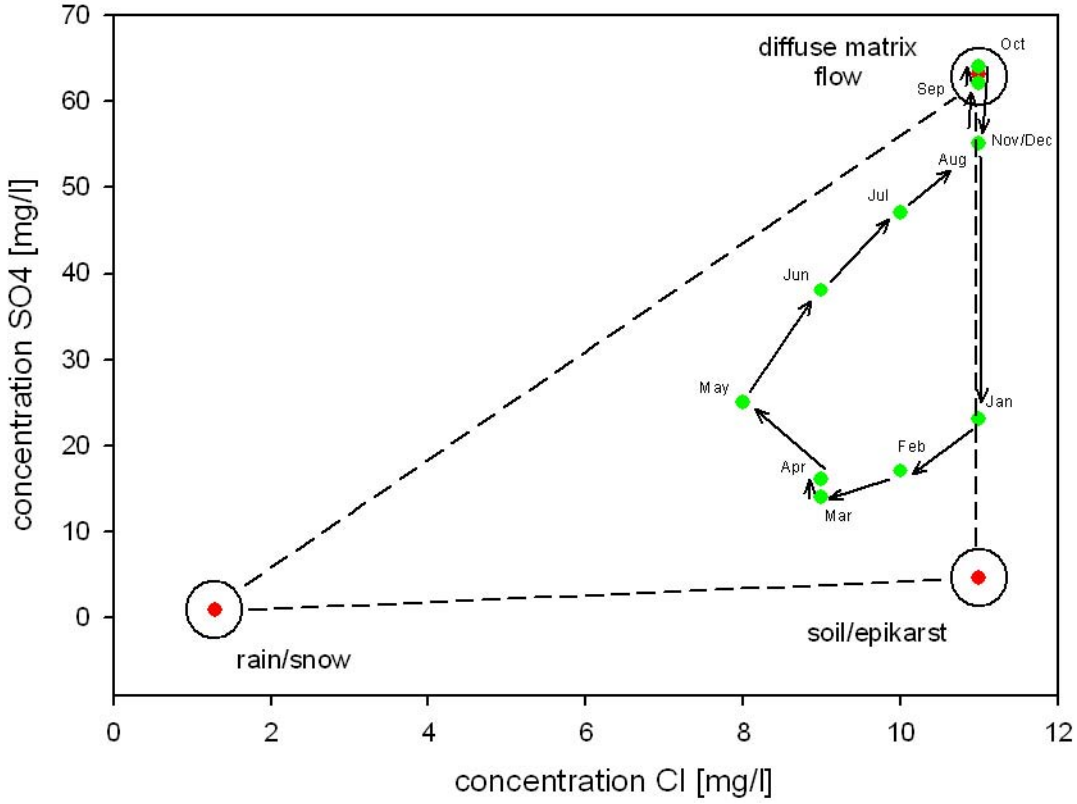

FIGURE 38: Mixing diagram of Cl and SO_4; red dots represent the end-members and the green dots the median mixing composition of the respective month

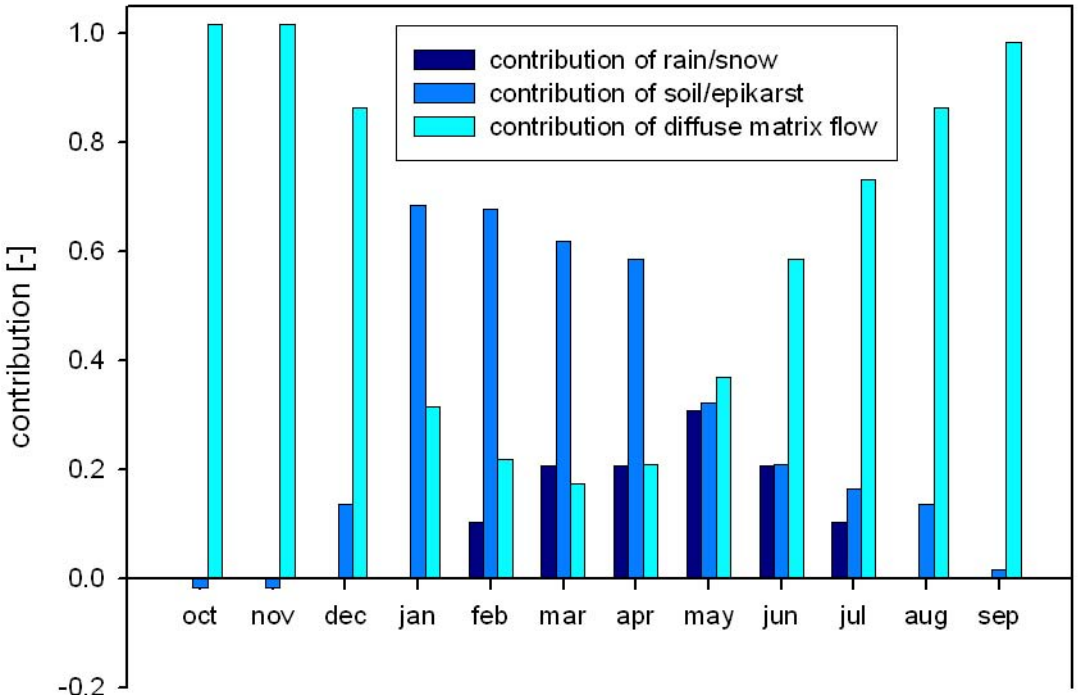

FIGURE 39: Contributions of the three components to total discharge

6.4.2 Dan Spring

BRIELMANN (2008) also performed a two-component hydrograph separation for Dan Spring assuming that there are just two different types of water inside the aquifer: newly arriving rain and snow water, and groundwater that resided in the aquifer for a longer period of time. Again she separated event and pre-event water using $\delta^{18}O$, SO_4 and Cl as tracers. The concentrations of event and pre-event waters for the hydrological years 2002/2003 and 2003/2004 are given in TABLE 8. Concentrations of event water were equally to the hydrograph separation for Banias Spring estimated using the rain and snow samples (TABLE 3). The concentrations of pre-event water were estimated by the baseflow concentration under low flow conditions (in this case October 2002 and October 2003).

TABLE 8: End-member concentrations for the hydrological years 2002/03 and 2003/04 at Dan Spring (BRIELMANN, 2008)

Hydrological	$\delta^{18}O$		SO_4		Cl	
Year	C_E [‰]	C_{PE} [‰]	C_E [mg/l]	C_{PE} [mg/l]	C_E [mg/l]	C_{PE} [mg/l]
2002/03	-8.19	-7.43	0.9	8.9	1.3	7.6
2003/04	-8.19	-7.4	0.9	7.6	1.3	6.6

The results of applying these end-member concentrations on the two-component separation are given in TABLE 9. Negative contributions are attributed to the low variations of the solutes and the $\delta^{18}O$ ratio and thus the relatively large analytical error (BRIELMANN, 2008).

TABLE 9: Contribution of event (E) and pre-event (PE) water to total discharge in 2002/03 and 2003/04 calculated with $\delta^{18}O$, SO_4 and Cl (BRIELMANN, 2008)

Hydr. year	Oct	Nov	Dec	Jan	Feb	Mar	Apr	May	Jun	Jul	Aug	Sep
2002/03												
P_E-$\delta^{18}O$ [%]	0	(-4)	(-4)	(-9)	(-13)	(-8)	0	19	24	-	-	-
P_{PE}-$\delta^{18}O$ [%]	100	-104	-104	-109	-113	-108	100	81	76	-	-	-
P_E-SO_4 [%]	0	10	12	9	1	(-6)	18	14	28	-	29	-
P_{PE}-SO_4 [%]	100	90	88	91	99	-106	82	86	72	-	71	-
P_E-Cl [%]	0	8	12	17	21	36	37	25	37	-	43	-
P_{PE}-Cl [%]	100	92	88	83	79	64	63	75	63	-	57	-
2003/04												
P_E-$\delta^{18}O$ [%]	0	(-6)	(-29)	(-23)	(-4)	14	18	9	15	12	-	-
P_{PE}-$\delta^{18}O$ [%]	100	-106	-129	-123	-104	86	82	91	85	88	-	-
P_E-SO_4 [%]	0	7	2	1	16	16	12	18	16	(-7)	-	-
P_{PE}-SO_4 [%]	100	93	98	99	84	84	88	82	84	-107	-	-
P_E-Cl [%]	0	1	0	(-3)	(-2)	7	8	20	19	(-12)	-	-
P_{PE}-Cl [%]	100	99	100	103	102	93	92	80	81	-112	-	-

Because of the strong uncertainties results were interpreted just qualitatively: they show that the pre-event component always contributes the major part of discharge regardless of the tracer considered. Generally first event water contributions can be observed in March. They reach their maximum in the early summer when contributions up to 37 % were calculated (Cl, June, 2002/2003). These results show that despite of the relatively continuous discharge behaviour of Dan Spring there is a fast component passing through. However its quantity is difficult to estimate due to the small variations of considered tracers and the thus resulting large analytical error as mentioned above (BRIELMANN, 2008). Yet there is still reason to assume the existence of a soil and epikarst component which is just not distinguishable from the diffuse matrix flow component because of the absence of geogene sources of SO_4 or other solutes as there are in the Banias Spring intake area.

6.4.3 Summary of hydrograph separations

Even though uncertainties in hydrograph separations allow more a qualitative interpretation (UHLENBROOK AND HOEG, 2003) they provided important information about the hydrological system of Mt. Hermon. The three-component hydrograph separations performed by BRIELMANN (2008) and the author of this diploma thesis prove that composition of Banias Spring water can be explained as the mixture of three sources: rain and snow melt the epikarst and deep, diffuse matrix flow groundwater. The contribution of a particular source is varying with the season with the soil/epikarst and the diffuse matrix flow component yielding the largest contributions in the rainy and the dry season, respectively. The Hydrograph separation for Dan Spring just showed that there is some contribution of event water. Since there was no way to separate more sources no information could be gained about the composition of pre-event water. The uncertainty of data was too large for further interpretations so no additional hydrograph separation was performed in this work. Instead of that a measurement campaign at Dan Spring was conducted to get some more information about its behaviour.

6.5 Measurement campaign

6.5.1 Preparation

Starting from 10th of January a measurement was started close to the Dan Spring outlet (see photos in the Appendix A.4: Photos of Dan Spring measurement campaign. The aim of drawing this data was to gain additional information about the small temporal scale behaviour of Dan Spring as well as to compare this data with the long-term data provided by the Mekorot. The devices used for this study are the CTD DIVER (water level, conductivity, water temperature) and the BARO DIVER (air temperature, air pressure) of Van Essen Instruments, and the 6920 V2 Multiparameter Water Quality Sonde of YSI incorporated (pH value, oxygen saturation). Since it was not available from the beginning, the YSI Water Quality Sonde was first installed 20th of February. Both DIVERs were programmed to log data every five minutes and the YSI Sonde was set to log every ten minutes.

The CTD DIVER measures the water level using a pressure sensor. It determines the whole pressure of water column and atmospheric pressure. Thus it needs to be corrected by the corresponding air pressure values measured by the BARO DIVER. The resolution of water level measurements is 2 cm and its accuracy is 0.1-0.2 % of the measured value. Temperature is measured by a semiconductor chip and it is used to correct temperature influence on the pressure measurements. Its resolution is 0.01 °C, and its accuracy 0.1 °C. Conductivity is measured by a four-electrode measurement cell. Temperature is again used for correction of measured conductivity to specific conductivity at 25 °C. Its precision is 1 % of the measured range and its resolution 1 µS/cm. Temperature and pressure measurement of the BARO DIVER work in the same way as the CDT DIVER. The YSI Sonde uses a field replaceable pH electrode for the determination of hydrogen ion concentration. The probe used thereby is a combination consisting of a proton sensitive glass reservoir filled with buffer at approximately pH 7 and an Ag/AgCl reference electrode. The potential difference between the buffer solution and the measured media is proportional to the pH of the media. Its accuracy is +/- 0.2 units and its resolution is 0.01 units. Dissolved oxygen is measured using the principle that dissolved oxygen quenches both the intensity and the lifetime of the luminescence associated with a certain dye. With this method the oxygen sensor reaches an accuracy of +/- 1% of the reading or of 1% air saturation (which ever is greater). Its resolution is 0.1 % air saturation.

6.5.2 Results

FIGURE 40 shows the data collected by the BARO DIVER and precipitation as vertical bars collected at El Rom meteorological station (about two kilometres west of Mt. Hermon at an elevation of 1050 m (data provided by Alon Rimmer). Air temperature shows an obvious diurnal variation and air pressure (expressed as cm water column) changes over some days representing the changing weather conditions.

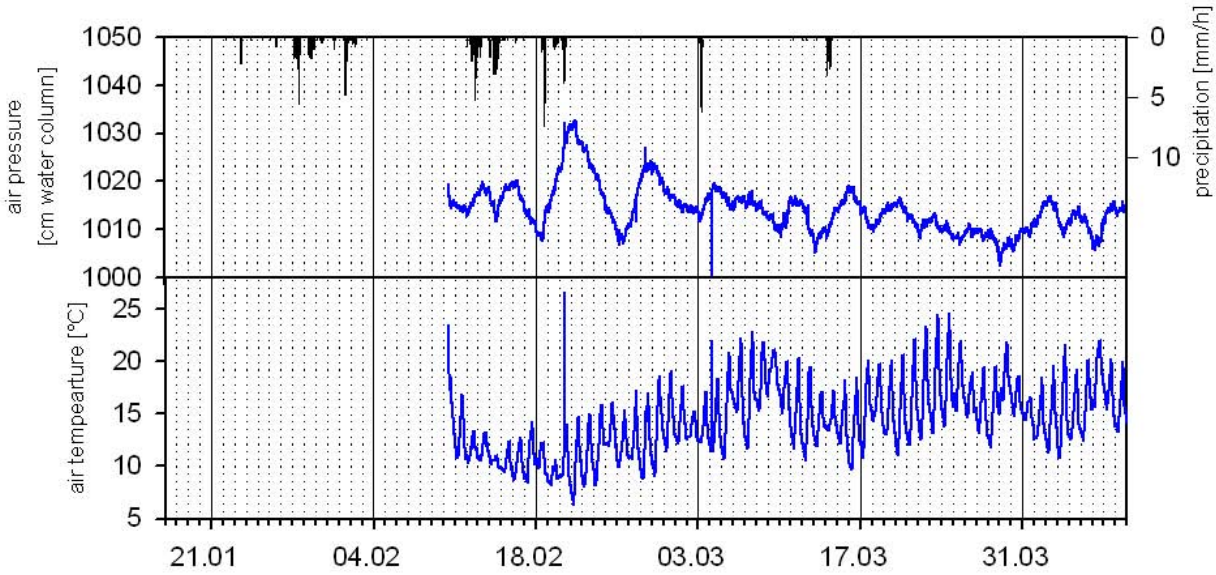

FIGURE 40: Air pressure and air temperature collected by the BARO DIVER

FIGURE 41 shows water level, conductivity and water temperature collected by the CDT DIVER and pH value and oxygen saturation collected by the YSI probe. Precipitation from El Rom meteorological station indicates that there was a rain event preceding the measurement campaign. This explains why water level is already rising from the 10th of January. Peak discharge is at the 15th of March. Then water level decreases first sharply then slower until the end of the campaign at 9th of April. Small fluctuation can be attributed to the influence of temperature and sunlight affecting the DIVER. Conductivity is decreasing in the first days of the campaign and then rising again until the end of February. After that it decreases again until 16th of March from then it keeps a constant value. Looking at the temperature one can see nearly the same behaviour: first, a slight decrease followed by an increase until 4th of March. Then again follows a decrease which ends quite simultaneous with the decrease of conductivity. The pH reacts in the same manner as the conductivity just in the opposite direction: at the beginning there is an increase of conductivity and a decrease of pH. Similarly the minimum value of pH is just at the conductivity maximum peak. Then it increases again

until it reaches a constant value at the end of February. The daily fluctuations can likewise be attributed to the fluctuations of temperature. Compared to the former variables variations of oxygen saturation can be divided into three parts. With the start of the campaign it decreases until 25th of February. This is followed by an increase to a plateau from the 29th of February to the 5th of March. Then it decreases rapidly to a nearly constant value within two days.

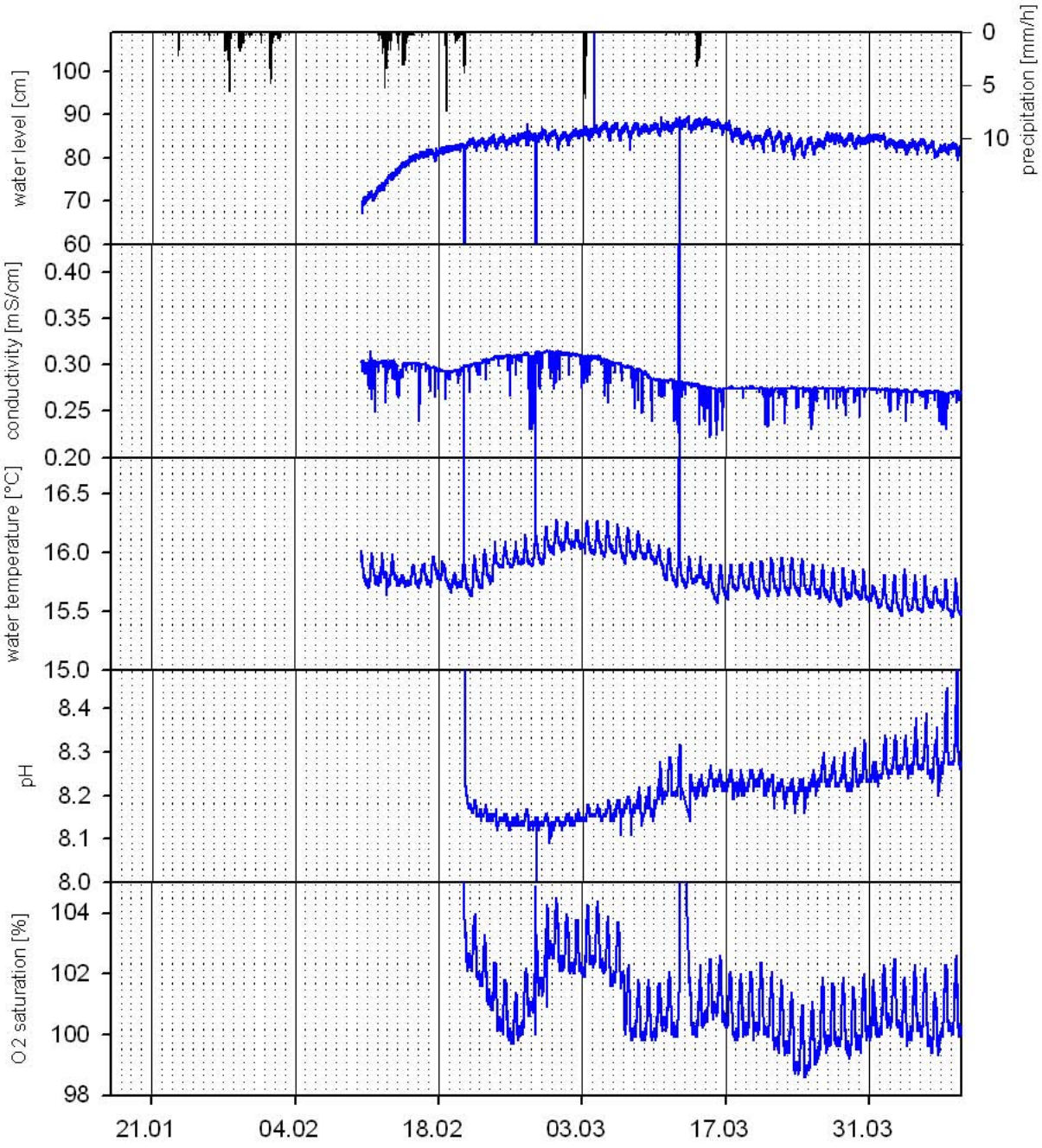

FIGURE 41: Water level, conductivity and , water temperature collected by the CTD DIVER, pH and O_2 saturation collected by the YSI Multiparameter Water Quality Sonde

6.5.3 Summary of measurement campaign

The behaviour of conductivity, water temperature and pH value might prove the pressing out of surface-near water. This would explain the higher conductivity which could then be attributed to the higher dissolution in the soil and epikarst (see chapter 3). Equally the lower pH might be an indicator of water which contains more free hydrogen ions due to decomposition processes in the soil. Higher values of water temperature also corroborate this theory: increasing temperature might be an indicator for warmer surface near water. This would imply that water reacing the counduits would come from lower regions than the water in the fissure storage which has a lower temperature. Only variations of oxygen are difficult to explain: the increase above 100 % saturation might only be explainable by the mixing of oxygen saturated waters with different temperatures which must have been taking place in the soil, the epikarst or the conduits if the theory established above is valid. However the major information that can be drawn from all variables in FIGURE 41 is that all of them recover to a constant value while water level is close to its peak value. This could be another proof that Dan Spring water is not only the mixture of rain/snow melt and a diffuse matrix component but also of an epikarst component. Whereby the diffuse matrix flow component, represented by the recovery values of the measured variables, is yielding a significant part to event discharge after the contribution of the surface-near waters already finished.

6.6 Conclusions

Hydrochemical characterisation showed that both springs have similar major ion compositions in the rainy season but they differ from each other hydrochemically during dry season. This was mainly attributed to diffuse matrix flow groundwater which came in contact with evaporates in the deeper layers of the bedrock. The comparison between the spring Cl and NO_3 variations gave reason to assume that both springs receive water from the same sources through out the seasons but in different proportions. Since there are no geogene sources for NO_3 its variation should have a superficial origin. However in dry season Banias Spring receives a significant contribution of SO_4 rich water which can be attributed to deep groundwater representing the diffuse matrix flow component of the system. Using hydrograph separation the contributions of rain/snow melt, surface-near soil/epikarst and diffuse matrix water could be estimated. Results showed that for Banias Spring the soil/epikarst contribution is yielding a large part of spring discharge ranging far into the dry season while the diffuse matrix water is dominates the dry season. Dan Spring hydrograph separation just showed that

this spring also receives some event (rain/snow melt) water but the accuracy of data was not good enough to draw more assumptions. This lack of information could partly be filled with the measurement campaign performed close to the Dan Spring outlet. Observations indicated that water reaching the spring during the time of observation originates from the soil and the epikarst. But its contribution finished almost in the middle of the hydrological event which is most probably caused by the switching of sources from the soil/epikarst to the diffuse matrix component. Thus the assumption of dominant contribution of diffuse matrix flow to Dan Spring can be supported whereas hydrograph separation showed that Banias Spring is more controlled by the soil/epikarst component. Hence both springs receive water from the same three sources: rain and snow melt, soil and epikarst and diffuse matrix flow. Just their individual contribution during the seasons is more or less pronounced: In the rainy season Banias Spring is dominated by water from the epikarst while Dan Spring still receives much water from the diffuse matrix component; event water contributions alternate with soil/epikarst water contributions. In the dry season both springs are dominated by diffuse matrix flow water slowly draining into the fissures and reaching the outlet. The different amounts of water from the epikarst and soil, and diffuse matrix flow at both springs might be a consequence of the different altitudes of their outlets; Dan Spring lies 159 m below Banias Spring, and karst exposures end below the Banias Spring level.

7 Development of a new model of groundwater flow: HYMKE_modified

As already shown in chapter 5 the groundwater module produced too strong smoothing of the solute concentrations at Dan Spring even though its predictions for the discharge were quite well. Similarly at Banias Spring discharge predictions were good but SO_4 variations could not be reproduced. Interpretation of hydrochemical data (chapter 6) gave clear evidence for a contribution of surface near originating water that is passed to both spring outlets quite rapidly. The contribution of SO_4 to Banias Spring discharge could be attributed to SO_4 enriched diffuse matrix flow water. Therefore a modification of the groundwater storage was necessary in which hydrochemical signal could be transferred rapidly to the spring's outlets without neglecting slow flow particularly for Dan Spring and, additionally, geogene contributions of SO_4 to the diffuse matrix flow component for Banias Spring had to be incorporated.

7.1 Incorporation of the duality of groundwater flow

In the new concept the incorporation of double porosity effects on groundwater flow, as introduced in chapter 3, was expected to lead to following results: on one hand, with the fast flow through the conduits, the input signal of the solute concentrations should be transposed rapidly to the spring outlet. And on the other hand slow discharge reaction should occur as a consequence of the slow draining fissure system. This process is typically taking place in karstic systems (chapter 3) and its abundance in Mt. Hermon hydrological system was proven in chapter 6. Therefore the conceptual model of HYMKE (FIGURE 20) was modified as described in FIGURE 42. For Dan and Banias Spring the groundwater reservoir was divided in two reservoirs: One reservoir representing the conduits and another representing the fissured storage. Exchange between the conduits and the fissured storage happens due to differences in water levels of the two reservoirs. Since the Dan Spring groundwater fissured storage is expected to be much larger than the Banias Spring groundwater its fissured storage was represented by a larger box (FIGURE 42). To exclude confusion the new version of HYMKE will be named HYMKE_modified to attribute for its modified groundwater routine.

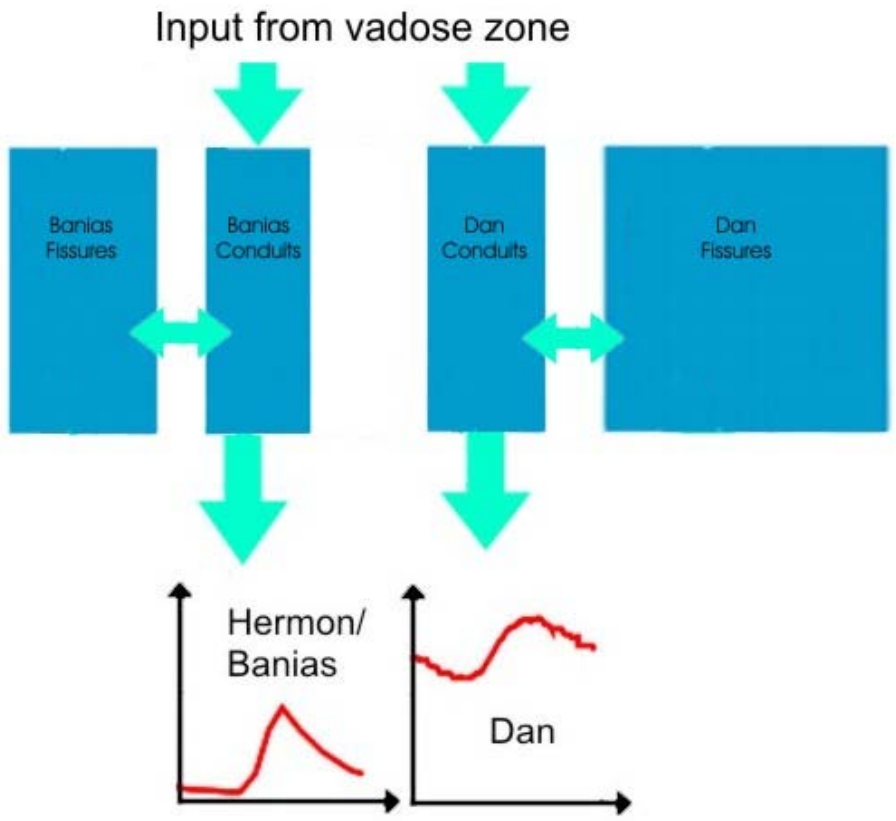

Figure 42: New conceptual model for the groundwater module in HYMKE

7.2 Mathematical application of the new conceptual model

7.2.1 Analytical solution for flows

For mathematical application a more schematic draft of the two exchanging groundwater systems was created (FIGURE 43). According to this conceptual model, and the assumption of linearity between water level and specific discharge, the specific flow between the conduit reservoir and the fissured aquifer $q_E(t)$ [m/day] is given by

$$q_E(t) = \frac{h_E(t)}{K_E}. \tag{15}$$

Here, $h_E(t)$ is the difference of water level of the two parallel reservoirs [m] and K_E is an exchange coefficient [day], similar to the α_0 used by MOHRLOCK (1995) in equation (8) and the K used by SUGARAWA (1995) in equation (10) as already shown in chapter 3.

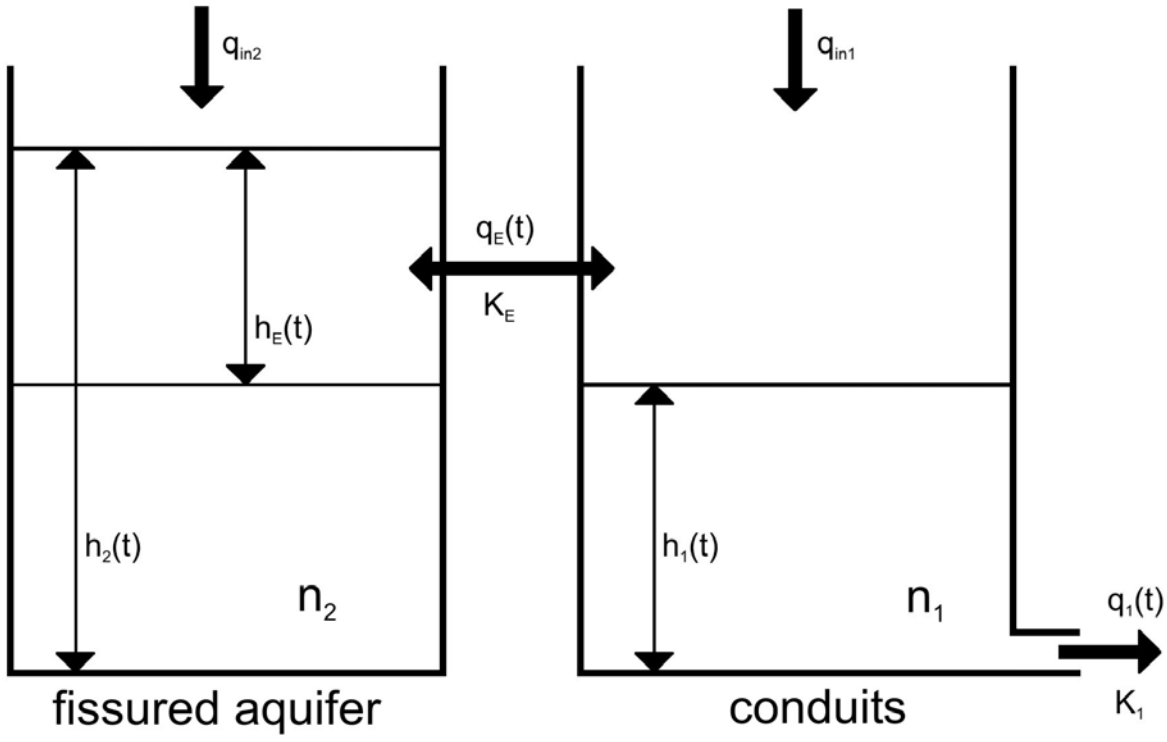

Figure 43: Schematic concept of the modified groundwater reservoir

Since linear reservoirs are based on the assumption that the outflow is linearly related to the stored volume the level of water column, which is obtained by dividing the volume by the catchment area, only represents the water level in a medium with a porosity of 100% or the porosity is included in the fitting parameter, the storage coefficient. However in media with two different porosities (FIGURE 43) a correction has to be performed to obtain the real difference of water levels $h_E(t)$. This is done by using the effective porosities of the two reservoirs n_1 and n_2:

$$h_E(t) = \frac{h_2(t)}{n_2} - \frac{h_1(t)}{n_1} \tag{16}$$

Whereby $h_1(t)$ and $h_2(t)$ are the levels of the water columns [m], and n_1 and n_2 are the effective porosities of the conduits and the fissured aquifer [-]. Note that in equation (10) SUGARAWA (1995) used the maximum volumes of the two parallel storages to reach the same goal. n_1 and n_2 can either be measured in the field before or be used as parameters in calibration if they are unknown. If $h_2(t) > h_1(t)$, $h_E(t)$ and thus $q_E(t)$ are positive; the exchange flow direction is from the fissured aquifer to the conduits. However if $h_1(t) > h_2(t)$, the opposite occurs. For the

linear relation of water level $h_1(t)$ and specific discharge of the conduits $q_1(t)$ simply the level of water column can be used because no comparison has to be made:

$$q_1(t) = \frac{h_1(t)}{K_1}. \tag{17}$$

Here K_1 represents the storage coefficient of the conduit reservoir [day]. Using again mass balance equations the change of water column $\partial h_1(t)/\partial t$ and $\partial h_2(t)/\partial t$ in the conduits and the fissured aquifer [m/day], respectively, can now be calculated:

$$\begin{aligned} \frac{\partial h_1(t)}{\partial t} &= -q_1(t) + q_E(t) + q_{in1} \\ \frac{\partial h_2(t)}{\partial t} &= -q_E(t) + q_{in2} \end{aligned} \tag{18}$$

Here q_{in1} and q_{in2} are the inflows to the conduits and the fissured aquifer and constant for each time step of the model [m/day]. Substituting equations (15), (16) and (17) into equation (18), and using the differential operator $D = \partial/\partial t$ [1/day], the following linear equation system can be obtained:

$$\begin{pmatrix} D + \left(\frac{1}{K_1} + \frac{1}{K_E n_1}\right) & -\frac{1}{K_E n_2} \\ -\frac{1}{K_E n_1} & D + \frac{1}{K_E n_2} \end{pmatrix} \cdot \begin{pmatrix} h_1(t) \\ h_2(t) \end{pmatrix} = \begin{pmatrix} q_{in1} \\ q_{in2} \end{pmatrix}. \tag{19}$$

For the following calculations, Cramer's rule will be used which is

$$Zx = c. \tag{20}$$

Whereby Z is a convertible square matrix, x a vector of n unknown variables and c a vector of n known constants. To eliminate all elements of x except i^{th} $x_i, 1 \le i \le n$, the determinant is used:

$$\det(Z)x_i = \det(Z_i). \tag{21}$$

Hereby Z_i is the matrix Z with the i^{th} column replaced by the vector c. Applying this rule on equation (19) gives

$$\frac{\partial^2 h_1(t)}{\partial t^2}+\left(\frac{1}{K_1}+\frac{1}{K_E n_1}+\frac{1}{K_E n_2}\right)\frac{\partial h_1(t)}{\partial t}+\frac{1}{K_E^2 n_1 n_2}h_1(t)=\frac{q_{in1}}{K_E n_2}+\frac{q_{in2}}{K_E n_2} \tag{22}$$

and

$$\frac{\partial^2 h_2(t)}{\partial t^2}+\left(\frac{1}{K_1}+\frac{1}{K_E n_1}+\frac{1}{K_E n_2}\right)\frac{\partial h_2(t)}{\partial t}+\frac{1}{K_E^2 n_1 n_2}h_2(t)=\frac{q_{in1}}{K_E n_1}+\frac{q_{in2}}{K_1}+\frac{q_{in2}}{K_E n_1} \tag{23}$$

The homogeneous parts of equations (22) and (23) are equal what means that the general part of both solutions is identical, too. To solve the homogeneous part the solution of the characteristic equation has to be calculated:

$$\begin{aligned}&\lambda^2+\left(\frac{1}{K_1}+\frac{1}{K_E n_1}+\frac{1}{K_E n_2}\right)\lambda+\frac{1}{K_1 K_E n_2}=0\\ &\Rightarrow \lambda_{1/2}=A_{1/2}=-\frac{1}{2}\left(\frac{1}{K_1}+\frac{1}{K_E n_1}+\frac{1}{K_E n_2}\right)\pm\sqrt{\frac{\left(\frac{1}{K_1}+\frac{1}{K_E n_1}+\frac{1}{K_E n_2}\right)^2}{4}-\frac{1}{K_1 K_E n_2}}\end{aligned} \tag{24}$$

Since they are constants the solutions of the characteristic equation will be substituted by $A_{1/2}$ in further formulations. With this the general solution of equations (22) and (23) is

$$h_{1/2}(t)=B_{1/3}\exp(A_1 t)+B_{2/4}\exp(A_2 t)\,. \tag{25}$$

Where B_1, B_2, B_3 and B_4 are constants [m] which will be determined later using the initial conditions. To include also the inhomogeneous part of equations (22) and (23), one particular solution of equations (22) and (23) has to be found. The is done by setting

$$h_1(t)=C_1 \tag{26}$$

and

$$h_2(t) = C_2 \tag{27}$$

Substituting equations (26) and (27) in equations (22) and (23), the special solutions can be obtained:

$$\begin{aligned} C_1 &= K_1(q_{in1} + q_{in2}) \\ C_2 &= K_1 \frac{n_2}{n_1}(q_{in1} + q_{in2}) + K_E n_2 q_{in2} \end{aligned} \tag{28}$$

Summarizing the general part (equation (25)) and the special part of the solution (equations (28)) yields the whole solution for both reservoirs:

$$\begin{aligned} h_1(t) &= B_1 \exp(A_1 t) + B_2 \exp(A_2 t) + C_1 \\ h_2(t) &= B_3 \exp(A_1 t) + B_4 \exp(A_2 t) + C_2 \end{aligned} \tag{29}$$

By using the initial conditions

$$\begin{aligned} h_1(t=0) &= h_{10} \\ h_2(t=0) &= h_{20} \end{aligned} \tag{30}$$

and

$$\begin{aligned} \frac{\partial h_1(t=0)}{dt} &= -\frac{h_{10}}{K_1} + \frac{h_{20}}{K_E n_2} - \frac{h_{10}}{K_E n_1} + q_{in1} \\ \frac{\partial h_2(t=0)}{dt} &= -\frac{h_{20}}{K_E n_2} + \frac{h_{10}}{K_E n_1} + q_{in2} \end{aligned} \tag{31}$$

the constants in equations (29) can be found:

$$
\begin{aligned}
B_1 &= \frac{\frac{\partial h_1(t=0)}{\partial t} - A_2 h_{10} + A_2 C_1}{A_1 - A_2} \\
B_2 &= h_{10} - B_1 - C_1 \\
B_3 &= \frac{\frac{\partial h_2(t=0)}{\partial t} - A_2 h_{20} + A_2 C_2}{A_1 - A_2} \\
B_4 &= h_{20} - B_3 - C_2
\end{aligned}
\tag{32}
$$

7.2.2 Analytical solution for mixing

To calculate solute concentrations at the spring outlets mass balance equations for the solutes were also applied to the modified groundwater reservoir:

$$
\begin{aligned}
\frac{\partial m_1(t)}{\partial t} &= -m_{out1}(t) + m_E(t) + m_{in1} \\
\frac{\partial m_2(t)}{\partial t} &= -m_E(t) + m_{in2} + m_{dif}
\end{aligned}
\tag{33}
$$

Hereby $\partial m_1(t)/\partial t$ and $\partial \mathrm{m}_2(\mathrm{t})/\partial \mathrm{t}$ are the change of solute mass [g/m²/day], m_{in1} and m_{in2} the constant input of mass into the conduits and the fissured aquifer each time step [g/m²/day], $m_{out1}(t)$ the outflow of solute mass at the spring outlet [g/m²/day] and $m_E(t)$ the exchange of solute mass between the two reservoirs [g/m²/day]. An additional constant m_{dif} was added to the fissured aquifer mass balance to account for intrinsic input of solute mass [g/m²/day] as it can be observed for the SO_4 at Banias Spring (chapter 6).

Now masses are substituted by the respective concentrations and volumes:

$$
\begin{aligned}
m_1(t) &= c_1(t) h_1(t) \\
m_2(t) &= c_2(t) h_2(t)
\end{aligned}
\tag{34}
$$

and

$$
m_{out1} = c_1(t) q_1(t) \tag{35}
$$

Hereby $c_1(t)$ and $c_2(t)$ are the concentrations [g/m³] of the considered solute in reservoir 1 and 2, respectively. It is assumed that outflow concentration $c_1(t)$ equals the concentration of water stored in reservoir 1 at time step t.

For exchange of solute mass between the reservoirs $m_E(t)$ a distinction of cases has to be performed since flow to one reservoir has always the concentration of the other reservoir where water and solute mass is coming from:

$$m_E(t) = \begin{cases} c_1(t) q_E(t) & \leftrightarrow \quad q_E(t) \leq 0 \\ c_2(t) q_E(t) & \leftrightarrow \quad q_E(t) > 0 \end{cases} \tag{36}$$

Substituting equations (34),(35) and (36) in (33), under the use of equations (15), (16) and (17), we obtain for $q_E(t) \leq 0$:

$$\begin{aligned} \frac{\partial(c_1(t)h_1(t))}{\partial t} &= -c_1(t)q_1(t) + c_1(t)q_E(t) + m_{in1} \\ \frac{\partial(c_2(t)h_2(t))}{\partial t} &= -c_1(t)q_E(t) + m_{in2} + m_{dif} \end{aligned} \tag{37}$$

And for $q_E(t) > 0$:

$$\begin{aligned} \frac{\partial(c_1(t)h_1(t))}{\partial t} &= -c_1(t)q_1(t) + c_2(t)q_E(t) + m_{in1} \\ \frac{\partial(c_2(t)h_2(t))}{\partial t} &= -c_2(t)q_E(t) + m_{in2} + m_{dif} \end{aligned} \tag{38}$$

First the case $q_E(t) \leq 0$ will be considered. Applying the product rule the change of concentration for each reservoir can be calculated:

$$\frac{\partial c_1(t)}{\partial t} h_1(t) = -c_1(t)q_1(t) + c_1(t)q_E(t) + m_{in1} - c_1(t)\frac{\partial h_1(t)}{\partial t} \tag{39}$$

and

$$\frac{\partial c_2(t)}{\partial t} h_2(t) = -c_1(t)q_E(t) + m_{in2} + m_{dif} - c_2(t)\frac{\partial h_2(t)}{\partial t} \tag{40}$$

Since the change of water level in the reservoirs $\partial h_1(t)/\partial t$ and $\partial h_2(t)/\partial t$ are known from equations (18), they can be substituted. This leads to

$$\frac{\partial c_1(t)}{\partial t} = -\frac{q_{in1}}{h_1(t)} c_1(t) + \frac{m_{in1}}{h_1(t)} \tag{41}$$

and

$$\frac{\partial c_2(t)}{\partial t} = -\frac{(-q_E(t) + q_{in2})}{h_2(t)} c_2(t) - \frac{q_E(t)}{h_2(t)} c_1(t) + \frac{m_{in2}}{h_2(t)} + \frac{m_{dif}}{h_2(t)} \tag{42}$$

Since equation (41) is not dependent on equation (42), it will be solved first. To do this more clearly, following substitutions will be made:

$$\begin{aligned} D_1(t) &= -\frac{q_{in1}}{h_1(t)} \\ E_1(t) &= \frac{m_{in1}}{h_1(t)} \end{aligned} \tag{43}$$

Using equations (43) the homogeneous part of equations (41) can easily be solved:

$$c_1(t) = K \exp\left(\int_{t_0}^{t} D_1(\tau) \partial \tau \right) \tag{44}$$

Where K is an unknown constant and t_0 is the starting point of integration which is also constant. Applying now the method of variation of parameters also the inhomogeneous part of equation (41) can be solved:

$$c_1(t) = K(t) \exp\left(\int_{t_0}^{t} D_1(\tau) \partial \tau \right) \tag{45}$$

$$\Downarrow$$

$$\frac{\partial c_1(t)}{\partial t} = \frac{\partial K(t)}{\partial t} \exp\left(\int_{t_0}^{t} D_1(\tau) \partial \tau \right) + D_1(t) c_1(t) \tag{46}$$

Substituting equation (46) in equation (41) results in

$$\frac{\partial K(t)}{\partial t} = E_1(t)\exp\left(-\int_{t_0}^{t} D_1(\tau)\partial\tau\right) \tag{47}$$

$$\Downarrow$$

$$K(t) = \int_{t_0}^{t} E_1(\tau)\exp\left(-\int_{t_0}^{\tau} D_1(\mu)\partial\mu\right)d\tau + C_3 \tag{48}$$

Where C_3 again is an unknown constant which will be determined later using the initial conditions. With equation (48) substituted in equation (45), the whole solution for $c_1(t)$ is provided:

$$c_1(t) = \left[\int_{t_0}^{t} E_1(\tau)\exp\left(-\int_{t_0}^{\tau} D_1(\mu)\partial\mu\right)d\tau + C_3\right]\exp\left(\int_{t_0}^{t} D_1(\tau)\partial\tau\right) \tag{49}$$

Now equation (42) can be solved equally by defining

$$D_2(t) = \left(\frac{q_E(t)}{h_2(t)} - \frac{q_{in2}}{h_2(t)}\right), \tag{50}$$

$$E_2(t) = -\frac{q_E(t)}{h_2(t)}c_1(t) + \frac{m_{in2} + m_{dif}}{h_2(t)} \tag{51}$$

and applying once again the method of variation of parameters, the solution of $c_2(t)$ is found:

$$c_2(t) = \left[\int_{t_0}^{t} E_2(\tau)\exp\left(-\int_{t_0}^{\tau} D_2(\mu)\partial\mu\right)d\tau + C_4\right]\exp\left(\int_{t_0}^{t} D_2(\tau)\partial\tau\right) \tag{52}$$

whereby C_4 is likewise unknown.

In the second case, $q_E(t) > 0$, an analogue proceeding is performed. Applying the product rule on equations (38) leads to

$$\frac{\partial c_1(t)}{\partial t}h_1(t) = -c_1(t)q_1(t) + c_2(t)q_E(t) + m_{in1} - c_1(t)\frac{\partial h_1(t)}{\partial t} \tag{53}$$

and

$$\frac{\partial c_2(t)}{\partial t} h_2(t) = -c_2(t) q_E(t) + m_{in2} + m_{dif} - c_2(t) \frac{\partial h_2(t)}{\partial t} \tag{54}$$

Substituting again the known changes of water level from equations (18) gives

$$\frac{\partial c_1(t)}{\partial t} = -\frac{q_E(t) + q_{in1}}{h_1(t)} c_1(t) + \frac{q_E(t)}{h_1(t)} c_2(t) + \frac{m_{in1}}{h_1(t)} \tag{55}$$

and

$$\frac{\partial c_2(t)}{\partial t} = -\frac{q_{in2}}{h_2(t)} c_2(t) + \frac{m_{in2} + m_{dif}}{h_2(t)} \tag{56}$$

In this case the change of concentration in reservoir 2 (equation (56)) is not dependent on the change of concentration in reservoir 1 (equation (55)). Thus equations (55) and (56) can be solved in the same way as it was done in the first case: defining

$$D_4(t) = -\frac{q_{in2}}{h_2(t)} \tag{57}$$

$$E_4(t) = \frac{m_{in2} + m_{dif}}{h_2(t)} \tag{58}$$

and

$$D_3(t) = -\frac{q_E(t)}{h_1(t)} + \frac{q_{in1}}{h_1(t)} \tag{59}$$

$$E_3(t) = \frac{q_E(t)}{h_1(t)} c_2(t) + \frac{m_{in1}}{h_1(t)} \tag{60}$$

results in

$$c_1(t) = \left[\int_{t_0}^{t} E_3(\tau) \exp\left(-\int_{t_0}^{\tau} D_3(\mu)\partial\mu \right) d\tau + C_5 \right] \exp\left(\int_{t_0}^{t} D_3(\tau)\partial\tau \right) \tag{61}$$

and

$$c_2(t) = \left[\int_{t_0}^{t} E_4(\tau) \exp\left(-\int_{t_0}^{\tau} D_4(\mu)\partial\mu \right) d\tau + C_6 \right] \exp\left(\int_{t_0}^{t} D_4(\tau)\partial\tau \right). \tag{62}$$

where C_5 and C_6 are unknown constants once again. Using the initial conditions

$$\begin{aligned} c_1(t=0) &= c_{10} \\ c_2(t=0) &= c_{20} \end{aligned} \tag{63}$$

and setting t_0=0 allows the determination of the unknown constants C_3, C_4, C_5 and C_6 in equations (49), (52), (61) and (62). Since integration is from t_0=0 to t=0 all integrals in this equations become zero. So the calculation of the unknown constants is fairly simple:

$$\begin{aligned} C_3 &= C_5 = c_{10} \\ C_4 &= C_6 = c_{20} \end{aligned} \tag{64}$$

With it the solution for the mixing in the modified reservoir is finally given by

$$\left.\begin{aligned} c_1(t) &= \left[\int_{t_0}^{t} E_1(\tau) \exp\left(-\int_{t_0}^{\tau} D_1(\mu)\partial\mu \right) d\tau + c_{10} \right] \exp\left(\int_{t_0}^{t} D_1(\tau)\partial\tau \right) \\ c_2(t) &= \left[\int_{t_0}^{t} E_2(\tau) \exp\left(-\int_{t_0}^{\tau} D_2(\mu)\partial\mu \right) d\tau + c_{20} \right] \exp\left(\int_{t_0}^{t} D_2(\tau)\partial\tau \right) \end{aligned}\right\} \text{for } q_E(t) \le 0 \tag{65}$$

and

$$\left.\begin{aligned} c_1(t) &= \left[\int_{t_0}^{t} E_3(\tau)\exp\left(-\int_{t_0}^{\tau} D_3(\mu)\partial\mu\right)d\tau + c_{10}\right]\exp\left(\int_{t_0}^{t} D_3(\tau)\partial\tau\right) \\ c_2(t) &= \left[\int_{t_0}^{t} E_4(\tau)\exp\left(-\int_{t_0}^{\tau} D_4(\mu)\partial\mu\right)d\tau + c_{20}\right]\exp\left(\int_{t_0}^{t} D_4(\tau)\partial\tau\right) \end{aligned}\right\} \text{for } q_E(t) > 0 \quad (66)$$

7.2.3 Acknowledgments

Since it was not possible to find primitives for the integrals in equations (65) and (66), they will be solved numerically in the model by using the trapezoidal rule. Source code for the implementations of these analytical solutions can be found in the Appendix A.5: Source codes of the modified groundwater routine.

8 Application of HYMKE_modified

8.1 Sensitivity analysis of the modified groundwater routine

To gain a better understanding of the new groundwater module behaviour synthetic data was applied. A five day rain event (20 mm/d) was created with a following dry period of 45 days. Initial water levels and initial solute masses $m_1(t=0)$ and $m_2(t=0)$ were set to arbitrary values. The synthetic data was applied in a loop until stationary conditions were reached (500 to 1000 loops). Whereby the porosities were taken as constant: n_1=0.01% and n_2=1.0% according to MALOSZEWSKI (2002) and BRIELMANN (2008). Very small storage constants K_1 were used for the conduit reservoir: K_1 = {5, 15, 25}. For each K_1 different exchange coefficients K_E were applied: K_E = {10, 50, 100, 200, 500, 1000}. K_E as introduced in equation (15), is an abstract number. To make it more comparable to the storage coefficients of common linear reservoirs equations (15) and (16) were rearranged as follows:

$$q_E = \frac{h_E(t)}{K_E} = \frac{h_2(t)}{K_E n_2} - \frac{h_1(t)}{K_E n_1} = \frac{h_2(t)}{K_{E2}} - \frac{h_1(t)}{K_{E1}} \tag{67}$$

The constants K_{E1} and K_{E2} now include the porosities of the particular reservoir. Imagine now that the water column level in reservoir 1, the conduits, would be equal to zero. Then the exchange flow from the fissured reservoir would be equal to the outflow of a common linear reservoir with a water column of $h_2(t)$ and a storage constant of K_{E2}. The same is valid for flow in the opposite direction (with a water column of $h_1(t)$ and a storage coefficient of K_{E1}). The relation between K_{E1} and K_{E2} is therefore given by

$$\frac{K_{E1}}{K_{E2}} = \frac{n_1}{n_2} \tag{68}$$

Since for explaining the recession behaviour of spring discharge the outflow from the fissured aquifer to the conduits is more important than the flow in the opposite direction K_{E2} will be used for calibration in the following chapters (but further referred to as K_E). The source code including the generation of the synthetic data and the solutions for water levels and input concentrations can be found in the Appendix A.5: Source codes of the modified groundwater routine.

Comparing first the conduit discharge for a constant K_1 and a varying K_E in FIGURE 44, FIGURE 45 and FIGURE 46 it can be observed that during the rain event peak discharge is decreasing with decreasing K_Es. That means that with smaller K_Es more water is exchanging to the fissured aquifer while less water exchanges with large K_Es. Looking at the exchange flow on the right side of the figures the most negative values of exchange flow during the events can be found for the smallest K_Es. During the dry period exchange flow is positive and has the highest values for small K_Es as well. This is logical because if there is much flow into the fissured aquifer during the events due to a small K_E more water will come back again in the dry period.

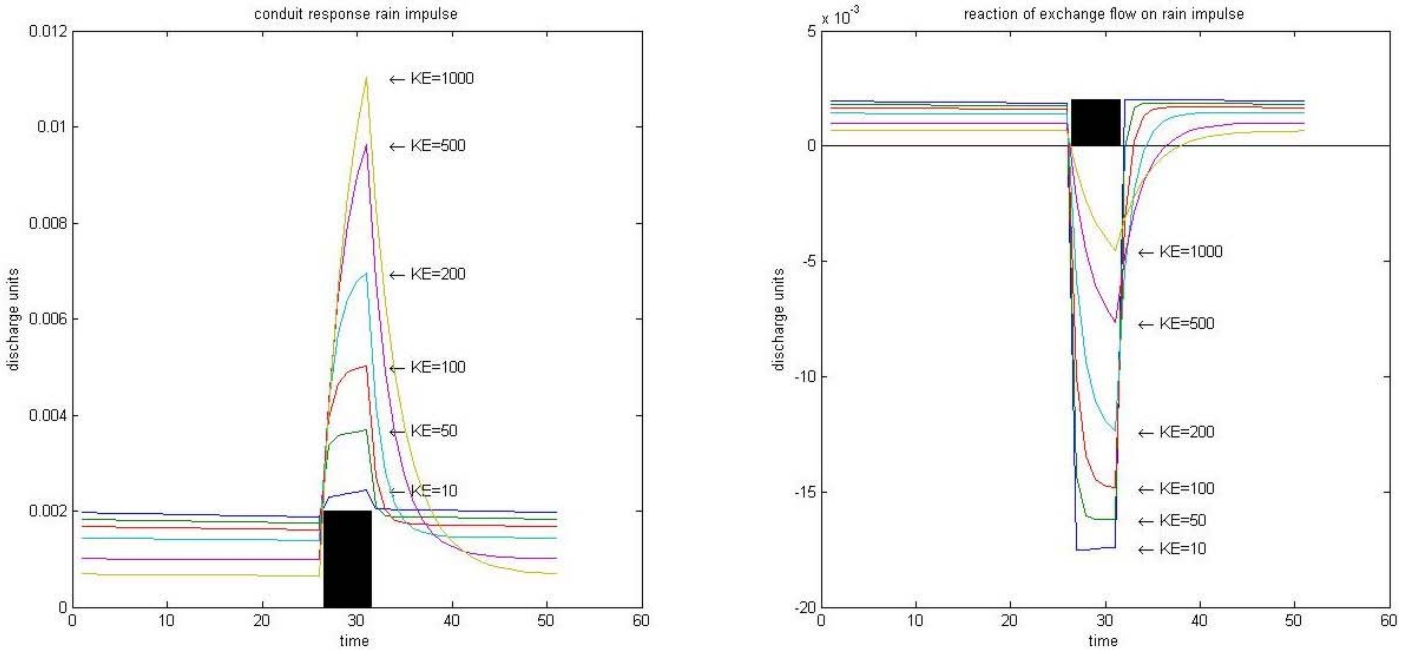

FIGURE 44: Response of the modified reservoir on a synthetic event using different K_Es and K_1=5 days; left: response of conduit outlet, right: response of exchange flow; the black bar represents the recharge event

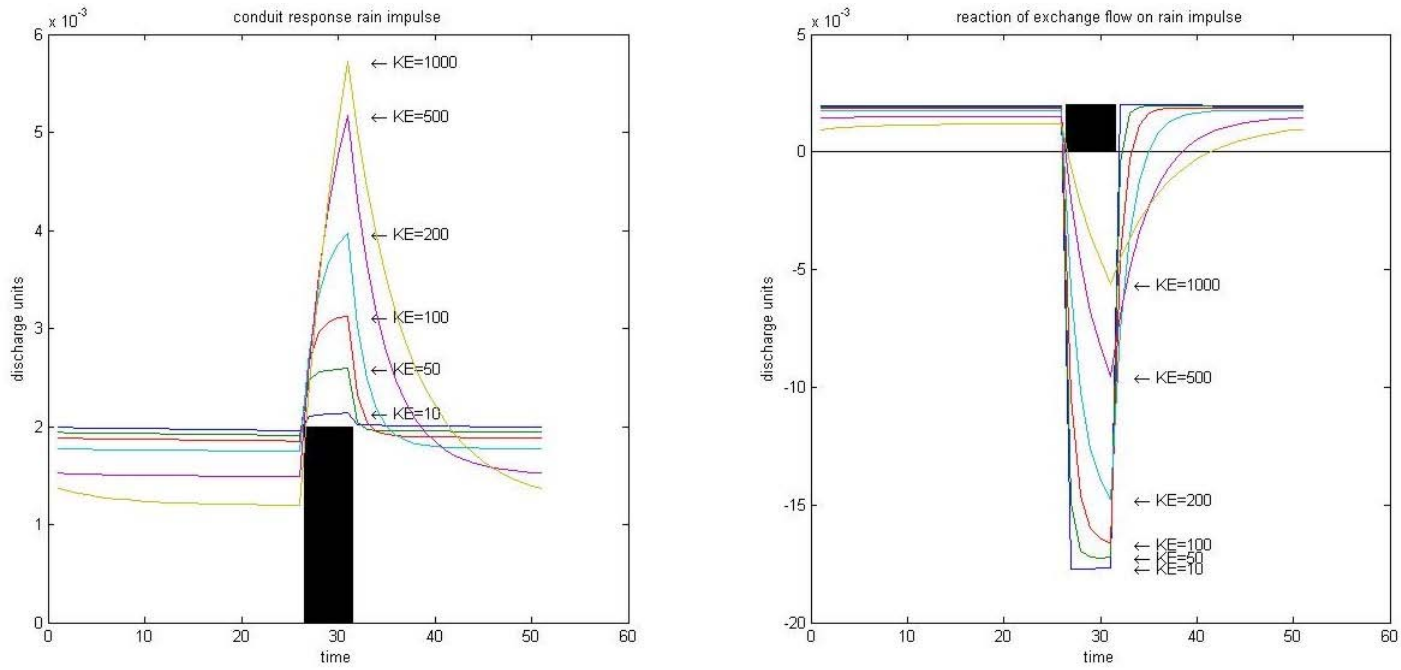

FIGURE 45: Response of the modified reservoir on a synthetic event using different K_Es and K_1=15; left: response of conduit outlet, right: response of exchange flow; the black bar represents the recharge event

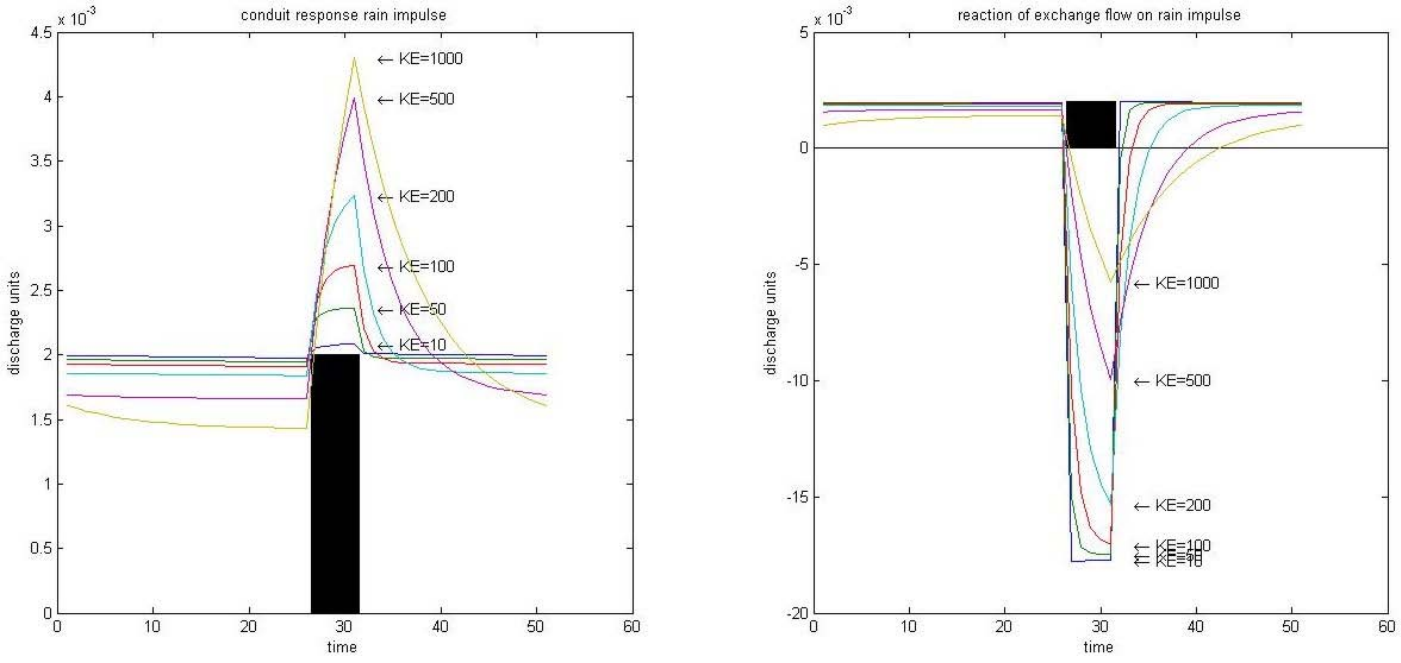

FIGURE 46: Response of the modified reservoir on a synthetic event using different K_Es and K_1=25; left: response of conduit outlet, right: response of exchange flow; the black bar represents the recharge event

Comparing now the response of the modified reservoir on different K_1s it can be observed that this parameter influences mainly the shape of the conduit discharge peak. For small K_1s peak discharge is higher and the event hydrograph is narrower. For large K_1s peak discharge is smaller whereas the event hydrograph is wider. Looking now at the exchange flow for

different K_1s no significant change is occurring. This is the consequence of two effects: first with larger K_1s there is more time for exchange and with smaller K_1s there is less time. Second with larger K_1s the peak value of conduit discharge is smaller. Thus there is less exchange flow to the fissured aquifer, due to the smaller difference in water levels. Whereas with smaller K_1s the peak value is larger and thus there is more exchange flow. These two effects act against each other and lead to the observed results.

To investigate how the modified reservoir is transposing a certain input of concentration to the outlet of reservoir 1 a course of concentration was added to the synthetic input data. An initial concentration of 2.5 mg/l was selected which gradually decreased to 0.5 mg/l during the input event. This should account for the washing out of solutes in the soil before the water enters the modified reservoir. Results are shown in FIGURE 47, FIGURE 48 and FIGURE 49. For each K_1, the maximum peak of concentration of different K_Es is nearly the same. Just as the concentrations in the fissured porous aquifer, which represent the mean concentration of exchange flow to the fissured aquifer, are nearly the same. But regarding the minimum peak of concentrations in the conduits there are obvious differences: the smaller K_E the smaller the minimum peak value. Also the recovery to the mean concentration of the fissured aquifer acts different: the larger K_E the slower recovery takes place. This is a consequence of water mixing in the conduits: if there is more water, due to larger K_Es and consequently less exchange, attenuation takes place and leads to less small minimum peaks and slower recovery. If the K_Es are small inflowing water dominates the course of concentration and after the event recovery happens faster. Looking at the differences for different K_1s no significant change happens for the fissured aquifer concentrations. For the conduit concentrations larger K_1s lead to an attenuation of the hydrochemical response due to bigger water volumes in the conduits. For small K_1s the signal is more distinctive.

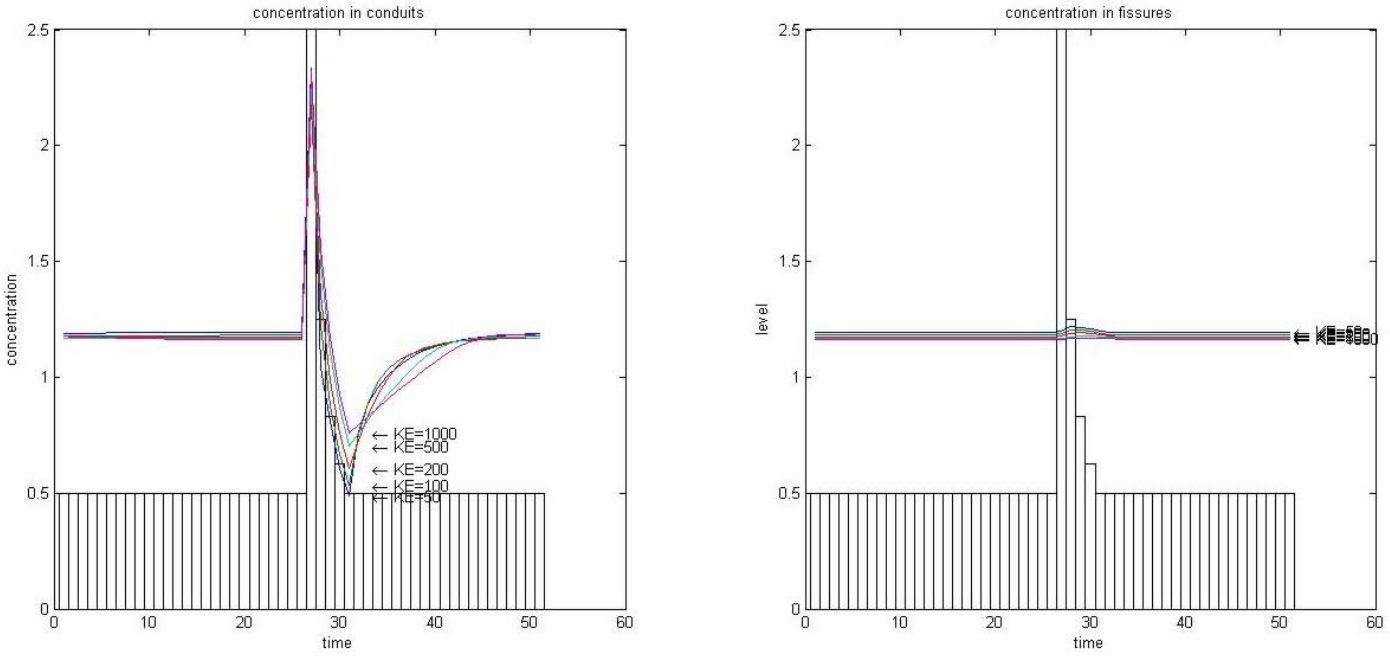

FIGURE 47: Hydrochemical response of the modified reservoir on a synthetic event with gradually decreasing concentration of input (bars) using different K_Es and K_1=5; left: response of conduit outlet, right: response of exchange flow

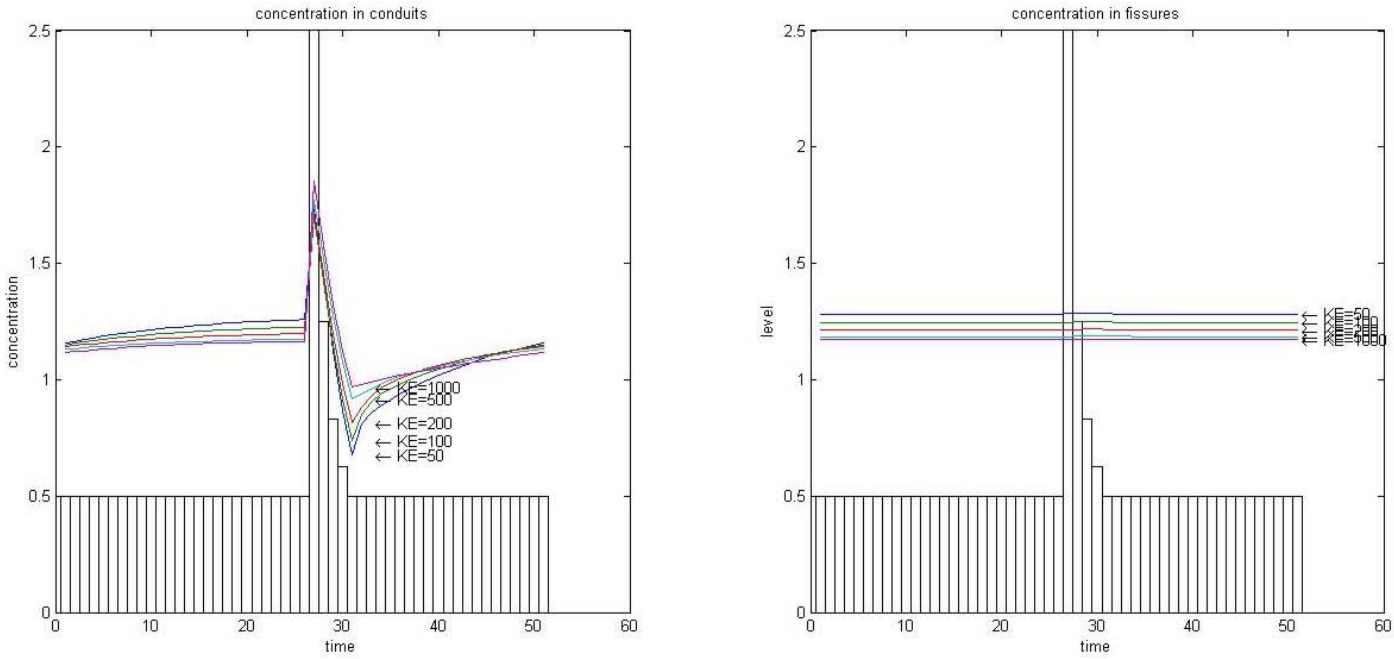

FIGURE 48: Hydrochemical response of the modified reservoir on a synthetic event with gradually decreasing concentration of input (bars) using different K_Es and K_1=15; left: response of conduit outlet, right: response of exchange flow

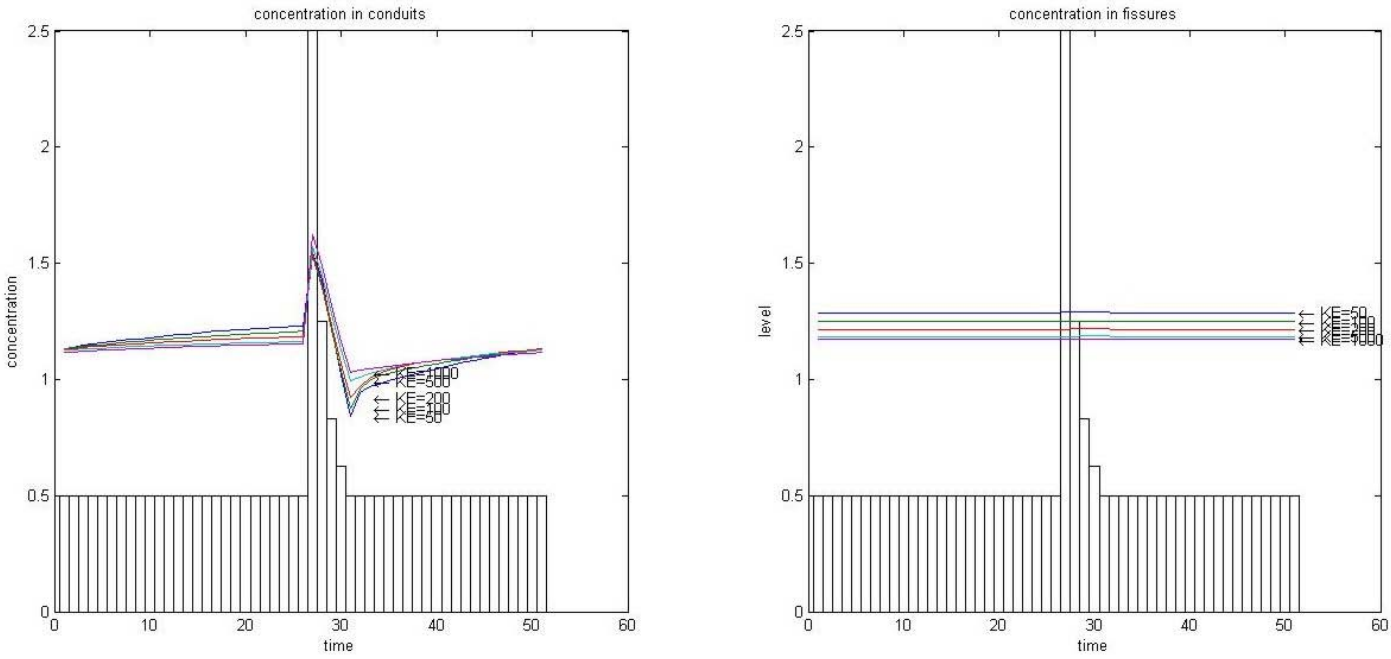

FIGURE 49: Hydrochemical response of the modified reservoir on a synthetic event with gradually decreasing concentration of input (bars) using different K_Es and K_1=25; left: response of conduit outlet, right: response of exchange flow

To examine how a constant flux of mass to the fissured aquifer, as introduced in equations (33), influences the solute concentrations a constant flux of mass was selected (1 mg/m²/day) and the concentration of input water was set constant (0.5 mg/l) for the whole event in order to exclusively observe the influence of the constant flux of mass. The so obtained chemographs are plotted in FIGURE 50, FIGURE 51 and FIGURE 52. Looking at first the concentrations in the fissured aquifer it can be seen that concentrations are increasing with increasing K_Es. This is due to the constant flux of mass to the fissured aquifer on the one hand; on the other hand this is a consequence to the transport of the accumulated mass out of the fissure system for different K_Es. If the exchanging water volume is small, due to large K_Es, a constant flux of mass will cause higher concentrations; and if exchanging water volume is big, due to small K_Es, lower concentrations in the fissure system can be observed. Regarding the concentrations in the conduits for different K_Es during the dry periods a recovery to the concentration to the respective fissured aquifer concentration is occurring. As soon as the event begins the concentrations fall down. Again the recovery to the fissured aquifer concentrations is dependent on the amount and rate exchange of water which is smaller for larger K_Es. Additionally the volume of water in the conduits, which is larger for large K_Es, is influencing the recovery: If there is more water in the conduits recovery is slower; if there is less water in the conduits it is faster. Looking at the fissured aquifer concentrations again a decrease of concentration for each K_E takes place when K_1 increases. This is due to the longer

time of recharge with diluted water, which occurs by increasing K_1. Differences in the conduit concentrations are, first that by increasing K_1 the concentration signal is attenuated, and second that the recovery to the fissured aquifer concentration is happening slower with increasing K_1s. Both effects are consequences of the larger water volumes in the conduits with larger K_1s.

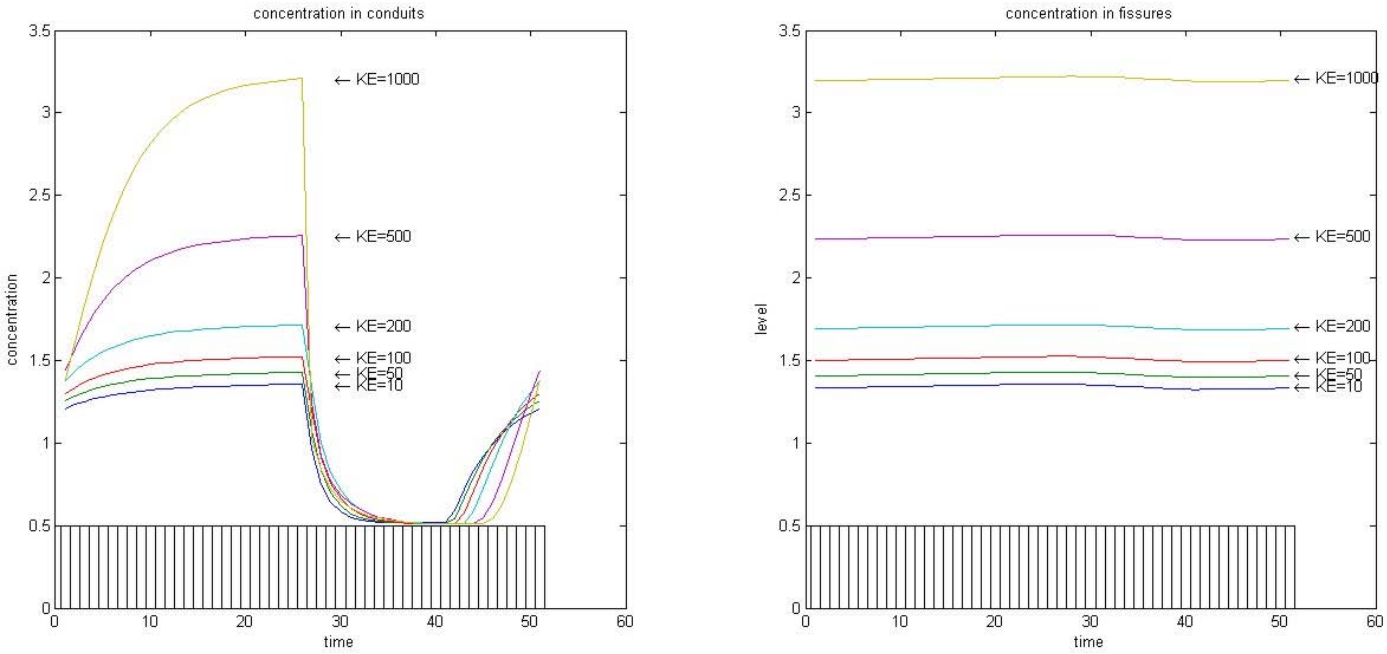

FIGURE 50: Hydrochemical response of the modified reservoir on a synthetic event with constant flux of mass to the fissured aquifer and a constant input concentration (bars) using different K_Es and K_1=5; left: response of conduit outlet, right: response of exchange flow

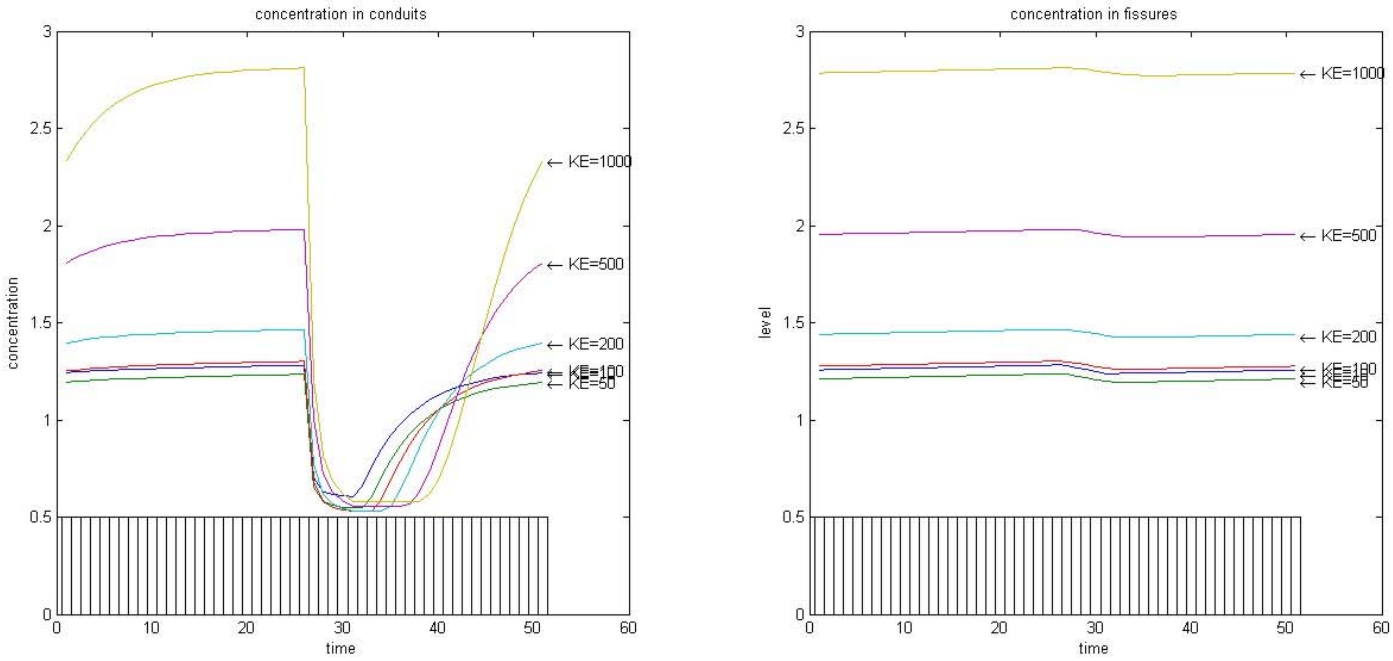

FIGURE 51: Hydrochemical response of the modified reservoir on a synthetic event with constant flux of mass to the fissured aquifer and a constant input concentration (bars) using different K_Es and K_I=15; left: response of conduit outlet, right: response of exchange flow

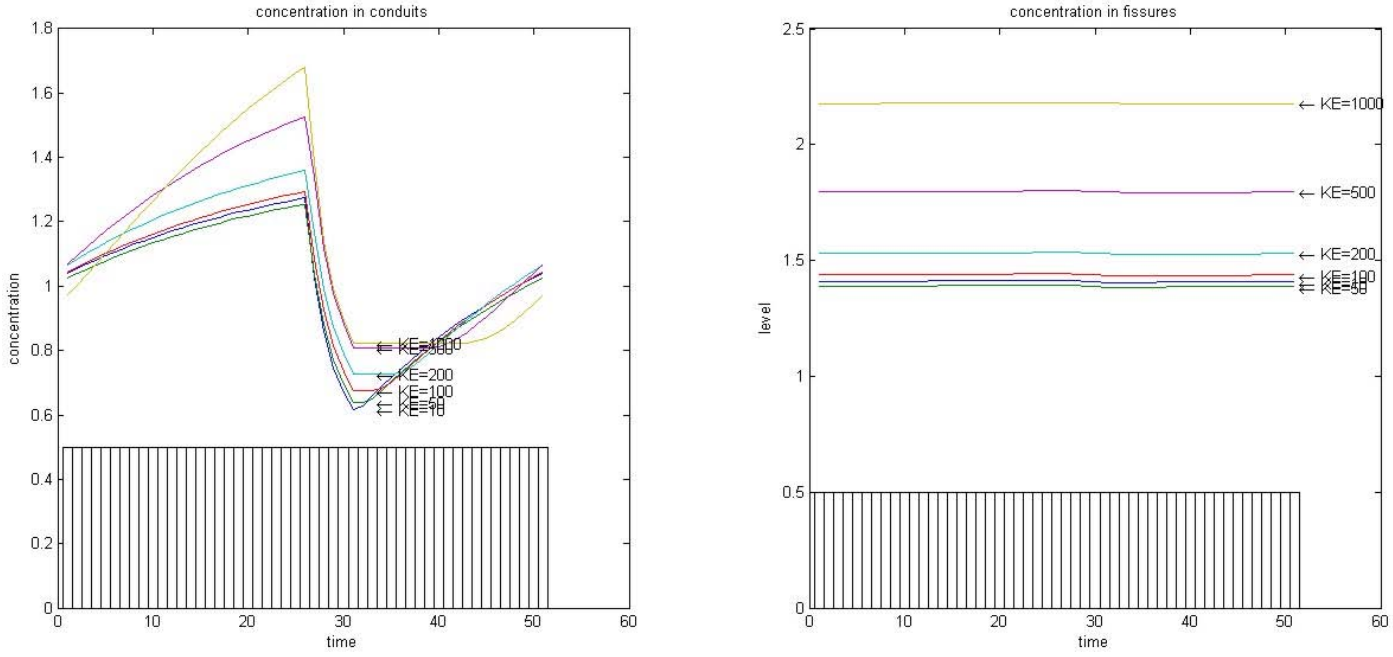

FIGURE 52: Hydrochemical response of the modified reservoir on a synthetic event with constant flux of mass to the fissured aquifer and a constant input concentration (bars) using different K_Es and K_I=25; left: response of conduit outlet, right: response of exchange flow

A summary of the analysis of the behaviour of the modified reservoir on synthetic data is given in TABLE 10. This knowledge will be used in the following chapter to find reasonable

choices of these parameters in the application of the modified groundwater reservoir on real data.

TABLE 10: Summary of impact of K_I and K_E on discharge and concentrations in the conduits and the fissured aquifer

Parameter	K_1	K_E
influence on		
conduit discharge	peak discharge peak width	peak discharge peak width
conduit concentration (variable input concentration)	attenuation	minimum peak recovery
conduit concentration (const. mass flux)	attenuation recovery	minimum peak recovery
exchange flow	recharge recharge duration	recharge recharge duration
fissured aquifer concentration (variable input concentration)	-	-
fissured aquifer concentration (const. mass flux)	mean concentration	mean concentration

8.2 Application of HYMKE_modified on the real data

To examine how the modified groundwater routine performs with real data HYMKE_modified calibrated to Dan and Banias Spring discharge and their concentrations. Since the surface layer routine is not affected by the modifications of the first version of HYMKE its output was taken as input for this simulation (FIGURE 53). Again the hydrological years 1990/1991 to 1999/2000 were chosen as simulation period to compare results with the results of the first version of HYMKE.

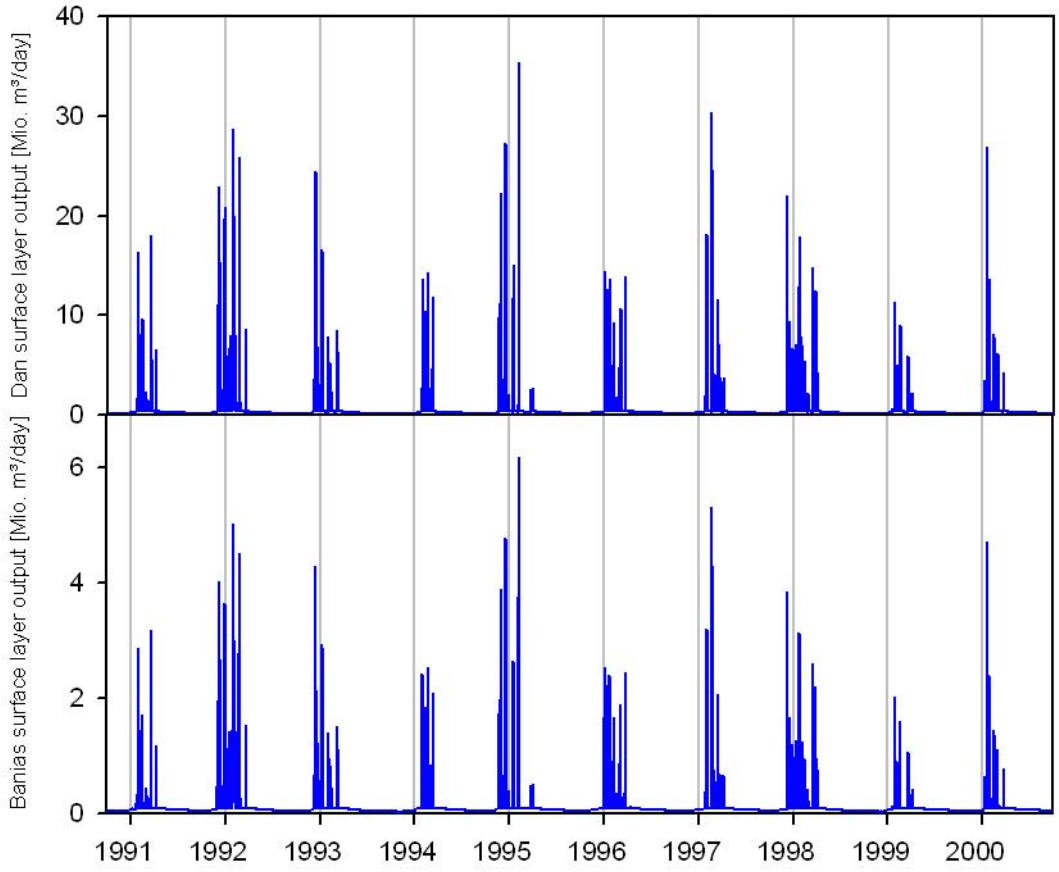

FIGURE 53: Output of the surface layer routine which serves as input for the simulations

As vadose zone storage coefficient the same value was chosen as found by RIMMER AND SALINGAR (2006): 71.8 days. It was assumed once again that only half the volume of water stored in the vadose zone reservoir takes part in mixing (see chapter 5). For Dan Spring and Banias Spring exchange coefficient K_E, the same value could be used: K_E = 50 days. The conduit storage constant K_1 at Banias Spring was set the half of the storage constant K_1 at Dan Spring: Banias Spring K_1=2.2 days and Dan Spring K_1=4.4 days. This is straightforward

explainable by the different sizes of the two subsurface catchments which were 368 km² for Dan Spring and 131.5 km² for Banias Spring. As mentioned in chapter 8.1 typical values for the effective porosity of a karstic system are 1% for the fissure porosity and 0.01% for the conduit porosity. These values were used for Dan Spring. To get a good fit for Banias Spring the conduit porosity was changed to 0.1%. This value could be explained by the higher solution which takes place in the shallow epikarst dominating Banias Spring system (BRIELMANN, 2008). That means that differences in terms of modelling between Dan Spring and Banias Spring could be mainly explained by different conduit porosities. No real calibration was performed just a rough optical fit since it should only be proven that the modifications would be able to improve model predictions. But already with this the results are quite good: Dan Spring discharge predictions (FIGURE 54) show nearly the same quality than the old model. Just in extreme years they differ: for the wet years of 1991/1992 to 1992/1993 the HYMKE_modified still overestimates the discharge but far not as strong as the first version of HYMKE. However regarding the dry year of 1998/1999 the recession of the new model is even worse than the old model.

Looking at the hydrochemistry in FIGURE 54 just for NO_3 the data resolution is fine enough to proper investigate the model predictions. For SO_4 and Cl the resolution of observed data can only proof that the range of predicted values is right. Compared to the results of the first version of HYMKE (green line) the new modelled output concentration is much better. In average years it follows well the observed variations of NO_3. Considering the dry year of 1998/1999 it also reproduces the weaker recession of the NO_3. However for the wet years 1991/1992 to 1992/1993 it underestimates the measured concentrations.

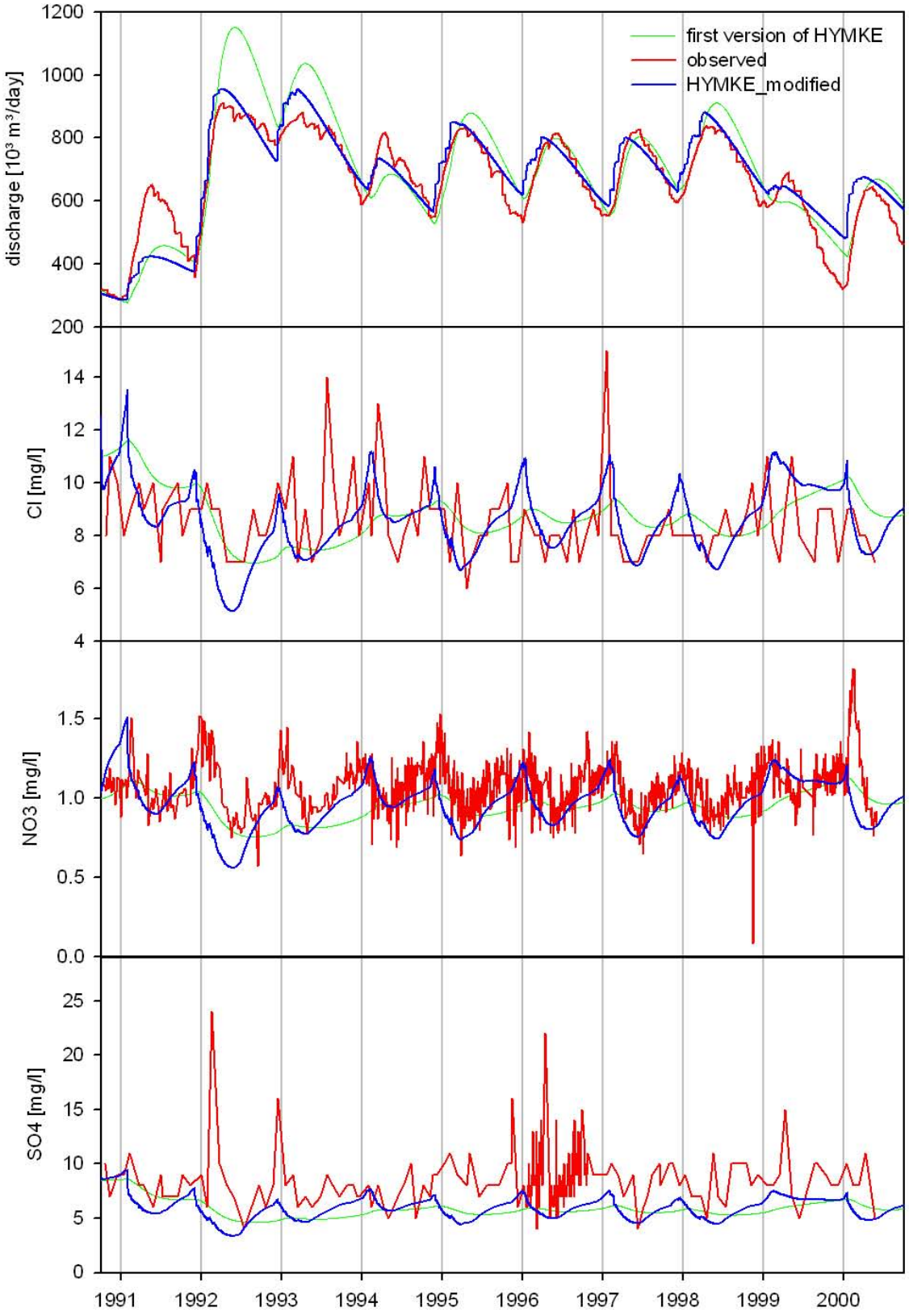

FIGURE 54: Discharge and concentrations of Cl, NO_3 and SO_4 at Dan Spring from 1990/1991 to 1999/2000 predicted by the old HYMKE and the modified HYMKE compared to the measured (base flow separated) and hydrochemical data

For the discharge predictions at Banias Spring in FIGURE 55 the first version of HYMKE and HYMKE_modified do not differ much from each other. Discharge peaks of the new model are slightly earlier than the peaks predicted by the old model. Overestimations during the falling tail of the measured discharge happen at the same time particularly in the dry year of 1998/1999. So there the modified reservoir did neither improve nor deteriorate the old model predictions.

Looking at the NO_3 concentration predictions the same conclusions as for the discharge predictions can be made: the old and new model data show the same behaviour. In the dry year of 1998/1999 the models predict, similar to the Dan Spring concentrations, a weaker decrease of NO_3. But this time, this cannot be seen in the observed data. Overall the old and new model predictions follow the course of the measured data even though they are slightly overestimating them.

Comparing now old and new model predictions for the SO_4 in FIGURE 55 finally strong differences can be seen: since the new mass balance equations (33) also include a possibility to add a geogene component as a constant flux of mass this possibility was applied to reproduce the SO_4 variations observed at Banias Spring outlet, which are totally different to Dan Spring SO_4 variations. As the results show this approach was very successful: course and peak value was good estimated. Even the phenomenon that independent to wet or dry conditions the SO_4 peak was always similar could be reproduced. This is caused by the constant flux of mass to the fissured aquifer. It leads to higher concentrations in the fissure reservoir when this storage contains smaller volumes of water in dry years and vice versa it leads to smaller concentrations in the storage in wet years. When the fissured storage drains during the dry season, after a dry year, little water with high concentrations enters the conduit storage and, after a wet year, much water with low concentrations enters the conduits. So the mixing with the water already stored in the conduit reservoir and coming from the vadose zone always leads to similar concentrations at the spring outlet.

For the Cl variations at Banias Spring the observed data resolution is still rough but compared to Dan Spring it is better. Peak values of modelled concentrations lie near to peak values of observed concentrations. In the dry yeas of 1998/1999, the same overestimation by the model as for NO_3 seems to take place.

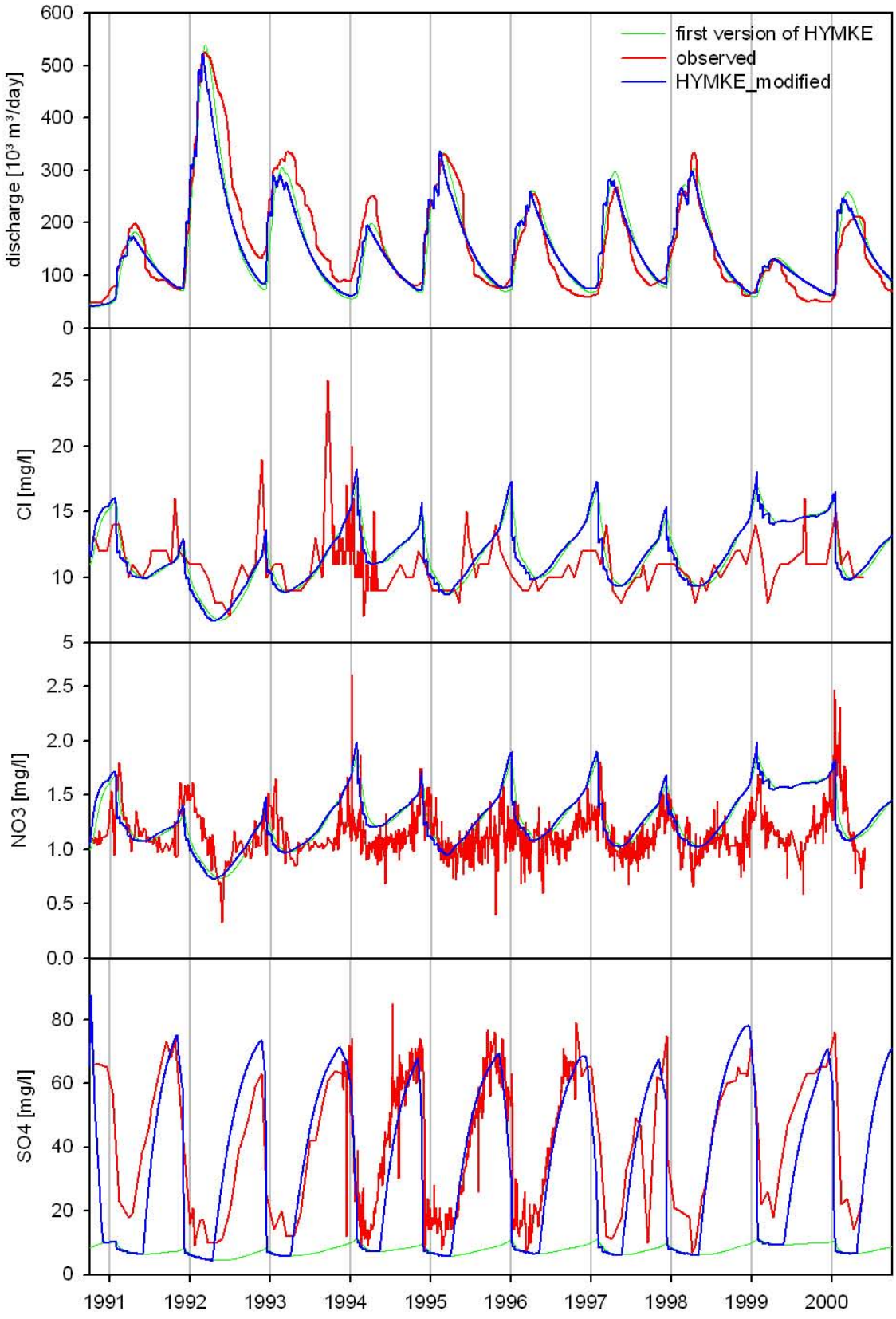

Figure 55: Discharge and concentrations of Cl, NO_3 and SO_4 at Banias Spring from 1990/1991 to 1999/2000 predicted by the old HYMKE and the modified HYMKE compared to the measured (base flow separated) and hydrochemical data

8.3 Intermediate conclusions

These results show that by solely replacing the groundwater reservoir of the first version of HYMKE by a routine which is able to reproduce the effects of double porosity on groundwater flow in karst systems hydrochemistry predictions could be improved significantly. Even discharge predictions improved slightly. This indicates that the duality of groundwater flow was one important process missung in the first version of HYMKE. During the modification the rest of the first version of HYMKE, including its parameters, has not been changed. This proves that the duality of groundwater flow is a major process in the Mt. Hermon system and that it is possible to reproduce this behaviour even though it is not possible to apply physically based ground water equations as they are used in distributive models (chapter 3). However the question is how far the upper routines of HYMKE_modified reflect the behaviour of a karst system as introduced in chapter 3. Is the surface layer really representing soil and epikarst? Is the separation of excess flow into preferential and surface near fast flow really necessary? And is flow in the vadose zone so significant that a proper routine has to be applied? These questions could be answered the best by going into the field and collecting much more data. But this was not possible in the frame of this diploma thesis. Instead of that a second approach for modelling the Mt. Hermon hydrological system was performed which will be introduced in the following chapters.

9 Incorporation of all major karst processes: HYMKE_DUAL

Encouraged by the successful results of the incorporation of the modified groundwater routine in HYMKE_modified another approach to model Mt. Hermon system was considered. This time no search for the most important modification necessary was performed. Instead of that a review of all recognized processes, as introduced in chapters 2 and recognised 6, was performed with particular focus on karst specific processes as introduced in chapter 3. The review yieled the following results: since Mt. Hermon altitude reaches altitudes above 2800 m ASL, the incorporation of a snow melt routine was regarded as necessary. This opened the question how to cope with the vadose zone module of the first version of HYMKE which should be more considered as a lumped "transfer function" representing delay effects – including the snow melt- of flow from the surface to the phreatic zone (RIMMER AND SALINGAR, 2006). Excluding delays of snowmelt from this transfer function and taking into account the hydrochemical evidence of the existence of an epikarst subsystem the question arose as to all delay processes be explained by an adequate modification of the surface module to represent the epikarstic behaviour identified in the chapter 6. Thus, it was decided to discard the vadose zone module in favour of the snow melt routine and a modified surface module. Finally, the assumption of two separate fissure aquifers in the HYMKE_modified in chapter 7 was examined anew. Even though the Sion Rachaya Fault divides Mt. Hermon range into a western and an eastern part (FIGURE 2) there is no reason to consider it is acting as a hydraulic barrier. Hydrochemical analysis in chapter 6 also corroborated this assumption. Hence, in the new approach a common fissure aquifer was developed which is connected to the two conduit systems of the Banias and Dan Spring. The development of the new routines is described in the following sections.

9.1 Snowmelt routine

As snowmelt routine the approach of the standard HBV (Hydrologiska Byråns Vattenbalansavdelning) model after BERGSTRÖM (1976) was adapted. Because of its robust and surprisingly generic structure, and in spite of its simplicity, the HBV model was applied successfully under various physiographic and climatological conditions (LINDSTRÖM ET AL., 1997). The HBV snowmelt routine is based on degree-day temperature-index approach. Temperature-index approaches have been developed because of the difficulty and expense of

meeting the data requirements of physically based energy-balance approaches (DINGMAN, 2002). The daily snowmelt given by the degree-day approach is given by

$$q_{melt} = ddf\left(T_{AIR} - T_M\right) \text{ if } T_{AIR} > T_M\,, \tag{69}$$

$$q_{melt} = 0 \text{ if } T_{AIR} \le T_M\,. \tag{70}$$

Where q_{melt} is the calculated snowmelt [mm/day], *ddf* the degree-day factor [mm/°C/day], T_{AIR} the mean daily temperature [°C] and T_M melting temperature [°C].

Additional the HBV snow melt routine includes the possibility for the snow pack to store water. The amount of water that can be stored in the snow pack, from now on referred to as retained liquid water *RLW* [mm], is controlled by the holding capacity *HC* [-], a parameter representing the fraction of the snow water equivalent *SWE* [mm] that can be retained in the snow pack in the liquid phase. First when the retained liquid water exceeds the liquid water retaining capacity *LWRC* [mm], which is *HC*SWE*, excess water enters the soil beneath the snow pack. The HBV snowmelt routine also allows liquid retained water to refreeze again if the air temperature falls below the melting temperature:

$$q_{refr} = RF \cdot ddf\left(T_M - T_{AIR}\right) \text{ if } T_{AIR} \le T_M \tag{71}$$

$$q_{refr} = 0 \text{ if } T_{AIR} > T_M \tag{72}$$

Where q_{refr} is the calculated amount of retained liquid water that is added to the snow pack again [mm/day] and *RF* [-] is a factor that describes how slow the refreezing occurs compared to the melting. Precipitation is added to the snow pack if $T_{AIR} \le T_M$ and if $T_{AIR} > T_M$ it is directly added to the liquid retained water. The HBV model divides the simulation area in different elevation and vegetation zones. Since the vegetation on Mt. Hermon is relatively homogeneous a simple division in different elevation zones was performed.

This could be done easily because HYMKE already had a subdivision into 56 altitude strips in order to calculate areal precipitation for the simulation area: RIMMER AND SALINGAR (2006) developed an empirical precipitation-elevation-seasonal equation:

$$R_M\left(JD_R, z\right) = \left(z + a_R\right) \cdot \left[A_R \sin\left(\lambda_R \cdot \left(JD_R + \omega_R\right)\right)\right] + b_R \tag{73}$$

Where R_M is the monthly precipitation [mm], JD_R the Julian Day number of the 15th day in each month (with counting beginning at the beginning of the rainy season), z the elevation of the gauging station [m], A_R the amplitude [mm/m], λ_R the angular frequency [rad] (λ_R=2*π/ 365.25), ω_R the phase shift, and a_R [m] and b_R [mm] are coefficients. The parameters in equation (73) where estimated by curve fitting with monthly averages of measured data from eight rain gauges in the Upper Jordan River Catchment, in elevation of -100 to 960 m ASL. To calculate the areal precipitation for the entire Hermon region RIMMER AND SALINGAR (2006) used GIS subroutines to divide the whole region into 56 strips of equal elevations from 75 m ASL to 2825 m ASL with 50 m increments. With the same GIS routines the area of each altitude strip was calculated. The results are given in FIGURE 56.

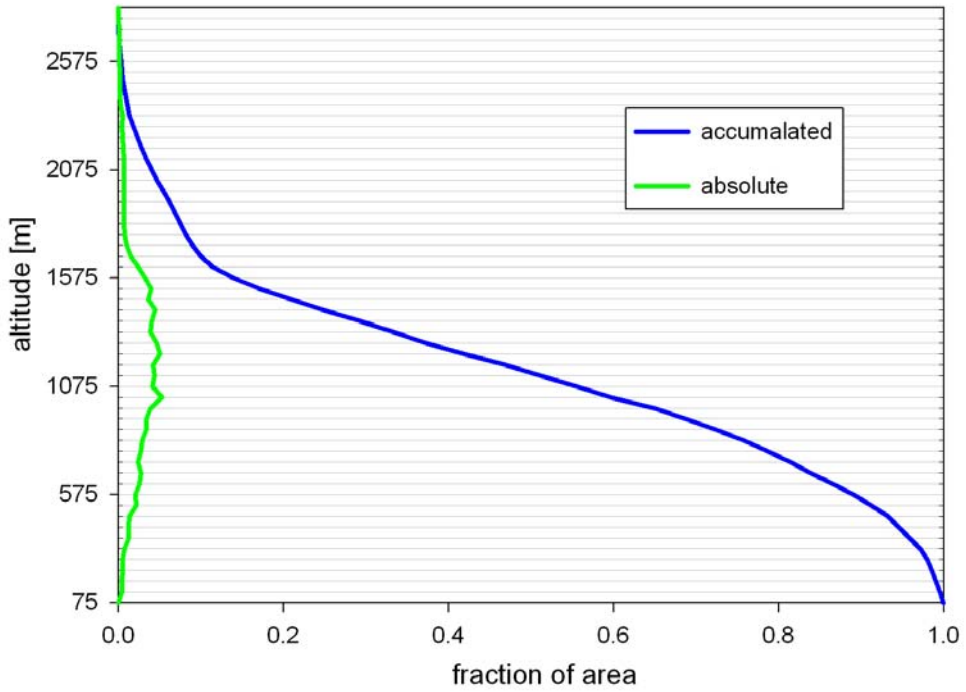

FIGURE 56: Altitude distribution of Mt. Hermon Range calculated by RIMMER AND SALINGAR (2006); grey lines indicate border between two altitude strips

Then the daily measured precipitation of four rain gauges in various elevations (Ein Ziwan at 948 m ASL, Golan Exp. Station at 960 m ASL, Malkya at 690 m ASL and Ma'ayan Barouch at 240 m ASL) were used to calculate a daily average factor $\overline{F_j}$ of the Julian day j:

$$\overline{F_j} = \frac{1}{4}\sum_{n=1}^{4}\frac{R_{nj}^{*}}{\left(R_M\left(JD_{Rj}\cdot z_n\right)/N_M\right)} \tag{74}$$

Where R_{nj}^{*} is the precipitation measured at station n at the j^{th} day of the year [mm], $R_M\left(JD_{Rj} \cdot z_n\right)$ is the precipitation of the j^{th} day of the year at the elevation of station n [mm] obtained by equation (73), and N_M is the number of day of the month the j^{th} day of the year belongs to. Using this average factor, the precipitation for each altitude strip R_{ij} [mm] ,altitude strip i and day of the year j, could be calculated:

$$R_{ij} = \overline{F_j}\left[R_M\left(JD_{Rj} \cdot z_i\right)/ N_M\right] \tag{75}$$

Where z_i is the mean elevation of altitude strip i (i = 1,…,56). Finally to obtain the entire areal precipitation RIMMER AND SALINGAR (2006) had to summarize the area weighted strip precipitations:

$$R_j = \frac{\sum_{i=1}^{56} R_{ij} A_i}{A} \tag{76}$$

Here, R_j is the daily areal precipitation at the j^{th} day of the year, A_i is the area of altitude strip i, and A is the whole study area.

However, since the aim was to apply the HBV snowmelt routine as described above for different elevation zones, the results of equation (75) were used as input to the snow routine, and snow melt calculations were performed in each time step for each altitude strip.
The implementation of the HBV degree-day approach mainly works as described above, but some special cases had to be incorporated into the source code to maintain mass balance: first if the refreezing equation (71) calculates more water to refreeze than is available only the available water refreezes. Secondly if the snow melt calculated by equation (69) is bigger than the snow water equivalent only this residual water will melt. More detailed descriptions can be found in the source code in the Appendix A.6.1: Source code of the snow melt routine.

9.2 Soil-Epikarst routine

The reason for developing a new surface module, the soil-epikarst routine, was to serve the objective of reproducing the epikarstic behaviour as summarized in chapter 3. It had to account for the slow type of flow to the fissures and the fast type of flow to the conduits as schematized by WILLIAMS (1983) and measured by ARBEL ET AL. (2008) in FIGURE 10 as well as for its functioning as storage and distribution system of the flows which enter fissures and conduits as introduced by GOLDSCHEIDER AND DREW (2007). Therefore a conceptual model similar to the conceptual model established by PERRIN (2003; FIGURE 18), was developed.

The new conceptualization consists of a double outlet reservoir which is divided in three parts: the soil, the upper epikarst and the lower epikarst (FIGURE 57). The soil is the layer which is exposed to evaporation and where precipitation or snow melt infiltrates. Flow types are matrix flow and preferential flow which will be explained more detailed in the following paragraphs of this section. Water leaving the soil layer enters the upper epikarst layer in which matrix and preferential flow can also occur. From there water can drain to the lower epikarst or leave the reservoir into the conduit system. This process of division of flows is very important and will be explained in more details later as well. In the lower epikarst only matrix flow takes place, entering slowly the fissure system.

In their approach to model the epikarst PERRIN ET AL. (2003) used a groundwater modelling software (FEFLOW by Wasy GmbH) to simulate saturated flow in the epikarst and a linear reservoir for the soil layer above (FIGURE 19). But in their discussion they mentioned that the use of unsaturated flow equations could lead to even better results. A very simple way to calculate unsaturated flow is the Buckingham-Darcy equation:

$$q(t) = K(\theta(t)) \cdot \left[\frac{\partial h(\theta(t))}{\partial z} - 1 \right] \tag{77}$$

Where *q(t)* [mm/day] is the flow in direction of the *z* axis at time *t*, *θ(t)* the volumetric water content [-] at time *t*, *K(θ(t))* the unsaturated conductivity at time *t* [mm/day], *h(θ(t))* the soil water matric potential head [m] at time *t* and *z* the depth [m]. Assuming that the matrix potential *h(θ(t))* is constant with depth equation (77) simplifies to

$$q(t) = K(\theta(t)). \tag{78}$$

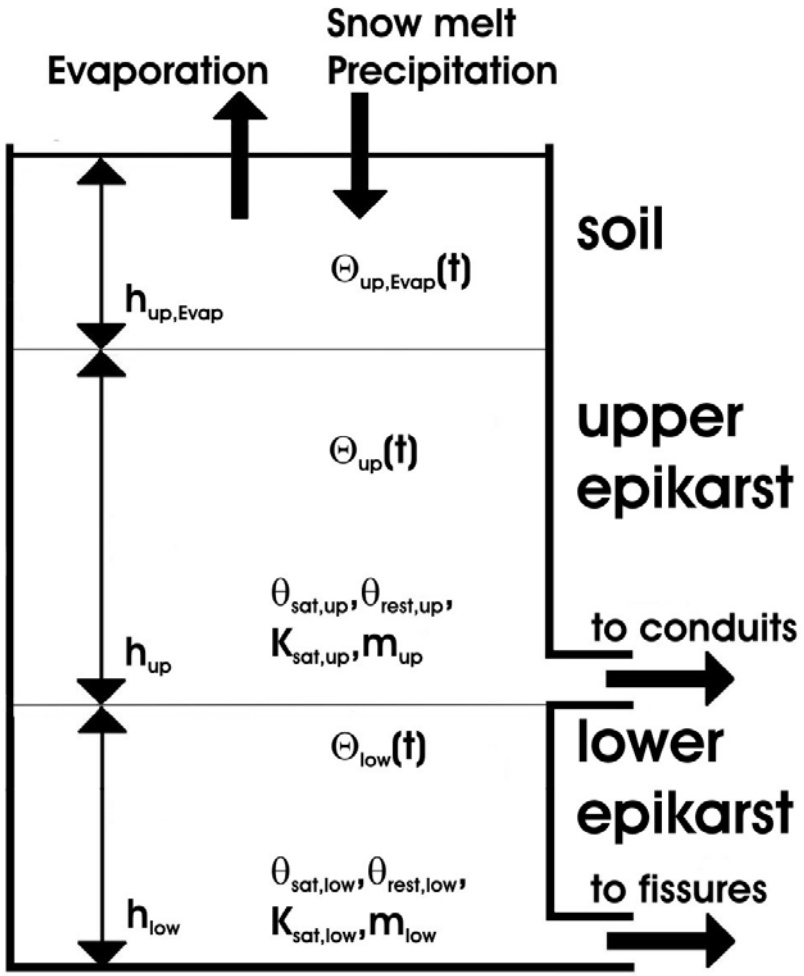

FIGURE 57: Geometry of the new soil-epikarst module

Thus knowing the unsaturated conductivity K(θ(t)) unsaturated flow in vertical direction can be calculated. A way to obtain the unsaturated conductivity is provided by the Mualem-Van Genuchten equation (RAWS ET AL., 1993):

$$K(\theta(t)) = K_{sat} \cdot \left(\left(\frac{\theta(t) - \theta_{rest}}{\theta_{sat} - \theta_{rest}} \right)^{1/2} \cdot \left\{ 1 - \left[1 - \left(\frac{\theta(t) - \theta_{rest}}{\theta_{sat} - \theta_{rest}} \right)^{1/m} \right]^{m} \right\}^{2} \right) \quad (79)$$

with

$$m = \left(\frac{\lambda}{\lambda + 1} \right) \quad (80)$$

Whereby K_{sat} is the saturated hydraulic conductivity [mm/day], $\theta(t)$ the relative water content at time t [-], θ_{rest} the residual relative water content [-], θ_{sat} the saturated relative water content [-], which is set equal to the porosity, and λ the Brooks-Corey grain size distribution index [-] as defined in RAWS ET AL. (1993). As mentioned in chapter 5 RIMMER AND SALINGAR (2006) used the Thornthwaite-Mather approach to simulate unsaturated flow in the surface layer of HYMKE. The calculation of the unsaturated conductivity followed the method proposed by BROOKS AND COREY (1964). In this case the model of Mualem-Van Genuchten (RAWS ET AL., 1993), including the soil water content and matric potential relationship introduced by VAN GENUCHTEN (1980), will be applied. The reason for this is that the model of VAN GENUCHTEN (1980) permits a representation of the whole water retention curves whereas the model described by BROOKS AND COREY (1964) explains only the portion of the curve for matric potentials less than the bubbling pressure, or pressure at which air will enter the soil (MAIDMENT, 1992).

To account for the epikarstic behaviour two sets of four parameters each where introduced: (1) a set for both, the soil layer and the upper epikarst ($K_{sat,up}$, $\theta_{rest,up}$, $\theta_{sat,up,}$ and m_{up}), and (2) another set for the lower epikarst ($K_{sat,low}$, $\theta_{rest,low}$, $\theta_{sat,low}$ and m_{low}). Water contents for the three layers at time t are $\theta_{up,Evap}(t)$, $\theta_{up}(t)$ and $\theta_{low}(t)$ for the soil, the upper epikarst and the lower epikarst, respectively. If $\theta_{up,Evap}(t)$ exceeds $\theta_{sat,up}$ excess water initiates preferential flow which is then bypassed directly to the upper epikarst layer without entering the soil layer matrix. Thus inflow to the upper epikarst layer is the sum of unsaturated matrix flow, as described above, and preferential flow. If $\theta_{up}(t)$ in the upper epikarst layer exceeds $\theta_{sat,up}$, excess water bypasses the upper epikarst layer and reaches the lower epikarst once again. At this point the division of flows takes place: as long $\theta_{low}(t)$ is below $\theta_{sat,low}$ all water leaving the upper epikarst, preferential flow and matrix flow, enters the lower epikarst from where it

reaches the fissure system outlet following the Buckingham-Darcy equation (77). However if $\theta_{low}(t)$ exceeds $\theta_{sat,low}$ no preferential flow takes place, only outflow to the conduit system through the upper outlet.

Precipitation and snow melt, given in [mm/day], are added to the whole depth of the soil layer $h_{up,Evap}$ [m]. Actual evaporation is calculated by

$$Evap(t) = Evap_{pot}(t) \text{ if } \theta_{up,Evap}(t) \geq Ept_{Thres} \tag{81}$$

$$Evap(t) = \frac{\theta_{up,Evap}(t)}{Ept_{Tres}} Evap_{pot}(t) \text{ if } \theta_{up,Evap}(t) < Ept_{Thres} \tag{82}$$

Where $Evap(t)$ is the actual evaporation [mm/day], $Evap_{pot}$(t) the potential evaporation [mm/day] and Ept_{Thres} a parameter which defines the minimum water content above which actual evaporation equals potential evaporation [-]. In the presence of snow (indicated by the snow melt routine) no evaporation takes place. Evaporation is equally subtracted from the whole depth of the soil layer. Inflow to the upper epikarst, as defined above, is also added to the whole depth of the upper epikarst layer h_{up} [m], as it is done for the lower epikarst and its depth h_{low} [m].

The whole numerical implementation of the soil-epikarst module can be found in the Appendix A.6.2: Source code of the soil/epikarst routine. Since for each layer of the soil-epikarst routine the same calculations had to be performed, but for different input data and parameters, a function to calculate unsaturated flow for every time step, every altitude strip and every layer was written. To fulfil mass balance, two special cases had to be introduced. Firstly when saturation water content is exceeded in the soil or upper epikarst layer excess water content is separated and transformed into preferential flow; the water content is set equal to the saturation water content. Secondly, if the calculated water content is smaller than the residual water content water content is set equal to the residual water content and the outflow (and evaporation in the soil layer) are corrected. The source code still contains the possibility of overland flow which can be separated from preferential flow with the help of a constant factor but in this study all flow was set to be preferential flow and no overland flow was assumed. The evaporation threshold Ept_{Thres} was set to 1 as well in order to reach potential evaporation just under saturated conditions in the soil layer.

Output of the soil/epikarst routine are matrix flow to the fissures [mm/day], matrix flow to the conduits [mm/day], preferential flow to the conduits [mm/day], matrix flow from the soil layer to the upper epikarst layer [mm/day], preferential flow from the soil layer to the upper epikarst layer [mm/day], matrix flow from the upper to the lower epikarst layer [mm/day], preferential flow from the upper to the lower epikarst layer [mm/day], water contents of the three layers [-] and actual evaporation from the soil layer [mm/day]. All calculations are performed for each time step and each altitude strip. But since the following groundwater routine is not distributed any more, mean output for each time step is calculated by weighting the output of each altitude strip by its area as performed in equation (76).

9.3 Groundwater routine

As already mentioned in the introduction of this chapter the assumption of two separated fissure reservoir made during the first modification in chapter 7 was reviewed once again. And it was decided to modify the groundwater routine again in order to have two separate conduit systems but one common fissure system. As shown in FIGURE 58 the Banias Spring conduit system and the Dan Spring conduit system exchange both with the common fissure storage depending on their respective difference of water level. Comparable to the groundwater routine developed in chapter 7 a conduit porosity n_1 and a fissure porosity n_2 were introduced to compare water levels. The essential difference to the modified groundwater reservoir of chapter 7 is that now water which leaves one conduit reservoir to the fissure storage may not come back the same way but can also leave the fissure system towards the other conduit system. The difference of hydrological base levels of the Dan and Banias Spring H_2 [m] is directly incorporated in the new routine. This will lead to a preferred flow direction from the Banias Spring conduit system towards the fissure storage and from there to the Dan Spring conduit system. Thus depending on H_2 the contribution of water from the fissure storage to the Dan Spring conduits is far larger than its contribution to the Banias Spring. As described in chapter 3 the fissure storage of a karst system can store a significantly larger amount of water and releases it much more continuously than the conduit system which acts more dynamically. So due to the difference of base levels the Banias Spring system should act more dynamically because of the smaller contribution from the fissure system, and Dan Spring should therefore act more continuously because of the bigger contribution of fissure ground water. This difference would fit quite well with the findings of chapter 6.

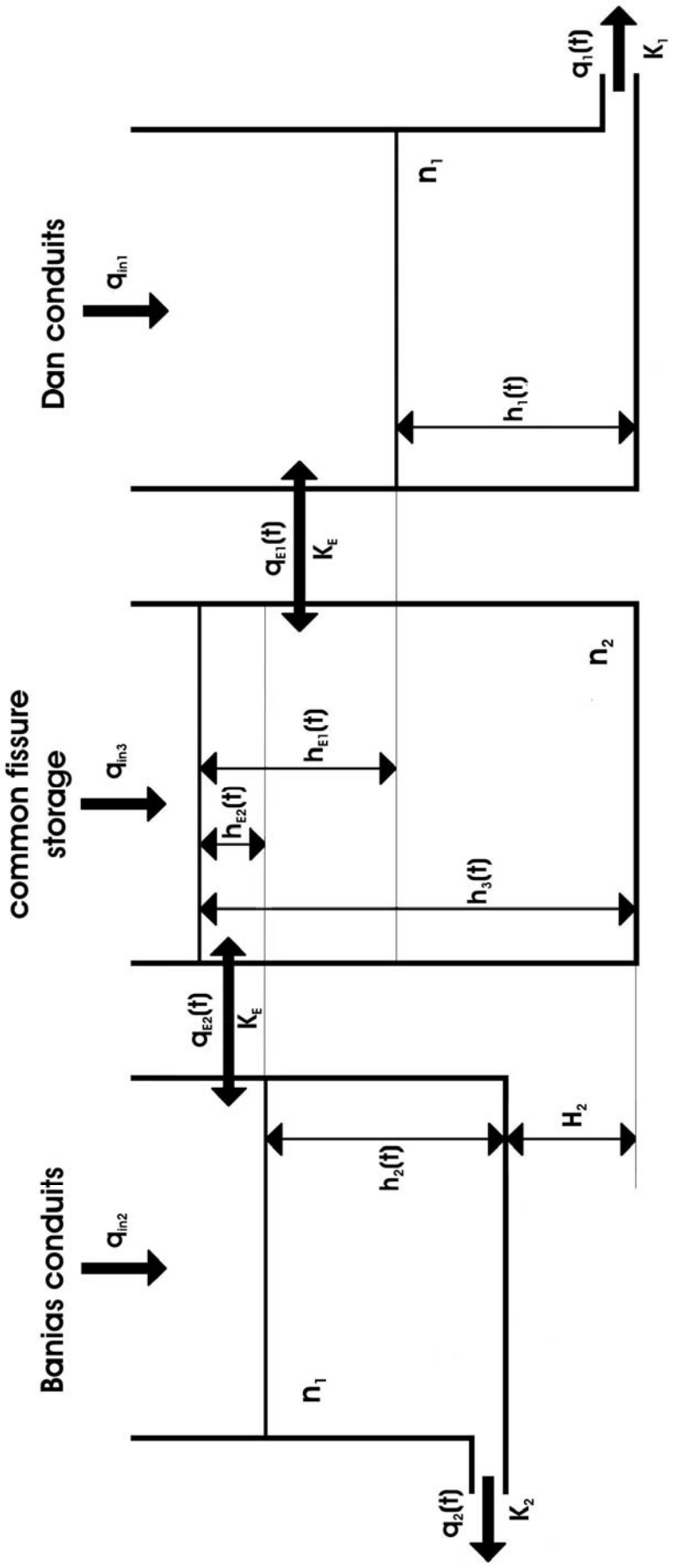

FIGURE 58: Geometry of the new groundwater module

Since no similar approach could be found in literature an analytical derivation of this groundwater system, as it is described in FIGURE 58, was performed once again. In the new approach there are two conduit systems interacting with one fissure system. That is the reason why two exchange flows have to be defined:

$$q_{E1}(t) = \frac{h_{E1}(t)}{K_E} \tag{83}$$

$$q_{E2}(t) = \frac{h_{E2}(t)}{K_E} \tag{84}$$

Where $q_{E1}(t)$ is the flow from the fissure reservoir to the Dan Spring conduit system [m/day] and $q_{E2}(t)$ is the flow to the Banias Spring conduit system [m/day] respectively. K_E is once again the exchange constant [day], which is assumed to be equal for the exchange from conduits to the fissures of both reservoirs and vice versa. The differences of water level $h_{E1}(t)$ and $h_{E2}(t)$ [m] are again rescaled using the assumed porosities of conduit and fissure systems n_1 and n_2 [-]:

$$h_{E1}(t) = \frac{h_3(t)}{n_2} - \frac{h_1(t)}{n_1} \tag{85}$$

$$h_{E2}(t) = \frac{h_3(t)}{n_2} - \left(\frac{h_2(t)}{n_1} + H_2 \right) \tag{86}$$

Where $h_1(t)$, $h_2(t)$, and $h_3(t)$ are the water levels in the Dan Spring conduit system, the Banias Spring conduit system and the fissure reservoir [m]. As already mentioned above H_2 is the level difference of the hydrologic bases [m], i.e. the spring outlets, of the Dan Spring conduit system and the Banias Spring conduit system. The outflows of the conduit systems $q_1(t)$ and $q_2(t)$ [m/day] are linear related to their water levels:

$$q_1(t) = \frac{h_1(t)}{K_1} \tag{87}$$

$$q_2(t) = \frac{h_2(t)}{K_2} \tag{88}$$

And K_1 and K_2 are the storage coefficients [day] of the Dan Spring conduit system and the Banias Spring conduits system, respectively. With the relations established above mass balance equations for the three reservoirs can be established:

$$\frac{\partial h_1(t)}{\partial t} = -q_1(t) + q_{E1}(t) + q_{in1} \tag{89}$$

$$\frac{\partial h_2(t)}{\partial t} = -q_1(t) + q_{E2}(t) + q_{in2} \tag{90}$$

$$\frac{\partial h_3(t)}{\partial t} = -q_{E1}(t) - q_{E2}(t) + q_{in3} \tag{91}$$

Hereby q_{in1}, q_{in2} and q_{in3} are the inflows [m/day] to the Dan Spring, Banias Spring and fissure system, respectively. Substituting $\partial/\partial t$ with the differential operator D and applying equations (83) to (88) allows the transformation of equations (89) to (91) into matrix form:

$$\begin{pmatrix} D + \left(\frac{1}{K_1} + \frac{1}{K_E n_1}\right) & 0 & -\frac{1}{K_E n_2} \\ 0 & D + \left(\frac{1}{K_2} + \frac{1}{K_E n_1}\right) & -\frac{1}{K_E n_2} \\ -\frac{1}{K_E n_1} & -\frac{1}{K_E n_1} & D + \frac{2}{K_E n_2} \end{pmatrix} \cdot \begin{pmatrix} h_1(t) \\ h_2(t) \\ h_3(t) \end{pmatrix} = \begin{pmatrix} q_{in1} \\ q_{in2} - \frac{H_2}{K_E} \\ q_{in3} + \frac{H_2}{K_E} \end{pmatrix} \tag{92}$$

To apply Cramer's rule, equations (20) and (21), once again the determinants of Z, Z_1, Z_2, and Z_3 have to be calculated. Z is the matrix in equation (92), and Z_i are the matrix Z with the i^{th} column replaced by the vector on right side of equation (92). Solving the determinant of Z gives:

$$D^3 + A \cdot D^2 + B \cdot D + C = 0 \tag{93}$$

With the coefficients:

$$A = \frac{1}{K_1} + \frac{1}{K_2} + \frac{2}{n_1 K_E} + \frac{2}{n_2 K_E} \tag{94}$$

$$B = \frac{1}{K_1 K_2} + \frac{1}{n_1 K_1 K_E} + \frac{1}{n_1 K_2 K_E} + \frac{1}{n_1^2 K_E^2} + \frac{2}{n_2 K_1 K_E} + \frac{2}{n_2 K_2 K_E} + \frac{2}{n_1 n_2 K_E^2} \tag{95}$$

$$C = \frac{1}{n_1 n_2 K_1 K_E^2} + \frac{1}{n_1 n_2 K_2 K_E^2} + \frac{2}{n_2 K_1 K_2 K_E} \tag{96}$$

This simplifies to three homogeneous third order differential equations describing the levels of the three reservoirs (i = 1,2,3):

$$\frac{\partial^3 h_i(t)}{\partial t^3} + A\frac{\partial^2 h_i(t)}{\partial t^2} + B\frac{\partial h_i(t)}{\partial t} + C h_i(t) = 0 \tag{97}$$

To solve this differential equation, the roots of its characteristic polynomial have to be calculated:

$$(-1)^3\left(\lambda^3 + A\lambda^2 + B\lambda + C\right) \stackrel{!}{=} 0 \tag{98}$$

Because the characteristic polynomial is of third order it has three roots which can be either all real or one real and two complex (complex number and its conjugate) depending on the choice of parameters. Therefore two solutions of the homogeneous part of equation (97) are calculated:

$$h_i(t) = \alpha_{i1}\exp(\lambda_1 t) + \alpha_{i2}\exp(\lambda_2 t) + \alpha_{i3}\exp(\lambda_3 t) \tag{99}$$

$$h_i(t) = \alpha_{i1} e^{\lambda_1 t} + \alpha_{i2}\exp(\mathrm{Re}(\lambda_2)t)\cos(\mathrm{Im}(\lambda_2)t) + \alpha_{i3}\exp(\mathrm{Re}(\lambda_2)t)\sin(\mathrm{Im}(\lambda_2)t) \tag{100}$$

Where solution (99) is in the case of three real λs and solution (100) for the case of one real λ_1 and two complex solutions λ_2 and $\overline{\lambda_2}$. α_{ij}, j=1, 2, 3, are constants which will be determined later.

The inhomogeneous parts of the of the differential equations $h_i(t)$ is determined by computing the determinants of Z_i:

$$\det(Z_1) = \frac{2q_{in1} + q_{in3}}{n_2 K_2 K_E} + \frac{q_{in1} + q_{in2} + q_{in3}}{n_1 n_2 K_E^2} - \frac{H_2}{n_2 K_2 K_E^2} \tag{101}$$

$$\det(Z_2) = \frac{2q_{in2} + q_{in3}}{n_2 K_1 K_E} + \frac{q_{in1} + q_{in2} + q_{in3}}{n_1 n_2 K_E^2} - \frac{H_2}{n_2 K_1 K_E^2} \tag{102}$$

$$\det(Z_3) = \frac{q_{in1} + q_{in2}}{n_1 K_2 K_E} + \frac{q_{in2} + q_{in3}}{n_1 K_1 K_E} + \frac{q_{in1} + q_{in2} + q_{in3}}{n_1^2 K_E^2} + \frac{q_{in3}}{K_1 K_2} + \frac{H_2}{K_1 K_2 K_E} + \frac{H_2}{n_1 K_2 K_E^2} \tag{103}$$

With it the three differential equations now including their inhomogeneous part are:

$$\frac{\partial^3 h_i(t)}{\partial t^3} + A\frac{\partial^2 h_i(t)}{\partial t^2} + B\frac{\partial h_i(t)}{\partial t} + C h_i(t) = \det(Z_i) \tag{104}$$

Then setting $h_i(t)$ equal to a constant γ_i makes all derivatives disappear leaving only one term on the left hand side, which yields the particular part of the general solution:

$$\gamma_i = \frac{\det(Z_i)}{C} \tag{105}$$

Thus a general solution of equations (89) to (91) for non-complex can be obtained:

$$h_1(t) = \alpha_{11}\exp(\lambda_1 t) + \alpha_{12}\exp(\lambda_2 t) + \alpha_{13}\exp(\lambda_3 t) + \gamma_1 \tag{106}$$

$$h_2(t) = \alpha_{21}\exp(\lambda_1 t) + \alpha_{22}\exp(\lambda_2 t) + \alpha_{23}\exp(\lambda_3 t) + \gamma_2 \tag{107}$$

$$h_3(t) = \alpha_{31}\exp(\lambda_1 t) + \alpha_{32}\exp(\lambda_2 t) + \alpha_{33}\exp(\lambda_3 t) + \gamma_3 \tag{108}$$

And for complex λ_i:

$$h_1(t) = \alpha_{11}\exp(\lambda_1 t) + \alpha_{12}\exp(\mathrm{Re}(\lambda_2)t)\cos(\mathrm{Im}(\lambda_2)t) + \alpha_{13}\exp(\mathrm{Re}(\lambda_2)t)\sin(\mathrm{Im}(\lambda_2)t) + \gamma_1 \tag{109}$$

$$h_2(t) = \alpha_{21}\exp(\lambda_1 t) + \alpha_{22}\exp(\mathrm{Re}(\lambda_2)t)\cos(\mathrm{Im}(\lambda_2)t) + \alpha_{23}\exp(\mathrm{Re}(\lambda_2)t)\sin(\mathrm{Im}(\lambda_2)t) + \gamma_2 \tag{110}$$

$$h_3(t) = \alpha_{31}\exp(\lambda_1 t) + \alpha_{32}\exp(\mathrm{Re}(\lambda_2)t)\cos(\mathrm{Im}(\lambda_2)t) + \alpha_{33}\exp(\mathrm{Re}(\lambda_2)t)\sin(\mathrm{Im}(\lambda_2)t) + \gamma_3 \tag{111}$$

Finally the α_{ij} will be determined. This is performed by using the initial conditions for the water levels in the three reservoirs h_{10}, h_{20} and h_{30} [m]:

$$\begin{aligned} h_1(t=0) &= h_{10} \\ h_2(t=0) &= h_{20} \\ h_3(t=0) &= h_{30} \end{aligned} \tag{112}$$

Since the differential equation is of third order, and three constants need to be determined, initial conditions of first and second order are required. First order initial conditions, h_{110}, h_{220} and h_{330} [m/day], can be taken from equations (89) to (91):

$$\begin{aligned} \frac{\partial h_1(t=0)}{dt} &= -\frac{h_{10}}{K_1} + \frac{h_{30}}{K_E n_2} - \frac{h_{10}}{K_E n_1} + q_{in1} = h_{110} \\ \frac{\partial h_2(t=0)}{dt} &= -\frac{h_{20}}{K_2} + \frac{h_{30}}{K_E n_2} - \frac{h_{20}}{K_E n_1} + q_{in2} - \frac{H_2}{K_E} = h_{220} \\ \frac{\partial h_3(t=0)}{dt} &= -\frac{2h_{30}}{K_E n_2} + \frac{h_{10}}{K_E n_1} + \frac{h_{20}}{K_E n_1} + q_{in3} + \frac{H_2}{K_E} = h_{330} \end{aligned} \tag{113}$$

And the second order initial conditions, h_{1110}, h_{2220} and h_{3330} [m/day²], from their derivatives:

$$\begin{aligned} \frac{\partial h_1^2(t=0)}{dt^2} &= -\frac{h_{110}}{K_1} + \frac{h_{330}}{K_E n_2} - \frac{h_{110}}{K_E n_1} = h_{1110} \\ \frac{\partial h_2^2(t=0)}{dt^2} &= -\frac{h_{220}}{K_2} + \frac{h_{330}}{K_E n_2} - \frac{h_{220}}{K_E n_1} = h_{2220} \\ \frac{\partial h_3^2(t=0)}{dt^2} &= -\frac{2h_{330}}{K_E n_2} + \frac{h_{110}}{K_E n_1} + \frac{h_{220}}{K_E n_1} = h_{3330} \end{aligned} \tag{114}$$

Substituting these initial conditions in (106) and (109) gives a system of linear equations

$$M \cdot \alpha_i = H_{i0} \tag{115}$$

Where α_i is a 3x1 vector consisting of the j=3 coefficients for the general solution of reservoir i in equations (106), (107), (108) or in equations (109), (110), (111), and H_{i0} a 3x1 vector including the initial conditions for reservoir i:

$$H_{i0} = \begin{pmatrix} h_{i0} - \gamma_i \\ h_{ii0} \\ h_{iii0} \end{pmatrix} \tag{116}$$

M is a 3x3 Matrix *M* deriving from first and second order derivatives of (106) and (109). As solution of equation (106), *M* is

$$M = \begin{pmatrix} 1 & 1 & 1 \\ \lambda_1 & \lambda_2 & \lambda_3 \\ \lambda_1^2 & \lambda_2^2 & \lambda_3^2 \end{pmatrix} \tag{117}$$

And as solution of equation (109), it is

$$M = \begin{pmatrix} 1 & 1 & 0 \\ \lambda_1 & \mathrm{Re}(\lambda_2) & \mathrm{Im}(\lambda_2) \\ \lambda_1^2 & \mathrm{Re}(\lambda_2)^2 + \mathrm{Im}(\lambda_2)^2 & 2\,\mathrm{Re}(\lambda_2)\mathrm{Im}(\lambda_2) \end{pmatrix} \tag{118}$$

Applying once again Cramer's rule yields the coefficients:

$$\alpha_{ij} = \frac{\det M_{ij}}{\det M} \tag{119}$$

Whereby, M_{ij} is the Matrix *M* with the j^{th} column replaced by H_{i0}.

The solutions for the water levels of the three reservoirs in FIGURE 58 as given in equations (106) to (111) where then implemented in a numerical code. Since measure of length now is [m] the water amounts [mm] coming from the soil-epikarst routine had to be divided by 1000. As shown in the Appendix A.6.3: Source code of the groundwater routine. Coefficients *A*, *B* and *C*, equations (95), (96) and (97), are calculated only once before the time loop begins. With them the characteristic polynomial, equation (98), is calculated, and its solution, either real or imaginary, determines which equations will be used for computing the water levels. Then the solution algorithm for the reservoir levels is applied each time step. At the end of each time step equations (83) to (88) are used to calculate the actual flow leaving the Banias Spring and Dan Spring conduit systems, as well as the exchange flows between the fissure storage and the two conduit systems. Since the solution is analytical no additional corrections as in the preceding chapters had to be performed.

9.4 Mixing routine for the soil-epikarst routine

To simulate the output concentrations of flows to the fissures and to the conduits mixing equations were applied to the previously calculated flows in and out of the soil-epikarst routine. Here the distinction was made between matrix flow and preferential flow: matrix flow was assumed to mix completely with the water already stored in the respective layer, and preferential flow was assumed to maintain the concentration of water before bypassing the respective layer.

Mixing calculations for the matrix component are similar to equations (11) and (12) in chapter 5. For flows and solute masses they follow the law of mass conservation:

$$\frac{\partial h(t)}{\partial t} = q_{in}(t) - q_{out}(t) - Evap(t) \tag{120}$$

$$\frac{\partial m(t)}{\partial t} = m_{in}(t) - m_{out}(t) + m_{UpRel}(t) \tag{121}$$

Whereby $h(t)$ is the water level in the respective reservoir [m], $q_{in}(t)$ the rate of water entering the reservoir [m/day], $q_{out}(t)$ the rate of water leaving the reservoir [m], $Evap(t)$ the actual evaporation from the reservoir [m/day], $m(t)$ the solute mass in the respective reservoir [g/m²], $m_{in}(t)$ the flux of solute mass entering the reservoir [g/m²/day], $m_{out}(t)$ the flux of solute mass leaving the reservoir [g/m²/day] and $m_{UpRel}(t)$ the solute mass uptake and release by micro-organisms and vegetation [g/m²/day] which will be used for the simulation of NO_3 concentrations. The variations of $m_{UpRel}(t)$ are required as input to the model and will be discussed later in section 10.1.4. Discretizing equations (120) and (121) gives

$$\frac{h(t) - h(t-1)}{\Delta t} = q_{in}(t) - q_{out}(t) - Evap(t) \tag{122}$$

$$\frac{m(t) - m(t-1)}{\Delta t} = m_{in}(t) - m_{out}(t) + m_{UpRel}(t) \tag{123}$$

with $h(t-1)$ and $m(t-1)$ from the previous time step and step size Δt (in this case $\Delta t = 1$ because of the model step size of one day). Assuming that the output concentration $c_{out}(t)$ of one reservoir [g/m³] at time step t equals

$$c_{out}(t) = \frac{m(t)}{h(t)} \tag{124}$$

and substituting in-flux and out-flux of solute mass in equation (123) by the product of their concentration ($c_{in}(t)$ and $c_{out}(t)$ [m³/day]) and their flow rate ($q_{in}(t)$ and $q_{out}(t)$ [m/day]) rearranging of equations (122), (123) and (124) yields

$$c_{out}(t) = \frac{m(t-1) + q_{in}(t)c_{in}(t) + m_{Up\,Rel}(t)}{h(t-1) + q_{in}(t) - Evap(t)} \tag{125}$$

and

$$m(t) = m(t-1) + q_{in}(t)c_{in}(t) - q_{out}(t)c_{out}(t) + m_{Up\,Rel}(t) \tag{126}$$

This numerical solution is implicit since it calculates $c_{out}(t)$ at the end of the time step instead of using the concentration of the preceding time step $c_{out}(t\text{-}1)$. Because of this approach some underestimations of concentration can occur during recharge, and vice versa some overestimations during draining of the respective reservoir.

Preferential flow bypassing the respective layer maintains its input concentration $c_{in}(t)$ and mixes then with the output of the respective layer yielding the final output concentration $c_{out,final}(t)$ [g/m³]:

$$c_{out,\,final}(t) = \frac{c_{out}(t)q_{out}(t) + c_{in}(t)q_{pref}(t)}{q_{out}(t) + q_{pref}(t)} \tag{127}$$

The calculations for mixing of matrix flow and preferential flow are performed for the soil layer and for the upper epikarst layer while evaporation, as well as uptake and release by micro-organisms and vegetation only take place in the soil layer. Input concentration for the soil layer is the concentration in snowmelt or precipitation, and for the upper epikarst layer the final output concentration of the soil layer. For the lower epikarst only mixing of matrix flow is taking place since there is no preferential flow as mentioned above in chapter 9. Thus output concentration to the conduits is the mixing of matrix flow and preferential flow leaving the upper epikarst reservoir, and output to the fissures is the concentration of matrix flow

leaving the lower epikarst. Since the ground water routine is not distributed any more (see chapter 9 and FIGURE 60) outflow concentrations of the soil-epikarst reservoirs have to be averaged. This is again done by weighting output of each altitude strip by its area similar to equation (76). However this time concentrations have to be weighted by the outflow of each strip as well:

$$c_{Cond}(t) = \frac{\sum_{i=1}^{56} q_{cond,i}(t) c_{cond,i}(t) A_i}{\sum_{i=1}^{56} q_{cond,i}(t) A_i} \tag{128}$$

$$c_{Fis}(t) = \frac{\sum_{i=1}^{56} q_{Fis,i}(t) c_{Fis,i}(t) A_i}{\sum_{i=1}^{56} q_{Fis,i}(t) A_i} \tag{129}$$

Whereby $c_{Cond}(t)$ and $c_{Fis}(t)$ are the weighted outflows to the conduits and to the fissures [g/m³], $q_{Cond,i}(t)$ the outflow to the conduits for the i^{th} altitude strip [m/day], $c_{Cond,i}(t)$ the outflow concentration of flow to the conduits for the i^{th} altitude strip [m/day], $q_{Fis,i}(t)$ the outflow to the fissures for the i^{th} altitude strip [m/day], $c_{Fis,i}(t)$ the concentration of flow to the fissures for the i^{th} altitude strip [g/m³] and A_i the area of the i^{th} altitude strip [m²]. The numerical implementation of the whole mixing subroutine can be found in the Appendix A.6.4: Source code of the soil-epikarst mixing routine.

9.5 Mixing for groundwater

The development of the mixing routine for the groundwater was once again based on the conservation of mass. Solute mass balance equations for each reservoir in FIGURE 58 were established:

$$\frac{\partial m_1(t)}{\partial t} = q_{in1}(t) c_{in1}(t) + q_{E1}(t) c_{E1}(t) - q_{out1}(t) c_{out1}(t) \tag{130}$$

$$\frac{\partial m_2(t)}{\partial t} = q_{in2}(t) c_{in2}(t) + q_{E2}(t) c_{E2}(t) - q_{out2}(t) c_{out2}(t) \tag{131}$$

$$\frac{\partial m_3(t)}{\partial t} = q_{in3}(t) c_{in3}(t) - q_{E1}(t) c_{E1}(t) - q_{E2}(t) c_{E2}(t) \tag{132}$$

Whereby $\partial m_i(t)/\partial t$ is the change of mass with time [g/m²/day], $q_{ini}(t)$ the inflow [m/day] and $c_{ini}(t)$ the inflow concentration [g/m³] for the Dan Spring conduits (i = 1), the Banias Spring conduits (i = 2) and the fissure aquifer (i = 3). $q_{E1}(t)$ is the exchange flow between the fissure aquifer and the Dan Spring conduits [m/day] with its respective exchange concentration $c_{E1}(t)$ [g/m³]; $q_{E2}(t)$ is the exchange flow between the fissure aquifer and Banias Spring conduits [m/day] with its exchange concentration $c_{E2}(t)$ [g/m³]. Likewise $q_{out1}(t)$ and $q_{out2}(t)$ are the outflows from Dan Spring conduits and Banias Spring conduits [m/day] with their respective outflow concentrations $c_{out1}(t)$ and $c_{out2}(t)$ [g/m³]. Similarly to the mixing model in chapter 9.4 it is assumed that the output flow concentrations of the three reservoirs $c_{outi}(t)$, i=1,2,3, [g/m³] equals the concentration of water stored in the respective reservoir:

$$c_{outi}(t) = \frac{m_i(t)}{h_i(t)} \tag{133}$$

With $m_i(t)$, i = 1,2,3, the mass stored in Dan Spring conduit reservoir (i = 1), Banias Spring conduit reservoir (i = 2) and the fissure reservoir (i = 3) [g/m²], and $h_i(t)$, i = 1,2,3, the water level in the respective reservoirs [m]. Discretising and rearranging of equations (130), (131), (132) and (133) gives:

$$-\frac{q_{E1}(t)}{h_1(t)}c_{E1}(t)+\left(1+\frac{q_{out1}(t)}{h_1(t)}\right)c_{out1}(t)=\frac{q_{in1}(t)}{h_1(t)}c_{in1}(t)+\frac{m_1(t-1)}{h_1(t)} \tag{134}$$

$$-\frac{q_{E2}(t)}{h_2(t)}c_{E2}(t)+\left(1+\frac{q_{out2}(t)}{h_2(t)}\right)c_{out2}(t)=\frac{q_{in2}(t)}{h_2(t)}c_{in2}(t)+\frac{m_2(t-1)}{h_2(t)} \tag{135}$$

$$-\frac{q_{E1}(t)}{h_1(t)}c_{E1}(t)-\frac{q_{E2}(t)}{h_2(t)}c_{E2}(t)+c_{out3}(t)=\frac{q_{in3}(t)}{h_3(t)}c_{in3}(t)+\frac{m_3(t-1)}{h_3(t)} \tag{136}$$

Writing equations (134), (135) and (136) in matrix form gives a linear equation system:

$$A_j(t)\cdot c_{out}(t)=b(t) \tag{137}$$

Hereby $c_{out}(t)$ is a 3x1 vector containing the concentrations $c_{outi}(t)$, i = 1,2,3, and $b(t)$ is a 3x1 vector containing the right sides of the equations (134), (135) and (136). $A_j(t)$ is a 3 x 3 matrix containing coefficients dependent on the case j that is occurring at time step t. Altogether j = 4 cases have to be distiguished:

Case 1: Water flows from the fissure aquifer to both the Dan Spring and Banias Spring conduit system (i.e. $c_{E1}(t) = c_{E2}(t) = c_{out3}(t)$). Thus

$$A_1(t) = \begin{pmatrix} 1+\frac{q_{out1}(t)}{h_1(t)} & 0 & -\frac{q_{E1}(t)}{h_1(t)} \\ 0 & 1+\frac{q_{out2}(t)}{h_2(t)} & -\frac{q_{E2}(t)}{h_2(t)} \\ 0 & 0 & 1+\frac{q_{E1}(t)}{h_3(t)}+\frac{q_{E2}(t)}{h_3(t)} \end{pmatrix} \quad (138)$$

Case 2: Water flows from the Banias Spring conduit system to the fissure aquifer and from the fissure aquifer to the Dan Spring conduits (i.e. $c_{E1}(t) = c_{out3}(t)$, $c_{E2}(t) = c_{out2}(t)$). Thus

$$A_2(t) = \begin{pmatrix} 1+\frac{q_{out1}(t)}{h_1(t)} & 0 & -\frac{q_{E1}(t)}{h_1(t)} \\ 0 & 1-\frac{q_{E2}(t)}{h_2(t)}+\frac{q_{out2}(t)}{h_2(t)} & 0 \\ 0 & \frac{q_{E2}(t)}{h_3(t)} & 1+\frac{q_{E1}(t)}{h_3(t)} \end{pmatrix} \quad (139)$$

Case 3: Water flows from the Dan Spring conduits to the fissure system and from the fissure aquifer to the Banias Spring (i.e. $c_{E1}(t) = c_{out1}(t)$, $c_{E2}(t) = c_{out3}(t)$). Thus

$$A_3(t) = \begin{pmatrix} 1-\frac{q_{E1}(t)}{h_1(t)}+\frac{q_{out1}(t)}{h_1(t)} & 0 & 0 \\ 0 & 1+\frac{q_{out2}(t)}{h_2(t)} & -\frac{q_{E2}(t)}{h_2(t)} \\ \frac{q_{E1}(t)}{h_3(t)} & 0 & 1+\frac{q_{E2}(t)}{h_3(t)} \end{pmatrix} \quad (140)$$

Case 4: Water flows from both the Dan Spring and Banias Spring conduit system, to the fissure system (i.e. $c_{E1}(t) = c_{out1}(t)$, $c_{E2}(t) = c_{out2}(t)$). Thus

$$A_4(t) = \begin{pmatrix} 1 - \frac{q_{E1}(t)}{h_1(t)} + \frac{q_{out1}(t)}{h_1(t)} & 0 & 0 \\ 0 & 1 - \frac{q_{E2}(t)}{h_2(t)} + \frac{q_{out2}(t)}{h_2(t)} & 0 \\ \frac{q_{E1}(t)}{h_3(t)} & \frac{q_{E2}(t)}{h_3(t)} & 1 \end{pmatrix} \quad (141)$$

Inverting $A_j(t)$ yields the concentrations of the outflows of the reservoirs $c_{out}(t)$ at time t:

$$c_{out}(t) = b(t)A_j(t)^{-1}, \quad (142)$$

whereby j is the number of the case which occurs at the respective time step t.

Additionally to account for geogene inputs of SO_4 into Banias Spring system, as mentioned in the chapter 6, a geogene input was added to the groundwater mixing model. Even though there is only one fissure aquifer the geogene contribution will be added to each spring system separately because water inside the fissure aquifer can pass different geological units on its way before it enters the respective conduit system. Thus different geogene contributions to solutes in this water can occur. A schematic picture of the groundwater mixing model, including the geogene contributions, is given in FIGURE 59. Compared to the first concept (FIGURE 58) two geogene mass reservoirs are interposed between the Dan Spring conduit system and the fissure aquifer, and between the Banias Spring and the fissure aquifer. At every time step a constant flux of mass m_{add1} and m_{add2} [g/m²/day] is added to the respective mass reservoir. The geogene contribution is only added to water when flow from the fissures to the respective system takes place; in the other direction it bypasses the geogene mass reservoir (FIGURE 59). Thus if exchange flow is going to the fissures the daily geogene mass contribution is only added to the geogene mass storage for the Dan and the Banias system without other changes:

$$m_{geo1}(t) = m_{geo1}(t-1) + m_{add1}, \quad (143)$$

$$m_{geo2}(t) = m_{geo2}(t-1) + m_{add2}. \quad (144)$$

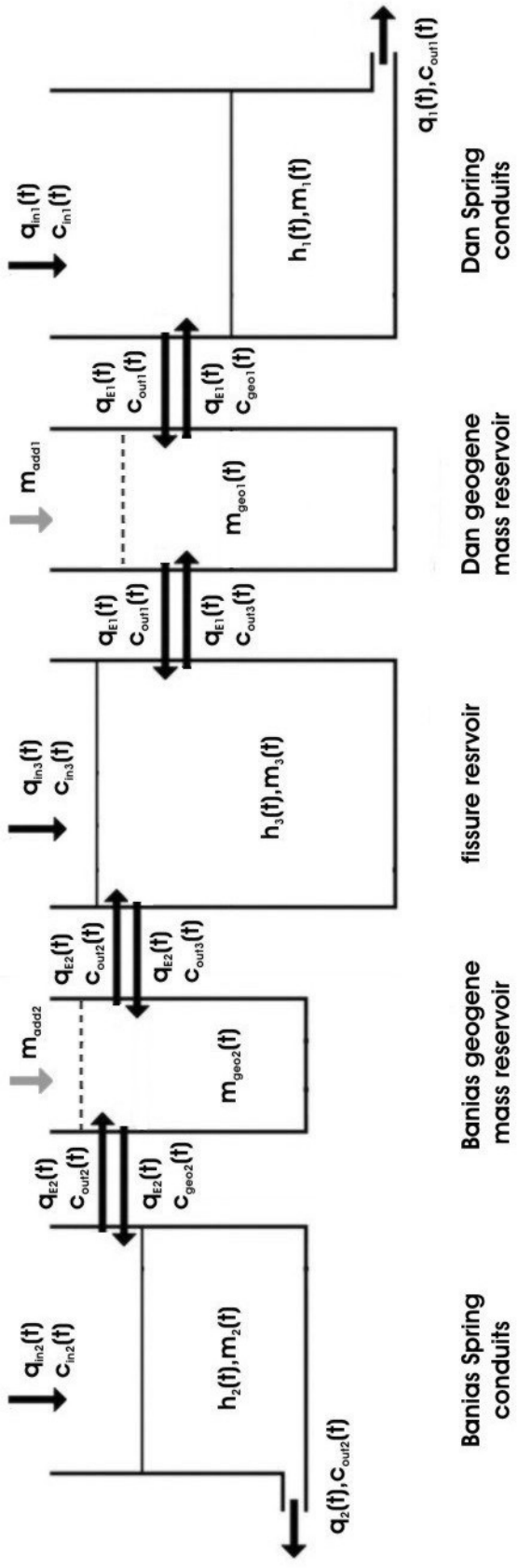

FIGURE 59: Schematic picture of the groundwater mixing model

But if exchange flow is going in the opposite direction to the respective conduit system mass is taken out of the geogene mass reservoir. This mass is calculated by assuming that the entire geogene mass reservoir is mixed with the water amount that causes the exchange flow. The resulting concentration is then attributed to the exchange flow to the respective conduit reservoir. This means for the Dan Spring system:

$$m_{geo1}(t) = m_{geo1}(t-1) + m_{add1} - \frac{m_{geo1}(t)}{h_3(t)} q_{E1}(t), \tag{145}$$

and for the Banias system

$$m_{geo2}(t) = m_{geo2}(t-1) + m_{add2} - \frac{m_{geo2}(t)}{h_3(t) - H_2 \cdot n_2} q_{E2}(t). \tag{146}$$

For the Banias system, the altitude difference of the two springs H_2 had to be considered. Since H_2 includes the porosity it had to be transformed using the fissure porosity n_2. Rearranging equations (145) and (146) gives the geogene mass in Dan and Banias Spring geogene mass storages $m_{geo1}(t)$ and $m_{geo2}(t)$ [g/m²] at time step t if flow from the fissures to the respective conduits system happens:

$$m_{geo1}(t) = \frac{m_{geo1}(t-1) + m_{add1}}{1 + \frac{q_{E1}(t)}{h_3(t)}} \tag{147}$$

$$m_{geo2}(t) = \frac{m_{geo2}(t-1) + m_{add2}}{1 + \frac{q_{E2}(t)}{h_3(t) - H_2 n_2}} \tag{148}$$

Knowing these masses the new concentrations can be calculated: As explained above if water flows to the fissures from the Dan or the Banias conduit system it bypasses the respective geogene mass reservoir. Hence its concentration $c_{out1}(t)$ and $c_{out2}(t)$ stay the same. But if water flows back to the respective conduit system the mass contributed from the respective geogene mass reservoir has to be added to the mass already stored in the respective conduit reservoir. This means for Dan Spring system:

$$c_{out1new}(t) = \frac{\frac{m_{geo1}(t)}{h_3(t)} q_{E1}(t) + c_{out1}(t) h_1(t)}{h_1(t)}, \tag{149}$$

and for the Banias Spring system

$$c_{out2new}(t) = \frac{\frac{m_{geo2}(t)}{h_3(t) - H_2 n_2} q_{E2}(t) + c_{out2}(t) h_2(t)}{h_2(t)} \tag{150}$$

Whereby $c_{out1new}(t)$ and $c_{out2new}(t)$ are the new concentrations in Dan and Banias Spring conduit system [g/m³] including the geogene contribution from there respective geogene mass reservoirs at time t.

The whole numerical implementation of the groundwater mixing model can be found in the Appendix A.6.5: Source code of the groundwater mixing routine.

9.6 Conclusions

Altogether adding these routines results in a model which includes a distributed snow melt routine, a distributed soil/epikarst routine and a lumped groundwater routine. This is summarized in FIGURE 60.

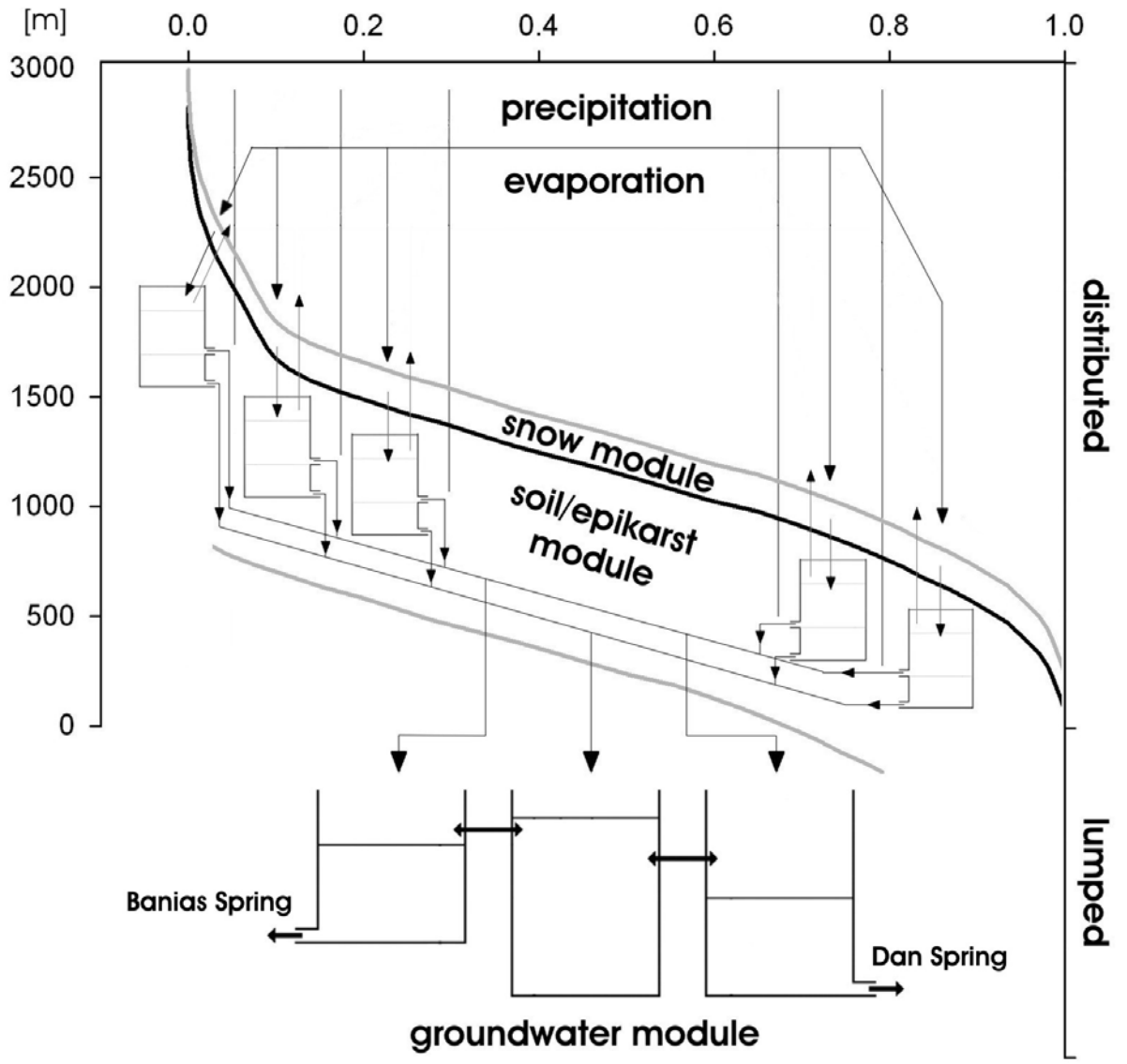

FIGURE 60: WHOLE MODEL STRUCTURE OF HYMKE_DUAL

The snow melt routine is based on the reliable routine of the HBV model (LINDSTRÖM ET AL, 1997). The soil-epikarst routine is based on the concept developed by PERRIN ET AL. (2003), as introduced in chapter 3.2.3, and the findings of ARBEL ET AL. (2008). Differences to the model of PERRIN ET AL. (2003) are that there is no saturated flow in the epikarst and no linear storage for the soil but unsaturated flow calculated by the Mualem-Van Genuchten equation

(RAWS ET AL., 1993). PERRIN ET AL. (2003) used numeric modelling of saturated flow with three different layers of saturated conductivity accounting for the decreasing hydraulic conductivity of epikarst with increasing depth. In the soil-epikarst routine of the present work only two layers of different saturated conductivity were incorporated: the upper epikarst and the lower epikarst layer. But similarly to PERRIN ET AL. (2003) the epikarst acts as storage and distribution system for slow diffuse matrix flow and fast conduit flow. It is assumed that no changes on solute concentration occur in the snow pack. Complete mixing in the soil layer is assumed for the soil-epikarst module similarly to PERRIN ET AL. (2003). However in the epikarst PERRIN ET AL. (2003) simulated solute transport numerically with the result that piston flow effects could be reproduced adequately. In this soil/epikarst routine the solute transport is modelled similar to the soil layer: Complete mixing is assumed for both, the upper epikarst and the lower epikarst layer. The modelling of groundwater was performed using two types of reservoirs: first a slow reacting large storage representing the fissures and second a fast reacting small storage representing the conduits. This is similar to the approaches of GEYER ET AL. (2008) and FLEURY ET AL. (2007) but with the big difference that in their approaches flow can not take place in both directions: only from the fissures to the conduits. In this approach flow from the conduits to the fissures can occur and vice versa as well as water entering the fissures from one conduit system can leave the fissures towards the other conduit system. The exchange between the two systems is based on the Double Continuum approach introduced by TEUTSCH (1988) but due to the scarcity of groundwater data in Mt. Hermon a lumped approach was used instead of numeric groundwater modelling based on Darcy's law (see FIGURE 60). Once again complete mixing is assumed. For the modelling of conduit water concentrations this assumption can be made since the conduit volume is very small compared to water entering during the rainy season and piston flow effects happen on time scale which is small compared to the model resolution of one day. The assumption of complete mixing of fissure groundwater will be discussed by examining the modelling results.

10 Application of HYMKE_DUAL

10.1 Input data

The hydrological years 1973/1974 to 1982/1983 were selected because snowmelt temperature data was available for that period (see section 10.1.2: Temperature).

10.1.1 Precipitation

Precipitation input for the simulation from 1973 to 1983 was provided by Ma'ayan Barukh (240 m ASL), Yiftah (445m ASL) and Malkya (690m ASL) meteorological stations situated in the region of the Upper Jordan River Catchments. Daily precipitation of these stations is shown in FIGURE 61. The choice of these stations was mainly justified by their complete data series for the simulation period.

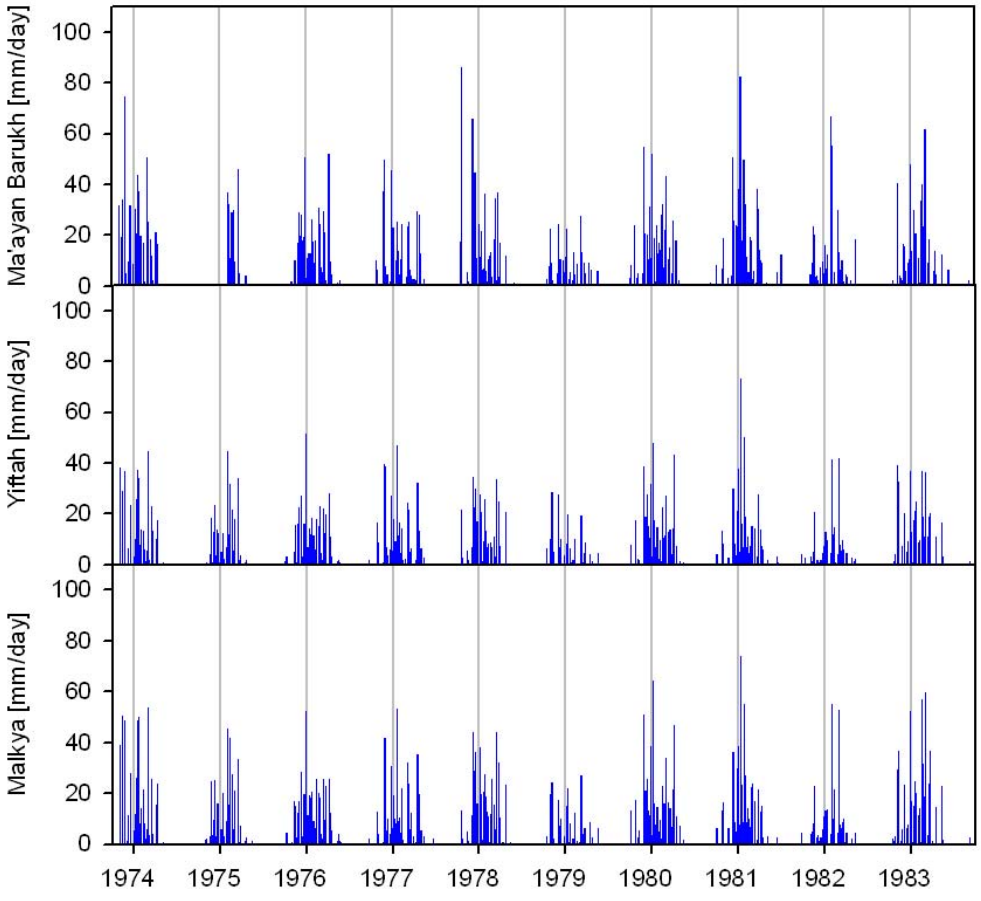

FIGURE 61: Daily precipitation of Ma'ayan Barukh, Yiiftah and Malkya meteorological stations from 1973 to 1983

10.1.2 Temperature

Since there was no temperature data available from stations directly inside the study area time series from Zefat meteorological station were used as temperature input (FIGURE 62). Zefat is located 40 km in the southern west of Mt. Hermon at an altitude of 934 m ASL. To apply this data to each altitude strip in the model the temperature from the altitude of Zefat station had to be transformed to the mean altitude of each altitude strip. This was done using a temperature altitude gradient AG = 0.55 °C/100m for this region according to BRIELMANN (2008) according to KESSLER (1980). Temperature $T_i(t)$ for each altitude strip i, i=1,…,56, at time t [°C] was then calculated by

$$T_i(t) = T_{Zefat}(t) + (Alt_i - Alt_{Zefat})\frac{AG}{100} \tag{151}$$

Whereby $T_{Zefat}(t)$ is the temperature at Zefat meteorological station [°C] at time t, Alt_i the mean altitude of altitude strip i [m] and Alt_{Zefat} the altitude of Zefat station [m]. Missing values were linearly interpolated. The whole algorithm to the method described above can be found in the Appendix A.7.2: Source code for interpolation and regionalization of temperature data.

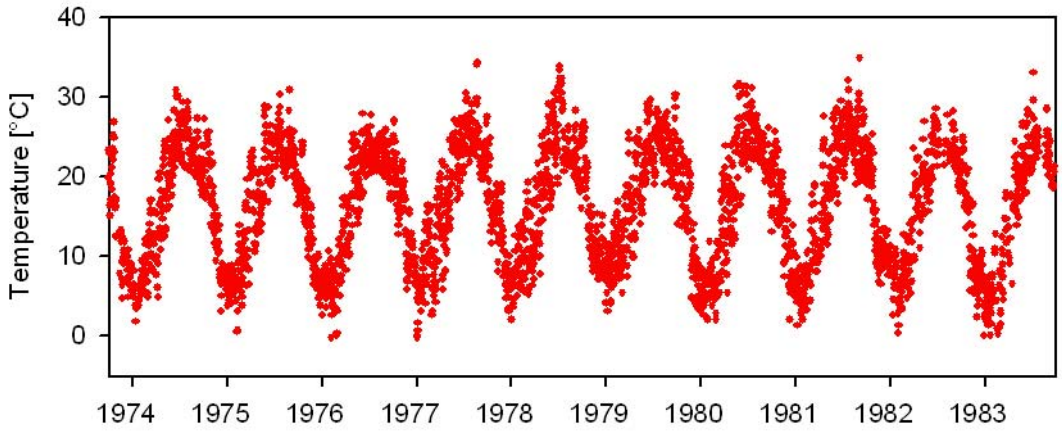

FIGURE 62: Temperature time series of Zefat station from 1973 to 1983

10.1.3 Evaporation

Data of potential evaporation bases on long term daily measurements of pan A evaporation (PONCE, 1989). Using three locations of long term measurements (Gamla, 380 m ASL, Ayelet HaShahar, 180 m ASL and Dafna, 150 m ASL) RIMMER AND SALINGAR (2006) calculated a mean seasonal evaporation trend for the entire Upper Catchments of the Jordan River whereby the average measured trend of pan A evaporation was an input for an optimization process in which parameters of the expected seasonal evaporation trend $E_p(JD)$ [mm/day]were determined (according to VINEY AND SIVAPALAN, 2000) as follows:

$$E_P(JD) = b_E\left[1 + a_E \sin\left(\lambda_E\left(JD + \omega_E\right)\right)\right] \tag{152}$$

Whereby *JD* is the day of the year according to the Julian calendar (beginning on the 1st of October) and a_E and b_E are constants [mm/day]. λ_E (=2*π/ 365.25) is the angular frequency and ω_E the phase shift. Parameters for equation (152) obtained by RIMMER AND SALINGAR (2006) are given in TABLE 11. To transform seasonal pan A evaporation values $E_p(JD)$ into land surface evaporation $Evap_{pot}(JD)$ these have to be multiplied with the so called pan A coefficient C_E. In this study this coefficient was set equal 0.54 following findings of a study performed by MÖLLER AND STANHILL (2007) in Bet Dagan, Israel.

$$Evap_{pot}\left(JD\right) = C_E E_p\left(JD\right) \tag{153}$$

TABLE 11: Parameters for seasonal pan A evaporation trend determined by RIMMER AND SALINGAR (2006)

Paramater	Value
a_E	5.4531
b_E	0.5686
λ_E	0.0172
ω_E	67.3105

Evaporation was also to be regionalized for all altitude strips. Hence a way had to be found to attribute a daily potential evaporation to each altitude strip. In order to achieve this the temperature based method of THORNTHWAITE (1948) was applied. This method uses a complex empirical formula for the computation of average monthly potential evapo-transpiration $E_{pt,mon}$ [mm/month] (DINGMAN, 2002) as a function of the mean monthly temperature $\overline{T_{mon}}$ [°C]:

$$E_{pt,mon} = 0.533 \cdot n \cdot \frac{S_0}{12}\left(\frac{10 \cdot \overline{T_{mon}}}{I}\right)^a \tag{154}$$

Where *a* and *I* are two parameters, *n* the number of days of the respective month and S_0 the mean daily astronomic sunshine length of the respective month [h]. The astronomic sunshine length of one day *S(JD)* is calculated by

$$S(JD) = \frac{24}{\pi}\arccos\left\{1 - \left[1 - \tan\left(\frac{lat}{180} \cdot \pi\right) \cdot \tan\left(\frac{Obl}{180} \cdot \pi \cdot \cos\left(\pi \frac{JD - diff_{JD}}{Per_{Sol}}\right)\right)\right]\right\} \tag{155}$$

Whereby *lat* is the latitude of Mt. Hermon (33.35°), *Obl* the obliquity of the ecliptic (23.439°), *PerSol* the period between the solstices (182.625 days) and $diff_{JD}$ is the difference of the *JD* of this system (beginning from 1st of October) and the day of the year for the astronomic sunshine length calculation (beginning from the winter solstice) which is 356 days. To compare *Evap(JD)* provided by equations (152) and (153) with estimations of evapo-transpiration obtained by Thornthwaite's approximate equation (154) has to be transformed to yield daily estimations of evapo-transpiration $E_{pt}(JD)$:

$$E_{pt}(JD) = 0.533 \cdot \frac{S_0}{12}\left(\frac{10 \cdot T_i(JD)}{I}\right)^a \tag{156}$$

Whereby $T_i(JD)$ is the daily temperature of altitude strip *i* where the pan A measurements were performed (the altitude strip with the mean altitude of 250 m ASL was regarded to be representative, i.e. $i = 4$) calculated as described in section 10.1.2. Now equation (156) can be fitted to equations (152) and (153) by optimizing parameters *I* and *a*. This was done using the Matlab function *lsqcurvefit* which is based on the interior-reflective Newton method described in COLEMAN AND LI (1996) and COLEMAN AND LI (1994). Results can be seen in FIGURE 63. Applying now equation (156) with the fitted parameters on the other altitude strips by substituting $T_i(JD), i = 1,2,3,5,\ldots,56$, gives the potential evaporation for each altitude strip.
The numerical implementation of the regionalisation described in this section can be found in the Appendix A.7.3: Source code for regionalisation of potential evaporation data.

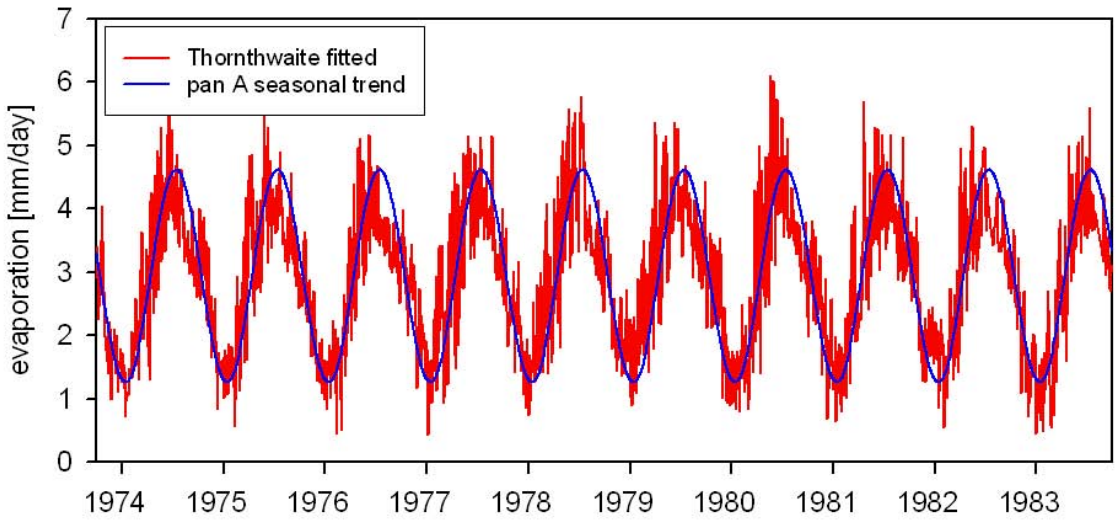

FIGURE 63: Seasonal pan coefficient corrected seasonal tren of pan A evaporation by RIMMER AND SALINGAR (2006) and fitted Thornthwaite evaporation for altitude strip 4

10.1.4 Plant uptake and release of NO_3 in the soil

The use of NO_3 for mixing calculations implies the estimation of uptake and release of NO_3 by the vegetation and micro-organisms. The transformation of organic nitrogen into inorganic nitrogen is the mineralization which is a microbial-driven soil process. Reduced nitrogen from the mineralization (e.g. NH_4) can then be transformed to NO_3 by a process called nitrification and therefore plays an important role in the nitrogen cycle (GELFAND AND YAKIR, 2008). There are two different groups involved in the nitrification process: ammonia oxidizing bacteria and nitrite oxidizing bacteria. These two groups have different tolerances to environmental stress such as temperature and water content (AVRAHAMI ET AL., 2003; AVRAHAMI AND CONRAD, 2005). The first step of nitrification, ammonia oxidation, is considered to be the rate limiting step of nitrification (KOWALCHUK AND STEPHEN, 2001). Compared to the first step of nitrification the oxidation of NO_2 to NO_3 is regarded to happen quickly. This is a reason for the rarity of higher concentrations of NO_2 in terrestrial systems (GELFAND AND YAKIR, 2008). Slow production of inorganic nitrogen in reduced forms (mainly NH_4) is taking place during the dry period. This occurs because of slow decomposition and mineralization processes which are again strongly influenced by the activity of abiotic enzymes like urease, protease and β-glucosidase (SARDANS ET AL., 2008). However, in the wet season, rapid recycling and uptake of reduced nitrogen can happen

(ZAADY, 2005; AUSTIN AND VIVANCO, 2006). Hence ammonium oxidizing bacteria play an important role in nitrogen cycling (AUSTIN ET AL., 2006).

These processes were partly identified in a study GELFAND AND YAKIR (2008) realized in the Yatir Forest, Israel. There they investigated the NH_4, NO_2 and NO_3 variations in the soil below the forest and the surrounding shrub lands. With annual precipitation of 280 mm the Yatir Forest is far dryer than Mt. Hermon but the seasonality of the wet and dry season is similar. FIGURE 64 shows the variations of NH_4, NO_2, NO_3 and total N in the soil below the Yatir Forest shrub land. As expected there are only low concentrations of NO_2. The small increase from May 04 can be explained by the greater drought tolerance of ammonia oxidizing bacteria compared to nitrite oxidizing bacteria (HASTINGS ET AL., 2000). NH_4 is negatively correlated with NO_3 which obviously is an indicator of the nitrification process. Variations in total nitrogen are explained by the reduction of the soil nitrogen pool by plant uptake whereas increased concentrations are explained by low demands by the vegetation and mineralization (BINKLEY AND HART, 1989, in GELFAND AND YAKIR, 2008).

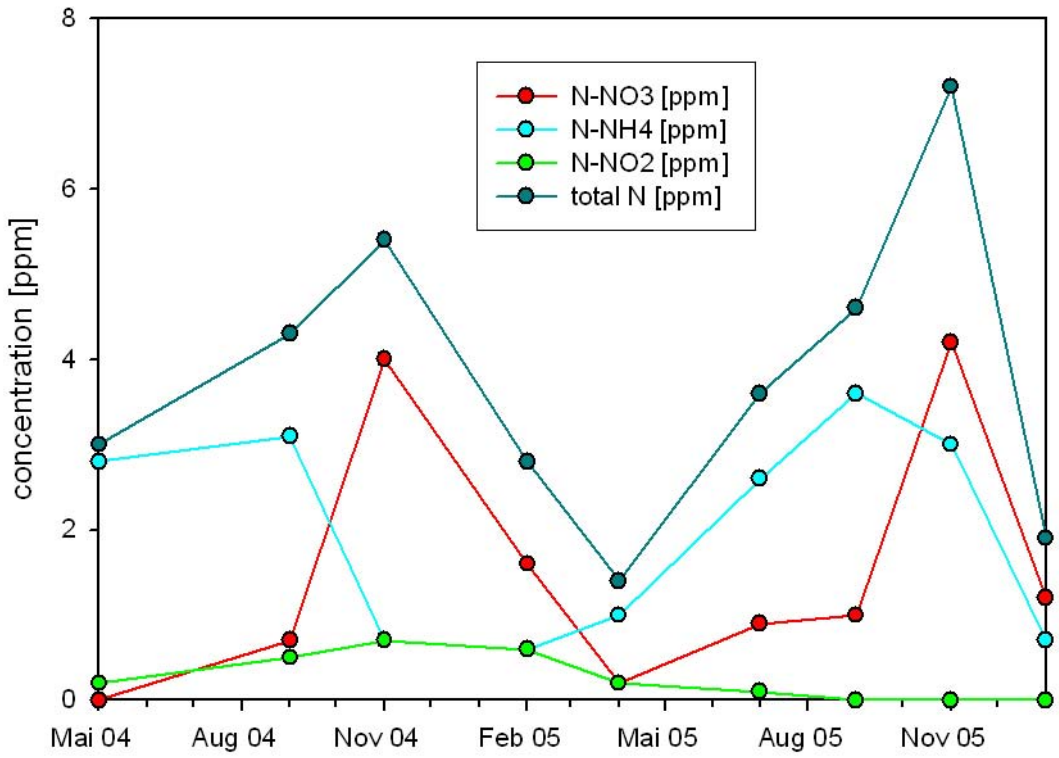

FIGURE 64: Variations of soil N-NO3, N-NH4, N-NO2 and total N [ppm] from May 2004 to January 2006 below the Yatir Forest shrub land as observed by GELFAND AND YAKIR (2008)

However the study of GELFAND AND YAKIR (2008) did not yield data of both mineralization rates and uptake by plant rates which are necessary for the estimation of this process in the soil layer of the soil/epikarst routine. This information could be found in a study performed by JOFFRE (1990) in the rangelands of southwestern Spain. The climate type of this region is, similar to that on Mt. Hermon, a sub-humid mediterranean type with temperate winters and with mean annual precipitation of 648 mm. Rainy season is from October to April. JOFFRE (1990) used two complementary methods to study nitrogen dynamics: first a method to characterize mineralization activity. This was done by incubating soil samples in the field and in the laboratory, and by measuring the amounts of ammonium and nitrate produced. With this method the dynamics of nitrogen mineralization over a year, as well as the maximum quantity of mineral nitrogen which can be absorbed by vegetation, can be determined (NADELHOFFER ET AL., 1984). The second method was a quantification of uptake by plants during the growing period. It was obtained from the nitrogen content of plant material and an estimation of the aerial and subterranean production of the vegetation studied. The results are shown in FIGURE 65 and FIGURE 66. Nitrogen mineralization stayed constant from October to April. Only in December it reaches a negative value what is attributed to immobilization by micro-organisms (JOFFRE, 1990). From April to June, mineralization increases strongly. This can be explained by decomposition of the root system and of the microbial biomass due to soil desiccation (MCGILL ET AL., 1981).

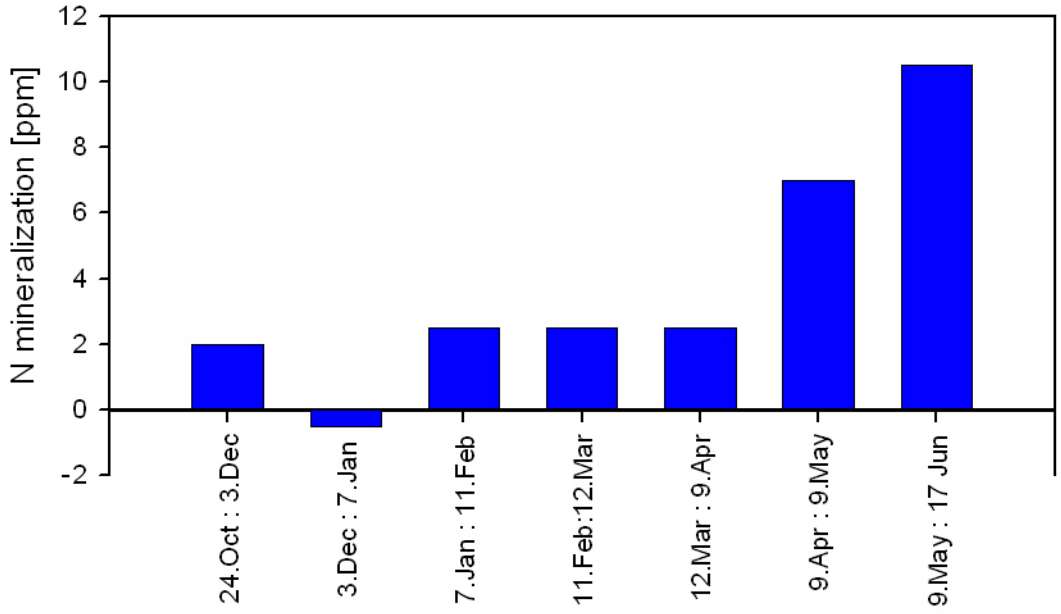

FIGURE 65: Accumulated nitrogen mineralization [ppm] for seven incubation periods from October 1985 to June 1986 observed by (JOFFRE, 1990)

Seasonal variations of nitrogen consumption reflect the growth dynamics of the vegetation. During the first period in FIGURE 66 nitrogen immobilization is due to root growth of the plants. During the second stage subterranean and aerial parts consumption area is the same order of magnitude but its sum is slightly smaller compared to the first observation period. In the last period, from March to June (end of vegetation period), the largest amount of nitrogen is consumed which can be manly attributed to growth of the aerial parts of the plants (JOFFRE, 1990).

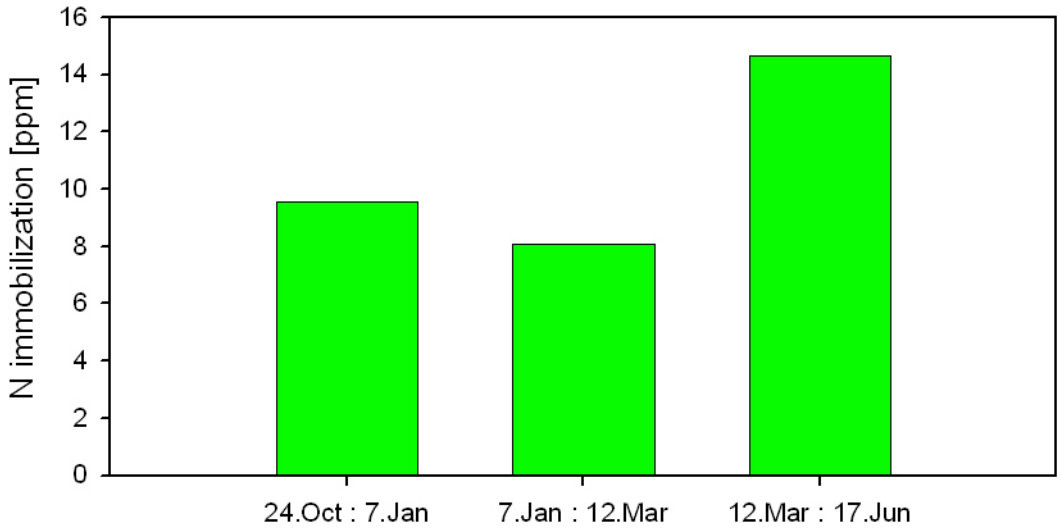

FIGURE 66: Accumulated plant nitrogen immoblization [ppm] for three periods from October 1985 to June 1986 observed by (JOFFRE, 1990)

Downscaling this data to daily values and assuming that the excess of immobilized nitrogen is mineralized during the dry season (as mentioned by GELFAND AND YAKIR, 2008) gives the annual variation of nitrogen mineralization and plant uptake. Assuming now that under wet conditions (i.e., enough water is available for the soil layer to drain downwards) nitrification is occurring rapidly the uptake and release of NO_3 by the vegetation can be estimated by the uptake and mineralization of nitrogen. Therefore, the difference between mineralization and immobilization gives an effective mineralization rate $m_{UpRel}(t)$ [ppm/day] which can be seen for a whole hydrological year in FIGURE 67. The source code of the sub-scaling algorithm can be found in the Appendix A.7.1: Source code for down-scaling of nitrogen mineralization and immobilization observations. Knowing the bulk density of the soil and the soil thickness these values can be converted into [g/m²/day].

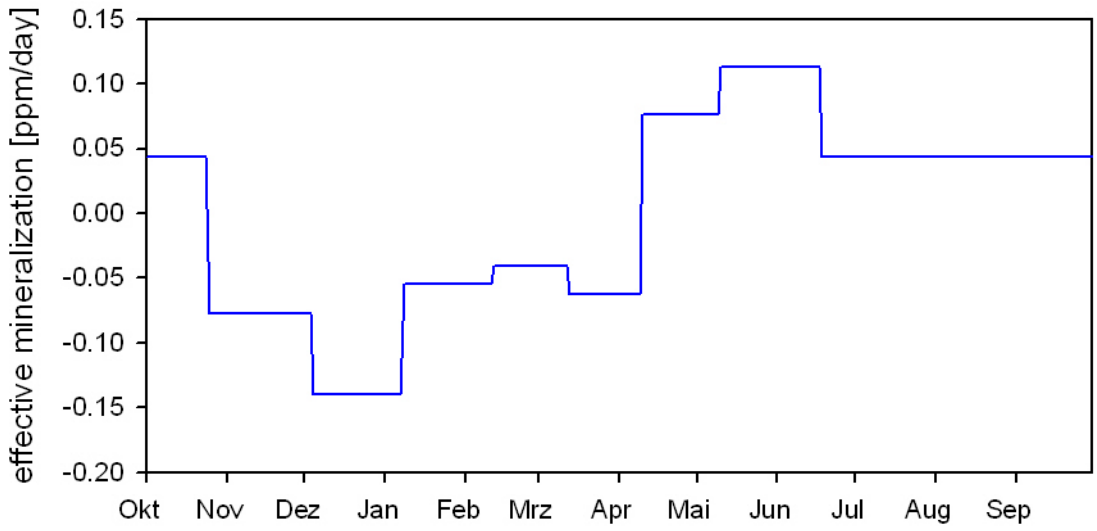

FIGURE 67: Effective mineralization of nitrogen, negative values stand for effective plant immobilization; data obtained from JOFFRE (1990).

10.2 Sensitivity analysis of the HYMKE_DUAL routines

To better understand the behaviour of HYMKE_DUAL on parameter changes a sensitivity analysis was performed. This was done separately for every routine by defining reasonable ranges for each parameter and varying the parameters within this range. The findings should support the calibration of the whole model on real data in section 10.3.

10.2.1 The snowmelt routine

In order to define a reasonable range of parameters for the snow melt routine literature was reviewed. Different sets of parameters found are listed in TABLE 12. Melting temperature T_M was always chosen to be 0 °C except in HAMILTON ET AL. (2000). Degree day factor *ddf* ranges from 1.65 to 4 mm/°C/day whereas the refreezing factor *RF* was between 0.05 and 1. Differences in holding capacity are not so large: values chosen are 0.05 and 0.1.

TABLE 12: Different sets of parameters applied in the HBV snow melt routine

parameter	description	HAMILTON ET AL. (2000)	MOORE (1993)	SEIBERT (1998)
T_M	melting temperature [℃]	-0.727	0	0
ddf	degree day factor [mm/℃/day]	1.65 to 2.55	2 to 4	1 .5 to 4
RF	refreezing factor [-]	0.41 to 0.63	0.5 to 1	0.05
HC	holding capacity of snow pack [-]	0.1	0.05	0.1

To check the sensitivity of the snowmelt routine to changes of them each parameter was varied from the lower to the upper end of its range as defined in TABLE 12 while the other parameters where set to default values (T_M = 0 °C, *ddf* = 2 mm/°C/day, *RF* = 0.05 and *HC* = 0.1). Results are shown in FIGURE 68.

The results in FIGURE 68 show the area weighted mean output of the snow epikarst routine. Only the years from 1978 to 1981 were plotted since differences of simulation results were minimal and would not be noticeable in a plot for the whole ten year simulation period. The most sensitive parameter of the analysis was the melting temperature T_M: setting the melting temperature to -0.727 °C resulted in a more precipitation like output of the snow melt routine, i.e. the small delays due to snow accumulation were smaller. Even though the maximum degree-day factor was more than double its minimum value, changes in the output were small. Only melt events were taking place more rapidly and thus led to a slightly higher melting peak. No significant changes could be recognized for the variation of the refreezing factor and the holding capacity.

The overall small sensitivity of the snow melt routine on changes of all included parameters is caused by the altitude distribution of Mt. Hermon. As it is visible in FIGURE 56 only about 10% of the study area is above 1500 m ASL. Snow is just accumulating were temperatures are below the melting temperature for long enough and this is only taking place in the upper regions of Mt. Hermon. Consequently snow melt contribution from these areas is just about 10% of the whole snow melt whereas the lower parts, which contribute the other 90%, are characterized by direct infiltration of rain or short time storage of snow since temperatures are too high. The major effect of the snow melt routine seems to be the attenuation of extreme rain events and then continuous release of water in small amounts as it can be seen in FIGURE 68. To maintain this effect parameters were set to T_M = 0 °C, *ddf* = 2 mm/°C/day, *RF* = 0.05 and *HC* = 0.1 for the further simulations.

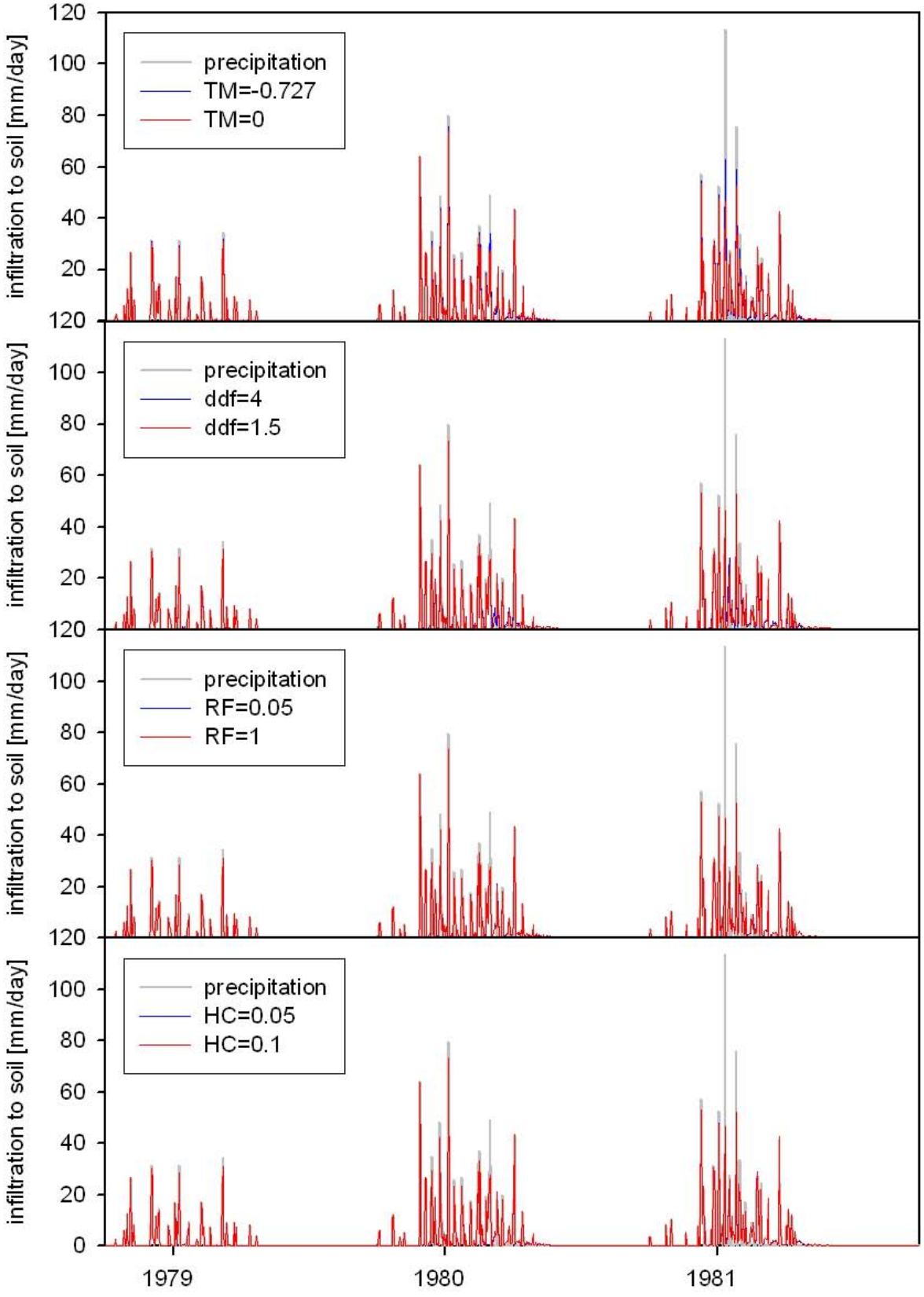

FIGURE 68: Results of sensitivity analysis of snow melt rotine

10.2.2 The soil/epikarst routine

Altogether there are 11 parameters in the soil/epikarst routine which have to be elected in a reasonable manner. Admittedly their number is high for just a single routine but all of them are either directly measurable or related to measurable parameters. All parameters and their descriptions are listed in TABLE 13. Unfortunately there was no specific data available for the study area. However literature was plentiful concerning hydraulic conductivities, depth of the epikarst and soils in northern Israel.

TABLE 13: Summary of the soil/epikarst routine parameters and description

parameter	description	unit
RD	thickness of soil layer [m]	[m]
h_{up}	thickness of upper epikarst [m]	[m]
h_{low}	thickness of lower epikarst [m]	[m]
$\theta_{sat,up}$	saturation water content of soil and upper epikarst [-]	[-]
$\theta_{rest,up}$	residual water content of soil and upper epikarst [-]	[-]
$K_{sat,up}$	saturated hydraulic conductivity of soil and upper epikarst[mm/day]	[mm/day]
m_{up}	parameter related to Brooks-Corey grain size index for soil and upper epikarst [-]	[-]
$\theta_{sat,low}$	saturation water content of lower epikarst [-]	[-]
$\theta_{rest,low}$	residual water content of lower epikarst [-]	[-]
$K_{sat,low}$	saturated hydraulic conductivity of lower epikarst [mm/day]	[mm/day]
m_{low}	parameter related to Brooks-Corey grain size index for lower epikarst [-]	[-]

Thickness of the whole epikarst layer was estimated by WILLIAMS (2008) to be 3 to 10 m whereas PERRIN ET AL. (2003) defined an epikarst thickness of 3.5 m in their study. No information about the lower epikarst could be found but the conceptual models introduced in chapter 3 let suggest that its thickness is smaller than the upper epikarst thickness. As mentioned in chapter 2 Mt. Hermon soils are primarily Terra Rossa soils which are relatively thin. PERRIN ET AL. (2003) estimated the soil thickness above the epikarst to be around 1 m. It is assumed that water storage in the soil and the epikarst is occurring mainly in weathering products of the limestone, i.e. the Terra Rossa. SINGER (2007) provides an overview of clay and silt contents found in the Israeli hill and mountain range: clay contents ranged from 60 to 75%, mostly increasing with depth, and silt contents from 15 to 30%, mostly decreasing with depth. Additionally SINGER (2007) found a decrease in organic matter content with depth from 6 to 2%. Using the SPAW Soil Water Characteristics tool (SAXTON, 2007, SAXTON AND RAWLS, 2006) this information could be transformed into saturation water contents, residual water contents, saturated hydraulic conductivities and Brooks-Corey grain size indices. For the soil and the upper epikarst a higher content of organic matter and silt was assumed by which saturation water contents from 48 to 55.3%, residual water contents from 33.9 to 35.2%, hydraulic conductivities from 2.16 to 115.2 mm/day and Brooks-Corey grain size

indices from 0.22 to 0.39 could be obtained. The same procedure was applied to the lower epikarst yielding water contents from 48.9 to 51%, residual water contents from 35.4 to 35.5%, hydraulic conductivities from 0.48 to 2.16 mm/day and Brooks-Corey grain size indices from 0.44 to 0.47 assuming that organic matter is nearly absent and silt content is also lower than in the soil and upper epikarst. It has to be mentioned that the SPAW Soil Water Characteristics tool only calculates soil characteristic parameters for clay contents lower than 60%. However, raising the clay content above 60% should lead to a farther decrease of the saturation water content and the saturated conductivity and a farther increase of residual water content and Brooks-Corey grain size index.

With this knowledge parameter ranges for the sensitivity analysis were determined (TABLE 14). Note that Brooks-Corey grain size indices were transformed with equation (80) to be applicable in the Mualem-Van Genuchten model. Similar to the sensitivity analysis of the snow melt routine default values in the middle of the defined range of the respective parameter were chosen. Simulation results for the maximum, minimum and default of each parameter were plotted while the other parameters kept their default values. For each parameter diagrams of actual evaporation, preferential flow to the conduits, matrix flow to the conduits and flow to the fissures were created.

TABLE 14: Parameter ranges chosen for sensitivity analysis of the soil/epikarst routine and their default values

parameter	range	default value	unit
RD	0.3 to 1.3	0.8	[m]
h_{up}	3 to 10	6.5	[m]
h_{low}	0.5 to 2	1.25	[m]
$\theta_{sat,up}$	0.45 to 0.553	0.5015	[-]
$\theta_{rest,up}$	0.339 to 0.37	0.3545	[-]
$K_{sat,up}$	0.5 to 115	57.75	[mm/day]
m_{up}	0.18 to 0.29	0.235	[-]
$\theta_{sat,low}$	0.45 to 0.51	0.48	[-]
$\theta_{rest,low}$	35.4 to 0.36	0.357	[-]
$K_{sat,low}$	0.05 to 0.5	0.275	[mm/day]
m_{low}	0.30 to 0.32	0.31	[-]

FIGURE 69 displays the sensitivity of the four output variables on changes of the thickness of the soil layer *RD*. Results indicate that more actual evaporation is occurring when the soil is thicker. Thus if the soil layer is thinner less actual evaporation takes place which leads to more preferential and matrix flow to the fissures and a more continuously discharging lower epikarst.

FIGURE 70 shows the sensitivity to changes on the thickness of the upper epikarst layer. Since the soil layer thickness is set to its default value (see TABLE 14) no influences on the actual evaporation can be observed. This changes if the preferential and matrix flow to the conduits are considered: if h_{Up} is smaller more preferential flow takes place whereas if it is larger more matrix flow to the conduits occurs. Higher matrix flow to the conduits also indicates a more continuous recharge to the lower epikarst which is consequently discharging more continuously as well.

Changes on h_{Low} only influence the behaviour of lower epikarst discharge: the discharge to the fissures is slightly less with smaller thickness of the lower epikarst (FIGURE 71). There is no influence on actual evaporation, preferential flow to conduits and matrix flow to conduits.

Varying the saturation water content of the soil and upper epikarst $\theta_{Sat,Up}$ in FIGURE 72 indicates that evaporation is higher if $\theta_{Sat,Up}$ is larger. Lowering $\theta_{Sat,Up}$ leads to more preferential flow to the conduits and less matrix flow to the conduits. However, higher peak values of matrix flow to the conduits can be attributed to lower values of $\theta_{Sat,Up}$ since it narrows the range of relative saturation and thus a reaching of saturated hydraulic conductivity happens more often. The more continuous matrix flow leads to more continuous recharge to the lower epikarst which then also discharge more continuously for larger $\theta_{Sat,Up}$s.

In FIGURE 73 it can be seen that variation of $\theta_{Rest,Up}$ only has a small impact on the soil/epikarst routine output variables: the actual evaporation is slightly higher with lower $\theta_{Rest,Up}$s as a consequence of higher water availability. Discharge to the conduits, preferential flow and matrix flow, is not changing significantly. And some more discharge to the fissures can be seen for lower $\theta_{Rest,Up}$s, too.

Changing $K_{Sat,Up}$ in the range set in TABLE 14 on output variables (FIGURE 74) caused actual evaporation to increase for low $K_{Sat,Up}$s. Additionally there is more preferential flow to the conduits when choosing a low $K_{Sat,Up}$. Despite of that there is more matrix flow to the conduits and more flow to the fissures with a large $K_{Sat,Up}$. Hence flow to the fissures once again depends on the amount of matrix flow in the upper epikarst.

Considering the m_{Up} parameter which is related to the Brooks-Corey grain size index in FIGURE 75 shows that actual evaporation is not changing greatly by varying m_{Up}. Low m_{Up}

causes more preferential flow to the conduits whereas there is more matrix flow to the conduits for large m_{Up}s. The highest peak values of matrix flow to discharge can be attributed to low m_{Up}s though. Matrix flow to fissures correlates again with the amount of matrix flow to the conduits: with larger m_{Up}s it increases.

In the lower epikarst sensitivity analysis showed that the parameters $\theta_{Sat,Low}$, $\theta_{Rest,Low}$ and m_{Low} do not change significantly the output of actual evaporation, matrix or preferential flow to the conduits as well as the outflow to the fissures (FIGURE 76, FIGURE 77 and FIGURE 79). Only $K_{Sat,Low}$ has an impact on discharge to the fissures (FIGURE 78): with large $K_{Sat,Up}$ there is logically more discharge to the fissures, but also more variation in the discharge behaviour. And if $K_{Sat,Low}$ is small there is less discharge but less variations in discharge. A lower hydraulic conductivity also causes ponding back in the upper epikarst which leads to slightly more discharge to the conduits.

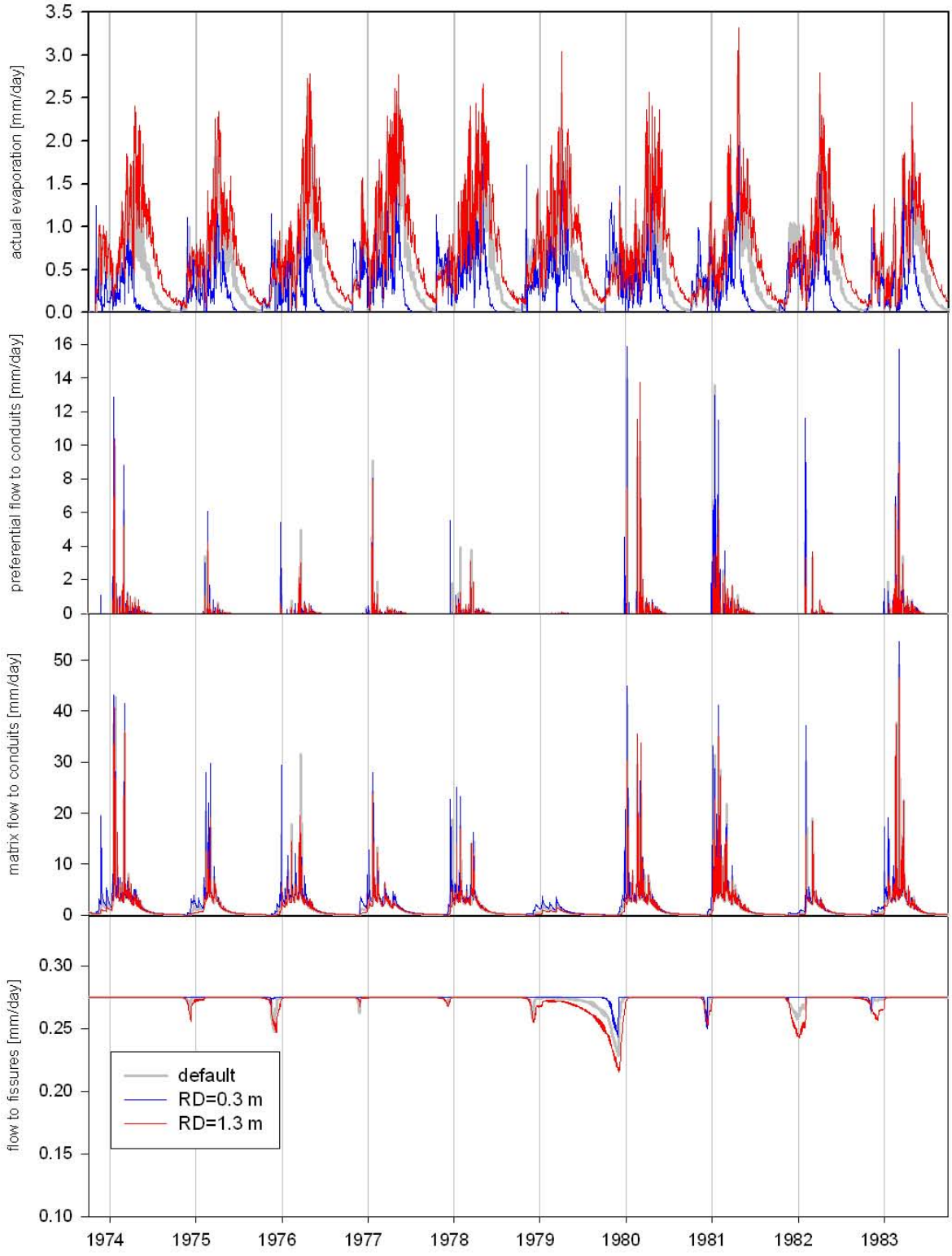

FIGURE 69: Sensitivity analysis for the thickness of the soil layer *RD*

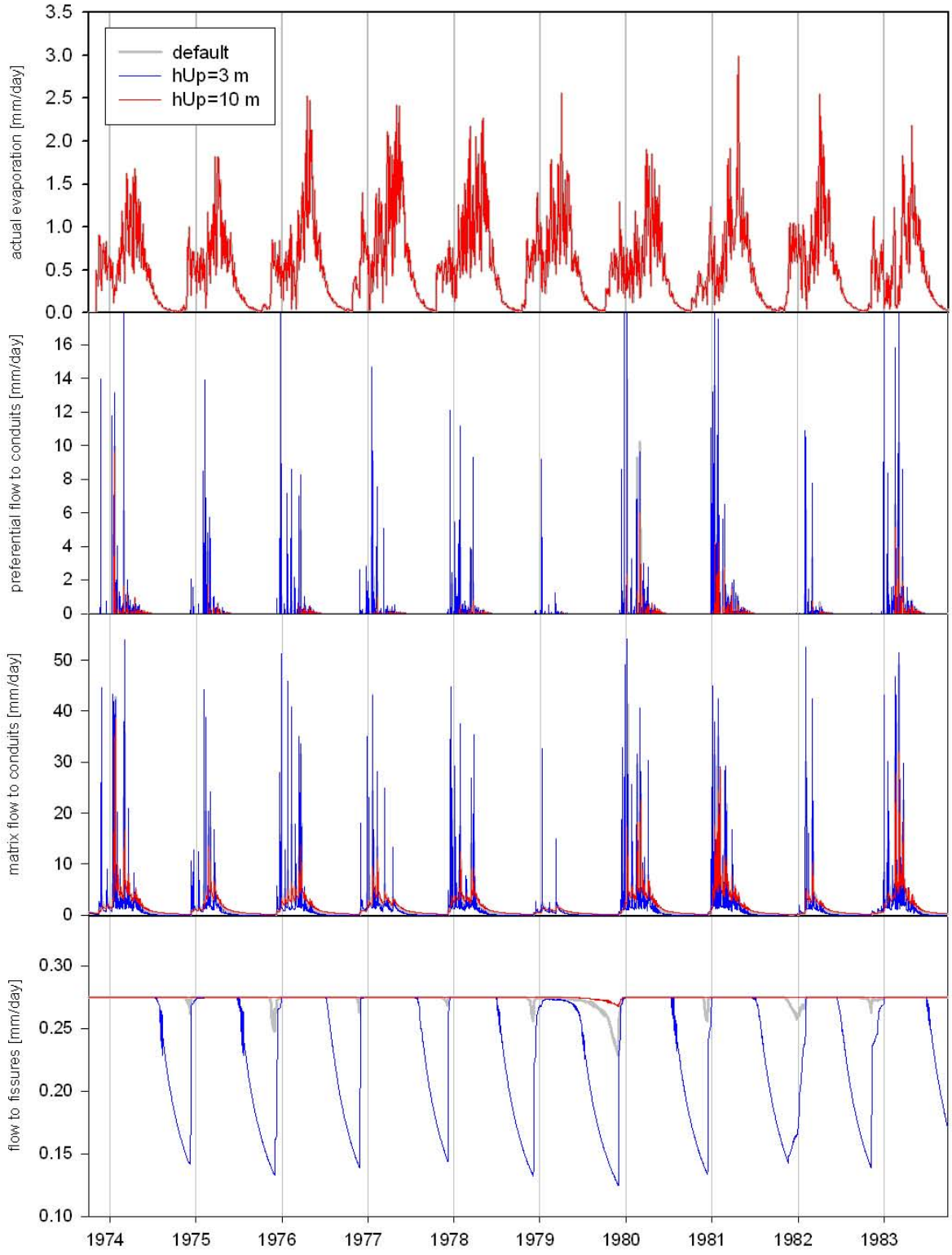

FIGURE 70: Sensitivity analysis for the thickness of the upper epikarst h_{Up}

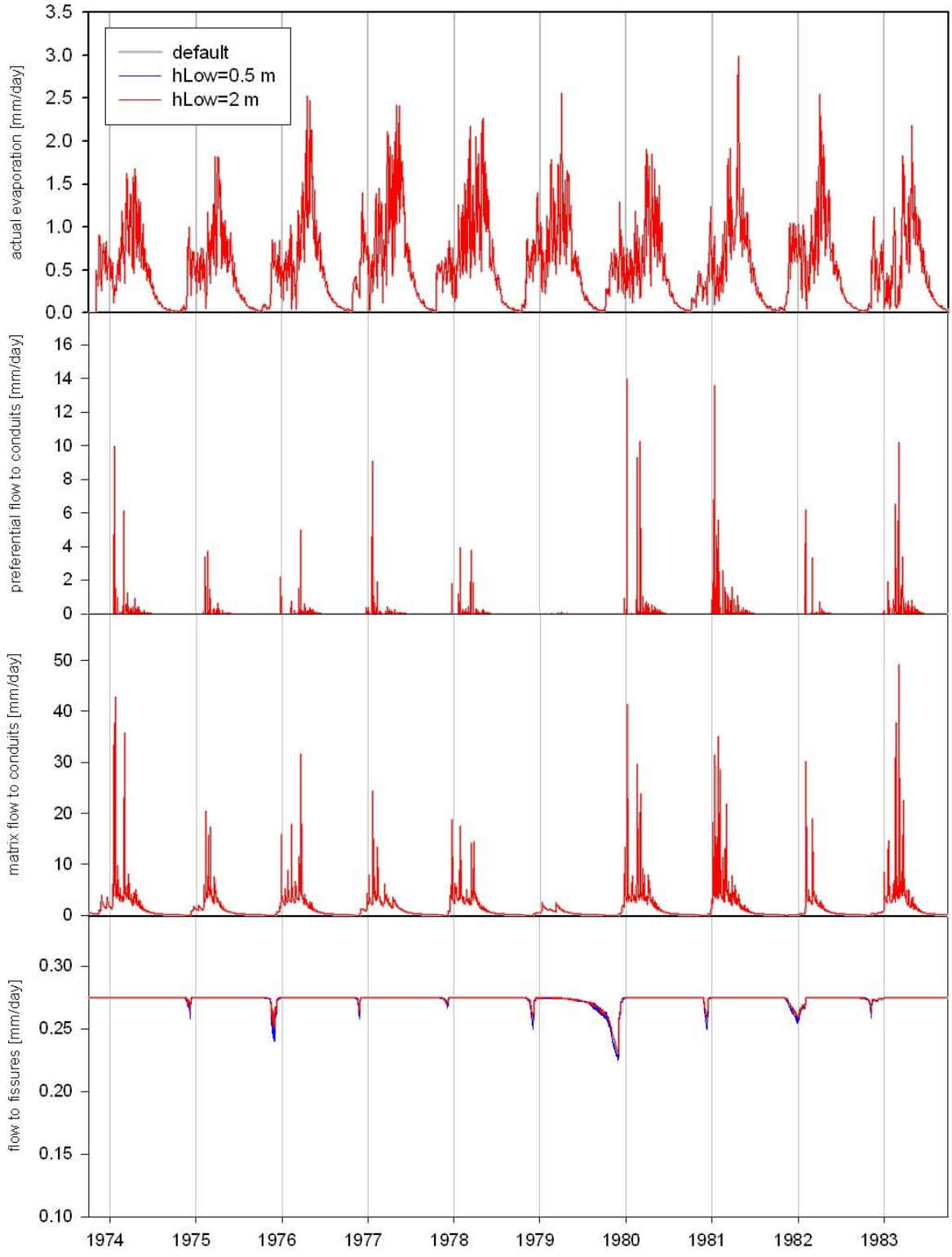

FIGURE 71: Sensitivity analysis for the thickness of the lower epikarst h_{Low}

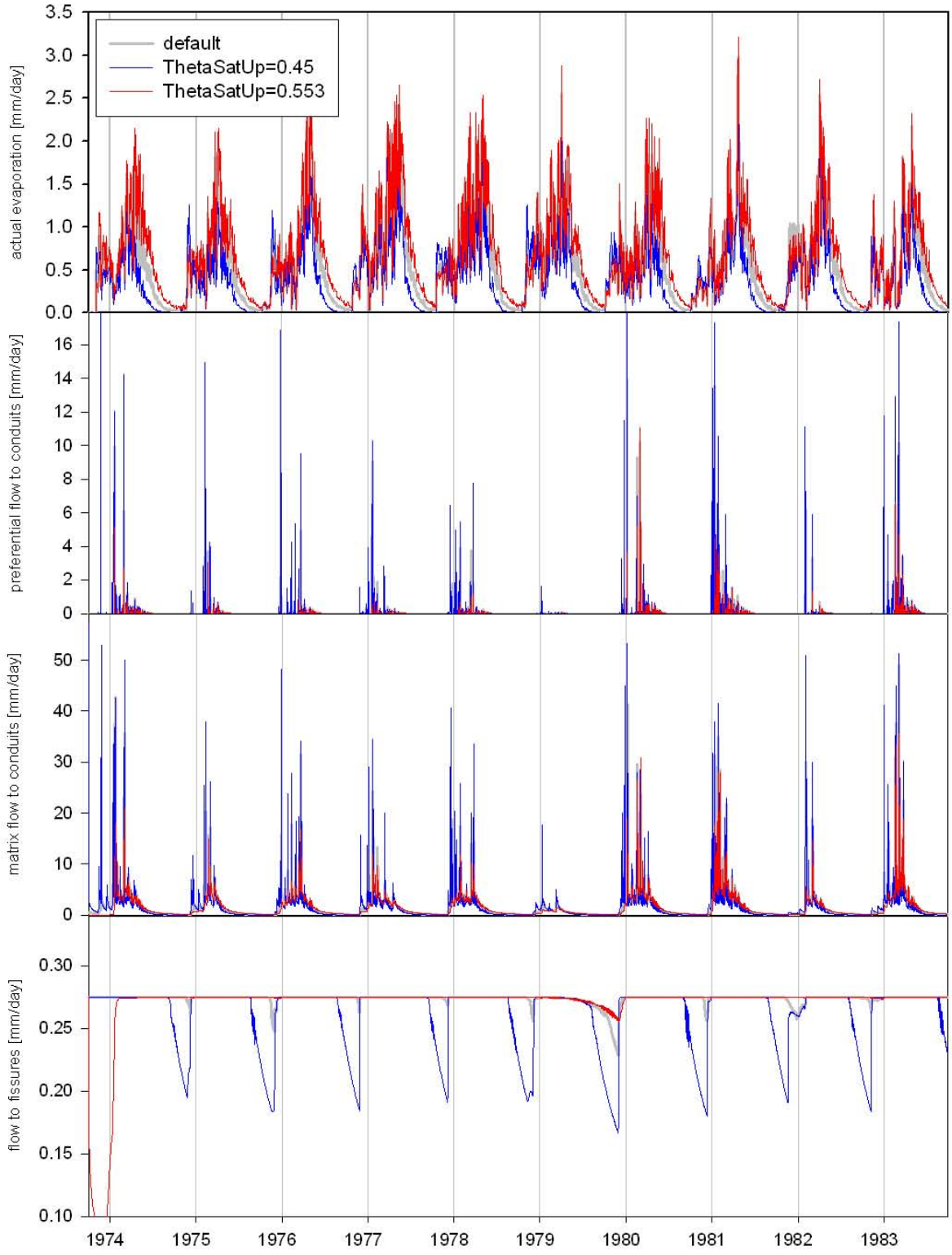

FIGURE 72: Sensitivity analysis for the saturation water content of the soil and upper epikarst $\theta_{Sat,Up}$

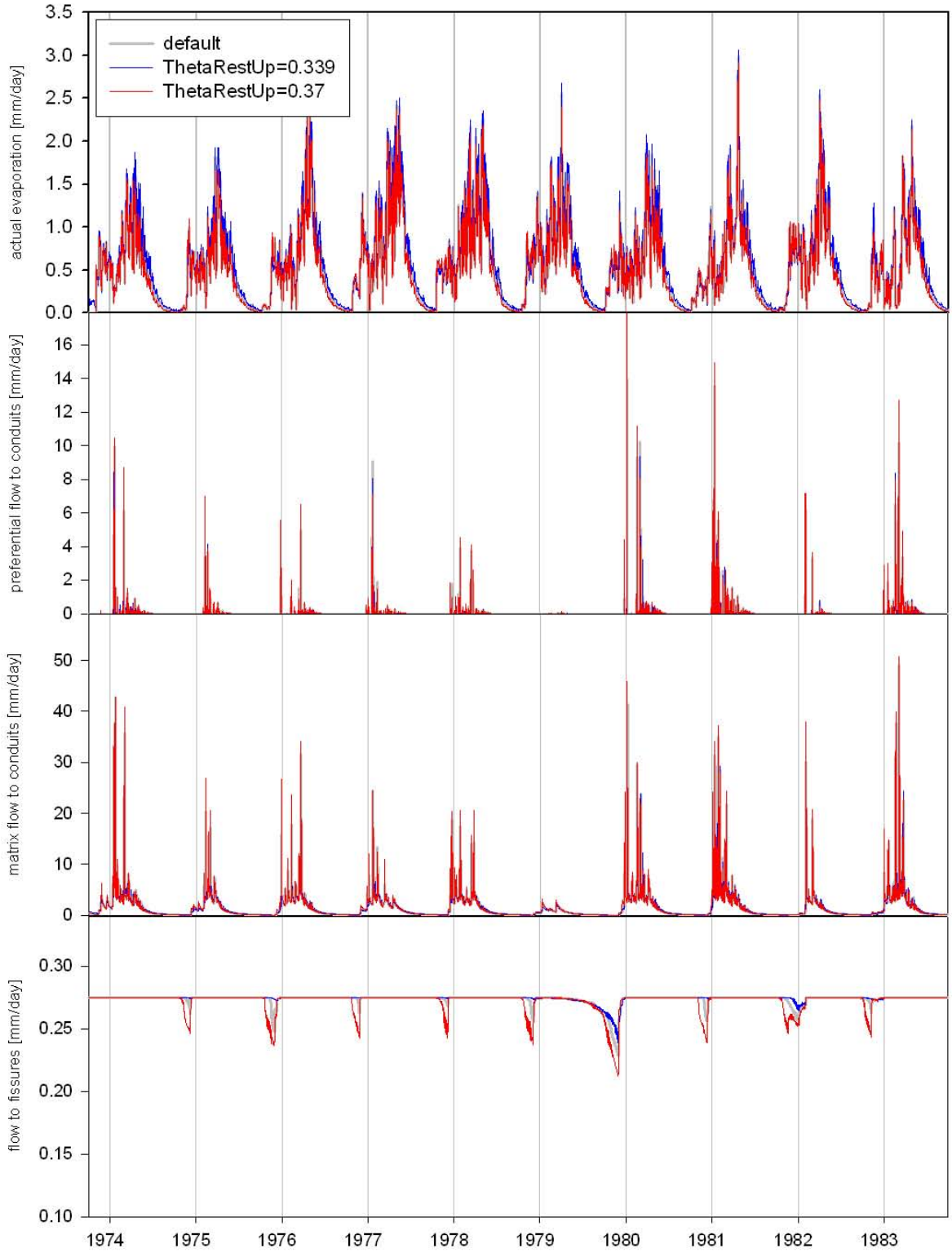

FIGURE 73: Sensitivity analysis for the residual water content of the soil and upper epikarst $\theta_{Rest,Up}$

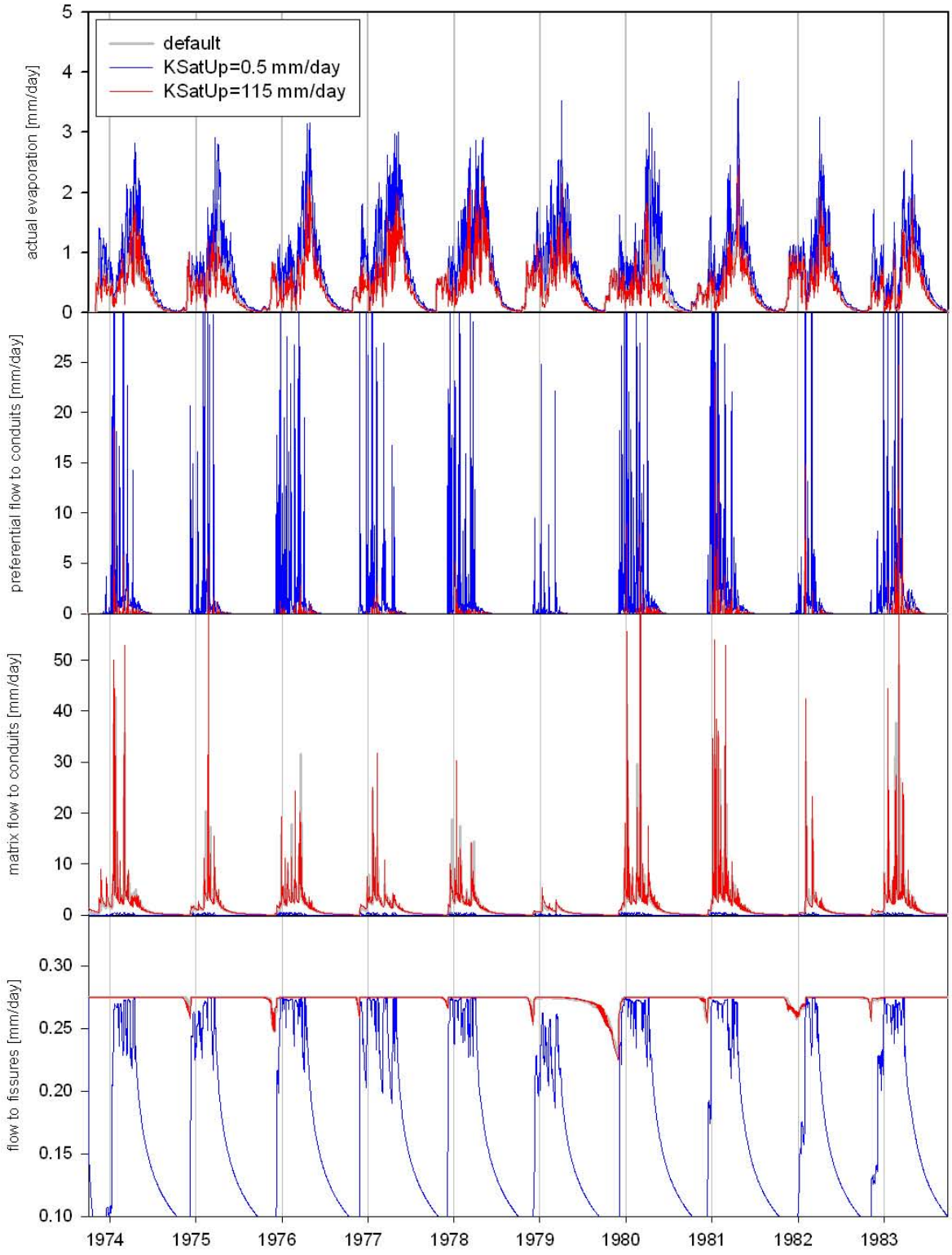

FIGURE 74: Sensitivity analysis for the saturated hydraulic conductivity of the soil and upper epikarst $K_{Sat,Up}$

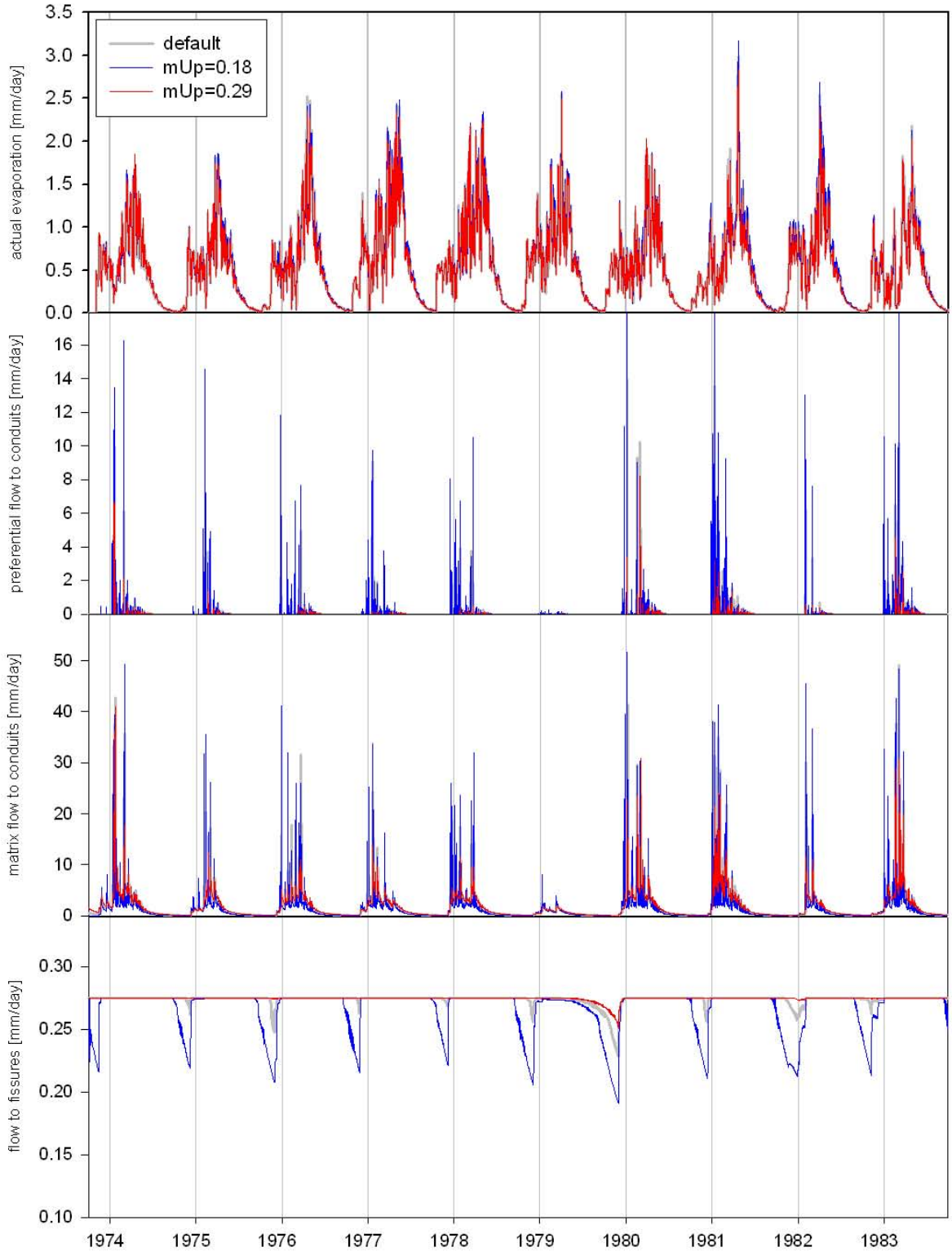

FIGURE 75: Sensitivity analysis for parameter which is related to the Brooks-Corey grain size index for the soil and upper epikarst m_{Up}

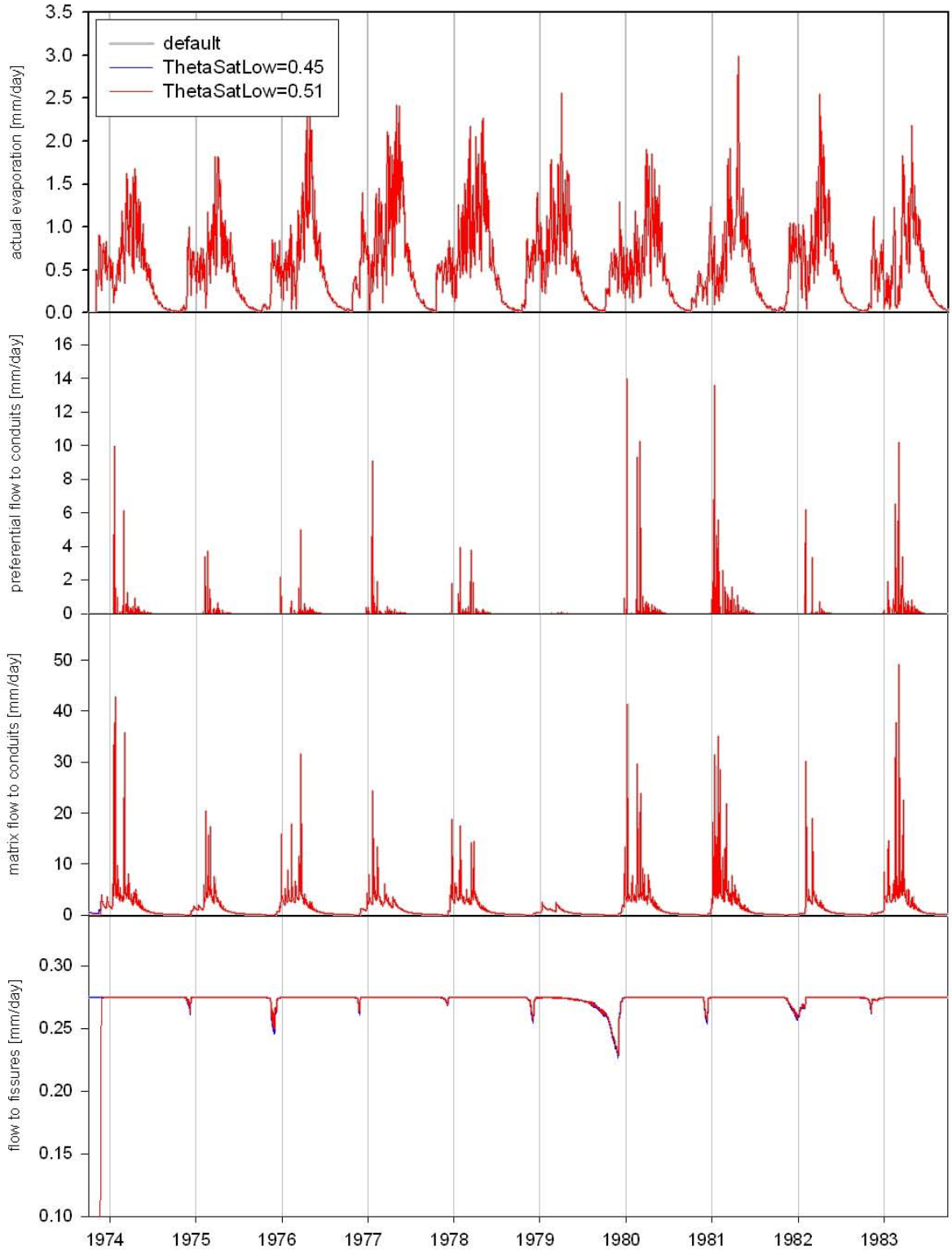

FIGURE 76: Sensitivity analysis for the saturation water content of the lower epikarst $\theta_{Sat,Low}$

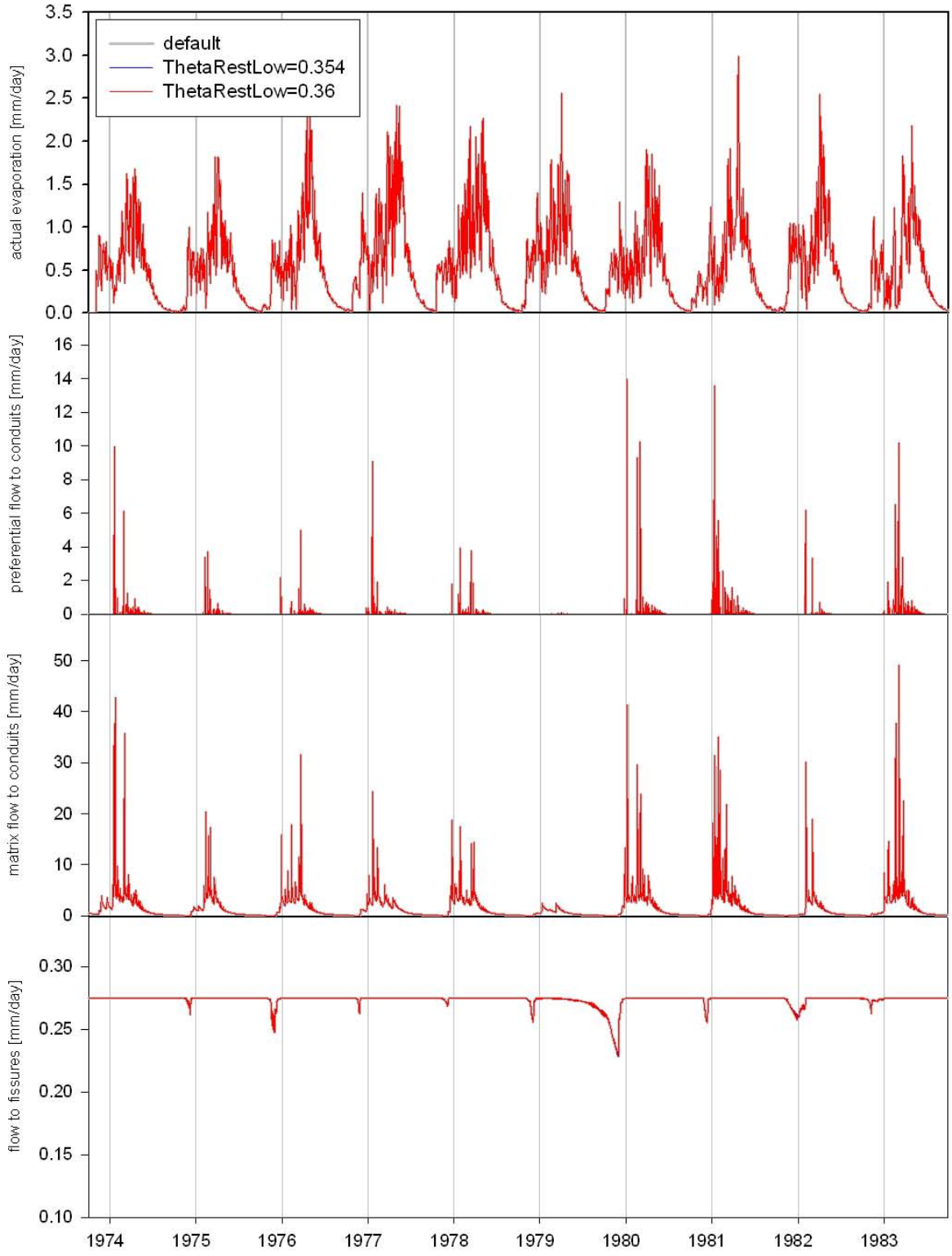

FIGURE 77: Sensitivity analysis for the residual water content of lower epikarst $\theta_{Rest,Low}$

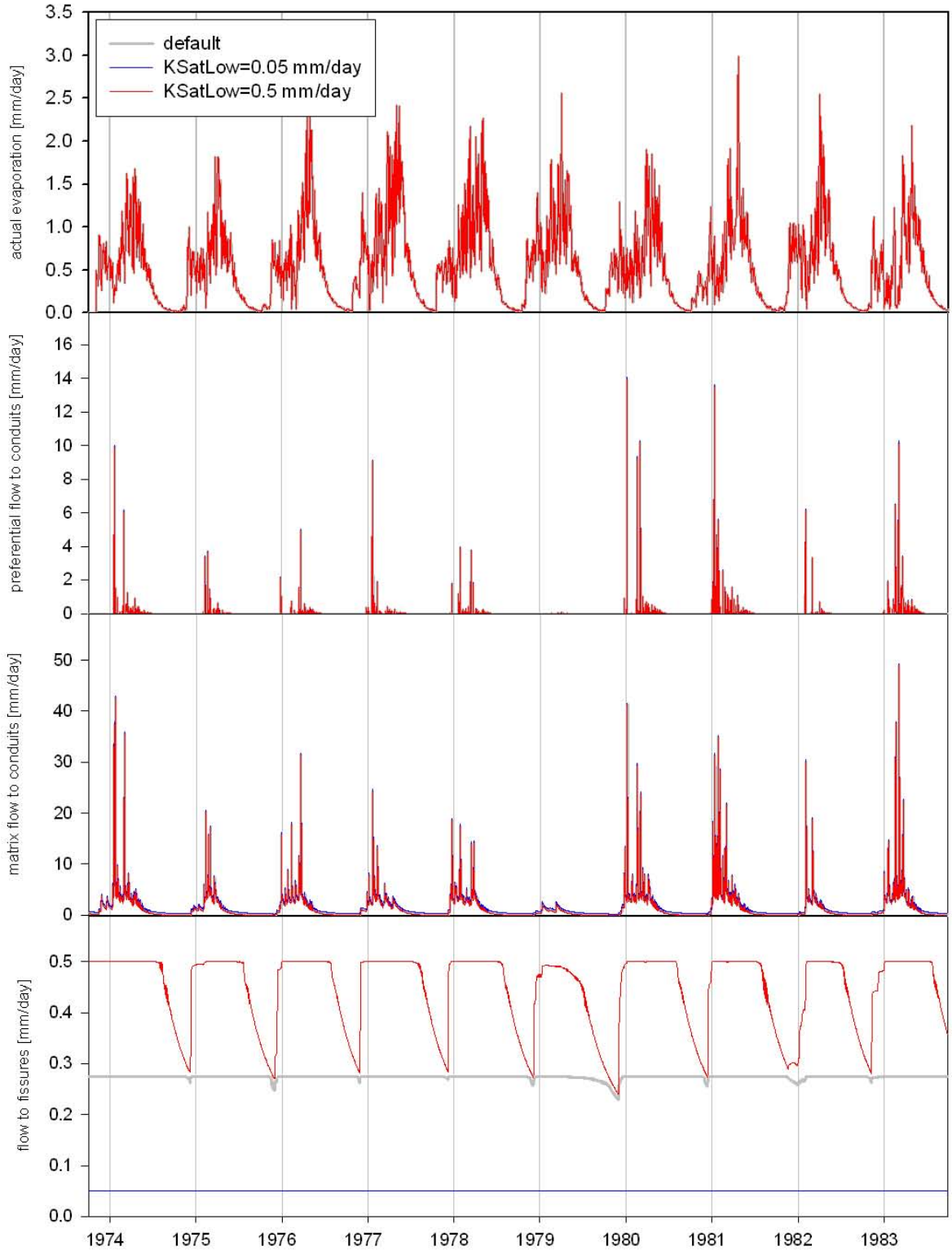

FIGURE 78: Sensitivity analysis for the saturated hydraulic conductivity of lower epikarst $K_{Sat,Low}$

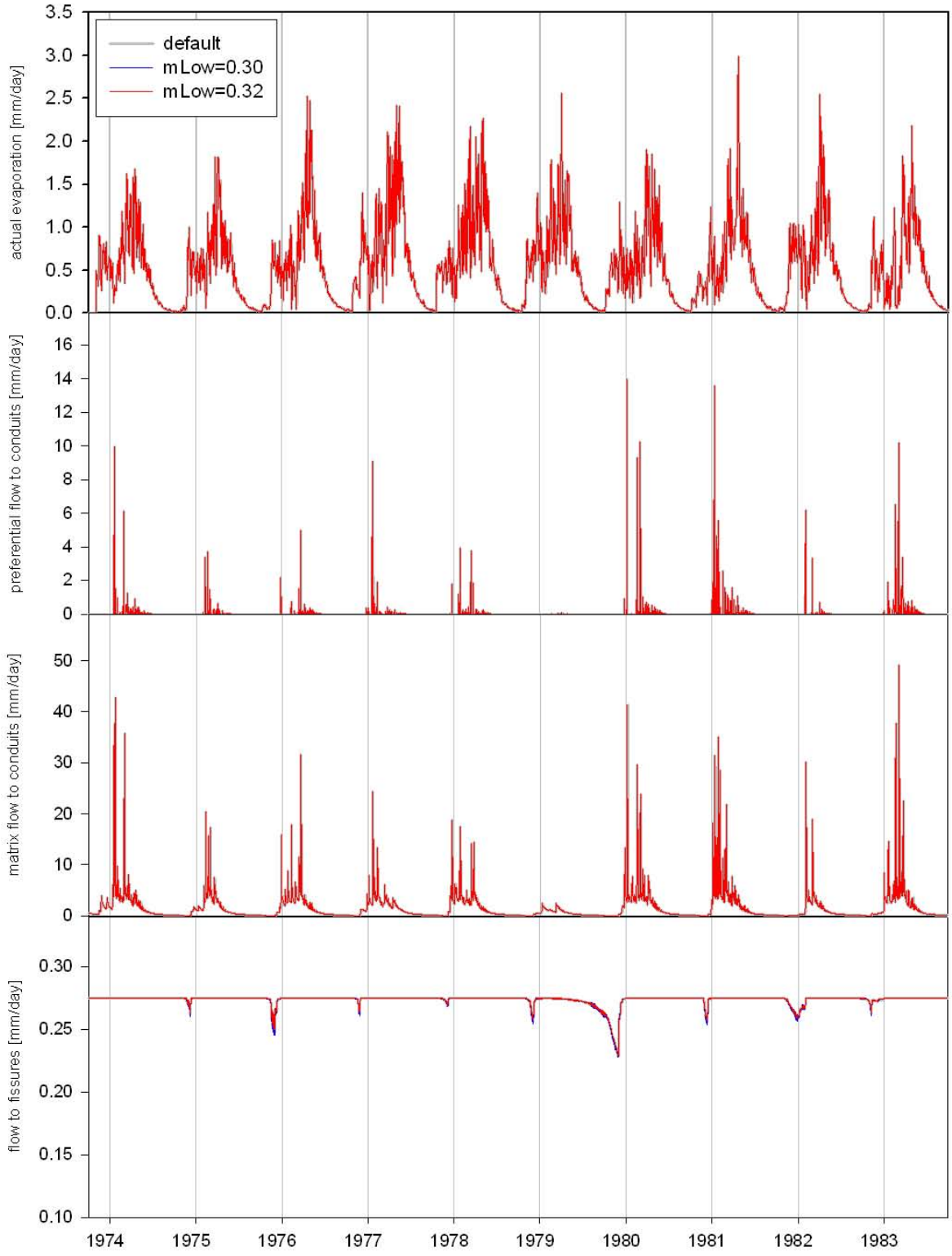

FIGURE 79: Sensitivity analysis for parameter which is related to the Brooks-Corey grain size index for the lower epikarst m_{Low}

Altogether there are 11 parameters which influence the four output variables of the soil/epikarst routine. But their influence on the different output variables is quite distinctive: the actual evaporation is mainly controlled by the root depth *RD* but $\theta_{Sat,Up}$ and $K_{Sat;up}$ also have a not negligible influence on it. Major parameters influencing preferential flow to the conduits are h_{Up} and $K_{Sat,Up}$ with a significant contribution of $\theta_{Sat,Up}$ and m_{Up}. The same parameters are influencing the matrix flow to the conduits in an opposite way: if a parameter increases the preferential flow to the conduits it automatically decreases the matrix flow to the conduits with the same strength. Since the lower epikarst, from where discharge to the fissures originates, is below the other layers, nearly all parameters of the superimposed layers have a certain impact on it. If a parameter increases matrix flow in the upper epikarst it also causes a more continuous recharge to the lower epikarst; which then leads to a more continuous discharge to the fissures. Compared to that the influence of the proper parameters of the lower epikarst is insignificant except for $K_{Sat,Low}$ which is obviously the major value controlling the outflow of this layer.

The thickness of the soil layer *RD*, the thickness of the upper soil layer h_{Up}, the saturated hydraulic conductivity of the upper epikarst $K_{Sat,Up}$ and the saturated hydraulic conductivity of the lower epikarst $K_{Sat,Low}$ were identified as most sensitive parameters of the soil/epikarst routine. For the following sensitivity analysis of the groundwater routine soil/epikarst parameters were set to their default values (TABLE 14).

TABLE 15: Influence of soil/epikarst routine parameters on output variables (+++: strong influence, ++: moderate influence, +: low influence, -: no influence)

Parameter	Actual evaporation	preferential flow to conduits	matrix flow to conduits	matrix flow to fissures
RD	+++	+	+	+
h_{up}	-	+++	+++	+
h_{low}	-	-	-	+
$\theta_{sat,up}$	++	++	++	+
$\theta_{rest,up}$	+	-	-	+
$K_{sat,up}$	++	+++	+++	++
m_{up}	+	++	++	+
$\theta_{sat,low}$	-	-	-	-
$\theta_{rest,low}$	-	-	-	-
$K_{sat,low}$	-	+	+	+++
m_{low}	-	-	-	-

10.2.3 The groundwater routine

Parameters included in the ground water routine, as shown in FIGURE 58, are listed in TABLE 16. K_1, K_2 and K_E are storage coefficients which describe the discharge behaviour of their respective storages. Since they are not measurable in the field they have to be regarded as abstract numbers. Even though they are measurable in nature the porosities n_1 and n_2 have to be calibrated, too, since there is no information about their values for Mt. Hermon (see chapter 4). The only parameter measurable and known is H_2 since a digital elevation model was available from which its value can be drawn. The fractions of the springs subsurface catchments, *a* and *b*, admittedly represent the real areas of the subsurface catchment but information about subsurface catchments of karstic systems is nearly impossible to obtain. They can only be estimated by the use of water balance equations.

TABLE 16: Parameters included in the groundwater routine, their descriptions and units

Parameter	Description	Unit
K_1	Storage coefficient of Dan Spring	[day]
K_2	Storage coefficient of Banias Spring	[day]
K_E	Exchange coefficient	[day]
n_1	Conduit porosity	[-]
n_2	Fissure porosity	[-]
H_2	Altitude difference between Dan and Banias Spring	[m]
a	fraction of Dan Spring subsurface catchment on total catchment area	[-]
b	fraction of Banias Spring subsurface catchment on total catchment area	[-]

Storage coefficients describing the outflow behaviour of Mt. Hermon Springs or other karst systems are listed in TABLE 17. Since the storage coefficients determined by GEYER ET AL. (2008) and FLEURY ET AL. (2007) were obtained in other karst systems they can only give the order of magnitude of the storage coefficients for the conduit and the fissure storages. The coefficients drawn from RIMMER AND SALINGER (2006) also have to be commented. They actually represent the storage coefficients of Banias Spring and Dan Spring. But as it was found out in chapter 6, the Banias Spring is dominated by the soil and epikarst while the Dan Spring is more controlled by the outflow of the fissure system. Thus the groundwater storage coefficient of Banias Spring is a measure of the transition of water through the conduits while Dan Spring storage coefficient estimates the draining of the fissure system.

TABLE 17: Storage coeffcients for conduit and fissure systems found in other studies

parameter	GEYER ET AL. (2008)	FLEURY ET AL. (2007)	RIMMER AND SALINGAR (2006)
K(conduits) [day]	2	16.7	20.5
K(fissures) [day]	100	167	300

In order to make the exchange coefficient K_E comparable to storage coefficients found for the fissure storages in TABLE 17 equations (67) and (68) were applied. Again, the variable name K_E will be used instead of K_{E2} (exchange coefficient of water exchange from the fissures to the conduits considering the porosities). Orders of magnitude for fissure and conduit porosity were found by MALOSZEWSKI ET AL. (2002) who determined a porous fissure porosity of 1.5% and a conduit porosity of 0.01%. However this was done in a karstic system in Austria where humid climates prevail. DOMENICO AND SCHWARTZ (1990) estimated the overall porosity of karstic rock to be 1 %. But first tries with these porosities showed that discharge behaviour was not reproducible while setting H_2 fixed to the real altitude difference. By decreasing the fissure porosity to 0.3% and the conduit porosity to 0.003% H_2 could be maintained and the model predictions stayed within a reasonable range. RIMMER AND SALINGAR (2006) estimated the fractions to the whole catchment area of Dan and Hermon Stream, which is mainly fed by the Banias Spring, subsurface catchments to 0.465 and 0.207, respectively. But since their model structure did not distinguish between conduit and fissure flow in the groundwater routine these numbers might not fit to the HYMKE_DUAL groundwater routine.

With this knowledge parameter ranges for the sensitivity analysis of the groundwater routine were set as listed in TABLE 18. K_1, K_2 and K_E vary between the values found in the literature review while n_1 and n_2 vary one order of magnitude around the values estimated with fixed H_2. Even though the exact value of H_2 is known from the digital elevation model it was included in the sensitivity analysis to investigate how changes on it would influence the routine output. Since there was not much information about the parameters *a* and *b* they were varied in a wide range. Similarly to the preceding sensitivity analyses single parameters were varied within the range defined in TABLE 18 while the other parameters were set to their default values.

TABLE 18: Parameter ranges chosen for sensitivity analysis of the groundwater routine and their default values

parameter	range	default values	unit
K_1	2 to 25	13.5	[day]
K_2	2 to 25	13.5	[day]
K_E	100 to 300	200	[day]
n_1	10^{-5} to 10^{-4}	$5.5*10^{-5}$	[-]
n_2	10^{-3} to 10^{-2}	$5.5*10^{-3}$	[-]
H_2	50 to 250	150	[m]
a	0.1 to 0.9	0.5	[-]
b	0.1 to 0.9	0.5	[-]

Results of varying K_1 are shown in FIGURE 80. It can be observed that for increasing K_1s there are overall higher water levels in the Dan and Banias conduits and in the fissure system. This is caused by lower draining of the fissure aquifer due to lower draining of the Dan conduit system which means that exchange flow to the Dan conduits decreases with increasing K_1s. Since the Dan conduits drain slower, the altitude difference each time step is smaller und thus exchange flow is smaller as well. As a consequence of the lower exchange flow to Dan conduits more exchange flow to Banias conduits occurs. The sum of these effects causes Dan Spring to discharge less and Banias Spring to discharge more by increasing K_1. For the minimum value of K_1 (K_1 = 2) no results could be obtained. The fissure storage was drained so fast that its level fell below the level of Banias Spring outlet. This case is not included in the model structure since hydrochemical investigations showed that Banias Spring always receives at least a small contribution of fissure flow.

Looking at changes on output by modifying K_2 lower water levels in the Dan Spring and Banias Spring conduits can be observed (FIGURE 81) for small K_2s. These let the water pass through the Banias conduit system rapidly and hence little exchange to the fissure system from Banias conduits takes place. Consequently there is also less exchange flow from the fissures to the Dan Spring conduits because there is less water in the fissures. This results again in less discharge for the Dan Spring. Only Banias system discharges more, caused by the small K_2. For increasing K_2s these conclusions can be reversed.

Varying the exchange constant K_E in FIGURE 82 shows that there are no big changes in the magnitude of all values. But there is a clear impact on the amplitudes of both the Dan and Banias conduit water levels: with decreasing K_Es they become more attenuated because more water can enter the fissures system in one time step instead of discharging directly at the

outlets. According to this the amplitudes of exchange flow grows, mainly in the negative direction, with decreasing K_Es. Additionally small K_Es cause the fissure aquifer to drain faster to the conduits systems in the dry season. The attenuation created by low K_Es can also be observed at the Dan and Banias Spring discharges: both show lower peak values with lower K_Es.

Looking at the routine's sensitivity on changes of n_1 large increases water levels in Dan conduits, Banias conduits and the fissure storage for decreasing n_1s can be observed (FIGURE 83). This can be explained simply by the change of porosity itself: a small porosity causes higher water levels without changing the amount of water in storage. However, since the fissure porosity stays constant changes of n_1 also influences the exchange capacity. Small n_1s cause a stronger exchange flow to the fissures since altitude difference increases. Thus decreasing n_1s also results in an attenuation which can be seen at the Dean Spring and Banias Spring discharges, too. But in the dry season the opposite effect occurs: due to smaller porosities the level difference of fissures and springs is smaller and thus there is less drainage from the fissures to the conduits.

Similar effects, but this time in a reverse way, can be seen by looking at changes of output on variations of the fissure porosity n_2 in FIGURE 84. Larger n_2 cause an attenuation of peak values in the Banias and Dan Spring water levels. But this attenuation is much weaker that the observed attenuation by changes of n_1 what causes the variations of the fissure water level to be quite small. This effect is more pronounced when decreasing exchange from the fissures to the conduits by increasing n_2 because water level difference between conduits and fissures decreases. This is the reason for the springs to show smaller peak values and small slopes of their recession curve during the dry season for large n_2s.

Increasing H_2 in FIGURE 85 leads to a shift of water levels for the Dan and Banias conduits and the fissure storage. Larger H_2 cause more exchange flow from the fissures to the Dan conduits and less exchange flow to the Banias conduits. Hence increasing H_2 causes Dan Spring to show more discharge and Banias Spring to show less discharge respectively.

Changing the fraction of Dan Spring subsurface catchment on the total area *a* means also an inverse change of the fraction of Banias Spring subsurface catchment on the total area *b* because it is assumed that they sum to one. Thus impact of changes of them on the

groundwater routine output will be explained in a single figure (FIGURE 86). If *a* decreases Dan Spring conduit levels show less reaction on recharge events and follow more the course of the fissure water level. Despite of that Banias Spring conduit levels vary mainly controlled by recharge events. Variations of *a* do not significantly influence the fissure water level and its course; only the origin of recharge water changes while changing *a*. This effect is observable in the changes of exchange flow following changes in the *a* value. The impacts of changes of parameter *a* on the conduit water levels propagates on to the spring discharges: Small *a* values cause the Dan Spring to discharge continuously following the course of fissure water level while large *a* causes the Banias Spring to react highly dynamically because it is more influenced by direct input than by the exchange flow from the fissures.

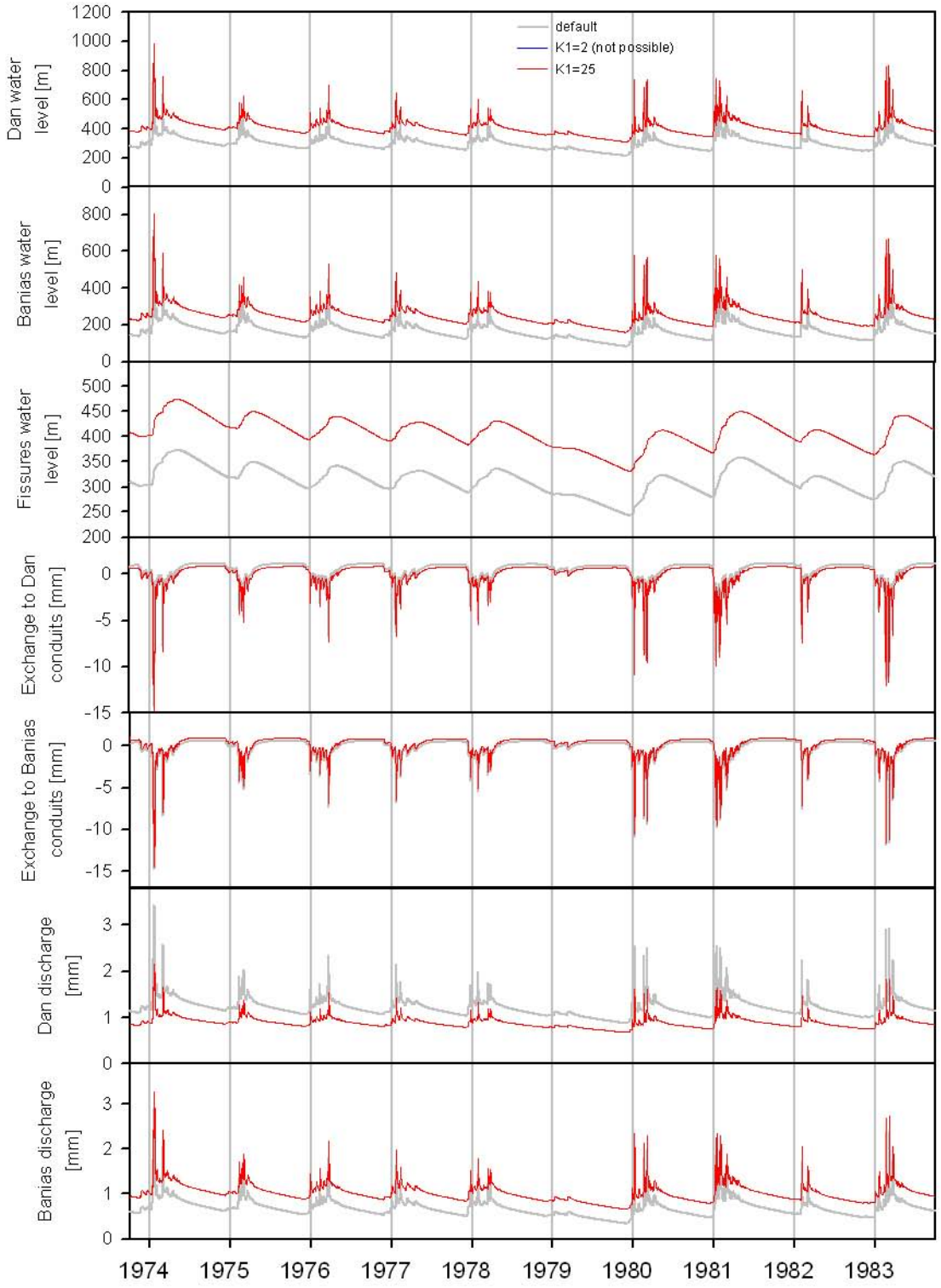

FIGURE 80: Sensitivity analysis for the storage coefficient of the Dan conduit system K_1

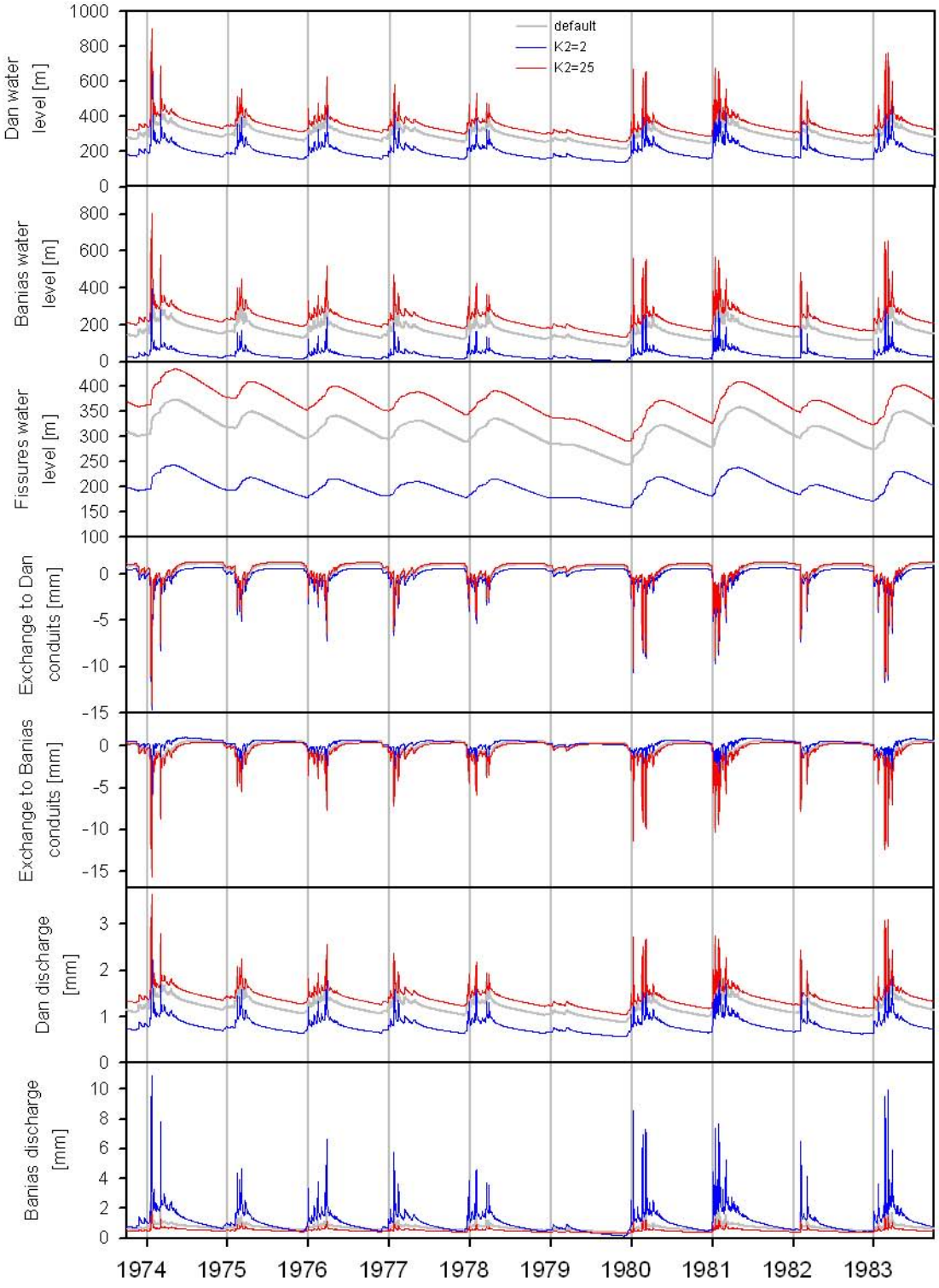

FIGURE 81: Sensitivity analysis for the storage coefficient of the Banias conduit system K_2

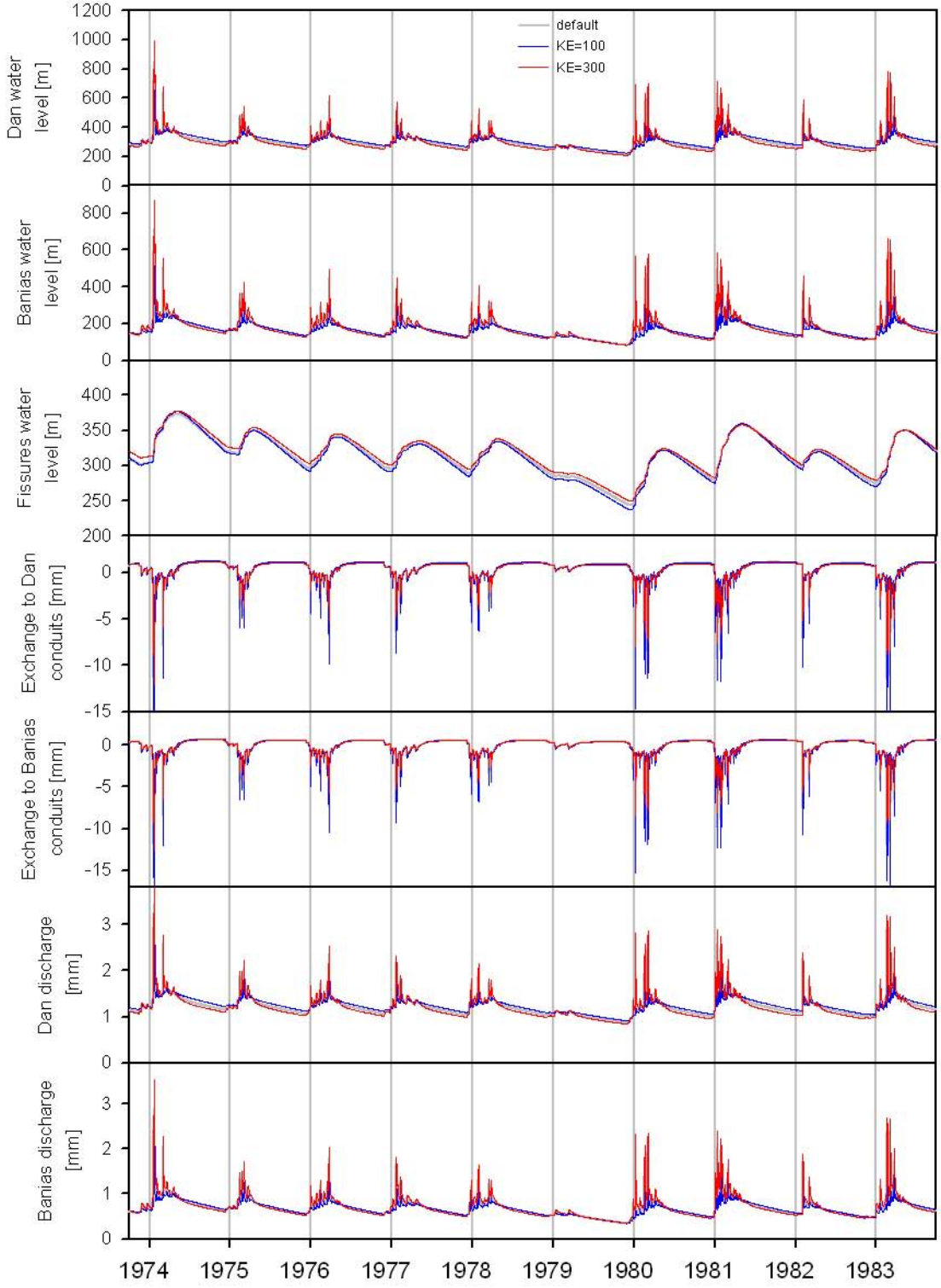

FIGURE 82: Sensitivity analysis for the exchange coefficient K_E

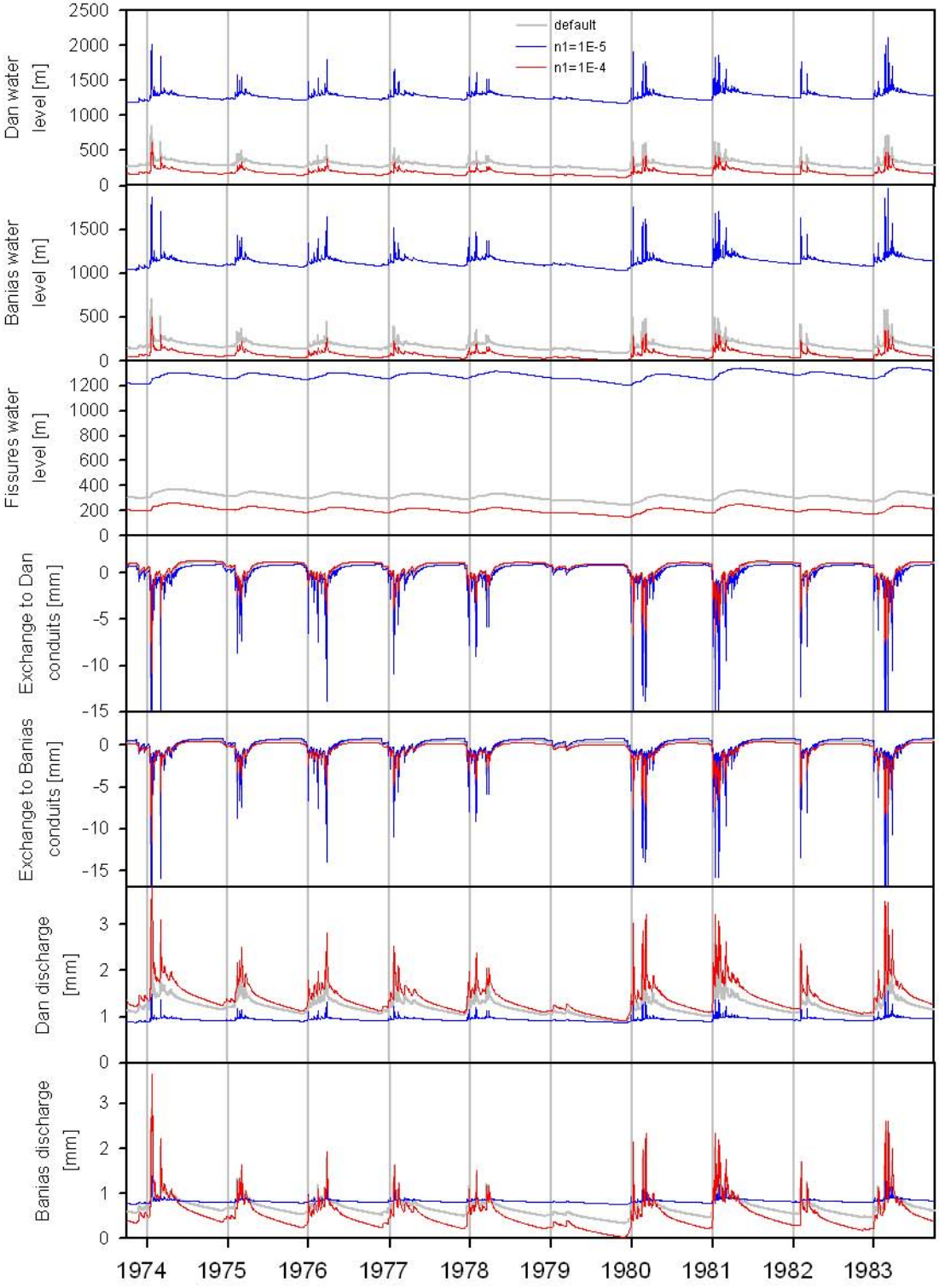

FIGURE 83: Sensitivity analysis for the conduit porosity n_1

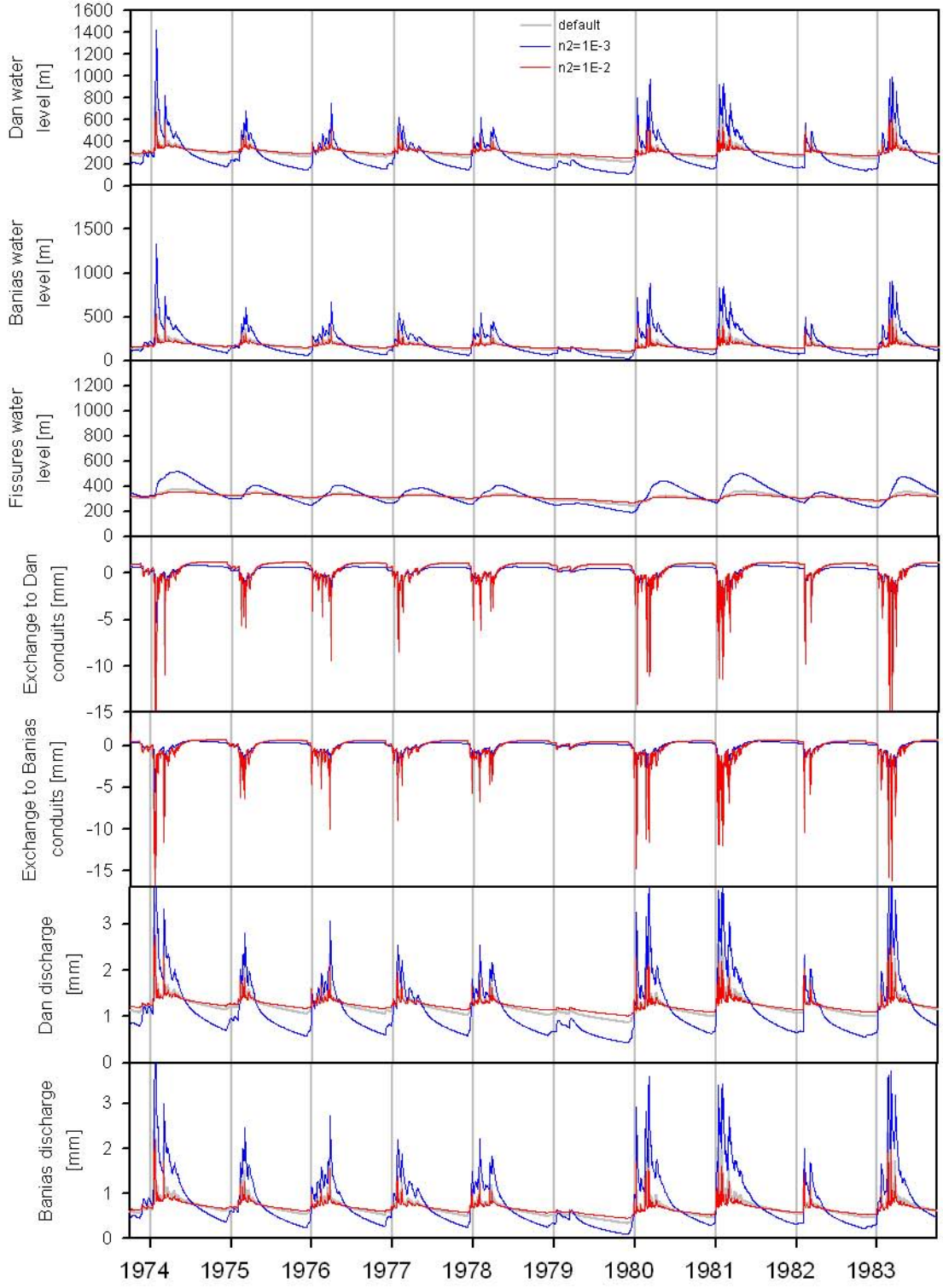

FIGURE 84: Sensitivity analysis for the fissure porosity n_2

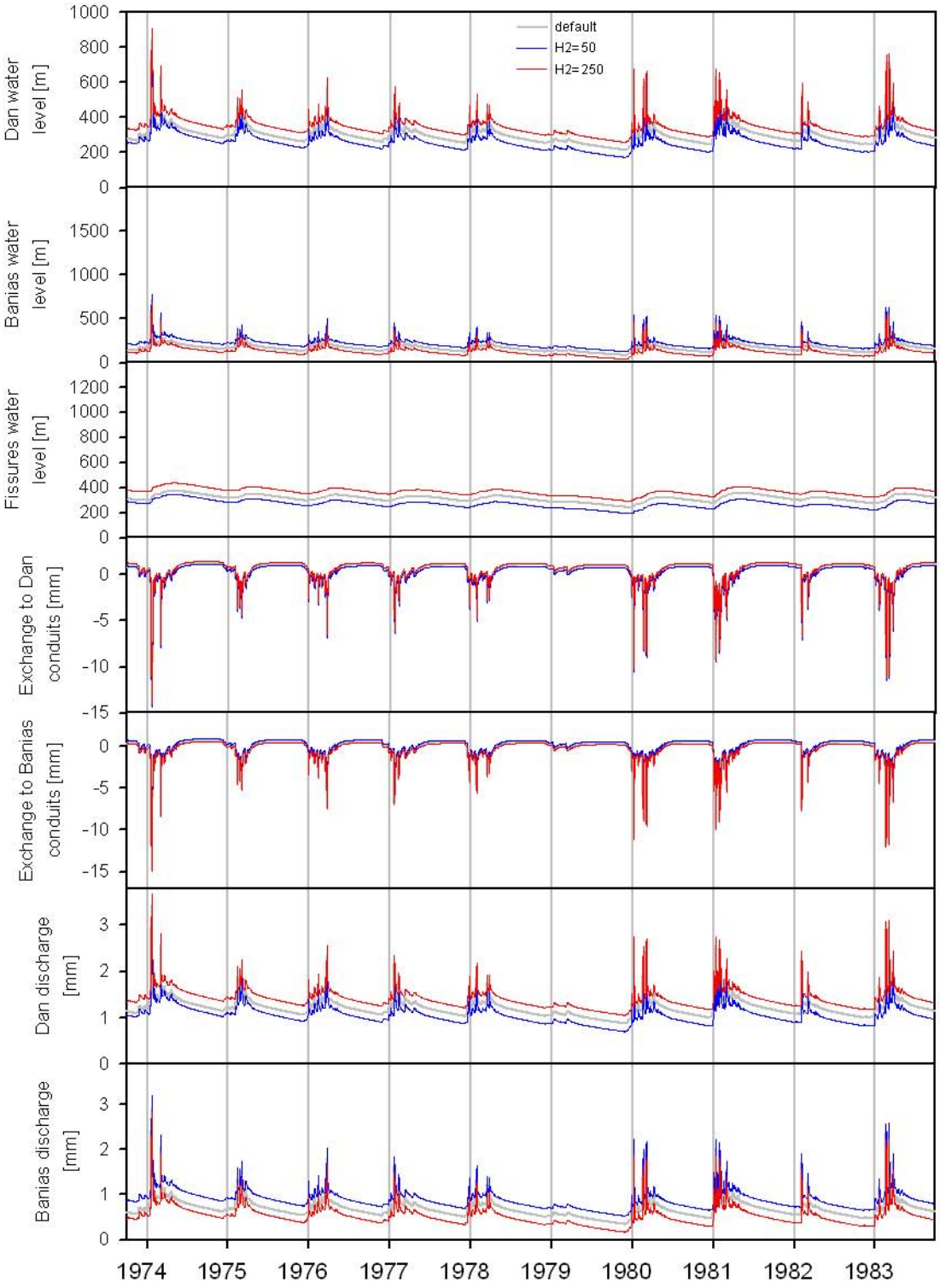

FIGURE 85: Sensitivity analysis for the altitude difference between Dan and Banias Spring outlet H_2

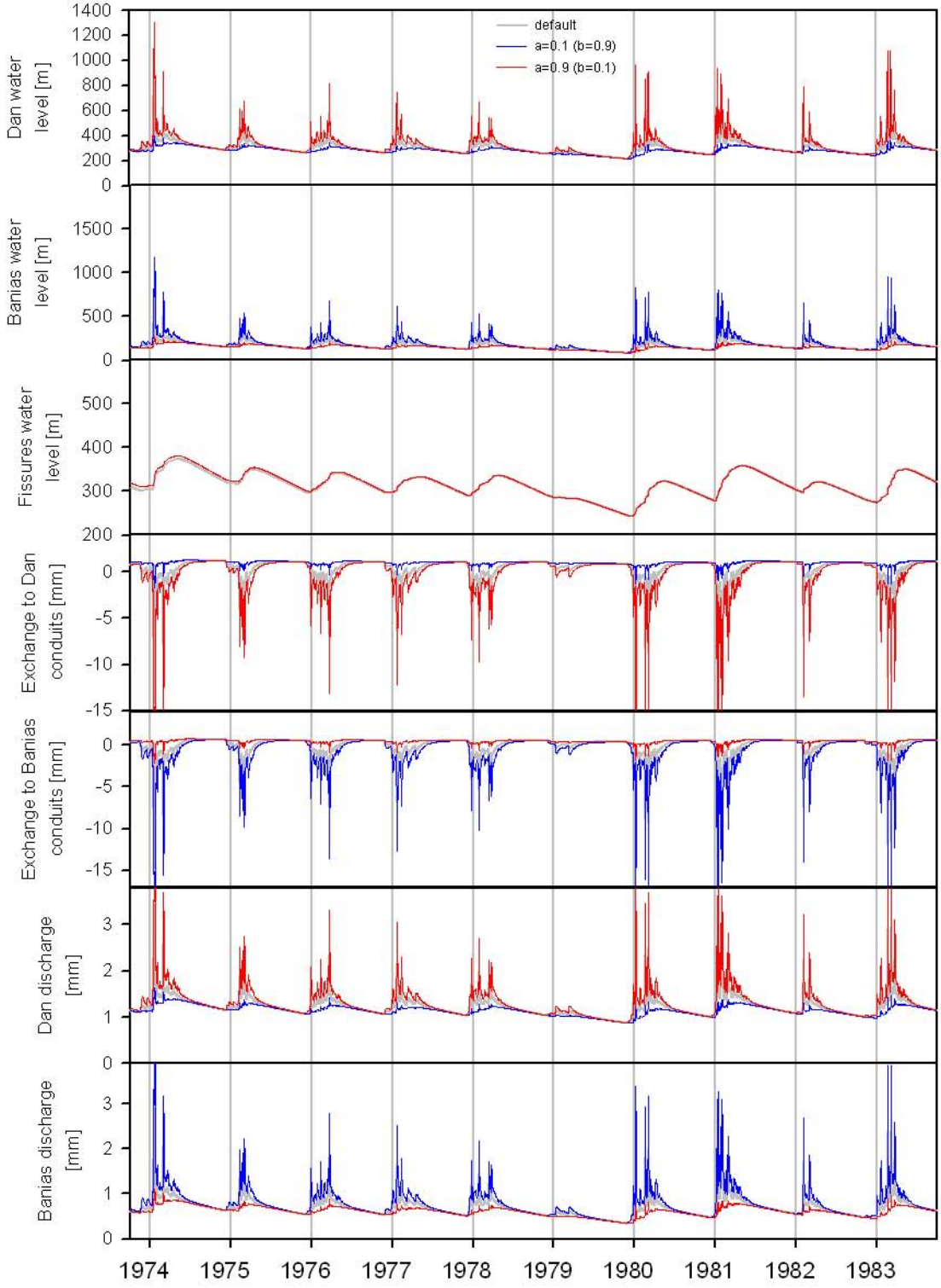

FIGURE 86: Sensitivity analysis for the fraction of Dan Spring subsurface catchment on the whole catchment area *a* (inverse to this the fraction of Banias Spring subsurface catchment area *b*)

Looking at the overall impact of the groundwater routine parameters on the output it can be seen that changes of one parameter mostly affect more than one output variable. This is different from the results of the sensitivity analysis of the soil/epikarst routine where one or two major parameters influencing just one output variable could be identified. Reason for this is the vertical structure of the soil/epikarst routine where one layer is placed below the other. In the groundwater routine the reservoirs are placed in a parallel order which enhances the impact of changes of one reservoir's parameter on the other two reservoirs. Hence the groundwater routine parameters can rather be attributed to different effects which have their particular impact on the output variables. Thus the parameter K_1 is controlling velocity the whole drainage of the system because it determines how fast water leaves the system at its lowest point. K_2 is responsible for the recharge to the fissures and thus the amount of water which can enter the Dan conduit system from there. The exchange parameter K_E is the main parameter controlling the attenuation of conduit peak values of water level and spring discharge. The major effect of changes on conduit porosity is of course the changes of conduit water levels because their calculation includes the use of n_1. But it also influences the exchange between conduits and fissures in two ways: Decreasing n_1 causes more flow from the conduits to the fissures but it also causes less flow back from the fissures to the conduits. Changes of n_2 have the same effect just in the opposite direction: Increasing n_2 causes more flow from the conduits to the fissures and less flow back. However for an increase of n_2 flow from conduits to fissures is not so pronounced and flow back to the conduits is also weaker compared to a decrease of n_1 in the same order of magnitude. Modifications on H_2 have also an influence on recharge to the fissures. Larger H_2s cause more recharge and thus shift up the water levels. The fractions of the Dan and Banias subsurface catchments of the whole catchment area *a* and *b* are the most important parameters to control the magnitude of influence of conduit flow or fissure flow. Small *a* lead to less influence of direct input events and to a major influence of fissure outflow which follows the water level in the fissures. Since H_2 is known it will not be used for calibration but the residual parameters listed in TABLE 16 will be used to fit the model prediction to the measured values at the spring outlets.

10.3 Application of HYMKE_DUAL on the real data

To understand how far HYMKE_DUAL can reproduce the discharge and the hydrochemistry at Dan and Banias Spring simulated data was compared to measured data at the spring outlets. Therefore the model had to be calibrated. As simulation period the hydrological years from 1973/1974 to 1982/1983 were selected since only then all input data was available (see section 10.1). This was done within the parameter ranges given for the snow melt routine, the soil/epikarst routine and the groundwater routine in TABLE 12, TABLE 14 and TABLE 18, respectively. At the beginning all values were set to their defaults as described in section 10.2. Then parameters were modified until the soil/epikarst output looked reasonable and that spring discharge and hydrochemistry predictions gave good approximations of the observed values. This was done by applying a trial-and-error method; hence the results shown below can thus be regarded as a good fit to the measured data but far not the best fit possible. First, using the water balance of all springs, the total catchment area of Dan and Banias Spring was determined which is 75% of the whole Mt. Hermon area (587.25 km²). As it was found out in the sensitivity analysis the snow melt routine is not so significant, having only an attenuation effect on big events. Therefore standard values were used which are listed in TABLE 19:

TABLE 19: Parameters chosen for the snow melt routine

parameter	value	unit
ddf	2	[mm/day]
HC	0.1	[-]
Tm	0	[°C]
RF	0.05	[-]

To obtain reasonable results for the soil/epikarst routine output only the most sensitive parameters were changed which are the soil layer thickness *RD*, the thickness of the upper epikarst h_{Up}, the saturated hydraulic conductivity of the soil and the upper epikarst $K_{Sat,Up}$ and the saturated hydraulic conductivity of the lower epikarst $K_{Sat,Low}$.

Unfortunately there are no measured data of epikarst outflow available for the Mt. Hermon area. But there was an epikarst experiment performed by ARBEL ET AL. (2008) in the limestone hills at Mt. Carmel, Israel. Their data gave useful information about the general behaviour and flow types beneath the epikarst. They identified three major flow types: (1) the perennial type of flow which gives low water rates in a very continuous manner; (2) the seasonal type which shows a seasonal variation and flow rates which are at their maximum about one order of magnitude above the perennial type flow rates; and (3) the post-storm type

which just activates after rain event and then dry off rapidly. With this knowledge the soil/epikarst routine output was calibrated so that flow to the fissures represents the perennial type of behaviour, matrix flow to the conduits the seasonal type of behaviour and preferential flow to the conduits the post-storm type. All parameters chosen are listed in TABLE 20. Deviations from the default values had to be made for *RD*, which was set a little lower to lower actual evaporation, for $K_{Sat;Up}$, which was set to about its 20% of its default value to force a faster initiation of preferential flow, and for $K_{Sat,Low}$, which was also set to its maximum value to obtain the perennial flow type behaviour.

TABLE 20: Parameters chosen for the soil/epikarst routine

parameter	value	unit
RD	0.65	[m]
h_{Up}	6.5	[m]
h_{Low}	1.25	[m]
$\theta_{Sat,Up}$	0.5015	[-]
$\theta_{Rest,Up}$	0.3545	[-]
$K_{Sat,Up}$	7.5	[mm/day]
l_{Up}	0.235	[-]
$q_{Sat,Low}$	0.48	[-]
$q_{Rest,Low}$	0.357	[-]
$K_{Sat,Low}$	0.5	[mm/day]
l_{Low}	0.31	[-]

Results are shown in FIGURE 87 in the uppermost plot. It can be seen that largest fluctuations happen for preferential and matrix flow to the conduits while the flow to the fissures is nearly constant and quite low compared to the flows to the conduits. In the dry season matrix and preferential flow fall dry; however the flow to the fissures stays constant throughout the year.

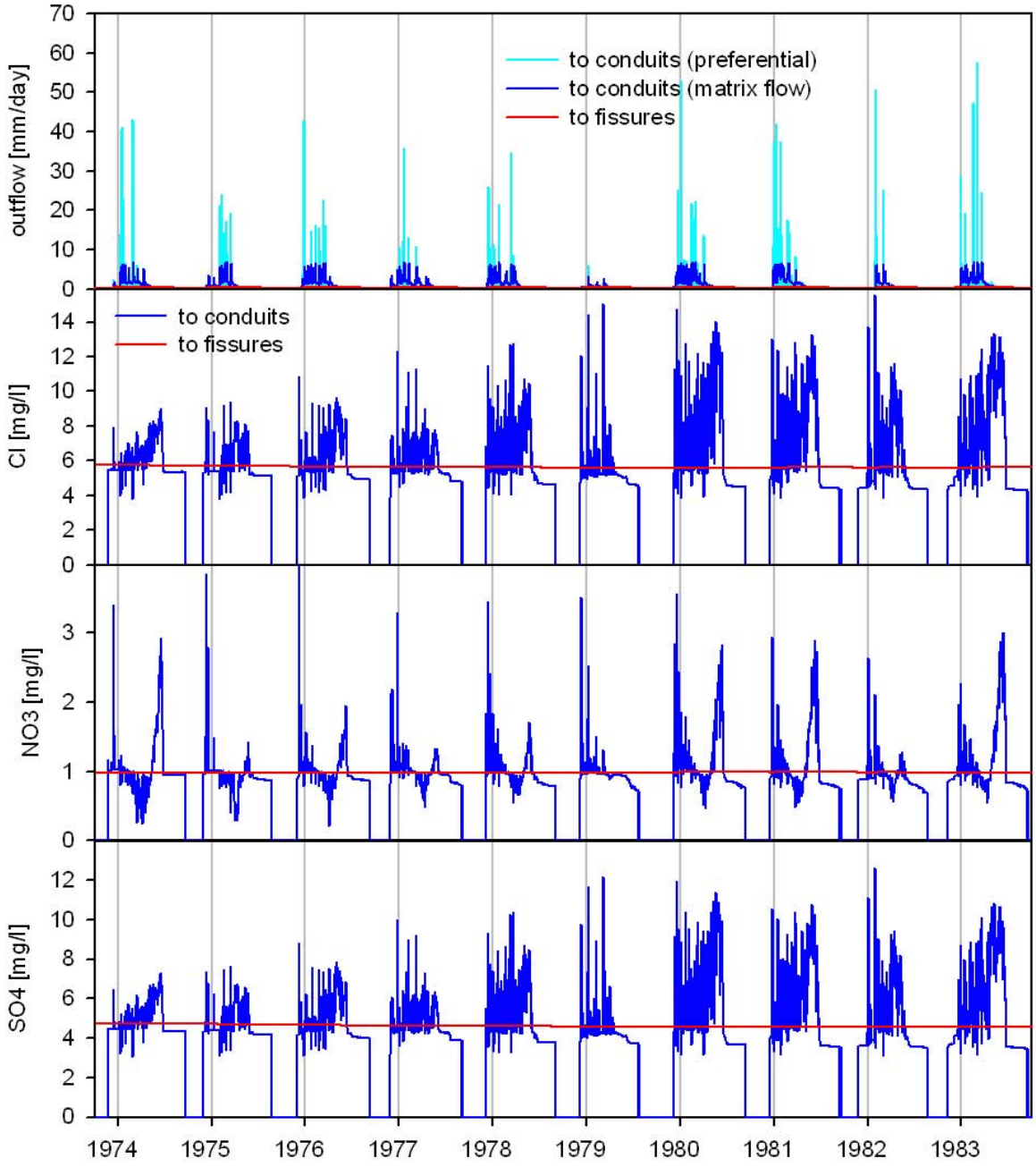

FIGURE 87: Output of soil epikarst routine; on the top: discharge to the fissures, matrix flow to the conduits and preferential flow to the conduits; below: concentrations of the sum of matrix and preferential flow to the conduits and flow to the fissures

To calibrate the groundwater routine all parameters were modified except the altitude difference between the Dan and Banias Spring which was set to its real value derived from the digital elevation model. The other values were changed until a good fit to the measured data at the spring's outlet was reached. Thereby the knowledge gained in the sensitivity analysis was applied. The parameters yielding to the best fit are shown in TABLE 21. Storage constant K_1

was set near the lower end of the defined range to produce the right recession of the Dan Spring hydrograph; whereas K_2 was set near the upper end of the defined range to produce the right recharge to the fissures. Note that this value is nearly the same as the one RIMMER AND SALINGAR (2006) used for the Banias Spring groundwater routine. The exchange constant K_E was again set at the lower end of the range defined to produce the right attenuation of the hydrographs. For the same reason the porosities n_1 and n_2 were lowered compared to their default values. The fraction of Dan Spring subsurface catchment area on the whole catchment a was set very small, even lower than in the range defined in the sensitivity analysis, to obtain the desired influence of the fissure system.

TABLE 21: Parameters chosen for the groundwater routine

parameter	value	unit
K_1	5	[day]
K_2	20	[day]
K_E	125	[day]
n_1	$2.5*10^{-5}$	[-]
n_2	2*10^3	[-]
H_2	159	[m]
a	0.06	[-]
b	0.87	[-]

Results are shown in FIGURE 88 for Banias Spring and in FIGURE 89 for Dan Spring. Overall simulation results of Banias Spring follow the course of observed discharge. Deviations from the measured discharge can be observed at some peak values which are sometimes underestimated. The recession of Banias Spring hydrographs in the dry season is also sometimes slightly overestimated. Looking at Dan Spring discharge predictions it can be seen that the recession behavior of the spring hydrograph fits much better the observed discharges. The maximum values are also approximated well except for the years 1981 and 1983 where the seasonal peak was overestimated.

To proof that the right parameter sets were chosen the mixing routines of HYMKE_DUAL were fed by constant input concentrations. If the model works properly the concentration predictions at the spring outlets would fit well to the observed concentrations. Therefore appropriate input concentrations had to be found. An estimation of input concentrations was given by BRIELMANN (2008) in TABLE 3 but first tries showed that Cl and SO_4 input concentrations had to be set higher and NO_3 input concentrations lower. The underestimation of Cl and SO_4 in the rain samples could be explained by the relatively strong dry deposition which might increase the input concentrations compared to the rain concentrations (see

chapter 2). Likewise there could be geogene contributions from sources that are not yet incorporated in the model structure. Concerning NO_3 the important uptake process by plants and mineralization of organic matter is incorporated (see section 10.1.4) but another important process, the denitrifcation, is not considered. This process is reducing NO_3 under anaerobe conditions and can even happen above the groundwater table in the soil and epikarst zone as shown by EINSIEDL ET AL. (2005) and EINSIEDL AND MAYER (2006). The final selected concentrations are listed in TABLE 22.

TABLE 22: Input concentration for HYMKE_DUAL mixing routines

solute	concentration	unit
Cl	3.7	[mg/l]
NO_3	0.75	[mg/l]
SO_4	3	[mg/l]

Results for mixing in the soil/epikarst routine can be seen in the three lower plots in FIGURE 87. Concentration of flow to the fissures stays very constant for all the three solutes while concentrations of flow to the conduits vary significantly. During the rainy season enrichment due to evaporation in the soil layer and dilution due to heavy rains alternate. At the end of each rainy season flow to the conduits ceases as a consequence of very low water contents, and no flow means a zero concentration. Focusing on NO_3 the course of uptake and mineralization by the vegetation and micro-organisms is influencing the enrichment and dilution processes. Therefore in a typical season there are two major peaks. The first peak is a result of the accumulation of NO_3 in the dry season which is caused by mineralization and enrichment due to evaporation. With the first rain this NO_3 is leached out of the soil to the lower parts of the system. The following decrease is explainable by the uptake by plants and dilution while the second peak is produced by the enhanced mineralization at the end of the seasonal vegetation period and the increasing evaporation.

The outflow of the soil/epikarst routine is feeding the groundwater systems of Banias and Dan Spring. In FIGURE 88 in the three lower figures the concentration predictions of Banias Spring discharge can be seen. Since there are geogene contributions intrinsic inputs of Cl and SO_4 were set to 12 g/m²/day and 100 g/m²/day, respectively. By adding this geogene component the variation of SO_4 could be approximated quite well while there are some overestimations of Cl at the beginning of the simulation period and some underestimations at the end of the simulation period. In the dry year of 1978/1979 both solute predictions overestimate the spring water concentrations. For NO_3 the model yields the best simulations: the measured

variations of NO_3 concentrations are accurately reproduced for the whole simulation period. Only at the end of the rainy season does the model sometimes show a second peak although this can be observed in the real data only in the years of 1974, 1977 and 1981. Even in the dry year it reproduces the small fluctuations observable in the measured concentrations.

Turning now our attention to the flow concentration predictions for the Dan Spring in FIGURE 89 too attenuated variations of Cl and NO_3 predictions can be observed. In the case of NO_3 it seems that the variations are right but their amplitude should be larger. For Cl the resolution of measured data unfortunately is too small to draw any conclusions but the amplitude of simulated concentrations is far smaller than the amplitude of observed Cl concentrations. To produce good predictions of SO_4 concentrations again a geogene contribution had to be added, although smaller than for the Banias Spring groundwater system (12 mg/m²/day). With it SO_4 variations could be reproduced at least better than for Cl but with some overestimations mostly in the second half of the rainy seasons.

For the interpretation of hydrochemical predictions of both springs it has to be kept in mind that uncertainty begins with the sampling. The measured data already have uncertainties of 0.12 mg/l, 0.1 mg/l and 0.13 mg/l for Cl, NO_3 and SO_4, respectively (see chapter 6). Since particularly for NO_3 the seasonal variations are within about 1 mg/l the relative error is already about 10%. Thus small variations could be also explained by the measurement error.

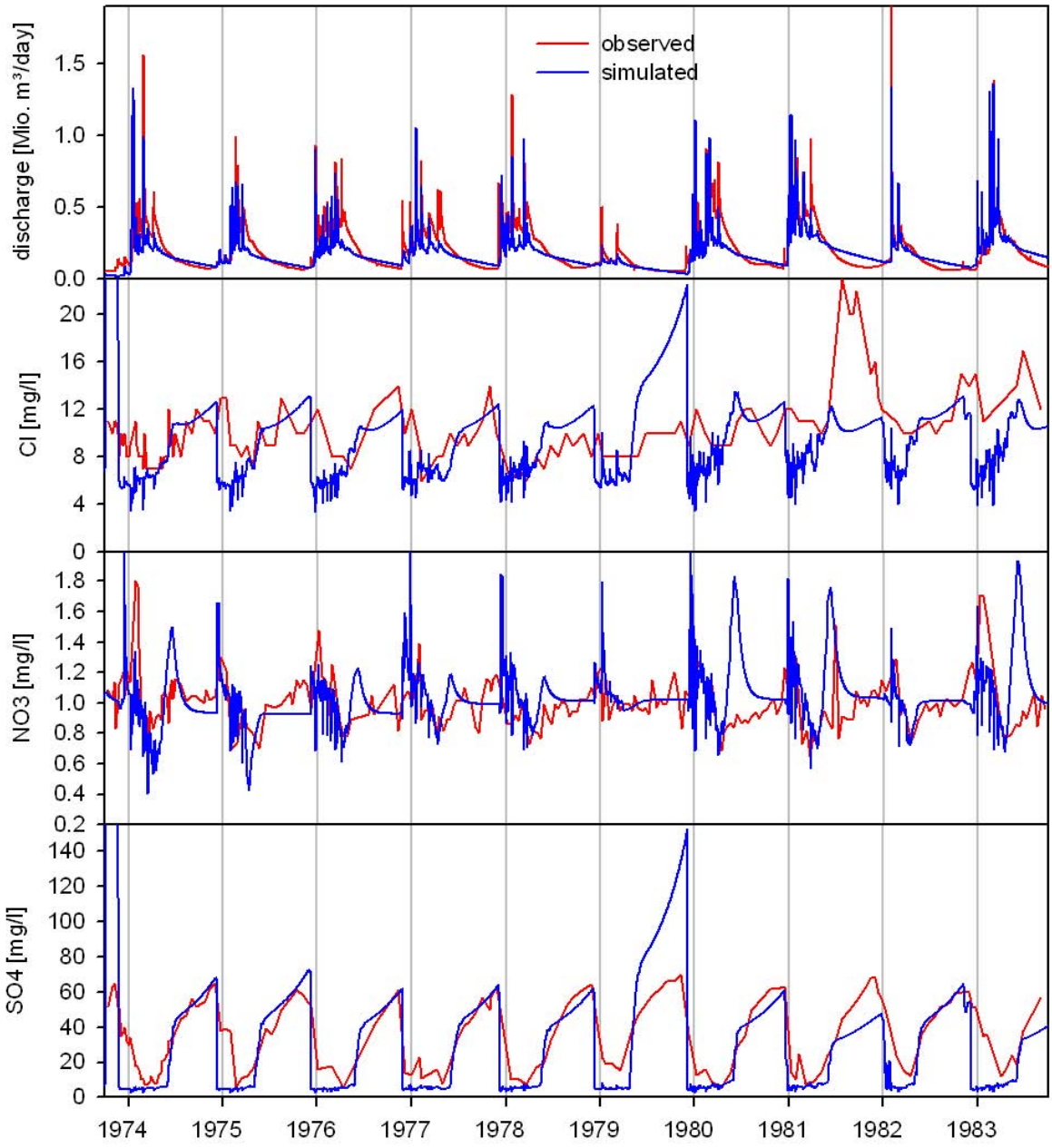

FIGURE 88: Output of groundwater routine for Banias Spring; on the top: observed and measured discharge; below: observed and measured concentrations of Cl, NO_3 and SO_4

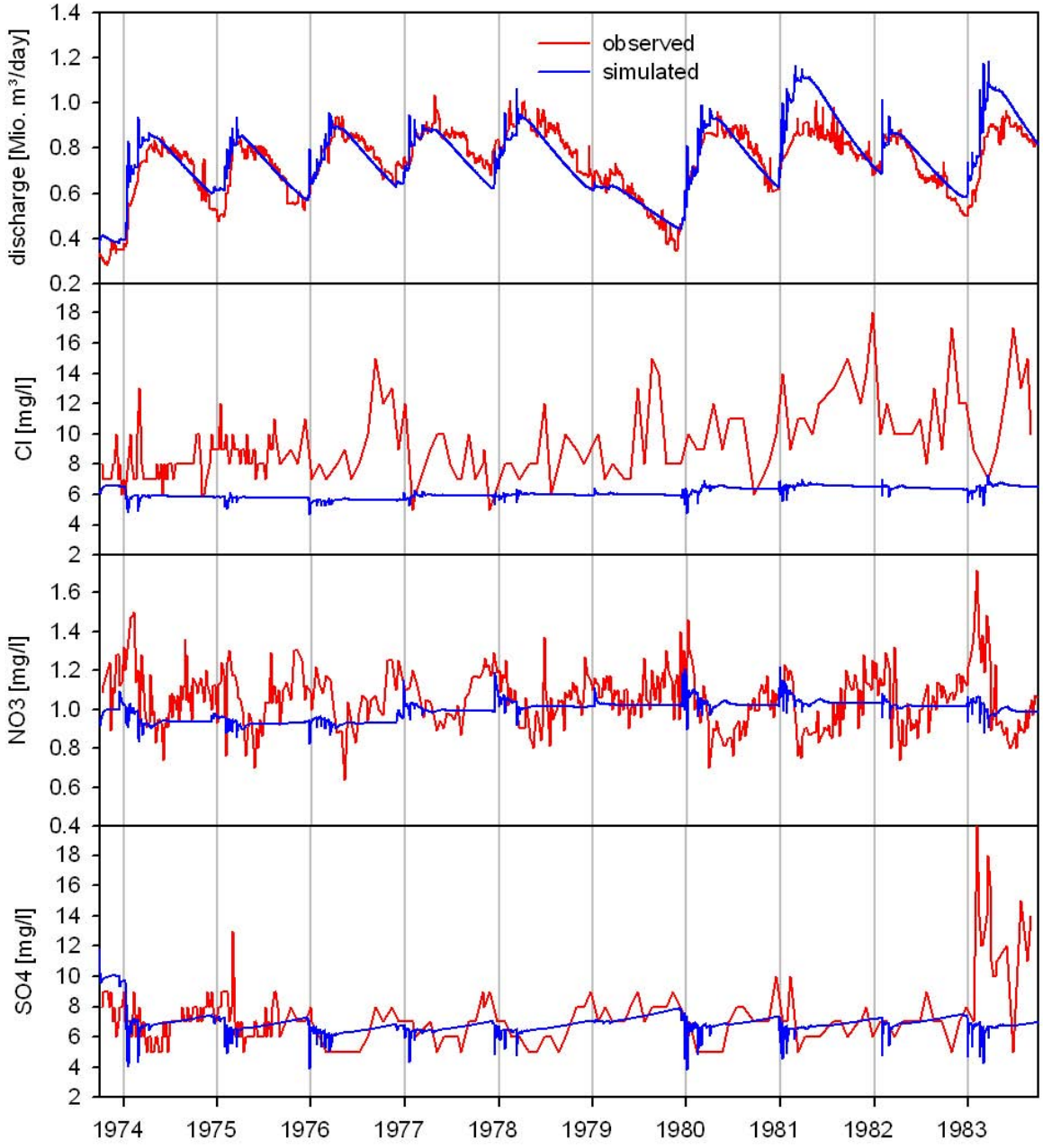

FIGURE 89: Output of groundwater routine for Dan Spring; on the top: observed and measured discharge; below: observed and measured concentrations of Cl, NO_3 and SO_4

10.4 Intermediate conclusions

Overall the results of the application of HYMKE_DUAL on the real data show that its new structure is able to reproduce the discharge behaviour of both springs quite well. The altitude difference and the right choice of parameters lead to more fissure exchange to the Dan conduits and more exchange flow from the Banias conduits to the fissures. This effect explains the different dynamics of the springs' discharge. Although the vadose zone and the Eckhard separation method of the first version of HYMKE were discarded it was possible to yield good discharge predictions. Hydrochemical results show that by applying simple mixing equations the hydrochemical variations at Banias Spring outlet can be well explained. Adding a geogene contribution to Cl and SO_4 fissure outflow concentrations at Banias Spring resulted in modelled chemographs very similar to the observed ones. Since the geogene contribution is coupled with the exchange flow from the fissures to the conduits this is an indicator that the groundwater routine for the flows is working properly. For the Dan Spring variation of simulated concentration was too small compared to the measured data except for the SO_4 concentrations. This might be an indicator that the exchange coefficient still is too large and the Dan Spring subsurface catchment is still too small. In the modelling of the springs with HYMKE_modified exchange coefficients of K_E = 50 and a subsurface catchment area of 368 km² lead too quite good results. Thus the range of reasonable K_Es determined in the sensitivity analysis should be revised once again and new tries with larger subsurface catchment areas should be performed. Equally the assumption of complete mixing for the fissures should be revised. Concentration course in the dry season, which is dominated by fissure discharge, is in the modelled concentration just a constant value which represents the concentration of the fissure storage. However observed data of NO_3 show a course from lower to higher concentrations. This could be explained by newly stored water draining out first and older water draining out later leading to a course of concentration which is not yet reproducible by the model. Looking at the NO_3 concentrations that come directly from the epikarst, which is dominant at Banias Spring outlet, they show that predicted variations fit well to the observed data. This would indicate that the soil/epikarst routine is working fine as well.

11 Final discussion and conclusions

As it was described in chapter 3 karst hydrology is characterised by a duality of recharge, flow, storage and discharge. Different approaches were introduced which can generally be divided in distributive models and global models. Distributive models require the availability of large amounts of data which means that the area under investigation should be well equipped with measurement devices and there should be information about system inside parameters and variables. This demand makes distributive models preferentially applicable in small scale catchments. Global models were once again divided in time series analyses, which do not posses predictive capabilities, and single event models. These models consist of different kinds of system functions. If theses system functions represent processes and storages naturally abundant in the real hydrological system the models are also called “grey box” models.

Due the scarceness of system inside data, as introduced in chapter 4, RIMMER AND SALINGAR (2006) developed such a “grey box” model by applying the system approach (see chapter 5): the first version of HYMKE. Even though HYMKE yielded good results for the predictions of spring discharges adding of mixing equations showed that it was not capable to yield good predictions of hydrochemistry as well. This was regarded as a sign that one storage or process at least was missing in the model structure.

Examination of long and short term hydrochemical data in chapter 6 showed that both, Dan and Banias Spring, receive event water, water from the epikarst and diffuse matrix flow water from a fissured matrix storage. Just the proportions were different for the two springs: in the rainy season Banias Spring was more dominated by event water and water from the epikarst while Dan Spring was more dominated by diffuse matrix flow from the fissure storage. In the dry season both springs only received water from the fissures. This indicates that the major karst processes, summarized as the duality of karstic systems, are also abundant in Mt. Hermon hydrological system.

To incorporate this knowledge in the first version of HYMKE two different approaches were used: (1) identifying the most important missing process, which was the duality of groundwater flow and storage, and adding it to the first version of HYMKE: development of HYMKE_modified (chapter 7). (2) Modifying all routines of the first version of HYMKE in a manner that they represent the all processes and stotrages of the Mt. Hermon hydrological

system as they were introduced in chapter 2 and recognized in chapter 6: development of HYMKE_DUAL (chapter 9).

11.1 Discussion of flow simulations

Both newly developed models yielded good predictions of spring discharges whereby HYMKE_modified was calibrated to fit to the separated base flow (see chapter 5) and HYMKE_DUAL was fitted to the real values observed at the spring outlets. Major differences regarding the simulations of flow inside the routines of HYMKE_modified and HYMKE_DUAL are as follows:

HYMKE_DUAL uses a snow melt routine which is not yet included in HYMKE_modified. However results showed that snowmelt is not so significant which is also indicated by the results of HYMKE_modified which yields good results without considering snow melt.

By adding the snow melt routine to HYMKE_DUAL also a subdivision of the study area in 56 altitude strips was performed. This distribution considers altitude effects on snow melt, precipitation and actual evaporation. HYMKE_modified just considered the altitude effect on precipitation. The subdivision in different altitude strips would also allow applying different sets of parameters on each level. However there was no spatial data available. Thus this subdivision did not lead to strong improvements of model results.

HYMKE_modified includes the assumption that parts of the excess flow of the surface layer are not transformed into preferential flow but into fast flow which does not enter the groundwater system. It leaves the surface layer and it is added to the spring outlet after it passed a surface flow routine implying that water is reaching the stream by travelling near to the surface. That assumption is not anymore included in HYMKE_DUAL. In its approach all water enters the groundwater system. As both models produce good results no statement can be given which assumption is the right one.

Recharge to the groundwater routines of both models is similar but the series of routines set above the groundwater routine producing these results are quite different: in HYMKE_modified infiltrating water either is stored in the surface layer reservoir

or it can pass by as preferential flow. Water stored inside the surface layer reservoir can leave as evaporation or as unsaturated matrix flow. The sum of unsaturated matrix flow and preferential flow enters the vadose zone from where it is draining to the conduit groundwater while it is following the assumption of linearity between stored volume and discharge. The vadose zone reservoir leads to a very even recharge to the groundwater. In HYMKE_DUAL infiltrating water once again can be either stored in the soil layer or it can pass by as preferential flow. Water stored in the soil layer is also exposed to evaporation and drains as unsaturated matrix flow. The sum of soil layer unsaturated matrix flow and soil preferential flow enters the epikarst layer. There, once again unsaturated matrix flow and preferential flow can take place. The sum of both can either enter the conduit groundwater system or the lower epikarst layer from where it drains as unsaturated flow to the fissure groundwater. Since preferential flow can occur until the outflow to the conduits even sharp flow signals can transposed. This is not possible in HYMKE_modified since the vadose zone includes no option for preferential flow. This ability allows that HYMKE_DUAL can be calibrated directly with the observed discharge values which also show strong variations.

In HYMKE_DUAL actual evaporation, which is subtracted from the soil layer water content, is a function of potential evaporation and relative saturation of the soil layer. In HYMKE_modified actual evaporation is calculated as a function of potential evaporation and dry days after the last rain event. Both models just allow evaporation from the uppermost layer.

The duality of groundwater flow and storage in HYMKE_modified is represented separately for Dan and Banias Spring system. However HYMKE_DUAL includes the possibility for groundwater to flow from one conduit system into the fissure system and leave from there to the other conduit system: water from Banias Spring conduits can reach Dan Spring conduit system passing the fissured matrix storage. By incorporating the real altitude difference between the springs this feature can explain the differences of spring dynamics.

Altogether different series of different types of parameters led to similar discharge results. Biggest differences of both models can be found in the transition of fast flow to the spring

outlets and the representation of the soil, the epikarst and the vadose zone. Fast flow in HYMKE_modified is not entering the groundwater system but reaches the stream as shallow fast flow by applying the surface flow routine. In HYMKE_DUAL fast flow enters the groundwater system and produces sharp discharge variations in the rainy season. There is not enough data available to prove or disprove any of these assumptions. In HYMKE_modified soil and epikarst are represented by just one layer. But as shown in chapter 3 at least soil and epikarst should be distinguished in modelling of epikarst since it performs as a temporal storage beneath the soil. However that epikarst is important in the Mt. Hermon system, too, was shown in chapter 6. Therefore just taking one storage for both, soil and epikarst, as it was done in HYMKE_modified, should result in bad to moderate predictions of solute concentrations. Since the structure of HYMKE_modified yields good results nevertheless the vadose zone routine might be more regarded as a storage representing the epikarst. With this assumption the partial mixing assumed for the vadose zone would represent a simple implementation of piston flow effect on hydrochemical predictions. The simulation of groundwater flow is similar in both approaches. The only difference is that in HYMKE_DUAL both conduit systems can exchange via the fissure system. This feature is a good explanation of the different dynamics of discharge observed for both springs.

11.2 Discussion of solute concentration simulations

Compared to the solute concentration predictions of the first version of HYMKE both models deliver good results once again whereby HYMKE_DUAL shows too small variations for all solute concentrations at Dan Spring. The improvement of predictions of both models were mainly due to the implementation of the duality of groundwater flow and storage which allows the fast transition of recharge concentration signals to the spring outlets. However groundwater concentration predictions are dependent on the concentration of recharge to the groundwater routine which in turn is dependent on the routines superimposed to the groundwater routine. The impact on the recharge concentration of the HYMKE_modified surface layer and vadose zone routine, and the HYMKE_DUAL soil/epikarst layer are as follows:

In HYMKE_modified actual evaporation can enrich water stored in the surface routine. Since the surface routine reservoir just stores little amounts of water in the low conductivity matrix much water can pass by as preferential flow which mixes with the matrix water leaving the surface routine. Hence the output concentration of

the whole routine fluctuates quite strong during the rainy season. Below it is mixed partially with the water already stored in the vadose zone routine. The special sequence of soil/epikarst routine and a following vadose zone is responsible for a very even hydrochemical signal of recharge reaching the groundwater. The partial mixing applied in the vadose zone evens the signal but does not dampen the signal too much. If complete mixing would be assumed the attenuation of the signal would be too strong.

In HYMKE_DUAL once again actual evaporation can enrich the solute concentrations in the soil layer. Unsaturated matrix flow leaving the soil layer mixes with preferential flow. Thus the overall concentration of flows leaving the soil layer is the mixing concentration of enriched soil layer matrix flow and preferential flow. Below it either mixed completely with the water already stored in the upper epikarst layer or it passes by as preferential flow maintaining its concentration from the soil layer output. Consequently outflow from the upper epikarst layer is again the mixing concentration of matrix flow from the upper epikarst and preferential flow. This flow is divided in flow to the conduit groundwater system and flow to the lower epikarst. In the lower epikarst it mixes again with the water already stored inside yielding the input concentration the fissure groundwater. There is no additional feature to include piston flow effects on flow in the epikarst. However due to the ability to produce preferential flow in the soil layer and the upper epikarst layer the sharp concentration signals can be transferred to the groundwater routine.

Both approaches delivered reasonable results for the groundwater recharge concentrations whereby the approach of HYMKE_DUAL was able transform sharp concentration signals to the spring outlets. Thus under extreme rainy conditions preferential flow can pass the soil and the epikarst layer, and reach the groundwater system from where at least a part of it can pass through to the spring outlet. That this process is really happening was proven in chapter 6 for both springs. The combination of surface layer and vadose zone with partial mixing in HYMKE_modified was able to reproduce the seasonal variations. But it was not able to reproduce sharp variations of concentrations at the spring outlets. However looking at its predictions for spring water concentrations its evened concentration signals could be transmitted successfully to both spring outlets which led to good approximations of the observed concentrations. This was a consequence of very small storage coefficients for the

conduit reservoirs combined with a small exchange coefficient. As mentioned above HYMKE_DUAL predictions for spring discharge concentrations just yielded good results for Banias Spring. Predictions for Dan Spring showed too small variations. This is due the big amount of fissure groundwater which attenuates the recharge concentration signal coming from the soil/epikarst layer. This effect is produced by the selection of a very small subsurface catchment area for the Dan Spring system, and an exchange coefficient which might be still too large. Additional the assumption of complete mixing of the water entering the fissure system should be reconsidered. It is most probable that water entering the fissures is not mixing totally with the water already stored in the fissure reservoir. Consequently water draining from the fissures after an event would first show the same concentrations as the event water before older water leaves the fissures.

11.3 Conclusions

Overall the implementation of two different approaches of modelling the Mt. Hermon hydrological system gave a lot of valuable information about the impact of their differing routines on their predictions of discharges and solute concentrations:

The snow melt routine did not change the results significantly due to the small fraction of area lying in the upper regions of Mt. Hermon. Thus its incorporation in a model system for Mt. Hermon groundwater system is not absolutely necessary.

The separation of the system in different altitude strips did not improve results significantly because there was no spatial information about surface properties available.

It could be demonstrated that modelling of the soil and epikarst requires the separation of soil and epikarst into two different storages. Thereby soil could be well approximated by a reservoir in which unsaturated flow and complete mixing is taking place with the possibility of preferential flow after exceeding saturation. For the epikarst either a linear reservoir or another unsaturated flow reservoir led to good discharge predictions. In respect to the mixing piston flow effects within the reservoir should be incorporated as well as the possibility of water passing by the epikarst after exceeding the storage capacity.

It could be shown that with a modified linear reservoir the effects of double porosity on groundwater flow could be adequately reproduced. This modification was the major improvement of both models compared to the first version of HYMKE. Thereby even the differences of spring dynamics could be explained by the coupling of both conduit systems and the fissure system, as it was done in HYMKE_DUAL.

Thus both approaches have their strengths and their weaknesses. Their biggest differences can be found in their approximation of the soil and the epikarst: the combination of soil/epikarst reservoir and vadose zone in HYMKE_modified convinces by its simplicity and the therefore resulting low number of parameters. Despite of that the approach applied in HYMKE_DUAL with its claim to reproduce epikarst behaviour, as described by PERRIN ET AL. (2003) and ARBEL ET AL. (2008), is more complex and thus demands for a larger number of parameters. However these parameters are measurable and they can be distributed over different altitude zones. The representation of the groundwater system was very similar for both approaches whereby HYMKE_DUAL with its interlinked fissure and conduit systems seems to be the most favourable choice since it explains best the differences in the dynamic behaviour of the springs; it even requires less parameters compared to the routine applied in HYMKE_modified. The application of the snow melt routine and the subdivision in different altitude strips in HYMKE_DUAL did not improve results significantly. However these features offer a big potential for the application of HYMKE_DUAL in other catchments with more system inside information available: due to the distributed calculation of snow melt and soil and epikarst behaviour distributed sets of parameters, representing spatial heterogeneities, can be applied, and spatial distributed results can be delivered. Unfortunately in Mt. Hermon there is no spatial data available about soil and epikarst properties. Hence these potential advantages have not much use in Mt. Hermon range. For HYMKE_DUAL they had to be estimated by using the results of other studies in similar regions.

Consequently a model with a lumped structure, similar to HYMKE_modified, including an approximation of the soil and epikarst, which unites the advantages of the approximations of HYMKE_modified and HYMKE_DUAL, and the groundwater routine developed for HYMKE_DUAL, might be the most reasonable choice to model the hydrological behaviour of Mt. Hermon system.

12 Outlook

In this diploma thesis two “grey box” models were developed based on karst specific and hydrochemical observations: HYMKE_modified and HYMKE_DUAL. Both models showed similar good results for discharge predictions of the two of the major springs of the Upper Jordan River: the Dan and Banias Spring. In order to proof the right choice of model structure and parameters flow predictions were coupled with solute concentration predictions. The hydrochemical predictions also showed adequate to good agreement with the observed data. Regarding these results it is most probable that the models reproduce the natural processes of the Mt. Hermon hydrological system. Thus it was possible to develop two process based “grey box” models which deliver reasonable predictions for a large scale hydrological system without having access to spatial system inside information. This is a big advantage to former approaches using distributive models which were only applicable in small scale catchments because of the large amount of system inside information required. As they are process based these models represent proper tools to be applied to scenarios of climate change. Wether HYMKE_modified or HYMKE_DUAL should be applied is dependent on the preciseness of data available and required: if there is just data about input, e.g. predictions of precipitation and temperature of climate scenarios, HYMKE_modified might be the better choice. If there is an additional demand for spatial distributed information, e.g. the impact of climate and landuse change on percolation in different altitude zones, HYMKE_DUAL might be more favourable. However this demand would also need more information about the spatial distribution of superficial and soil parameters.

In the past when Caesar built a temple of white marble at the footslopes of Mt. Hermon close to the major spring of the Jordan River, the Dan Spring, he already appreciated the importance of this river. In the present it did not loose any of this importance – it even rose. Facing increasing water demands of the Eastern Mediterranean countries and impacts of climate change plans for an equitable distribution of its water must be developed to avoid aggreviation of the political tensions already abundant in this region. Predictions of the future water availability can provide the base for these distribution plans. Therefore the models developed in this diploma thesis would be an appropriate tool.

13 References

ALPERT, P. (2004): The water crisis in the E. Mediterranean – and relation to global warming? In: Water in the Middle East and in North Afrikca – Resources, Protection and Management, eds: Zereini, F. and Jaeschke, W., Springer Verlag Berlin Heidelberg New York, 369 p.

ALPERT, P., OSETINSKY, I., ZIV, B., SHAFIR, H. (2004a): A new seasons definition based on classified daily synoptic systems: an example for the Eastern Mediterranean. International Journal of Climatology, 24, 1013-1021.

ALPERT, P., OSETINSKY, I., ZIV, B., SHAFIR, H. (2004b): Semi-objective classification for daily synoptic systems: application to the Eastern Mediterranean climate change. International Journal of Climatology, 24, 1001-1011.

AQUILINA, L., LADOUCHE, B., DOERFLIGER, N. (2006): Water storage and transfer in the epikarst of karstic systems during high flow periods. Journal of Hydrology 327(3-4), 472-485.

ARBEL, Y., GREENBAUM, N., LANGE, J., INBAR, M. (2008): Infiltration Processes and Flow Rates – Monitoring Environmental and Artificial Tracers in Cave Drippings- Mt. Carmel, Israel, in preparation.

AUSTIN, A.T., VIVANCO, L. (2006): Plant litter decomposition in semi-arid ecosystem controlled by photodegradation. Nature 442 (3), 555–558.

AUSTIN, A.T., SALA, O.E., JACKSON, R.B. (2006): Inhibition of nitrification alters carbon turnover in the Patagonian steppe. Ecosystems 9 (8), 1257–1265.

AVRAHAMI, S., CONRAD, R. (2005): Cold-temperate climate: a factor for selection of ammonia oxidizers in upland soil? Canadian Journal of Microbiology 51, 709–714.

AVRAHAMI, S., LIESACK, W., CONRAD, R. (2003): Effects of temperature and fertilizer on activity and community structure of soil ammonia oxidizers. Environmental Microbiology 5 (8), 691–705.

BARENBLATT, G.I., ZHELTOV, I.P., KOCHINA I.N. (1960): Basic concepts in the theory of seepage of homogeneous liquids in fissured rocks. Journal of Applied Mathematics and Mechanics, 24, 1286-1303.

BEAUMONT, P. (2000): The Quest for Water Efficiency - Restructuring of Water Use in the Middle East. Water, Air, & Soil Pollution 123(1-4): 551-564.

BEAUMONT, P., BLAKE, G.H., WAGSTAFF, J.M. (1988): The Middle East - a geographical study, David Fulton Publishers, London, 572 p.

BEN-GAI, T., BITAN, A., MANES, A., ALPERT, P., RUBIN, S. (1999): Spatial and temporal trends of temperature patterns in Israel. Theoretical and Applied Climatology, Vol. 64, 163-177.

BERGSTRÖM, S. (1976): Development and application of a conceptual runoff model for Scandinavian catchments. SMHI RH07, Norrköping.

BEVEN, K.J. & KIRKBY, M.J. (1979): A physically based, variable contributing area model of basin hydrology. Hydrological Sciences Bull., 24, 43-69.

BEVEN, K.J. (2001): Rainfall-Runoff Modeling. The Primer, John Wiley and Sons Ltd., 360 p.

BINKLEY, D., HART, S.C. (1989): The components of nitrogen availability assessments in forest soils. Advances in Soil Science 10, 57–112.

BOX, G.E.P., JENKINS, G.M. (1976): Time series analysis: forecasting and control. San Francisco: Holden Day, 576 p.

BRIELMANN, H. (2008): Recharge and discharge mechanism and dynamics in the mountainous northern Upper Jordan River Catchment, Israel. PhD-Thesis, Faculty of Geosciences at Ludwig-Maximilians-University Munich.

BROOKS, R.H., AND COREY, A.J. (1964): Hydraulic properties of porous media. Hydrol. Paper 3, Colo. State Univ., Fort Collins, CO.

CACAS, M.C., LEDOUX, E., DE MARSILY, G., TILIE, B., BARBREAU, A., DURAND, E., FEUGA, B., PEAUDERCERF, P. (1990): Modeling fracture flow with a stochastic discrete fracture network model: calibration and validation, 1. the flow model. Water Resources Research, 26, 479-489.

CAMBI, C., DRAGONI, W. (2000): Groundwater yield, climatic changes and recharge variability: considerations arising from the modelling of a spring in the Umbria-Marche Apennines. Hydrogéologie, 4, 11–25.

CHRISTOPHERSEN, N., HOOPER, R.P. (1992): Multivariate analysis of stream water chemical data: The use of principal components analysis for the end-member mixing problem. Water Resources Research, 28, 99–107.

CHRISTOPHERSEN, N., NEAL, C., HOOPER, R.P., VOGT, R.D., ANDERSEN, S. (1990): Modelling streamwater as a mixture of soilwater end-members – a step towards second-generation acidification models, J. Hydrol. 116, 307–320

COLEMAN, T.F., Y. LI (1996): An Interior, Trust Region Approach for Nonlinear Minimization Subject to Bounds. SIAM Journal on Optimization, Vol. 6, pp. 418-445.

COLEMAN, T.F. AND Y. LI (1994): On the Convergence of Reflective Newton Methods for Large-Scale Nonlinear Minimization Subject to Bounds. Mathematical Programming, Vol. 67, Number 2, pp. 189-224.

CORNELL, R.M., SCHWERTMANN, U. (1996): The iron oxides. Structure, properties, reactions, occurence and uses. VCH Weinheim, 395-432.

DAN, J. (1983): Soil chronosequences of Israel. Catena, 10, 287-319.

DANIN, A. (2004): Distribution atlas of plants in the flora Palaestina area. Israel Academy for Science and Humanities, Jerusalem.

DERSHOWITZ, W.S., LA POINTE, P.R., DOE, T.W. (2004): Advances in discrete fracture network modelling. Proceedings of the U.S. EPA/NGWA Fractured Rock Conference, Portland.

DERSHOWITZ, W.S., TOXFORD, T., SUDICKY, E., SHUTTLE, D.A., EIBEN, T., AHLSTROM, E. (1998): PA Works pathways analysis for Discrete Fracture Networks with LTG solute transport. User Documentatiom, Golder Associates Inc., Redmont, Washington

DESMARAIS, K., ROJSTACZER, S. (2002): Inferring groundwater flow paths from measurements of carbonate spring response to storms. Journal of Hydrology 260, 118-134.

DINGMAN, S. L. (2002): Physical Hydrology. Macmillan, 646 p.

DOERFLIGER, N., JEANNIN, P.-Y., ZWAHLEN, F. (1999): Water vulnerability assessment in karst environments: a new method of defining protection areas using a multi-attribute approach and GIS tools (EPIK method). Environmental Geology, 39, 2, 165-176.

DOMENICO, P.A., SCHWARTZ, F.W. (1990): Physical and chemical hydrogeology. John Wiley and Sons, New York, 824 p.

DVERSTORP, B., ANDERSSON, J., NORDQVIST, W. (1992): Discrete fracture network interpretation of field tracer migration in sparsely fractured rock. Water Resources Research, 28, 2327-2343

EATON, A.D., LENORE, S.C., RICE, E.W., GREENBERG A.E. (2005): Standard Methods for Examination of Water & Wastewater. American Public Health Association, 21, 1368 p.

ECKHARDT, K. (2005): How to construct recursive digital filters for baseflow separation. Hydrological Processes, 19, 507–515.

EINSIEDL, F. (2005): Flow system dynamics and water storage of a fissured-porous karst aquifer characterized by artificial and environmental tracers. Journal of Hydrology, 312: 312-321.

EINSIEDL, F., MAYER, B. (2006): Hydrodynamic and microbial processes governing nitrate in a fissured-porous karst aquifer. Environmental Science and Technology, 40, 6697-6702

EINSIEDL F., MALOSZEWSKI P., AND STICHLER W. (2005): Estimation of denitrification potential in a karst using the ^{15}N and ^{18}O isotopes of NO_3. Biogeochemistry 72(1), 67-86.

EISENLOHR, L., KIRÁLY, L., BOUZELBOUDJEN, M., ROSSIER, I. (1997b): Numerical versus statistical modeling of natural response of a karst hydrogeological system. Journal of Hydrology, 202, 244-262.

FETTER, C.W. (1994): Applied HYDROGEOLOGY. PRENTICE-HALL, NEW JERSEY. EDITION?

FLEURY, P., Plagnes, V., Bakalowicz, M. (2007): Modelling of the functioning of karst aquifers with a reservoir model: Application to Fontaine de Vaucluse (South of France). Journal of Hydrology Volume 345, Issues 1-2, 38-49.

FORD, D.C. AND WILLIAMS,P.W. (2007): Karst Hydrogeology and Geomorphology. Chichester, Wiley: 561 pp.

GANOR, E., MAMANE, Y. (1982): Transport of Saharan dust across the eastern Mediterranean. Atmospheric Environment, 16, 581-587.

GELFAND, I., YAKIR, D. (2008): Influence of nitrite accumulation in association with seasonal patterns and mineralization of soil nitrogen in a semi-arid pine forest, Soil Biology and Biochemistry Volume 40, Issue 2, 415-424.

GEYER, T., BIRK, S., LIEDL, R., SAUTER, M. (2008): Quantification of temporal distribution of recharge in karst systems from spring hydrographs. Journal of Hydrology Volume 348, Issues 3-4, 452-463.

GILAD, D., BONNE, J. (1990): Snowmelt of Mt. Hermon and its contribution to the sources of the Jordan River. Journal of Hydrology, 114, 1–15.

GILAD, D., SCHWARTZ, S. (1978): Hydrogeology of the Jordan sources aquifers. Isr. Hydrol. Serv. Rep. Hydro/5/78 58 pp (in Hebrew).

GOLDBERG, M., HIRSCH, F., MIMRAN, Y. (1981): The Jurassic sequence of Mount Hermon. Israeli Geological Society, Proceedings of the Annual Meeting, Abstract.

GOLDSCHEIDER, N., DREW, D. (2007): Methods in Karst Hydrogeology. International Association of Hydrogeologists, Taylor & Francis Group, 264 p.

GOPHEN, M. (2004): Hydrology and management of Lake Kinneret aimed at water quality protection. In: Water in the Middle East and in North Afrikca – Resources, Protection and Management, eds: Zereini, F. and Jaeschke, W., Springer Verlag Berlin Heidelberg New York, 369 p.

GRASSO, D. A. (1998): Interprétation des réponses hydrauliques et chimiques des sources karstiques. Ph.D. thesis, Centre of Hydrogeology (CHYN) University of Neuchatel, Switzerland.

GRASSO, D.A., JEANNIN, P.Y. (1994): Etude critique des methods d'analyse de la réponse globale des systèmes karstiques. Application au site du Bure (JU, Suisse). Bulletin d'Hydrogéologie, 13, 87-113.

GRASSO, D.A., JEANNIN, P.Y. (1998): Statistical approach to the impact of climatic variations on karst spring hydrochemical response. Bulletin d'Hydrogéologie, 16, 59-74.

GUR, D., BAR-MATTHEWS, M., SASS, E. (2003): Hydrochemistry of the main Jordan River sources: Dan, Banias, and Kezinim springs, north Hula Valley, Israel. Israel Journal of Earth Science, 52, 155–178.

HAMILTON, A.S., HUTCHINSON, D.G. AND MOORE, R.D. (2000): Estimation of winter streamflow using a conceptual streamflow model. Journal of Cold Regions Engineering 14:158-175.

HASTINGS, R.C., BUTLER, C., SINGLETON, I., SAUNDERS, J.R., MCCARTHY, A.J. (2000): Analysis of ammonia-oxidizing bacteria populations in acid forest soil during conditions of moisture limitation. Letters in Applied Microbiology 30 (1), 14–18.

HEIMANN, A. (1990): The development of the Dead Sea Rift and its margins in Northern Israel during the Pliocene and the Pleistocene. PhD-Thesis, Hebrew University Jerusalem and GSI Rep.28/90, 76 pp. (in Hebrew, English abstract).

HÖTZL, H. (2004): Natural scarcity of water resources in semi-arid and arid Middle East and its economical implications. In: Water in the Middle East and in North Afrikca – Resources, Protection and Management, eds: Zereini, F. and Jaeschke, W., Springer Verlag Berlin Heidelberg New York, 369 p.

HORNBERGER, G.M., BENCALA, K.E., MCKNIGHT, D.M. (1994): Hydrological Controls on Dissolved Organic Carbon during Snowmelt in the Snake River near Montezuma, Colorado. Biogeochemistry, 25, 3, 147-165.

HUGHES, D.A., HANNART, P., WATKINS, D. (2003): Continuous baseflow separation from time series of daily and monthly streamflow data. Water SA, 29, 1, 43–48.

HUYAKORN, P.S., PINDER, G.F. (1983): Computational methods in subsurface flow. London: Academic Press.

IPCC (2007): Summary for Policymakers of the Synthesis Report of the IPCC Fourth Assessment Report; http://ipcc-wg1.ucar.edu/ (19. Dezember 2007)

JENKINS, G.M., WATTS, D.G. (1968): Spectral analysis and its applications. San Francisco: Holden Days.

JEANNIN, P.-Y., GRASSO, D.A. (1997): Permeability and hydrodynamic behavior of karstic environment. In: Gunay, G., Johnson, A.I. (Eds.): Karst Waters Environmental Impact. A.A. Balkema, Roterdam, Netherlands, 335–342.

JEANNIN, P.-Y. (1996): Structure et comportement hydraulique des aquifères karstiques. Neuchâtel, 237 pp.

JENNINGS, J.N. (1985): Karst Geomorphology. Basil Blackwell Ltd., Oxford, p. 293.

JU'UB, G.A., SCHETELING, K. (2004): The Jordan River: Natural flow and current consumtion by riparian countries. In: Water in the Middle East and in North Afrikca – Resources, Protection and Management, eds: Zereini, F. and Jaeschke, W., Springer Verlag Berlin Heidelberg New York, 369 p.

JOFFRE, R. (1990): Plant and soil nitrogen dynamics in mediterranean grasslands: a comparison of annual and perennial grasses. Oecologia 85, 142–149.

KAFRI, U., LANG, B., HALICZ, L., YOFFE, O. (2002): Geochemical characterization and pollution phenomena of aquifer waters in northern Israel. Environmental Geology, 42, 370-386.

KESSLER, J. (1980): Mount Hermon Climate. Mt. Hermon – Nature and Landscape (eds. A. Shmida and M. Livne), Kibbutz Hamoudchad, Tel Aviv, 275 pp.

KINZELBACH, W. (1986): Groundwater modelling. Elsevier, Int. Edition.

KIRÁLY, L. (1975): Rapport sur l'état actuel des connaissances dans le domaine des caractères physiques des roches karstiques. In Burger, A. & Dubertret, L. (Eds.), Hydrogeology of karstic terrains (pp. 53-67). IAH, International Union of Geological Sciences, Series B, 3.

KIRÁLY, L. (1979): Remarques sur la simulation des failles et du réseau karstique par elements finis dans les modèles d'écoulement. Bulletin d'Hydrogéologie de l'Université de Neuchatel, 3, 155-167.

KIRÁLY, L. (1985): FEM-301, A three dimensional model for groundwater flow simulation. NAGRA Technical Report 84-49, 96 p.

KIRÁLY, L. (1988): Large-scale 3D groundwater flow modeling in highly heterogeneous geologic medium. In Custodio (Ed.), Groundwater flow and quality modeling, D. Riedel Publishing Company, pp. 761-776.

KIRALY, L. (1998): Modelling karst aquifers by the combined discrete channel and continuum approach. Bulletin d'Hydrogéologie, 16, 77-98.

KIRÁLY, L. (2002): Karstification and Groundwater Flow. Proceedings of the Conference on Evolution of Karst: From Prekarst to Cessation. Postojna-Ljubljana, 155-190.

KIRÁLY, L., MOREL, G. (1976a): Etude de regularisation de l'Areuse par modèle mathématique. Bulletin du Centre d'Hydrogéologie, Neuchatel, 1, 19-36.

KIRÁLY, L., MOREL, G. (1976b): Remarques sur l'hydrogramme des sources karstiques simule par modèles mathématiques. Bulletin du Centre d'Hydrogéologie, Neuchatel, 1. 37-60.

KIRÁLY, L., PERROCHET, P., ROSSIER, Y. (1995): Effect of epikarst on the hydrograph of karst springs: a numerical approach. Bulletin d'Hydrogéologie, 14, 199-220.

KLAER, W. (1962): Eine Landnutzungskarte von Libanon. Heidelberger Geographische Arbeiten 10, Heidelberg.

KOVÁCS, A. (2003): Geometry and hydraulic parameters of karst aquifers: A hydrodynamic modelling approach. Ph.D. thesis, University of Neuchatel, Switzerland, 131 p.

KOVÁCS, A., PERROCHET, P., KIRÁLY, L., JEANNIN, P.-Y. (2005): A quantitative method for the characterization of karst aquifers based on spring hydrograph analysis. Journal of Hydrology, 303, 152-64.

KOWALCHUK, G.A., STEPHEN, J.R. (2001): Ammonia-oxidizing bacteria: a model for molecular microbial ecology. Annual Review of Microbiology 55, 485–529.

LAROQUE, M., MANGIN, A., RAZACK, M., BANTON, O. (1998): Characterization of the La Rochefoucauld karst aquifer (Charente, France) using correlation and spectral analysis. Bulletin d'Hydrogéologie, 16, 49-57.

LEE, E. S. AND KROTHE, N.C. (2003): Delineating the karstic flow system in the upper Lost River drainage basin, south central Indiana: using sulphate and 34S-SO4 as tracers. Applied Geochemistry 18(1): 145-153.

LEE, E. S., KROTHE, N.C. (2001): A four-component mixing model for water in a karst terrain in south-central Indiana, USA. Using solute concentration and stable isotopes as tracers. Chemical Geology 179:129-143.

LINDSTROM, G., JOHANSSON, B., PERSSON, M., GARDELIN, M., AND BERGSTROM, S. (1997): Development and test of the distributed HBV-96 hydrological model Journal of Hydrology, 201, 272–288.

MACLEOD, D.A. (1980): The origin of the Red Mediterranean soils in Epirus, Greece. Journal of Soil Science, 31, 126-136.

MALOSZEWSKI, P., STICHLER, W., ZUBER, A., RANK, D. (2002): Identifying the flow systems in a karstic-fissured-porous aquifer, the Schneealpe, Austria, by modelling of environmental 18O and 3H isotopes. Journal of Hydrology, 256, 48-59.

MAIDMENT, D.R. (1992): Handbook of hydrology. In D.R. Maidment (ed.) McGraw-Hill, New York, NY.

MAILLET, E. (1905): Essais d'hydraulique souterraine et fluviale. Paris: Hermann.

MANGIN, A. (1971): Etude des debits classes d'exutoires karstiques portent sur un cycle hydrologique. Annales de spéléologie, 28, 21-40.

MANGIN, A. (1975): Contribution a l'étude hydrodynamique des aquifers karstiques. Thèse, Institut des Sciences de la Terre de l'Université de Dijon.

MANGIN, A. (1981): Utilisation des analyses corrélatoire et spectrale dans l'approche des systèmes hydrologiques. Comptes Rendus de l'Académie des Sciences, Série III, 293, 401-404.

MANGIN, A. (1982): L'approche systémique du karst, consequences conceptuelles et méthodologiques. Proc. Réunion Monographica sobre el karst, Larra., 141-157

MANGIN, A. (1984): Pour une meilleure connaissance des systèmes hydrologiques à partir des analyses correlatoire et spectrale. Journal of Hydrology, 67, 25-43.

MAZOR, E. (2004): Chemical and Isotopic Groundwater Hydrology. third edition; Marcel Dekker Publ., New York; 451 p.

MCGILL, W.B., HUNT, H.W., WOODMANSEE, R.G., REUSS, J.O. (1981): Phoenix - a model of the dynamics of carbon and nitrogen in a grassland soil. In: Clark, F.E., Rosswall, T. (eds.): Terrestrial nitrogen cycles. Ecology Bulletin (Stockholm) 33, 49 115.

MÖLLER, M., STANHILL, G. (2007): Hydrological changes in evotranspiration and precipiation: two case studies in semi-arid and humid climates. Hydrological Sciences, 52 (6), 1216-1231.

MOHRLOK, U. (1996): Parameter-Identifikation in Doppel-Kontinuum-Modellen am Beispiel von Karstaquiferen. Tübinger Geowissenschaftliche Arbeiten TGA, Reihe C31.

MOORE, R.D. (1993): Application of a conceptual stream-flow model in a glacierized drainage basin. Journal of Hydrology 150, 151-168.

NADELHOFFER, K.J., ABER, J.D. (1984): Leaf-litter production and soil organic matter dynamics along a nitrogen-availability gradient in southern Wisconsin (USA). Canadian Journal of Forest Research 13,12-21.

NATHAN, R.J., MCMAHON, T.A. (1990): Evaluation of automated techniques for base flow and recession analyses. Water Resources Research ,26, 1465–1473.

NATIV, R., MAZOR, E. (1987): Rain events in an arid environment – their distribution and ionic and isotopic composition patterns: Makhtesh Ramon Basin. Israel Journal of Hydrology, 89, 205-237.

NIHLEN, T., OLSSON, S. (1995): Influence of eolian dust on soil formation in the Aegean area. Zeitschrift für Geomorphologie, 39, 341-361.

NISSENBAUM, A. (1978): Sulfur isotope distribution in sulfates from surface waters from the northern Jordan Valley, Israel. Environmental Science and Technology, 12, 962-964.

ODA, M. (1995): Permeability tensor for discontinuous rock masses. Geotechnique, 35, 483-495.

PADILLA, A., PULIDO-BOSCH, A. (1995): Study of hydrographs of karstic aquifers by means of correlation and cross spectral analysis. Journal of Hydrology, 168, 73-89.

PALMER, A.N., PALMER, V., SASOWSKY, I. (1999): Karst Modelling. SP5, Karst Water Institute, Akron, Ohio, 265 p.

PE'ER, G., SAFRIEL, U.N. (2000): Climate change: Israel national report under the United Nations Framework Convention on Climate Change: Impact, vulnerability and adaptation (http://www.bgu.ac.il/BIDR/rio/Global91-editedfinal.html, 08.2008).

PERANGINANGIN, N., SAKTHIVADIVEL, R., SCOTT, N.R., KENDY, E., STEENHUIS, T.S. (2004): Water accounting for conjunctive groundwater/surface water management: case of the Singkarak–Ombilin River basin, Indonesia. Journal of Hydrology, 292, 1–22.

PERRIN, P. (2003): A conceptual model of flow and transport in a karst aquifer based on spatial and temporal variations of natural tracers. PhD-Thesis, Institut de Géologie, Université de Neuchatel.

PERRIN, J., JEANNIN, P.-Y., ZWAHLEN, F. (2003): Epikarst storage in a karst aquifer: conceptual model based on isotopic data, Milandre test site, Switzerland. Journal of Hydrology 279: 106-124.

PONCE, V.M. (1989): Engineering Hydrology – Principles and Practices. Prentice-Hall, Englewood Cliffs, New Jersey.

RAWS W.J., AHUJA L.R., BRAKENSIEK D.L., SHIRMOHAMMADI A. (1993): Handbook of Hydrology, chap. 5, McGraw Hill, ISBN 0-07-039732-5.

RIMMER A., SALINGAR Y. (2006): Modelling precipitation-streamflow processes in karst basin: The case of the Jordan River sources, Israel. Journal of Hydrology, 331, 524-542.

RIMMER, A., HURWITZ, S., GVIRTZMAN, H. (1999): Spatial and temporal characteristics of saline springs: Sea of Galilee, Israel. Ground Water 37, 663-673.

SARDANS, J., PENUELAS, J., ESTIARTE, M. (2008): Changes in soil enzymes related to C and N cycle and in soil C and N content under prolonged warming and drought in a Mediterranean shrubland. Applied Soil Ecology Volume 39, Issue 2, 223-235.

SAXTON, K.E. (2007): SPAW Soil-Plant-Atmosphere-Water Field & Pond Hydrology. (http://hydrolab.arsusda.gov/SPAW/Index.htm, 08.2008)

SAXTON, K.E., RAWLS, W. (2006): Soil Water Characteristics Estimates by Texture and Organic Matter for Hydrologic Solutions. Soil Sci. Soc. Am. J. vol. 70, pp. 1569-1578.

SEIBERT, J. (1997): HBV light, version 1.2, User's manual. Uppsala University, Department of Earth Sciences, Hydrology (1997), p. 31.

SEILER, K.-P., GAT, J.R. (2007): Groundwater recharge from run-off and infiltration.. Springer Verlag, Dordrecht, 241p.

SEILER, K.P., MALOSZEWSKI, P., BEHRENS, H. (1989): Hydrodynamic Dispersion in Karstified Limstones and Dolomites in the Upper Jurassic of the Franconian Alb, F.R.G.. Journal of Hydrology, 108, 235-247.

SHIMRON, A.E. (1989): Geochemical exploration and new geological data along the SE flanks of the Hermon range. Geological Survey of Israel, Jerusalem, Report GSI/32/89.

SIMONSON, R.W. (1995): Airborne dust and ist significance to soils. Geoderma, 65, 1-43.

SIMPSON, B., CARMI, I. (1983): The hydrology of the Jordan tributaries, Israel. Hydrographic and isotopic investigation. Journal of Hydrology, 62, 225–242.

SIMUNEK, J., JARVIS, N.J., VAN GENUCHTEN, M.T., GÄRDENÄS, A. (2003): Review and comparison of models for describing nonequilibrium and preferential flow and transport in the vadose zone. Journal of Hydrology 272, 14–35.

SINGER, A. (2007): The Soils of Israel. Springer Verlag Berlin Heidelberg,, 306 p.

SINGER, A., SCHWERTMANN, U., FRIEDL, J. (1998): Iron oxide mineralogy of Terre Rosse and Rendzinas in relation to their moisture and temperature regimes. European Journal of Soil Science, 49, 385-395.

SINGH, V.P. (1988): Hydrologic Systems, Rainfall-Runoff Modeling. Prentice-Hall, New Jersey.

SKLASH, M.G., FARVOLDEN, R.N. (1979): The role of groundwater in storm runoff; J. Hydrol. 43, 4565

SMAKHTIN, V.U. (2001): Estimating continuous monthly baseflow time series and their possible applications in the context of the ecological reserve. Water SA, 27, 2, 213–217.

STEENHUIS, T.S., VAN DER MOLEN, W.H. (1986): The Thornthwaite–Mather procedure as a simple engineering method to predict recharge. Journal of Hydrology, 84, 221–229.

STEINBERGER, E.H., YAARI, N.G. (1996): Recent changes in the spatial distribution of annual rainfall in Israel. J. Climate, Vol. 9, pp. 3328-3336.

STRICKLAND, J.D.H AND PARSONS, T.R. (1968): A Practical Handbook of Seawater Analysis. Ottawa: Fisheries Research Board of Canada, Bulletin 167, 293 p.

SUGAWARA, M. (1995): Tank model. In: Singh, V.P. (Ed.): Computer Models of Watershed Hydrology. Water Resources Publications, Colorado, pp. 165–214.

SZEKELY, E. (1979): Method and reagents for detection, estimation and quantitative determination of nitrate ions. Isreal Patent Number 46677.

TAHA, M.F., HARB, S.A., NAGIB, M.K., TANTAWY, A.H. (1981): The climate of the Near East. In Takahasi, K. [HRSG.]: World Survey of Climatology, Bd. 9: Climates of Southern and Western Asia. –Amsterdam.

TEUTSCH, G. (1988): Grundwassermodelle im Karst: Praktische Ansätze am Beispiel zweier Einzugsgebiete im Tiefen und Seichtem Malmkarst der Schwäbischen Alb. Ph.D. thesis, University of Tübingen

TEUTSCH, G., SAUTER, M. (1991): Groundwater modeling in karst terrains: Scale effects, data acquisition and field validation. 3rd Confernece on hydrology, ecology, monitoring and management of groundwater in karst terrains, Nashville, USA.

TEUTSCH, G., SAUTER, M. (1998): Distrinuted parameter modelling approaches in karst-hydrological investigations. Bulletin d'Hydrogéologie, 16, 99-109

THORNTHWAITE, C.W., MATHER, J.R. (1957): Instructions and tables for computing potential evapotranspiration and the water balance. Publ. Climatol. 10, 181–311. ???

THORNTHWAITE, C.W., MATHER, J.R. (1955): The water balance. Publ. Climatol. 8, 1–104.

THORNTHWAITE, C.W. (1948): An Approach toward a Rational Classification of Climate. Geographical Review, Vol. 38, No. 1, pp. 55-94

UHLENBROOK, S., HOEG, S. (2003): Quantifying uncertainties in tracer-based hydrographseparations: a case study for two, three and five component hydrograph separation in a mountainous catchment. Hydrological Processes 17: 431-453.

VAN GENUCHTEN, M.TH. (1980): A closed-form equation for predicting the hydraulic conductivity of unsaturated soils. Soil Sci. Soc. Am. J. 44:892–898.

VINEY, N.R., SIVAPALAN, M. (2000): LASCAM User Manual, Centre for Water Research, University of Western Australia.

WANG, H.F., ANDERSON, M.P. (1982): Introduction to groundwater modeling. San Francisco: W.H. Freeman & Co.

WHISTON, W. (1987): The Works of Josephus. Hendrickson Publishers Twentieth Printing 2007, 926 p.

WILLIAMS, P.W. (2008): The role of the epikarst in karst and cave hydrogeology: a review. International Journal of Speleology, 37(1), 1-10.

WILLIAMS, P.W. (1985): Subcutaneous hydrology and the development of doline and cockpit karst. Zeitschrift für Geomorphologie NF 29, 463–482.

WILLIAMS P.W., (1983): The role of the subcutaneous zone in karst hydrology. Journal of Hydrology, 61: 45–67.

WOLFART, R (1967): Geologie von Syrien und dem Libanon. Beiträge zur Regionalen Geologie der Erde, Bd. 6, 103-111.

YAALON, D.H. (1997): Soils in the Mediterranean region: what makes them different? Catena 28, 157-169.

YAALON, D.H., GANOR, E. (1973): The influence of dust on soils during the Quaternary. Soil Science, 116, 146-155.

ZAADY, E. (2005): Seasonal change and nitrogen cycling in a patchy Negev Desert: a review. Arid Land Research and Management 19 (2), 111–124.

ZILBERMAN, E., AMIT, R., HEIMANN, A., PORAT, N. (2000): Changes in Holocene Paleoseismic activity in the Hula pull-apart basin, Dead Sea Rift, northern Israel. Tectonophysics, 321, 237-252.

A Appendix

A.1 Long term data of hydrochemical variables for Banias and Dan Spring

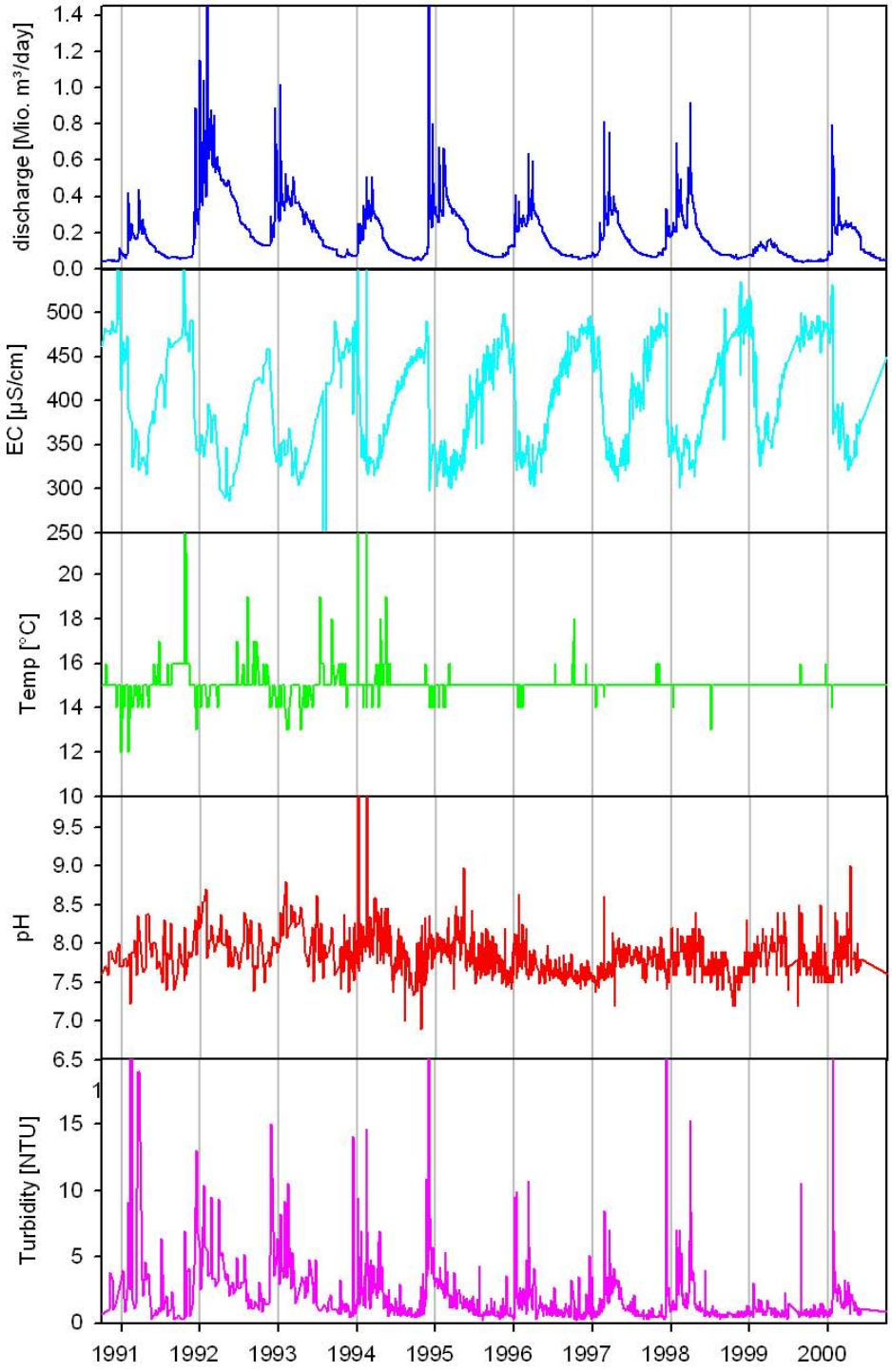

FIGURE 90: Discharge, electric conductivity, temperature. pH value and turbidity courses of Banias Spring from 1990 to 2000

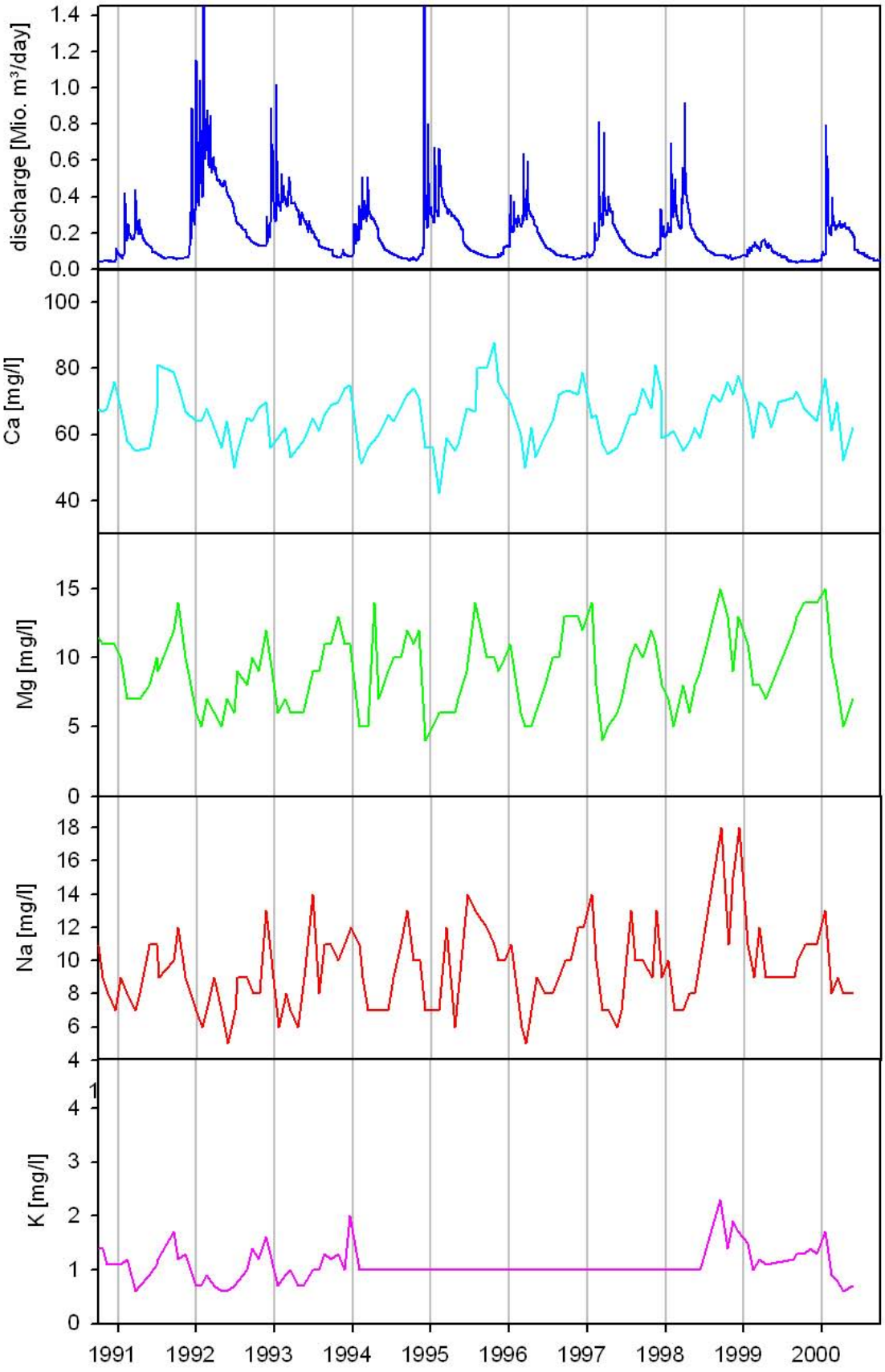

FIGURE 91: Major cation courses of Banias Spring from 1990 to 2000

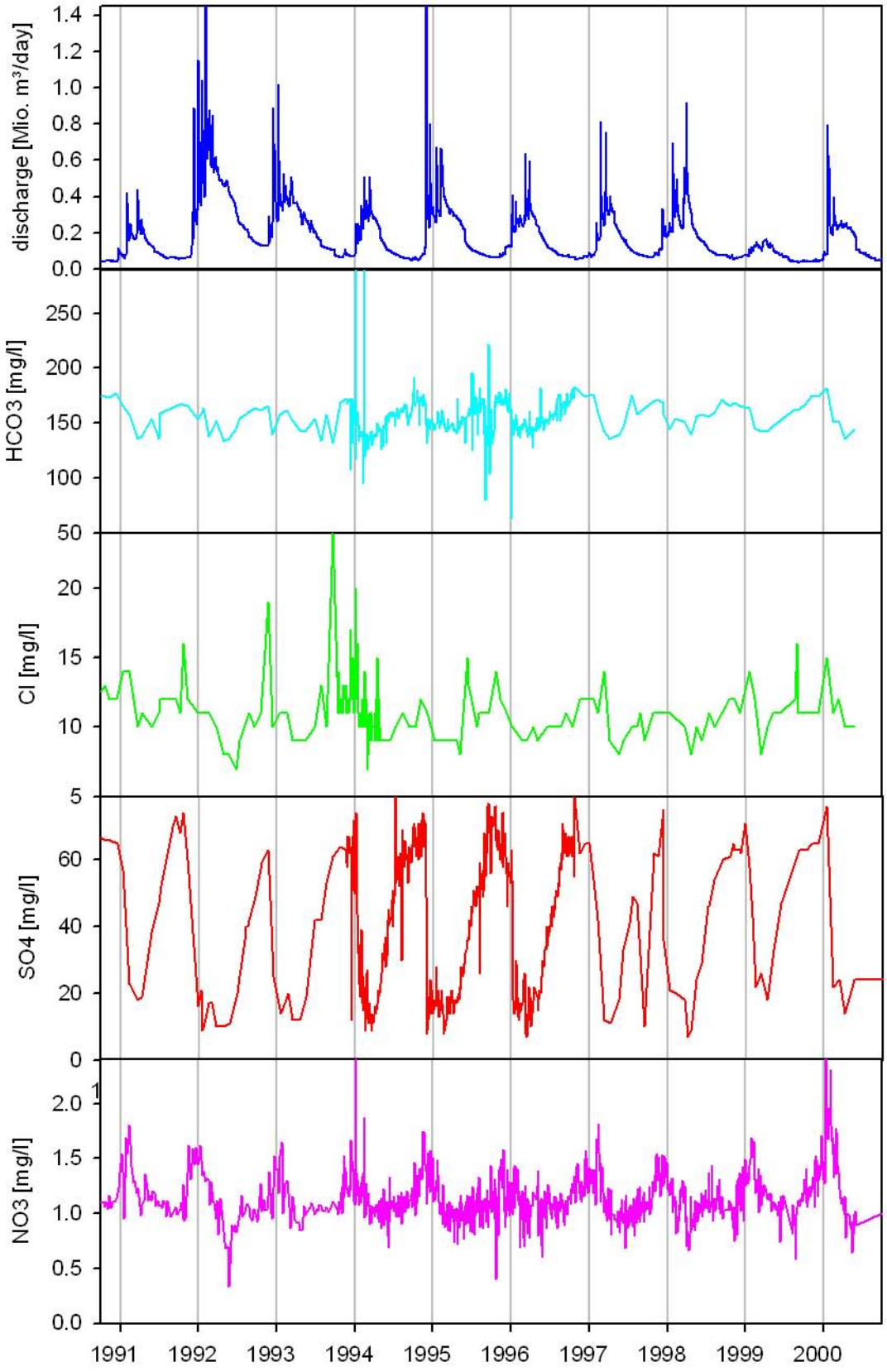

FIGURE 92: Major anion courses of Banias Spring from 1990 to 2000

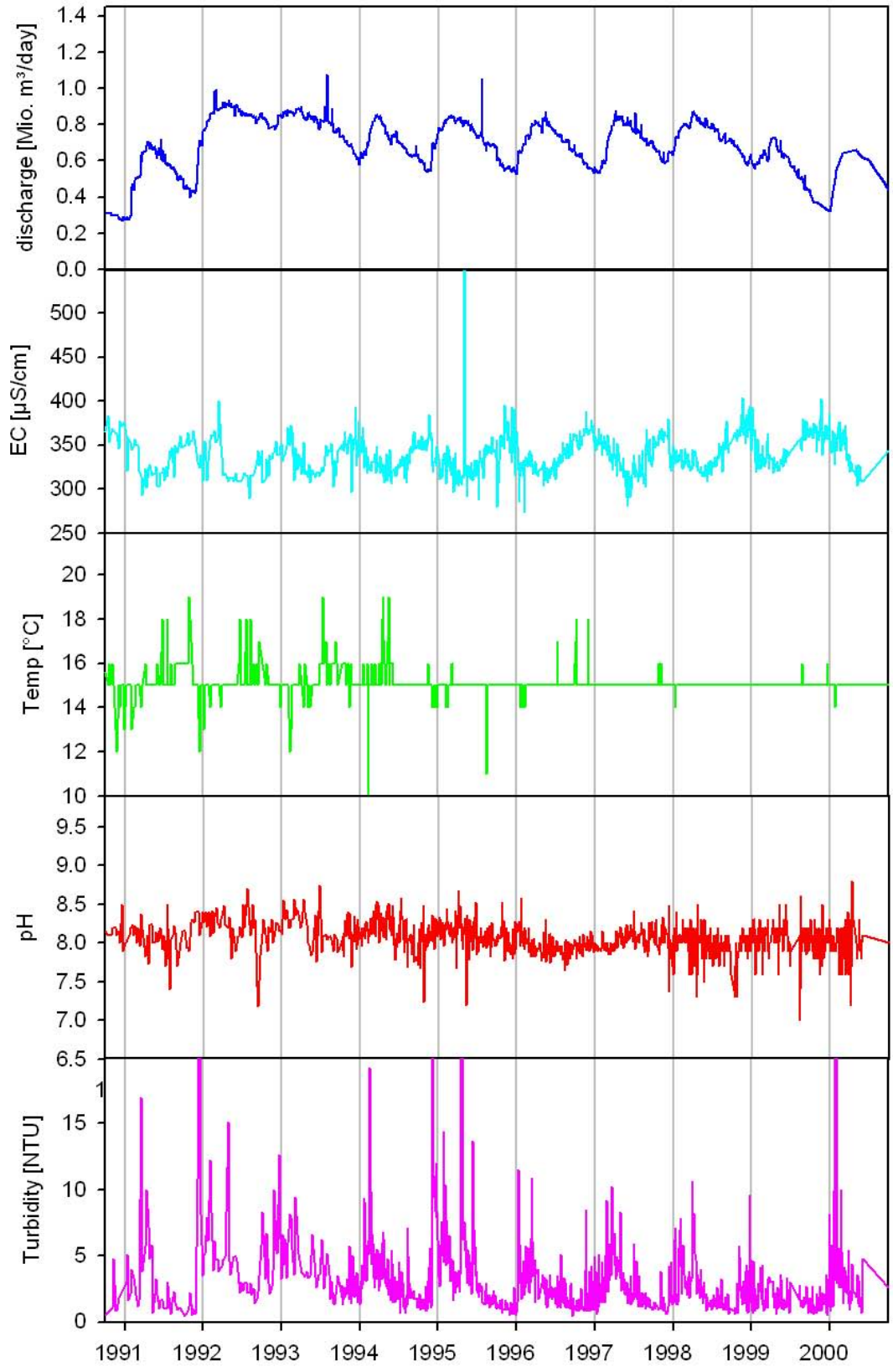

FIGURE 93: Discharge, electric conductivity, temperature. pH value and turbidity courses of Dan Spring from 1990 to 2000

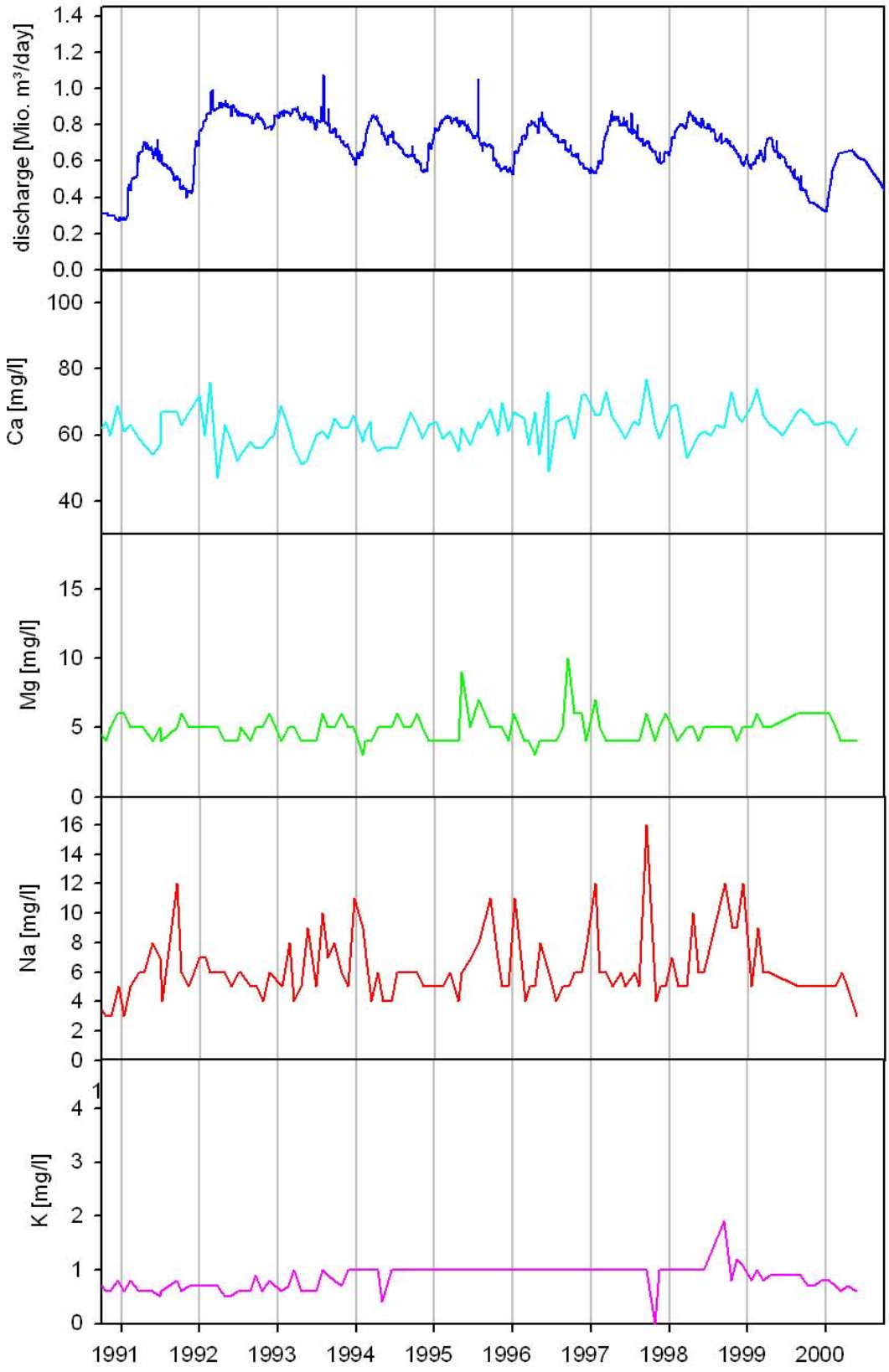

FIGURE 94: Major cation courses of Dan Spring from 1990 to 2000

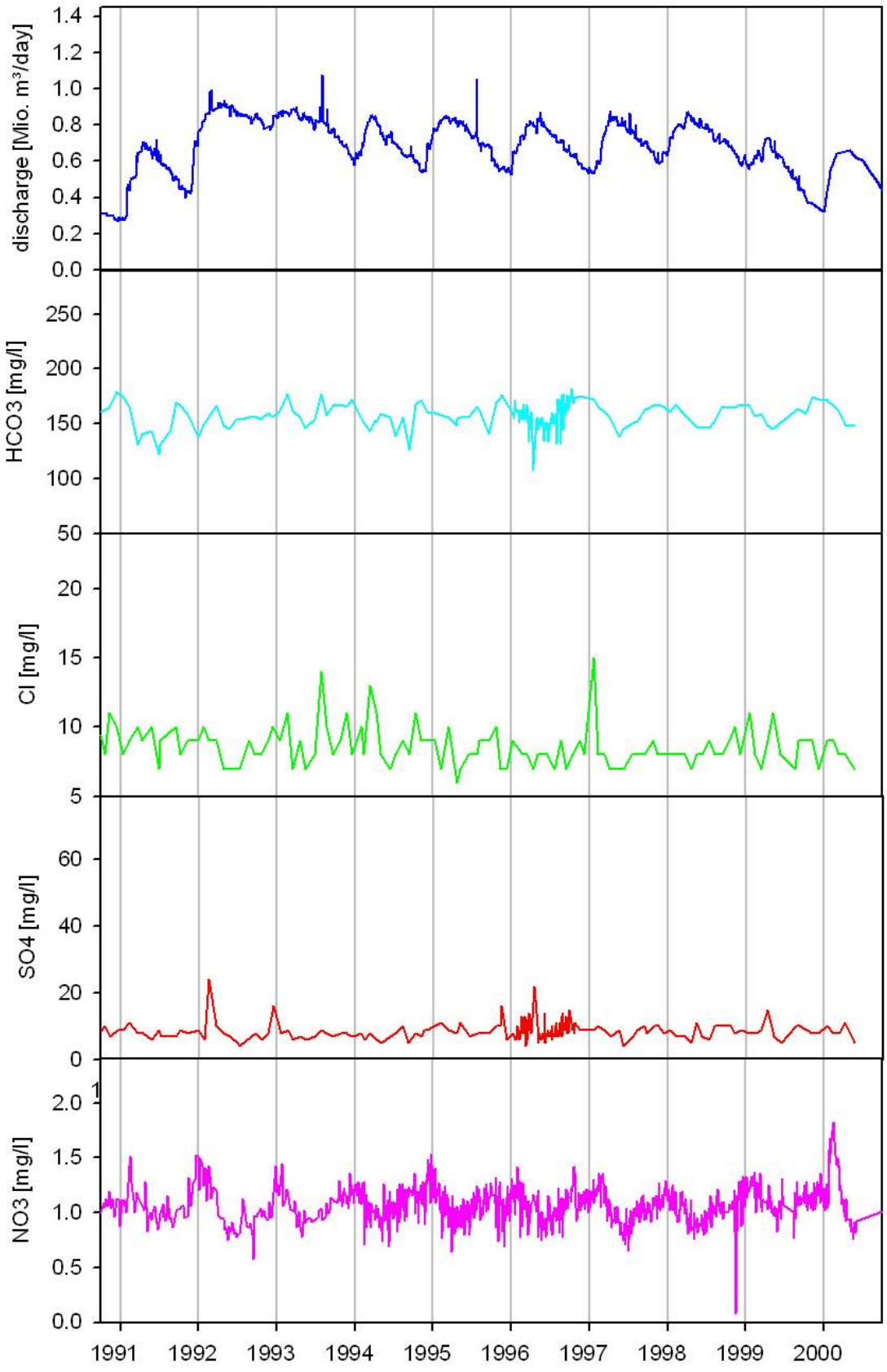

FIGURE 95: Major anion courses of Banias Spring from 1990 to 2000

A.2 Data used for the Piper and Schoeller diagrams

TABLE 23: Banias Spring major ion concentrations for different seasons (rainy or wet) under different pre-conditions in the year before

season	average conditions in the year before	date	Na [meq/l]	K [meq/l]	Ca [meq/l]	Mg [meq/l]	Cl [meq/l]	SO_4 [meq/l]	HCO_3 [meq/l]	TDS [meq/l]
rainy	wet	19.03.1978	0.22	0.02	2.79	0.33	0.17	0.17	2.29	5.99
rainy	dry	09.03.1980	0.26	0.02	3.09	0.41	0.25	0.19	2.49	6.72
dry	wet	06.11.1977	0.35	0.04	3.44	0.99	0.37	1.19	2.69	9.05
dry	dry	11.11.1979	0.52	0.04	3.69	1.13	0.31	1.46	2.82	9.97
rainy	wet	17.03.1985	0.13	0.03	2.89	0.41	0.17	0.42	2.38	6.42
rainy	dry	01.03.1987	0.09	0.03	2.69	0.41	0.20	0.29	2.34	6.05
dry	wet	10.11.1985	0.57	0.05	3.84	1.07	0.25	1.37	2.72	9.87
dry	dry	14.09.1986	0.30	0.03	3.49	1.32	0.25	1.54	3.15	10.08
rainy	wet	06.04.1997	0.30	0.03	2.69	0.41	0.25	0.23	2.23	6.15
rainy	dry	26.04.1992	0.30	0.02	2.79	0.41	0.23	0.21	2.20	6.15
dry	wet	16.11.1997	0.57	0.03	4.04	0.91	0.31	1.27	2.80	9.92
dry	dry	11.11.1990	0.35	0.03	3.39	0.91	0.34	1.37	2.84	9.22

TABLE 24: Dan Spring major ion concentrations for different seasons (rainy or wet) under different pre-conditions in the year before

season	average conditions in the year before	date	Na [meq/l]	K [meq/l]	Ca [meq/l]	Mg [meq/l]	Cl [meq/l]	SO_4 [meq/l]	HCO_3 [meq/l]	TDS [meq/l]
rainy	wet	28.05.1978	0.13	0.01	2.74	0.25	0.23	0.10	2.43	5.89
rainy	dry	18.05.1980	0.22	0.01	2.79	0.30	0.25	0.10	2.49	6.17
dry	wet	06.11.1977	0.17	0.02	3.19	0.41	0.25	0.17	2.69	6.90
dry	dry	11.11.1979	0.26	0.02	3.24	0.49	0.23	0.19	2.82	7.24
rainy	wet	12.05.1985	0.17	0.03	2.84	0.25	0.25	0.17	2.46	6.17
rainy	dry	10.05.1987	0.04	0.03	4.04	0.16	0.17	0.08	2.44	6.97
dry	wet	10.11.1985	0.22	0.03	3.19	0.41	0.31	0.17	2.74	7.06
dry	dry	14.09.1986	0.04	0.03	3.19	0.49	0.25	0.19	2.69	6.88
rainy	wet	18.05.1997	0.26	0.03	3.04	0.33	0.20	0.19	2.28	6.32
rainy	dry	24.05.1992	0.22	0.01	2.94	0.33	0.20	0.15	2.38	6.22
dry	wet	16.11.1997	0.22	0.03	2.94	0.41	0.23	0.21	2.75	6.78
dry	dry	11.11.1990	0.13	0.02	2.99	0.41	0.31	0.15	2.70	6.71

A.3 Data used for the three-component hydrograph separation

TABLE 25: median, mean, minimum and maximum monthly concentrations of Cl; n is the total number of samples taken for the respective calculations

month	median	mean	min	max	n
Oct	11	11.4	8	16	42
Nov	11	11.4	7	19	54
Dec	11	11.6	7	17	48
Jan	11	10.9	6	20	54
Feb	10	9.8	5	14	49
Mar	9	8.8	6	14	47
Apr	9	9	5	15	45
May	8	8.9	5	14	37
Jun	9	9.8	5	17	39
Jul	10	10.4	7	23	28
Aug	11	11.2	9	20	29
Sept	11	11.7	8	25	31

TABLE 26: median, mean, minimum and maximum monthly concentrations of NO_3; n is the total number of samples taken for the respective calculations

month	median	mean	min	max	n
Oct	1.105	1.11	0.4	1.47	170
Nov	1.24	1.24	0.75	1.75	195
Dec	1.27	1.3	0.88	1.95	207
Jan	1.29	1.33	0.55	2.61	205
Feb	1.175	1.22	0.68	2.31	186
Mar	1.07	1.07	0.5	1.74	200
Apr	0.98	0.97	0.66	1.36	151
May	0.99	0.98	0.33	1.39	194
Jun	1.04	1.05	0.68	3.39	186
Jul	1.07	1.07	0.77	1.51	172
Aug	1.06	1.06	0.59	1.33	181
Sept	1.06	1.05	0.44	1.44	148

TABLE 27: median, mean, minimum and maximum monthly concentrations of SO_4; n is the total number of samples taken for the respective calculations

month	median	mean	min	max	n
Oct	64	63.8	50	79	67
Nov	64	63.3	21	76	78
Dec	55	47.3	8	87	85
Jan	23	31.3	8	76	91
Feb	17	18.9	6	52	82
Mar	14	14.7	7	27	75
Apr	16	16	5	29	62
May	25	25.9	8	47	85
Jun	38	37.7	9	54	87
Jul	47	48.8	25	85	75
Aug	55	55	26	72	80
Sept	62	61.7	10	77	61

A.4 Photos of Dan Spring measurement campaign

FIGURE 96: DIVER fixed on cable and lock

FIGURE 97: Hydrologist Yuri Lechinsky, Kinneret Limnological Laboratory staff, installing the DIVER in the Dan stream

A.5 Source codes of the modified groundwater routine

```
%%%%%%%%%%%%%%%%%%%%%%%%%%%%%%%%%%%%%%%%%%%%%%%%%%%%%%%%%%%%%%%%%%%%%%%%%%%%%%%%
% algorithm for application of synthetic data on modified groundwater
% routine (by Andreas Hartmann)
%%%%%%%%%%%%%%%%%%%%%%%%%%%%%%%%%%%%%%%%%%%%%%%%%%%%%%%%%%%%%%%%%%%%%%%%%%%%%%%%

dummy=[10 50 100 200 500 1000]; % desired KEs

for j=1:length(dummy) %loop for all KEs
    %initial comditions
    h10=1;
    h20=1;
    c10=1;
    c20=1;
    K1=5;
    KE=dummy(j);
    n1=0.0001;
    n2=0.01;
    li=5;  %lenght of rain impulse in days
    en=50; %length of whole simulated period
    ken=1000; %runs for staionary conditions
    m_dif=0.001;
```

```
    %create rain impulse
    in1=[];
    in2=[];
    for k=1:ken
        in1=[in1,ones(1,li),zeros(1,en-li)];
        in2=[in2,zeros(1,en)];
    end
    in1=.1/li*in1; %100mm input uniform distributed over the whole impulse

    %create rain concentration course
    cin=[];
    cstart=2.5; %concentration if rainwater in 1st rain event time step
    c_rain=.5;
    h = waitbar(0, 'processing synthetic data');
    for k=1:ken
        for l=1:li
            %constant for geogene mass input
            ctemp(l)=c_rain;
            %continuously decreasing
%             ctemp(l)=cstart/l; %linaer decrease of concetration
        end
        cin=[cin,ctemp,ones(1,en-li)*c_rain];
        h = waitbar(k/ken,h);
    end
    close(h);

    %apply reservoir for heads and concentrations
    [h1(j,:) h2(j,:) q1(j,:) qE(j,:) c1(j,:) c2(j,:)]= ...
        mod_res(in1,in2,h10,h20,K1,KE/n2,cin,zeros(1,length(cin)), ...
        c10,c20,m_dif,n1,n2);

end
%-------------------------------------------------------------------------



%%%%%%%%%%%%%%%%%%%%%%%%%%%%%%%%%%%%%%%%%%%%%%%%%%%%%%%%%%%%%%%%%%%%%%%%%%%%
% time loop for modified groundwater routine (by Andreas Hartmann)
%%%%%%%%%%%%%%%%%%%%%%%%%%%%%%%%%%%%%%%%%%%%%%%%%%%%%%%%%%%%%%%%%%%%%%%%%%%%

function [h1 h2 q1 qE c1 c2]=mod_res(in1,in2,h10,h20,K1,KE, ...
    c_in1,c_in2,c10,c20,m_dif,n1,n2)

n=length(in1);

%1st step
[h1(1) h2(1) q1(1) qE(1) c1(1) c2(1)]=simpel_1step(K1,KE,in1(1),in2(1), ...
    h10,h20,c_in1(1),c_in2(1),c10,c20,m_dif,n1,n2);
%2nd timestep
for t=2:n %through all time steps
    [h1(t) h2(t) q1(t) qE(t) c1(t) c2(t)]=simpel_1step(K1,KE,in1(t), ...
        in2(t),h1(t-1),h2(t-1),c_in1(t),c_in2(t),c1(t-1), ...
        c2(t-1),m_dif,n1,n2);
end
%-------------------------------------------------------------------------



%%%%%%%%%%%%%%%%%%%%%%%%%%%%%%%%%%%%%%%%%%%%%%%%%%%%%%%%%%%%%%%%%%%%%%%%%%%%
```

```
% solution for water levels in modified groundwater reservoir with
% consideration of switch of exchange flow direction
% (by Andreas Hartmann)
%%%%%%%%%%%%%%%%%%%%%%%%%%%%%%%%%%%%%%%%%%%%%%%%%%%%%%%%%%%%%%%%%%%%%%%%%%%%

function [h1 h2 q1 qE c1 c2]=simpel_1step(K1,KE,in1,in2, ...
    h10,h20,c_in1,c_in2,c10,c20,m_dif,n1,n2)
%%%%%%%%%%%%%%%%%%%%%%%%%%%%%%%%%%%%%%%%%%%%%%%%%%%%%%%%%%%%%%%%%%%%%%%%%%%%
%water levels in parallel reservoirs
%constants
h110=-h10/K1-h10/KE/n1+h20/KE/n2+in1;
h220=-h20/KE/n2+h10/KE/n1+in2;
A1=-1/2*(1/K1+1/KE*(1/n1+1/n2))+sqrt((1/K1+1/KE*(1/n1+1/n2))^2/4 ...
    -1/n2/K1/KE);
A2=-1/2*(1/K1+1/KE*(1/n1+1/n2))-sqrt((1/K1+1/KE*(1/n1+1/n2))^2/4 ...
    -1/n2/K1/KE);
C1=K1*(in1+in2);
C2=C1*n2/n1+n2*KE*in2;
B1=(h110-A2*h10+A2*C1)/(A1-A2);
B2=h10-B1-C1;
B3=(h220-A2*h20+A2*C2)/(A1-A2);
B4=h20-B3-C2;

%equations
h1=B1*exp(A1)+B2*exp(A2)+C1;
h2=B3*exp(A1)+B4*exp(A2)+C2;
q1=h1/K1;
qE=(h2/n2-h1/n1)/KE;
qE0=(h20/n2-h10/n1)/KE;
%%%%%%%%%%%%%%%%%%%%%%%%%%%%%%%%%%%%%%%%%%%%%%%%%%%%%%%%%%%%%%%%%%%%%%%%%%%%

%%%%%%%%%%%%%%%%%%%%%%%%%%%%%%%%%%%%%%%%%%%%%%%%%%%%%%%%%%%%%%%%%%%%%%%%%%%%
%mixing
min1=in1*c_in1;
% recognize change of exchange flow direction for separating time step into
% two separate steps with each having just one direction of exchange flow
if ((h20/n2-h10/n1)/KE>0 && qE<=0) || ((h20/n2-h10/n1)/KE<=0 && qE>0)
    %find time of equal water levels in the reservoirs
    f=@(t) ((B3*exp(A1*t)+B4*exp(A2*t)+C2)/n2- ...
        (B1*exp(A1*t)+B2*exp(A2*t)+C1)/n1);
    z=fzero(f,.5);
    %intermediate water level
    h1z=(B1*exp(A1*z)+B2*exp(A2*z)+C1);
    h2z=(B3*exp(A1*z)+B4*exp(A2*z)+C2);
    %exchange flow at time of equal levels qEz is zero
    qEz=0;
    %calculate input for first part of separated time step
    in1z1=in1*z;
    in2z1=in2*z;
    m_in1_z1=c_in1*in1z1;
    m_in2_z1=c_in2*in2z1;
    m_dif_z1=m_dif*z;
    %apply mixing equations for first part of separated time step
    [c1z c2z] = simple_1step_conc(in1z1,qE0,qEz,h10,h1z,h20,h2z, ...
        m_in1_z1,c10,c20,z,m_dif);
    %calculate input for second part of separated time step
    in1z2=in1*(1-z);
    in2z2=in2*(1-z);
    m_in1_z2=c_in1*in1z2;
    m_in2_z2=c_in2*in2z2;
    m_dif_z2=m_dif*(1-z);
    %apply mixing equations for second part of separated time step
```

```
    [c1 c2] = simple_1step_conc(in1z2,qEz,qE,h1z,h1,h2z,h2, ...
        m_in1_z2,c1z,c2z,(1-z),m_dif);
else
    [c1 c2] = simple_1step_conc(in1,qE0,qE,h10,h1,h20,h2,min1, ...
        c10,c20,1,m_dif);
end
%--------------------------------------------------------------------------


%%%%%%%%%%%%%%%%%%%%%%%%%%%%%%%%%%%%%%%%%%%%%%%%%%%%%%%%%%%%%%%%%%%%%%%%%%%
% solution for concentration of outflows for both directions of
% exchange flow (by Andreas Hartmann)
%%%%%%%%%%%%%%%%%%%%%%%%%%%%%%%%%%%%%%%%%%%%%%%%%%%%%%%%%%%%%%%%%%%%%%%%%%%

function [c1 c2]= ...
    simple_1step_conc(in1,qE0,qE,h10,h1,h20,h2,min1,c10,c20,dt,m_dif)

if qE<=0 && qE0<=0
    c1=((min1/h10+min1/h1*exp((in1/h10+in1/h1)*.5*dt))*.5*dt+c10)* ...
        exp(-(in1/h10+in1/h1)*.5*dt);
    c2=(-(qE0/h20*c10-m_dif/h20+(qE/h2*c1-m_dif/h2)* ...
        exp(-(qE0/h20+qE/h2)*.5*dt))*.5*dt+c20)* ...
        exp((qE0/h20+qE/h2)*.5*dt);
elseif qE>=0 && qE0>=0
    c2=(m_dif/h20+m_dif/h2)*.5*dt+c20;
    c1=(((qE0/h10*c20+min1/h10)+(qE/h1*c2+min1/h1)* ...
        exp((qE0/h10+in1/h1+qE/h1+in1/h1)*.5*dt))*.5*dt+c10)* ...
        exp(-(qE0/h10+in1/h10+qE/h1+in1/h1)*.5*dt);
end
%--------------------------------------------------------------------------
```

A.6 Source codes of the model routines of HYMKE_DUAL

A.6.1 Source code of the snow melt routine

```
%%%%%%%%%%%%%%%%%%%%%%%%%%%%%%%%%%%%%%%%%%%%%%%%%%%%%%%%%%%%%%%%%%%%%%%%%%%
%snow melt routine (by Andreas Hartmann)
%%%%%%%%%%%%%%%%%%%%%%%%%%%%%%%%%%%%%%%%%%%%%%%%%%%%%%%%%%%%%%%%%%%%%%%%%%%

h = waitbar(0, 'Calculating new snowmelt series'); %initiates progress bar
for i=2:length(DateRain0) %first loop for all time steps
    for j=1:length(HermonTopo) %second loop for all altitude strips
        if TopoTemp(i,j)<=Tm %if air temperature of altitude strip is
                             %bigger than the melting temperature
            refr=RF*ddf*(Tm-TopoTemp(i,j)); %refreezing of retained liquid
                                            %water
            if refr<RLW(i-1,j) && RLW(i-1,j)>0%standard case: enough liquid
                                              %water is available
                RLW(i,j)=RLW(i-1,j)-refr;
                SWE(i,j)=SWE(i-1,j)+StripRainfall(i,j)/HermonTopo(j,1) ...
                    /AreaFactor+refr;
                StripSnowMelt(i,j)=0;
            elseif refr>=RLW(i-1,j) && RLW(i-1,j)>0%1st special case: not
                                                   %enough liquid water
                RLW(i,j)=0;
                SWE(i,j)=SWE(i-1,j)+StripRainfall(i,j)/HermonTopo(j,1) ...
                    /AreaFactor+RLW(i-1,j);
                StripSnowMelt(i,j)=0;
            elseif RLW(i-1,j)==0 %2nd special case: no liquid water
                RLW(i,1)=0;
```

```
                SWE(i,j)=SWE(i-1,j)+StripRainfall(i,j)/HermonTopo(j,1) ...
                    /AreaFactor;
                StripSnowMelt(i,j)=0;
            end
        elseif TopoTemp(i,j)>Tm %if air temperature of altitude strip is
                                %smaller than the melting temperature
            melt=ddf*(TopoTemp(i,j)-Tm);%snow melt
            if melt<SWE(i-1,j) && SWE(i-1,j)>0
                SWE(i,j)=SWE(i-1,j)-melt;
                RLW(i,j)=RLW(i-1,j)+StripRainfall(i,j)/HermonTopo(j,1) ...
                    /AreaFactor+melt;
                LWRC=HC*SWE(i,j); %amount of water which can be retained
                                  %in the snowpack
                if RLW(i,j)>LWRC
                    StripSnowMelt(i,j)=RLW(i,j)-LWRC; %excess water is
                                                      %released to the soil
                    RLW(i,j)=LWRC;
                end
            elseif melt>=SWE(i-1,j) && SWE(i-1,j)>0%1st special case: snow
                                                   %melt is bigger than
                                                   %snow water equivalent
                SWE(i,j)=0;
                RLW(i,j)=0;
                StripSnowMelt(i,j)=RLW(i-1,j)+StripRainfall(i,j) ...
                    /HermonTopo(j,1)/AreaFactor+SWE(i-1,j);
            elseif SWE(i-1,j)==0%2nd special case: no snow water equivalent
                                %available
                SWE(i,j)=0;
                RLW(i,j)=0;
                StripSnowMelt(i,j)=StripRainfall(i,j)/HermonTopo(j,1) ...
                    /AreaFactor;
            end
        end
        if SWE(i,j)>0
            SnowLog(i,j)=1;% snow cover? Yes.
        else
            SnowLog(i,j)=0;% snow cover? No.
        end
        StripPrecip(i,j)=StripRainfall(i,j)/HermonTopo(j,1)/AreaFactor;
    end
    %areal snowmelt for plotting
    HermonSnowMelt(i)=StripSnowMelt(i,:)*HermonTopo(:,1)*AreaFactor/783;
    h = waitbar(i/length(DateRain0),h);
end
close(h);
%-------------------------------------------------------------------------
```

A.6.2 Source code of the soil/epikarst routine

```
%%%%%%%%%%%%%%%%%%%%%%%%%%%%%%%%%%%%%%%%%%%%%%%%%%%%%%%%%%%%%%%%%%%%%%%%%%%%
% soil-epikarst routine (by Andreas Hartmann)
%%%%%%%%%%%%%%%%%%%%%%%%%%%%%%%%%%%%%%%%%%%%%%%%%%%%%%%%%%%%%%%%%%%%%%%%%%%%
for i=2:dim(1) %first loop for all time steps
    for j=1:dim(2) %second loop for all altitude strips
        %upper soil layer
        [ThetaUpEPT(i,j) qUpExcEPT(i,j) qOutUpEPT(i,j) qFastEPT(i,j) ...
            Evap(i,j)]= UnsatFlow(ThetaUpEPT(i-1,j),StripMeltData(i,j), ...
            TopoPotEvap(i,j),SnowLog(i,j),ThetaRestUp,ThetaSatUp, ...
            KSatUp,lUp,RD,f,EptThres);
        %upper soil storage below evaporation layer
        [ThetaUp(i,j) qUpExc(i,j) qOutUp(i,j) qFast(i,j) EvapUp(i,j)]= ...
```

```
            UnsatFlow(ThetaUp(i-1,j),qUpExcEPT(i,j)+qOutUpEPT(i,j),0, ...
            0,ThetaRestUp,ThetaSatUp,KSatUp,lUp,hUp-RD,1,1);
        %lower soil storage
        [ThetaLow(i,j) qLowExc(i,j) qOutLow(i,j) qFastLow(i,j) ...
            EvapLow(i,j)]=UnsatFlow(ThetaLow(i-1,j), ...
            qUpExc(i,j)+qOutUp(i,j),0,0,ThetaRestLow,ThetaSatLow, ...
            KSatLow,lLow,hLow,1,1);
        %calculate flows between the storages and to the conduits and
        %fissures
        qUpEPTUpPref(i,j)=qUpExcEPT(i,j);
        qUpEPTUpSlow(i,j)=qOutUpEPT(i,j);
        qFisSlow(i,j)=qOutLow(i,j);
        TotOutUp=qUpExc(i,j)+qOutUp(i,j);
        if TotOutUp~=0
            qCondPref(i,j)=qUpExc(i,j)/TotOutUp*qLowExc(i,j);
            qCondSlow(i,j)=qOutUp(i,j)/TotOutUp*qLowExc(i,j);
            qUpLowPref(i,j)=qUpExc(i,j)/TotOutUp* ...
                (1-qLowExc(i,j)/TotOutUp)*TotOutUp;
            qUpLowSlow(i,j)=qOutUp(i,j)/TotOutUp* ...
                (1-qLowExc(i,j)/TotOutUp)*TotOutUp;
        else
            qCondPref(i,j)=0;
            qCondSlow(i,j)=0;
            qUpLowPref(i,j)=0;
            qUpLowSlow(i,j)=0;
        end
    end
    h = waitbar(i/dim(1)); %information for progress bar
    %calculate areal values for over all altitude strips
    ThetaUpEPTHermon(i)=ThetaUpEPT(i,:)*HermonTopo(:,1)/ ...
        HermonTopo(length(HermonTopo),3);
    ThetaUpHermon(i)=ThetaUp(i,:)*HermonTopo(:,1)/ ...
        HermonTopo(length(HermonTopo),3);
    ThetaLowHermon(i)=ThetaLow(i,:)*HermonTopo(:,1)/ ...
        HermonTopo(length(HermonTopo),3);
    PotEvapHermon(i)=TopoPotEvap(i,:)*HermonTopo(:,1)/ ...
        HermonTopo(length(HermonTopo),3);
    EvapHermon(i)=Evap(i,:)*HermonTopo(:,1)/ ...
        HermonTopo(length(HermonTopo),3);
    qCondSlowHermon(i)=qCondSlow(i,:)*HermonTopo(:,1)/ ...
        HermonTopo(length(HermonTopo),3);
    qCondPrefHermon(i)=qCondPref(i,:)*HermonTopo(:,1)/ ...
        HermonTopo(length(HermonTopo),3);
    qFisSlowHermon(i)=qFisSlow(i,:)*HermonTopo(:,1)/ ...
        HermonTopo(length(HermonTopo),3);
end
close(h);



%%%%%%%%%%%%%%%%%%%%%%%%%%%%%%%%%%%%%%%%%%%%%%%%%%%%%%%%%%%%%%%%%%%%%%%%%%%%%%%
%Function unsaturated flow (by Andreas Hartmann)
%%%%%%%%%%%%%%%%%%%%%%%%%%%%%%%%%%%%%%%%%%%%%%%%%%%%%%%%%%%%%%%%%%%%%%%%%%%%%%%

function [Theta qExc qOut qFast Evap]=UnsatFlow(Theta0,In0,Evap0, ...
    SnowLog,ThetaRest,ThetaSat,KSat,m,h,f,EptThres)

%calculate relative saturation and unsaturated conductivity
if Theta0>=ThetaRest
    relSat=(Theta0-ThetaRest)/ ...
        (ThetaSat-ThetaRest);
    K=KSat*relSat^.5*(1-(1-relSat^(1/m))^m)^2; %Mualem Van Genuchten
```

```
else
    relSat=0;
    K=0;
end
qOut=K; %downward flow

%calculate actual evaporation
if relSat>=EptThres && SnowLog~=1
    Evap=Evap0;
elseif relSat<EptThres && SnowLog~=1 && relSat>0
    Evap=relSat/EptThres*Evap0;
elseif SnowLog==1 || relSat==0
    Evap=0;
end

%calculate potential water content
PotTheta=Theta0+(In0-Evap-qOut)/h/1000;

%calculate new water content of upper soil storage and saturation
%excess
if PotTheta<=ThetaSat && PotTheta>ThetaRest %standard case
    Theta=PotTheta;
    ExcTheta=0;
elseif PotTheta>ThetaSat && PotTheta>ThetaRest %1st special case: potential
                                               %water content bigger than
                                               %saturation water content
    Theta=ThetaSat;
    ExcTheta=PotTheta-ThetaSat;
elseif PotTheta<=ThetaRest %2nd special case: potential water content
                           %smaller than minimum water content
    Theta=ThetaRest;
    ExcTheta=0;
    qOut=(Theta0-ThetaRest)*h*1000+(In0-Evap);
    if qOut<0
        Evap=Evap+qOut;
        qOut=0;
    end
end
qExc=f*h*1000*ExcTheta; %preferential flow
qFast=(1-f)*h*1000*ExcTheta; %overland flow
%-------------------------------------------------------------------------
```

A.6.3 Source code of the groundwater routine

```
%%%%%%%%%%%%%%%%%%%%%%%%%%%%%%%%%%%%%%%%%%%%%%%%%%%%%%%%%%%%%%%%%%%%%%%%%%%%
% function ThreeResGWFun (by Andreas Hartmann)
%%%%%%%%%%%%%%%%%%%%%%%%%%%%%%%%%%%%%%%%%%%%%%%%%%%%%%%%%%%%%%%%%%%%%%%%%%%%

function [h1 h2 h3 q1 q2 qE1 qE2]= ...
    ThreeResGWFun(in1,in2,in3,h10,h20,h30,K1,K2,KE,n1,n2,H2)

%constants
%-------------------------------------------------------------------------
    %coefficients in homogeneous approach (stay constant fow whole
    %simualtion)
    A=1/K1+1/K2+2/n1/KE+2/n2/KE;
    B=1/K1/K2+1/n1/K1/KE+1/n1/K2/KE+2/n2/K1/KE+2/n2/K2/KE+2/n1/n2/KE^2+ ...
        1/n1^2/KE^2;
    C=2/n2/K1/K2/KE+1/n1/n2/K1/KE^2+1/n1/n2/K2/KE^2;
```

```
    %solutions of characteristic polynomial
    lambda=roots([-1 -A -B -C])
%-------------------------------------------------------------------------

%1st step
%-------------------------------------------------------------------------
h = waitbar(0, 'calculating groundwater'); %initiates progress bar
% solve groundwater equations for this time step
[h1(1) h2(1) h3(1) q1(1) q2(1) qE1(1) qE2(1)]= ...
    ThreeResGW1Step(in1(1),in2(1),in3(1),h10,h20,h30,K1,K2,KE,n1,n2,H2, ...
    A,B,C,lambda);
h = waitbar(1/length(in1),h);
%-------------------------------------------------------------------------

% 2nd step until end
%-------------------------------------------------------------------------
for t=2:length(in1) % loop through all time steps
    % solve groundwater equations for this time step
    [h1(t) h2(t) h3(t) q1(t) q2(t) qE1(t) qE2(t)]= ...
        ThreeResGW1Step(in1(t),in2(t),in3(t), ...
        h1(t-1),h2(t-1),h3(t-1),K1,K2,KE,n1,n2,H2,A,B,C,lambda);
    h = waitbar(t/length(in1),h);
end
close(h);
%-------------------------------------------------------------------------



%%%%%%%%%%%%%%%%%%%%%%%%%%%%%%%%%%%%%%%%%%%%%%%%%%%%%%%%%%%%%%%%%%%%%%%%%%%
% function ThreeResGWFun (by Andreas Hartmann)
%%%%%%%%%%%%%%%%%%%%%%%%%%%%%%%%%%%%%%%%%%%%%%%%%%%%%%%%%%%%%%%%%%%%%%%%%%%

function [h1 h2 h3 q1 q2 qE1 qE2]= ...
    ThreeResGW1Step(qin1,qin2,qin3,h10,h20,h30,K1,K2,KE,n1,n2,H2, ...
    A,B,C,lambda)

%initial conditions
%-------------------------------------------------------------------------
    h110=-(1/K1+1/n1/KE)*h10+1/n2/KE*h30+qin1; %first order
    h220=-(1/K2+1/n1/KE)*h20+1/n2/KE*h30+qin2-H2/KE;
    h330=1/n1/KE*h10+1/n1/KE*h20-2/n2/KE*h30+qin3+H2/KE;
    h1110=-(1/K1+1/n1/KE)*h110+1/n2/KE*h330; %second order
    h2220=-(1/K2+1/n1/KE)*h220+1/n2/KE*h330;
    h3330=1/n1/KE*h110+1/n1/KE*h220-2/n2/KE*h330;
%-------------------------------------------------------------------------

%constants
%-------------------------------------------------------------------------

    %right side of inhomogeneos approach
    qin=[qin1;qin2-H2/KE;qin3+H2/KE];
    Z=[1/K1+1/n1/KE 0 -1/n2/KE
        0 1/K2+1/n1/KE -1/n2/KE
        -1/n1/KE -1/n1/KE 2/n2/KE];
    for i=1:3
        Zi=Z;
        Zi(:,i)=qin;
        gamma(i)=det(Zi)/C;
    end
```

```
    %case distinction for real and complex lambdas
    H0(:,1)=[h10-gamma(1);h110;h1110];
    H0(:,2)=[h20-gamma(2);h220;h2220];
    H0(:,3)=[h30-gamma(3);h330;h3330];
    if isreal(lambda)~=0
        M=[1 1 1
            lambda(1) lambda(2) lambda(3)
            lambda(1)^2 lambda(2)^2 lambda(3)^2];
        for i=1:3
            for j=1:3
                Mij=M;
                Mij(:,j)=H0(:,i);
                a(i,j)=det(Mij)/det(M);
            end
        end
    elseif isreal(lambda)==0
        for k=1:3
            if isreal(lambda(k))==0
                co=k;
            elseif isreal(lambda(k))~=0
                re=k;
            end
        end
        M=[1 1 0
            lambda(re) real(lambda(co)) abs(imag(lambda(co)))
            lambda(re)^2 real(lambda(co))^2+abs(imag(lambda(co)))^2 2* ...
            real(lambda(co))*abs(imag(lambda(co)))];
        for i=1:3
            for j=1:3
                Mij=M;
                Mij(:,j)=H0(:,i);
                a(i,j)=det(Mij)/det(M);
            end
        end

    end
%-------------------------------------------------------------------------

%solutions for the three reservoirs
%-------------------------------------------------------------------------
for t=1:length(qin1)
    if isreal(lambda)~=0
        h1(t)=a(1,1)*exp(lambda(1)*t)+a(1,2)*exp(lambda(2)*t)+ ...
            a(1,3)*exp(lambda(3)*t)+gamma(1);
        h2(t)=a(2,1)*exp(lambda(1)*t)+a(2,2)*exp(lambda(2)*t)+ ...
            a(2,3)*exp(lambda(3)*t)+gamma(2);
        h3(t)=a(3,1)*exp(lambda(1)*t)+a(3,2)*exp(lambda(2)*t)+ ...
            a(3,3)*exp(lambda(3)*t)+gamma(3);
    elseif isreal(lambda)==0
        h1(t)=a(1,1)*exp(lambda(re)*t)+ ...
            a(1,2)*exp(real(lambda(co))*t)*cos(abs(imag(lambda(co)))*t) ...
            +a(1,3)*exp(real(lambda(co))*t) ...
            *sin(abs(imag(lambda(co)))*t)+gamma(1);
        h2(t)=a(2,1)*exp(lambda(re)*t)+ ...
            a(2,2)*exp(real(lambda(co))*t)*cos(abs(imag(lambda(co)))*t) ...
            +a(2,3)*exp(real(lambda(co))*t) ...
            *sin(abs(imag(lambda(co)))*t)+gamma(2);
        h3(t)=a(3,1)*exp(lambda(re)*t)+ ...
            a(3,2)*exp(real(lambda(co))*t)*cos(abs(imag(lambda(co)))*t) ...
            +a(3,3)*exp(real(lambda(co))*t) ...
            *sin(abs(imag(lambda(co)))*t)+gamma(3);
    end
```

```
    if h2(t)/n1<0
        warning(['BRUTAL ERROR 734C: h2(t=' num2str(t) ...
            ') below 0 m(in respect to the spring outlet level)']);
        break
    end
    q1(t)=h1(t)/K1;
    q2(t)=h2(t)/K2;
    hE1(t)=(h3(t)/n2-h1(t)/n1);
    hE2(t)=(h3(t)/n2-h2(t)/n1-H2);
    qE1(t)=hE1(t)/KE;
    qE2(t)=hE2(t)/KE;
end
%-------------------------------------------------------------------------
```

A.6.4 Source code of the soil-epikarst mixing routine

```
%%%%%%%%%%%%%%%%%%%%%%%%%%%%%%%%%%%%%%%%%%%%%%%%%%%%%%%%%%%%%%%%%%%%%%%%
% mixing calculations in soil-epikarst routine (by Andreas Hartmann)
%%%%%%%%%%%%%%%%%%%%%%%%%%%%%%%%%%%%%%%%%%%%%%%%%%%%%%%%%%%%%%%%%%%%%%%%


function [cinCHermon cinFHermon]=MixingSoilEpiEPT(DateRain,qinF, ...
    qUpEPTUpSlow,qUpEPTUpPref,qUpLowSl,qUpLowPref,qinCSl, ...
    qinCPref,ThetaUpEPT,ThetaUp,ThetaLow,Evap,qFast,StripMeltData, ...
    HermonTopo,ThetaUpEPT0,ThetaUp0,ThetaLow0,cMelt,RD,hUp,hLow, ...
    cUpEPT0,cUp0,cLow0,mUpRel)

%function that calculates the mixing in the soil routines which consists of
%mixing in the soil layer, the upper epikarst layer and the lower epikarst
%and the mixing with preferential flow below the soil and upper epikarst
%layer
%-------------------------------------------------------------------------
dim=size(StripMeltData);

%mixing in the soil layer which is exposed to evaporation (diffuse matrix
%component)
%-------------------------------------------------------------------------
qIn=StripMeltData-qUpEPTUpPref-qFast; %inflows to the layer
qOut=qUpEPTUpSlow; %outflows of the layer
cIn=cMelt*ones(size(qIn)); %input concentration

%applying mixing equations
[mUpEPTSl cOutUpEPTSl]=StripMixing(cIn, qIn, qOut, Evap, ...
    ThetaUpEPT*RD*1000,mUpRel,ones(1,length(HermonTopo))*cUpEPT0, ...
    ones(1,length(HermonTopo))*ThetaUpEPT0*RD*1000);

%mass balance to test for numerical errors
input=qIn.*cIn+mUpRel*ones(1,length(HermonTopo));
output=qOut.*cOutUpEPTSl;
deltaS=diff([ones(1,length(HermonTopo))*ThetaUpEPT0*RD*1000.* ...
    ones(1,length(HermonTopo))*cUpEPT0;mUpEPTSl]);
balance=sum(input-output-deltaS);
total_error_upper_soil_slow_component_mixing_EPT_part= ...
    sum(balance./sum(input))
%-------------------------------------------------------------------------

%mixing of soil layer matrix flow and preferential flow
%-------------------------------------------------------------------------
n = waitbar(0, 'Running soil mixing'); %progress bar
```

```
for i=1:dim(1) %loop for all time steps
    for j=1:dim(2) %loop for all altitude strips
        if (qOut(i,j)+qUpEPTUpPref(i,j))~=0 %perform mixing of matrix and
                                            %preferential flwo
            cOutUpEPTTot(i,j)=(cOutUpEPTSl(i,j)*(qUpEPTUpSlow(i,j))+ ...
                cMelt*(qUpEPTUpPref(i,j)))./ ...
                (qOut(i,j)+qUpEPTUpPref(i,j));
        else
            cOutUpEPTTot(i,j)=0;
        end
    end
    n = waitbar(i/dim(1));
end
close(n);

cinUp=cOutUpEPTTot; %concentration of outflow to the conduits equals the
                    %total output concentration of the upper soil storage
%--------------------------------------------------------------------------


%mixing in the upper epikarst layer (slow matrix component)
%--------------------------------------------------------------------------
qIn=qUpEPTUpPref+qUpEPTUpSlow-qUpLowPref-qinCPref; %inflows
qOut=qUpLowSl+qinCSl; %outflows
cIn=cinUp; %input concentration

%perform mixing calculations for this layer
[mUpSl cOutUpSl]=StripMixing(cIn, qIn, qOut, zeros(dim), ...
    ThetaUp*(hUp-RD)*1000,zeros(length(cIn),1), ...
    ones(1,length(HermonTopo))*cUp0,ones(1,length(HermonTopo)) ...
    *ThetaUp0*(hUp-RD)*1000);

%mass balance to check for numerical errors
input=qIn.*cIn;
output=qOut.*cOutUpSl;
deltaS=diff([ones(1,length(HermonTopo))*ThetaUp0*(hUp-RD)*1000.* ...
    ones(1,length(HermonTopo))*cUp0;mUpSl]);
balance=sum(input-output-deltaS);
total_error_upper_soil_slow_component_mixing=sum(balance./sum(input))
%--------------------------------------------------------------------------

%mixing of upper soil storage slow flow and prferential flow
%--------------------------------------------------------------------------
n = waitbar(0, 'Running soil mixing');
for i=1:dim(1) % loop for all time steps
    for j=1:dim(2) % loop for all altitude strips
        if (qOut(i,j)+qUpLowPref(i,j)+qinCPref(i,j))~=0 %mixing of
                                                        %preferential and
                                                        %matrix flow
            cOutUpTot(i,j)=(cOutUpSl(i,j)*(qUpLowSl(i,j)+qinCSl(i,j))+ ...
                cinUp(i)*(qUpLowPref(i,j)+qinCPref(i,j)))./ ...
                (qOut(i,j)+qUpLowPref(i,j)+qinCPref(i,j));
        else
            cOutUpTot(i,j)=0;
        end
    end
    n = waitbar(i/dim(1));
end
close(n);

cinC=cOutUpTot; %concentration of outflow to the conduits equals the total
```

```
                %output concentration of the upper soil storage
%-------------------------------------------------------------------------

%
%-------------------------------------------------------------------------
qIn=qUpLowPref+qUpLowSl; %inflow
qOut=qinF; %outflow
cIn=cOutUpTot; %input concentration equals the mixing concentration of
               %preferntial and matrix flow leaving the upper epikarst
               %layer

%apply mixing equations
[mLowSl cOutLowSl]=StripMixing(cIn, qIn, qOut, zeros(dim), ...
    ThetaLow*hLow*1000,zeros(length(cIn),1), ...
    ones(1,length(HermonTopo))*cLow0, ones(1,length(HermonTopo))* ...
    ThetaLow0*hLow*1000);

%mass balance to check for numerical errors
input=qIn.*cIn;
output=qOut.*cOutLowSl;
deltaS=diff([ones(1,length(HermonTopo))*ThetaLow0*hLow*1000.* ...
    ones(1,length(HermonTopo))*cLow0;mLowSl]);
balance=sum(input-output-deltaS);
total_error_lower_soil_slow_component_mixing=sum(balance./sum(input))

cinF=cOutLowSl; %concentration of outflow to the fissures equals the output
                %concentration of the lower soil storage
%-------------------------------------------------------------------------

%aggregating data for whole Hermon Range
%-------------------------------------------------------------------------
n = waitbar(0, 'Aggregating data');
for i=1:dim(1)
    cOutUpEPTSlHermon(i)=(cOutUpEPTSl(i,:).*ThetaUpEPT(i,:) ...
        *HermonTopo(:,1)/HermonTopo(length(HermonTopo),3))/ ...
        (ThetaUpEPT(i,:)*HermonTopo(:,1)/ ...
        HermonTopo(length(HermonTopo),3));
    cOutUpSlHermon(i)=(cOutUpSl(i,:).*ThetaUp(i,:)*HermonTopo(:,1)/ ...
        HermonTopo(length(HermonTopo),3))/ ...
        (ThetaUp(i,:)*HermonTopo(:,1)/ ...
        HermonTopo(length(HermonTopo),3));
    cOutLowSlHermon(i)=(cOutLowSl(i,:).*ThetaLow(i,:)*HermonTopo(:,1)/ ...
        HermonTopo(length(HermonTopo),3))/ ...
        (ThetaLow(i,:)*HermonTopo(:,1)/ ...
        HermonTopo(length(HermonTopo),3));
    mUpEPTSlHermon(i)=mUpEPTSl(i,:)*HermonTopo(:,1)/ ...
        HermonTopo(length(HermonTopo),3);
    mUpSlHermon(i)=mUpSl(i,:)*HermonTopo(:,1)/ ...
        HermonTopo(length(HermonTopo),3);
    mLowSlHermon(i)=mLowSl(i,:)*HermonTopo(:,1)/ ...
        HermonTopo(length(HermonTopo),3);
    if sum(qinCSl(i,:)+qinCPref(i,:))~=0
    cinCHermon(i)=(((qinCSl(i,:)+qinCPref(i,:)).*cinC(i,:)) ...
        *HermonTopo(:,1)/HermonTopo(length(HermonTopo),3))/ ...
        ((qinCSl(i,:)+qinCPref(i,:))* ...
        HermonTopo(:,1)/HermonTopo(length(HermonTopo),3));
    else
        cinCHermon(i)=0;
    end
    if qinF(i,:)~=0
    cinFHermon(i)=((qinF(i,:).*cinF(i,:))*HermonTopo(:,1)/ ...
        HermonTopo(length(HermonTopo),3))/(qinF(i,:)* ...
```

```
        HermonTopo(:,1)/HermonTopo(length(HermonTopo),3));
    else
        cinFHermon(i)=0;
    end
    n = waitbar(i/dim(1));
end
close(n);
%------------------------------------------------------------------------



%%%%%%%%%%%%%%%%%%%%%%%%%%%%%%%%%%%%%%%%%%%%%%%%%%%%%%%%%%%%%%%%%%%%%%%%%%%
% mixing equations applied for every layer of the soil-epikarst routine to
% calculate mixing of matrix flow (by Andreas Hartmann)
%%%%%%%%%%%%%%%%%%%%%%%%%%%%%%%%%%%%%%%%%%%%%%%%%%%%%%%%%%%%%%%%%%%%%%%%%%%

for i=2:dim(1) % loop for time steps
    for j=1:dim(2) % loop for altitude strips
        if (h(i-1,j)+qIn(i,j)-Evap(i,j))>=0.01 %check if denominator of
                                               %fraction is not too small
            cOut(i,j)=(m(i-1,j)+qIn(i,j)*cIn(i,j)+mIn(i))/ ...
                (h(i-1,j)+qIn(i,j)-Evap(i,j)); %implicite calculation of
                                               %new concentration
        else
            cOut(i,j)=0;
        end
        %new mass in layer
        m(i,j)=m(i-1,j)+qIn(i,j)*cIn(i,j)-qOut(i,j)*cOut(i,j)+mIn(i);
    end
    n = waitbar(i/dim(1));
end
close(n);
%------------------------------------------------------------------------
```

A.6.5 Source code of the groundwater mixing routine

```
%%%%%%%%%%%%%%%%%%%%%%%%%%%%%%%%%%%%%%%%%%%%%%%%%%%%%%%%%%%%%%%%%%%%%%%%%%%
% groundwater mixing (by Andreas Hartmann)
%%%%%%%%%%%%%%%%%%%%%%%%%%%%%%%%%%%%%%%%%%%%%%%%%%%%%%%%%%%%%%%%%%%%%%%%%%%

for t=2:dim %loop through all time steps
    b=[in1(t)/h1(t)*cin1(t)+m1(t-1)/h1(t)
        in2(t)/h2(t)*cin2(t)+m2(t-1)/h2(t)
        in3(t)/h3(t)*cin3(t)+m3(t-1)/h3(t)]; %right part of equation system
    %coefficient matrices of equation system under different conditions
    if h3(t)/n2>h1(t)/n1 && h3(t)/n2>h2(t)/n1+H2
        A=[1+q1(t)/h1(t) 0 -qE1(t)/h1(t)
            0 1+q2(t)/h2(t) -qE2(t)/h2(t)
            0 0 1+qE1(t)/h3(t)+qE2(t)/h3(t)];
        a=1;
    elseif h2(t)/n1+H2>=h3(t)/n2 && h3(t)/n2>=h1(t)/n1
        A=[1+q1(t)/h1(t) 0 -qE1(t)/h1(t)
            0 1-qE2(t)/h2(t)+q2(t)/h2(t) 0
            0 +qE2(t)/h3(t) 1+qE1(t)/h3(t)];
        a=2;
    elseif h1(t)/n1>=h3(t)/n2 && h3(t)/n2>=h2(t)/n1+H2
        A=[1-qE1(t)/h1(t)+q1(t)/h1(t) 0 0
            0 1+q2(t)/h2(t) -qE2(t)/h2(t)
            qE1(t)/h3(t) 0 1+qE2(t)/h3(t)];
        a=3;
```

```
elseif h1(t)/n1>h3(t)/n2 && h2(t)/n1+H2>h3(t)/n2
    A=[1-qE1(t)/h1(t)+q1(t)/h1(t) 0 0
        0 1-qE2(t)/h2(t)+q2(t)/h2(t) 0
        qE1(t)/h3(t) qE2(t)/h3(t) 1];
    a=4;
end
%solve system
sol=A\b;
cOut1(t)=sol(1);
cOut2(t)=sol(2);
cOut3(t)=sol(3);
%calculate solute masses
m1(t)=cOut1(t)*h1(t);
m2(t)=cOut2(t)*h2(t);
m3(t)=cOut3(t)*h3(t);

%adding of geogene contributions
if a==1
    mGeo1(t)=(mGeo1(t-1)+mAdd1)/(1+qE1(t)/h3(t));
    cGeo1(t)=(mGeo1(t)/h3(t)*qE1(t)+cOut1(t)*h1(t))/h1(t);
    mGeo2(t)=(mGeo2(t-1)+mAdd2)/(1+qE2(t)/(h3(t)-H2*n2));
    cGeo2(t)=(mGeo2(t)/(h3(t)-H2*n2)*qE2(t)+cOut2(t)*h2(t))/h2(t);
elseif a==2
    mGeo1(t)=(mGeo1(t-1)+mAdd1)/(1+qE1(t)/h3(t));
    cGeo1(t)=(mGeo1(t)/h3(t)*qE1(t)+cOut1(t)*h1(t))/h1(t);
    mGeo2(t)=mGeo2(t-1)+mAdd2;
    cGeo2(t)=cOut2(t);
elseif a==3
    mGeo1(t)=mGeo1(t-1)+mAdd1;
    cGeo1(t)=cOut1(t);
    mGeo2(t)=(mGeo2(t-1)+mAdd2)/(1+qE2(t)/(h3(t)-H2*n2));
    cGeo2(t)=(mGeo2(t)/(h3(t)-H2*n2)*qE2(t)+cOut2(t)*h2(t))/h2(t);
elseif a==4
    mGeo1(t)=mGeo1(t-1)+mAdd1;
    cGeo1(t)=cOut1(t);
    mGeo2(t)=mGeo2(t-1)+mAdd2;
    cGeo2(t)=cOut2(t);
end

%mass balance to check for numerical errors
%define exchange concentrations
if a==1
    cE1(t)=cOut3(t);
    cE2(t)=cOut3(t);
elseif a==2
    cE1(t)=cOut3(t);
    cE2(t)=cOut2(t);
elseif a==3
    cE1(t)=cOut1(t);
    cE2(t)=cOut3(t);
elseif a==4
    cE1(t)=cOut1(t);
    cE2(t)=cOut2(t);
end
%reservoir 1
input1(t)=in1(t)*cin1(t)+qE1(t)*cE1(t);
output1(t)=q1(t).*cOut1(t);
deltaS1(t)=diff([m1(t-1),m1(t)]);
%reservoir 2
input2(t)=in2(t)*cin2(t)+qE2(t)*cE2(t);
output2(t)=q2(t).*cOut2(t);
deltaS2(t)=diff([m2(t-1),m2(t)]);
```

```
    %reservoir 3
    input3(t)=in3(t)*cin3(t);
    output3(t)=qE1(t)*cE1(t)+qE2(t)*cE2(t);
    deltaS3(t)=diff([m3(t-1),m3(t)]);
end
%-------------------------------------------------------------------------
```

A.7 Input data

A.7.1 Source code for down-scaling of nitrogen mineralization and immobilization observations

```
%%%%%%%%%%%%%%%%%%%%%%%%%%%%%%%%%%%%%%%%%%%%%%%%%%%%%%%%%%%%%%%%%%%%%%%%%%%%
% down-scalling of experimental nitrogen mineralization and immobilization
% data (by Andreas Hartmann)
%%%%%%%%%%%%%%%%%%%%%%%%%%%%%%%%%%%%%%%%%%%%%%%%%%%%%%%%%%%%%%%%%%%%%%%%%%%%

function [mUpRel]=N_Correction(ModelStart,NumberOfYears,mTotUpRel)

cd 'nitrog~1';
%load annual experimental values measured Joffre 1990
%date in these date is one year begining in october 1900 (excel time)
Min=load('min_ann.txt');
Imm=load('imm_ann.txt');
%convert excel to matlab dates
Min=[x2mdate(Min(:,1:2)) Min(:,3)];
Imm=[x2mdate(Imm(:,1:2)) Imm(:,3)];

%down-scalling of mineralization data
MinDailyBars=[];
[yyyy mm dd]=datevec(ModelStart); %date vector of model start
[yyyy1 mm1 dd1]=datevec(Min(1,1)); %date vector of Mineralization data
YearDiff=yyyy-yyyy1; %difference of years between model and mineralization
for n=1:NumberOfYears %loop number equals number of simulation years
    for i=1:length(Min)
        [yyyy1 mm1 dd1]=datevec(Min(i,1)); %start date vector of respective
                                           %mineralization period
        [yyyy2 mm2 dd2]=datevec(Min(i,2)); %end date vector of respective
                                           %minarlization period
        %new array for the respective simulation year
        MinTemp=[datenum(yyyy1+YearDiff+n-1,mm1,dd1) ...
            datenum(yyyy2+YearDiff+n-1,mm2,dd2) Min(i,3)];
        numDayMin(i)=MinTemp(2)-MinTemp(1); %number of day in this period
        %down-scalling by dividing the value for this period by its number
        %of days
        for d=MinTemp(1):MinTemp(2)
            NewMin=[d,MinTemp(3)/(numDayMin(i)+1)];%daily mineralization
            L=find(MinDailyBars==NewMin(1));%if date allready exists (for
                                            %example in overlying periods
            if L
                NewMin=[];                  %no new colums in
                                            %mineralization vector wil be
                                            %produced
            end
            MinDailyBars=[MinDailyBars;NewMin]; %add new sub-scalled values
                                                %to allready sub-scalled
                                                %mineralization data
        end
```

```
    end
end

%down-scalling of mineralization data (description see above)
ImmDailyBars=[];
[yyyy mm dd]=datevec(ModelStart);
[yyyy1 mm1 dd1]=datevec(Imm(1,1));
YearDiff=yyyy-yyyy1;
for n=1:NumberOfYears
    for i=1:length(Imm)
        [yyyy1 mm1 dd1]=datevec(Imm(i,1));
        [yyyy2 mm2 dd2]=datevec(Imm(i,2));
        ImmTemp=[datenum(yyyy1+YearDiff+n-1,mm1,dd1) ...
            datenum(yyyy2+YearDiff+n-1,mm2,dd2) Imm(i,3)];
        numDayImm(i)=ImmTemp(2)-ImmTemp(1);
        for d=ImmTemp(1):ImmTemp(2)
            NewImm=[d,ImmTemp(3)/(numDayImm(i)+1)];
            L=find(ImmDailyBars==NewImm(1));
            if L
                NewImm=[];
            end
            ImmDailyBars=[ImmDailyBars;NewImm];
        end
    end
end

%difference of Mineralization/Immobilization
NRatio=[MinDailyBars(:,1) MinDailyBars(:,2)-ImmDailyBars(:,2)];
%convert values to g/m²/day
mUpRel=[NRatio(:,1) mTotUpRel/365.25*NRatio(:,2)];

%------------------------------------------------------------------------
```

A.7.2 Source code for interpolation and regionalization of temperature data

```
%%%%%%%%%%%%%%%%%%%%%%%%%%%%%%%%%%%%%%%%%%%%%%%%%%%%%%%%%%%%%%%%%%%%%%%%%%%
% Interpolation and regionalization of temperature (by Andreas Hartmann)
%%%%%%%%%%%%%%%%%%%%%%%%%%%%%%%%%%%%%%%%%%%%%%%%%%%%%%%%%%%%%%%%%%%%%%%%%%%

%clip meteorological data to simulation period and interpolate
%------------------------------------------------------------------------
%progres bar
h = waitbar(0, 'Interpolating missing temperature observation days');
for j=1:length(DateRain0) % loop for all time steps
    index1=find(TempDateArray==DateRain0(j));% find the common dates
    if index1>0
        TempSeries(j)=TempData(index1); %transfer value to new data series
        indexold=index1; %index for interpolation of missing observations
        position=0; %setting zero the interpolation position
        %routine for filling dates without measurements via interpolation
        %works just if the 1st of october is measured as well as the 30th
        %september
    %interpolation if no common dates exist
    elseif isempty(index1) && (DateRain0(j)>=StartDate) && ...
            (DateRain0(j)<=EndDate)
        %number of missing observations+1
        dist=TempDateArray(indexold+1)-TempDateArray(indexold);
        position=position+1; %increment interpolation position
        frac=position/dist; %fraction of difference of measured values
                            %added to the lower measured value
```

```
        TempSeries(j)=TempData(indexold)+(TempData(indexold+1)- ...
            TempData(indexold))*frac; %interpolation
    end
    h = waitbar(j/length(DateRain0),h);
end
close(h);
%-----------------------------------------------------------------------

%allocating temparature to the temperature strips
%-----------------------------------------------------------------------
h = waitbar(0, 'allocating temparature to the temperature strips');
for i=1:length(DateRain0)
    for j=1:length(HermonTopo)
            TopoTemp(i,j)=TempSeries(i)+(HermonTopo(j,2)-SAlt)*AG/100;
    end
    h = waitbar(i/length(DateRain0),h);
end
close(h);
%-----------------------------------------------------------------------
```

A.7.3 Source code for regionalisation of potential evaporation data

```
%%%%%%%%%%%%%%%%%%%%%%%%%%%%%%%%%%%%%%%%%%%%%%%%%%%%%%%%%%%%%%%%%%%%%%%%
% Regionalization of potential evaporation (by Andread Hartmann)
%%%%%%%%%%%%%%%%%%%%%%%%%%%%%%%%%%%%%%%%%%%%%%%%%%%%%%%%%%%%%%%%%%%%%%%%

%parameters for Pan A Evap function
%-----------------------------------------------------------------------
EvapCoef = 5.4531;      % from analysis of Pan A
AngFreq = 0.0172;       % from analysis of Pan A
Phase = 67.3105;        % from analysis of Pan A
Amp  = 0.5686;          % from analysis of Pan A
[Y,M,D] = datevec(DateRain);
%-----------------------------------------------------------------------

%Pan A Evap function
%-----------------------------------------------------------------------
PanPotentialEvap=EvapCoef*(1+Amp*sin(AngFreq*(30.44*(M-1)+D)+Phase));
PotentialEvap=PanACoeff*PanPotentialEvap;
%-----------------------------------------------------------------------

%daily astronomic sunshine length
%-----------------------------------------------------------------------
    Obl=23.439; %Obliquity of the ecliptic
    PerSol=182.625; %period between solstices
    diffJD=datenum('21.12.0000','dd.mm.yy'); %correction from calendar year
                    %to astronomic year (begins with winter solstice)

%astronomic sunshine length
%-----------------------------------------------------------------------
for t=1:length(DateRain)
    asl(t)=24*(acos(1-(1-tan(lat/180*pi)*tan(Obl/180*pi * ...
        cos(pi*(t-diffJD)/PerSol))))/pi);
end
%-----------------------------------------------------------------------

%fit Thornthwaite to corrected Pan A observations
%-----------------------------------------------------------------------
```

```
%function handle of Thornthwaite formula for daily values
%(without number of days of month)
f_th=@(x,y) 0.533.*y(:,1)./12.*(10.*y(:,2)/x(1)).^x(2);
%estimation of parameters
x0(1)=(mean(TopoTemp(:,4))/5)^1.514;
x0(2)=(.0675*x0(1)^3-7.71*x0(1)^2+1792*x0(1)+49239)*10^-5;
%fit thornthwaite to Pan A evaporation at 250m Strip; x are new parameters
x=lsqcurvefit(f_th,x0,[asl' TopoTemp(:,4)],PotentialEvap);
%--------------------------------------------------------------------------

%regionalize potential Evaporation
%--------------------------------------------------------------------------
h = waitbar(0, 'allocating potential evaporation to altitude Strips');
for i=1:length(DateRain)
    for j=1:length(HermonTopo)
        if TopoTemp(i,j)>0
            TopoPotEvap(i,j)=0.533.*asl(i)./12.*(10.*TopoTemp(i,j) ...
                /x(1)).^x(2);
        else
            TopoPotEvap(i,j)=0;
        end
    end
    h = waitbar(i/length(DateRain),h);
end
close(h)
%--------------------------------------------------------------------------
```